

1992

Parameter uncertainty and modeling of sludge dewatering in one dimension

Joseph H. Plaskett
Portland State University

Follow this and additional works at: https://pdxscholar.library.pdx.edu/open_access_etds



Part of the [Civil and Environmental Engineering Commons](#)

Let us know how access to this document benefits you.

Recommended Citation

Plaskett, Joseph H., "Parameter uncertainty and modeling of sludge dewatering in one dimension" (1992).
Dissertations and Theses. Paper 4432.
<https://doi.org/10.15760/etd.6316>

This Thesis is brought to you for free and open access. It has been accepted for inclusion in Dissertations and Theses by an authorized administrator of PDXScholar. Please contact us if we can make this document more accessible: pdxscholar@pdx.edu.

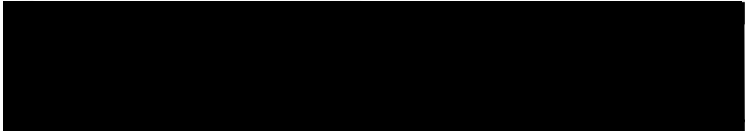
AN ABSTRACT OF THE THESIS OF Joseph H. Plaskett for the Master of Science in Civil Engineering presented June 10, 1992.

Title: Parameter Uncertainty and Modeling of Sludge Dewatering in One Dimension.

APPROVED BY THE MEMBERS OF THE THESIS COMMITTEE:


Scott Wells, Chair


Roy W. Koch


Gerald Reutenwald

Separation of liquid from solids is a necessary step in the ultimate disposal of wastewater sludges. Most commonly, sludges are dewatered by pressure-filtration methods. Mathematical models of the physics of the sludge dewatering process would provide the ability to predict dewatering performance and optimize the design and operation of dewatering facilities.

This study focuses on a physically-based, one-dimensional dewatering model developed by Wells (1990a), which is driven

by an empirical representation of the properties of the sludge in the form of two constitutive equations.

A literature review of previous modeling efforts applicable to the problem of sludge dewatering is presented.

Simulation experiments were conducted to show the model's range of predictive capability. Model output was compared to the experimental data of Bierck, Wells and Dick (1988). The results of computer simulations indicated that the constitutive relationships proposed by Wells (1990a) may not be accurate at low suspended solids concentrations.

Although the model gave good results for slurries which have undergone sedimentation prior to filtration, inaccurate results were obtained when predicting the dewatering behavior of a well-mixed suspension. In order to allow the model to make accurate predictions for suspensions having uniform initial suspended solids concentrations, the artificial viscosity method of von Neuman and Richtmeyer was implemented. This is shown to be a significant improvement to the Wells (1990a) model, giving the model the capability to give accurate results using initially uniform suspended solids concentration profiles as input, while not unduly affecting model output for runs with initial concentration profiles resulting from a period of gravity sedimentation.

In order to quantify the effect of uncertainty and variability of the model constitutive relationships on model output, a stochastic, or Monte Carlo simulation was performed.

The results are presented and discussed.

A new constitutive relationship for the coefficient of volume compressibility, m_v , is proposed, which better fit the experimental data of Bierck, Wells and Dick (1988).

PARAMETER UNCERTAINTY AND MODELING OF SLUDGE DEWATERING
IN ONE DIMENSION

by

JOSEPH H. PLASKETT

A thesis submitted in partial fulfillment of the
requirements for the degree of

MASTER OF SCIENCE
in
CIVIL ENGINEERING

Portland State University
1992

TO THE OFFICE OF GRADUATE STUDIES:

The members of the Committee approve the thesis of Joseph H. Plaskett presented June 10, 1992.

[Redacted Signature]

Scott Wells, Chair

[Redacted Signature]

Roy W. Koch

[Redacted Signature]

Gerald Rectenwald

APPROVED:



[Redacted Signature]

Franz Rad, Chair, Department of Civil Engineering

[Redacted Signature]

C. William Savery, Vice Provost for Graduate Studies and Research

TABLE OF CONTENTS

		PAGE
	LIST OF TABLES.....	v
	LIST OF FIGURES.....	vii
	LIST OF SYMBOLS.....	xxiii
 CHAPTER		
I	INTRODUCTION.....	1
II	BACKGROUND.....	5
III	MODELING OF ONE-DIMENSIONAL SLUDGE DEWATERING. 10	
	Small Strain Theories.....	10
	Finite Strain Theories.....	15
IV	WELLS MODEL OF CAKE FILTRATION.....	36
	Solution Strategy.....	38
	Model Calibration and Verification.....	46
V	FURTHER EXPERIMENTS WITH THE WELLS MODEL.....	62
	Simulations With Uniform Initial Porosity Profiles.....	87
VI	WELLS MODEL WITH ARTIFICIAL VISCOSITY.....	97
	Derivation of Wells Compressible Cake Filtration Model With Artificial Viscosity.....	99
	Finite Difference Form of Governing Equation With Artificial Viscosity..	103
	Calibration of the Artificial Viscosity Constant.....	105

VII	DETERMINATION OF CONSTITUTIVE RELATIONSHIPS FROM SPECIFIC RESISTANCE TESTS.....	129
VIII	MODELING OF CAKE FILTRATION WITH UNCERTAINTY..	180
	Dewatering Model Uncertainty Analysis....	185
	A New Constitutive Equation For m_v	200
IX	CONCLUSIONS AND RECOMMENDATIONS FOR FURTHER RESEARCH.....	203
	REFERENCES.....	206
	APPENDICES	
A	MODIFIED SLUDGE DEWATERING MODEL COMPUTER CODE.....	211
B	RESULTS OF DEWATERING MODEL SIMULATIONS.....	227
C	COMPUTER CODE FOR GENERATING MODEL PARAMETER VALUES.....	232
D	UNIX SHELL PROCEDURE TO CONTROL MONTE CARLO SIMULATION.....	237
E	MONTE CARLO SIMULATION RESULTS.....	239

LIST OF TABLES

TABLE		PAGE
I	Summary and Comparison of Dewatering Models .	34
II	Summary of Results From Computer Simulations Using Wells Cake Filtration Model ($c_i=0.31 \text{ g/cm}^3$)	50
III	Statistics From Data-Model Comparison of Porosity and Distance Over Time ($c_i=0.31 \text{ g/cm}^3$)	61
IV	Summary of Results From Computer Simulations Using Wells Cake Filtration Model ($c_i=0.47 \text{ g/cm}^3$)	63
V	Statistics From Data-Model Comparison of Porosity and Distance Over Time ($c_i=0.47 \text{ g/cm}^3$)	74
VI	Summary of Results From Computer Simulations Using Wells Cake Filtration Model ($c_i=0.14 \text{ g/cm}^3$)	75
VII	Statistics From Data-Model Comparison of Porosity and Distance Over Time ($c_i=0.14 \text{ g/cm}^3$)	86
VIII	Summary of Results From Computer Simulations Using Wells Cake Filtration Model With Uniform Initial Porosity Distributions .	88
IX	Summary of Results of Simulations Using the Wells (1990a) Sludge Dewatering Model With Artificial Viscosity.	110
X	Effect of Artificial Viscosity on CHES Runs With Prior Gravity Sedimentation	113
XI	Summary of Dewaterability Parameters Obtained From Specific Resistance Tests	134

XII	Summary of Converted Dewaterability Parameters Used In Dewatering Model	135
XIII	Summary of Results From Computer Simulations Using Constitutive Relationships For Kaolin Sludge Calculated From Specific Resistance Tests	137
XIV	Comparison of Results for Model Runs With Kaolin Sludge Using Constitutive Equations Determined From Specific Resistance Tests. Percent Change in Selected Output From That Obtained From Calibrated Constitutive Relationships. .	168
XV	Statistics From Data-Model Comparisons of Porosity and Distance Over Time for Simulations of a Kaolin Suspension Using Constitutive Equations Calculated From Specific Resistance Tests.	169
XVI	Summary of Results From Computer Simulations Using Constitutive Relationships Calculated From Specific Resistance Tests For Anaerobic Sludge With and Without Chemical Conditioning.	171
XVII	Mean and Standard Deviation of Parameter- Dependent Quantities For 500 Runs of Wells (1990a) Dewatering Model.. . . .	189

LIST OF FIGURES

FIGURE	PAGE
1.	Boundary conditions of compressible cake filtration dewatering, where n_i is the initial porosity, n_0 is the terminal porosity, v_0 is the liquid velocity at $z=0$ and Q is the rate of filtrate production. 6
2.	Coordinate system and domain for cake filtration models of Atsumi and Akiyama (1975), Wakeman (1978) and Tosun (1986). 28
3.	Finite difference grid near moving boundary as treated in the model of Lee and Sills (1979). 30
4.	Semi-log plot of effective stress versus porosity data from CHESSE experiments with exponential best fit of Equation 35. 39
5.	Semi-log plot of permeability versus porosity data from CHESSE experiments with exponential best fit of Equation 33. 39
6.	Treatment of moving boundary by Wells (1990a) dewatering model. 45
7.	Computation algorithm for Wells (1990) cake filtration dewatering model. 47
8.	Semi-log plot of calibrated effective stress versus porosity relationship superimposed over CHESSE data. 48
9.	Semi-log plot of calibrated permeability versus porosity constitutive relationship superimposed over CHESSE data. 48
10.	Data-model comparison of concentration profiles at 30 s intervals under conditions of CHESSE run KDMK9 (100 kPa, 0.31 g/cm ³). 51
11.	Error frequency histogram for run KDMK9, paired data-model observations of porosity and time as in Figure 10. 51

12.	Data-model comparison of filtrate production with time under conditions of CHESS run KDMK9 (103 kPa, 0.31 g/cm ³).	52
13.	Data-model comparison of concentration profiles at 30 s intervals under conditions of CHESS run KDM2 (172 kPa, 0.31 g/cm ³).	53
14.	Error frequency histogram for run KDM2, paired data-model observations of porosity and time as in Figure 13.	53
15.	Data-model comparison of filtrate production with time under conditions of CHESS run KDM2 (172 kPa, 0.31 g/cm ³).	54
16.	Data-model comparison of concentration profiles at 30 s intervals under conditions of CHESS run PMK3 (345 kPa, 0.31 g/cm ³).	55
17.	Error frequency histogram for run PMK3, paired data-model observations of porosity and time as in Figure 16.	55
18.	Data-model comparison of filtrate production with time under conditions of CHESS run PMK3 (345 kPa, 0.31 g/cm ³).	56
19.	Data-model comparison of concentration profiles at 30 s intervals under conditions of CHESS run PMK4 (517 kPa, 0.31 g/cm ³).	57
20.	Error frequency histogram for run PMK4, paired data-model observations of porosity and time as in Figure 19.	57
21.	Data-model comparison of filtrate production with time under conditions of CHESS run PMK4 (517 kPa, 0.31 g/cm ³).	58
22.	Data-model comparison of concentration profiles at 30 s intervals under conditions of CHESS run PMK5 (682 kPa, 0.31 g/cm ³).	59
23.	Error frequency histogram for run PMK5, paired data-model observations of porosity and time as in Figure 22.	59
24.	Data-model comparison of filtrate production with time under conditions of CHESS run PMK5 (682 kPa, 0.31 g/cm ³).	60

25.	Data-model comparison of concentration profiles at 30 s intervals under conditions of CHES run KDMK8 (103 kPa, 0.47 g/cm ³).	64
26.	Error frequency histogram for run KDMK8, from paired data-model observations of porosity and time as in Figure 25.	64
27.	Data-model comparison of filtrate production with time under conditions of CHES run KDMK8 (103 kPa, 0.47 g/cm ³).	65
28.	Data-model comparison of concentration profiles at 30 s intervals under conditions of CHES run KDM6 (172 kPa, 0.47 g/cm ³).	66
29.	Error frequency histogram for run KDM6, from paired data-model observations of porosity and time as in Figure 28.	66
30.	Data-model comparison of filtrate production with time under conditions of CHES run KDM6 (172 kPa, 0.47 g/cm ³).	67
31.	Data-model comparison of concentration profiles at 30 s intervals under conditions of CHES run KDM4 (345 kPa, 0.47 g/cm ³).	68
32.	Error frequency histogram for run KDM4, from paired data-model observations of porosity and time as in Figure 31.	68
33.	Data-model comparison of filtrate production with time under conditions of CHES run KDM4 (345 kPa, 0.47 g/cm ³).	69
34.	Data-model comparison of concentration profiles at 30 s intervals under conditions of CHES run PMK9 (517 kPa, 0.47 g/cm ³).	70
35.	Error frequency histogram for run PMK9, from paired data-model observations of porosity and time as in Figure 34.	70
36.	Data-model comparison of filtrate production with time under conditions of CHES run PMK9 (517 kPa, 0.47 g/cm ³).	71
37.	Data-model comparison of concentration profiles at 30 s intervals under conditions of CHES run PMK6 (682 kPa, 0.47 g/cm ³).	72

38.	Error frequency histogram for run PMK6, from paired data-model observations of porosity and time as in Figure 37.	72
39.	Data-model comparison of filtrate production with time under conditions of CHESS run PMK6 (682 kPa, 0.47 g/cm ³).	73
40.	Data-model comparison of concentration profiles at 30 s intervals under conditions of CHESS run KDM7 (103 kPa, 0.14 g/cm ³).	76
41.	Error frequency histogram for run KDM7, paired data-model observations of porosity and time as in Figure 40.	76
42.	Data-model comparison of filtrate production with time under conditions of CHESS run KDM7 (103 kPa, 0.14 g/cm ³).	77
43.	Data-model comparison of concentration profiles at 30 s intervals under conditions of CHESS run KDM5 (172 kPa, 0.14 g/cm ³).	78
44.	Error frequency histogram for run KDM5, paired data-model observations of porosity and time as in Figure 43.	78
45.	Data-model comparison of filtrate production with time under conditions of CHESS run KDM5 (172 kPa, 0.14 g/cm ³).	79
46.	Data-model comparison of concentration profiles at 30 s intervals under conditions of CHESS run KDM3B (345 kPa, 0.14 g/cm ³).	80
47.	Error frequency histogram for run KDM3B, paired data-model observations of porosity and time as in Figure 46.	80
48.	Data-model comparison of filtrate production with time under conditions of CHESS run KDM3B (345 kPa, 0.14 g/cm ³).	81
49.	Data model comparison of concentration profiles at 30 s intervals under conditions of CHESS run PMK10 (517 kPa, 0.14 g/cm ³).	82
50.	Error frequency histogram for run PMK10, paired data-model observations of porosity and time as in Figure 49.	82

51.	Data-model comparison of filtrate production with time under conditions of CHES run PMK10 (517 kPa, 0.14 g/cm ³).	83
52.	Data-model comparison of concentration profiles at 30 s intervals under conditions of CHES run PMK7 (682 kPa, 0.14 g/cm ³).	84
53.	Error frequency histogram for run PMK7, paired data-model observations of porosity and time as in Figure 52.	84
54.	Data-model comparison of filtrate production with time under conditions of CHES run PMK7 (682 kPa, 0.14 g/cm ³).	85
55.	Concentration profiles at 30 s intervals under conditions of CHES run KDMK8 with uniform initial porosity profile as predicted by Wells (1990a) dewatering model.	89
56.	Filtrate production versus time for conditions of CHES run KDMK8 with and without prior gravity sedimentation as predicted by Wells (1990a) dewatering model.	89
57.	Plot of porosity gradient versus time for CHES run KDMK8 with prior sedimentation.	94
58.	Plot of porosity gradient versus time for CHES run KDMK8 without prior sedimentation.	94
59.	Plot of porosity gradient versus time for CHES run KDMK9 with prior sedimentation.	95
60.	Plot of porosity gradient versus time for CHES run KDMK9 without prior sedimentation.	95
61.	Plot of diffusive and convective terms of governing equation versus time for CHES run KDMK8 with prior sedimentation at grid point number 2.	96
62.	Plot of diffusive and convective terms of governing equation over time for CHES run KDMK9 without prior sedimentation at grid point number 2.	96
63.	Porosity profile immediately after application of the external pressure gradient ($P_{app}=103$ kPa), for a slurry with an initially uniform porosity of 0.88.	97

64.	Plot of porosity gradient versus time for CHESS run KDMK9 without prior gravity sedimentation using artificial viscosity at node 2.	107
65.	Plot of diffusive and convective terms of governing equation versus time with artificial viscosity for CHESS run KDMK9 without prior gravity sedimentation at grid point 2.	108
66.	Plot of diffusive and convective terms of governing equation versus time with artificial viscosity for CHESS run KDMK9 without prior gravity sedimentation at grid point 5.	109
67.	Plot of diffusive and convective terms of governing equation versus time with artificial viscosity for CHESS run KDMK9 without prior gravity sedimentation at grid point 10.	109
68.	Concentration profiles at 30 s intervals under conditions of CHESS run KDMK8 (103 kPa, 0.47 g/cm ³) without prior gravity sedimentation.	114
69.	Filtrate production versus time for run KDMK8 without prior gravity sedimentation.	114
70.	Concentration profiles at 30 s intervals under conditions of CHESS run KDM6 (170 kPa, 0.47 g/cm ³) without prior gravity sedimentation.	115
71.	Filtrate production versus time for run KDM6 without prior gravity sedimentation.	115
72.	Concentration profiles at 30 s intervals under conditions of CHESS run KDM4 (345 kPa, 0.47 g/cm ³) without prior gravity sedimentation.	116
73.	Filtrate production versus time for run KDM4 without prior gravity sedimentation.	116
74.	Concentration profiles at 30 s intervals under conditions of CHESS run PMK9 (520 kPa, 0.47 g/cm ³) without prior gravity sedimentation.	117
75.	Filtrate production versus time for run PMK9 without prior gravity sedimentation.	117
76.	Concentration profiles at 30 s intervals under conditions of CHESS run PMK6 (690 kPa, 0.47 g/cm ³) without prior gravity sedimentation.	118

77.	Filtrate production versus time for run PMK6 without prior gravity sedimentation.	118
78.	Concentration profiles at 30 s intervals under conditions of CHESS run KDMK9 (103 kPa, 0.31 g/cm ³) without prior gravity sedimentation. .	119
79.	Filtrate production versus time for run KDMK9 without prior gravity sedimentation.	119
80.	Concentration profiles at 30 s intervals under conditions of CHESS run KDM2 (170 kPa, 0.31 g/cm ³) without prior gravity sedimentation. .	120
81.	Filtrate production versus time for run KDM2 without prior gravity sedimentation.	120
82.	Concentration profiles at 30 s intervals under conditions of CHESS run PMK3 (345 kPa, 0.31 g/cm ³) without prior gravity sedimentation. .	121
83.	Filtrate production versus time for run PMK3 without prior gravity sedimentation.	121
84.	Concentration profiles at 30 s intervals under conditions of CHESS run PMK4 (520 kPa, 0.31 g/cm ³) without prior gravity sedimentation. .	122
85.	Filtrate production versus time for run PMK4 without prior gravity sedimentation.	122
86.	Concentration profiles at 30 s intervals under conditions of CHESS run PMK5 (690 kPa, 0.31 g/cm ³) without prior gravity sedimentation. .	123
87.	Filtrate production versus time for run PMK5 without prior gravity sedimentation.	123
88.	Concentration profiles at 30 s intervals under conditions of CHESS run KDM7 (103 kPa, 0.14 g/cm ³) without prior gravity sedimentation. .	124
89.	Filtrate production versus time for run KDM7 without prior gravity sedimentation.	124
90.	Concentration profiles at 30 s intervals under conditions of CHESS run KDM5 (170 kPa, 0.31 g/cm ³) without prior gravity sedimentation. .	125
91.	Filtrate production versus time for run KDM5 without prior gravity sedimentation.	125

92.	Concentration profiles at 30 s intervals under conditions of CHES run KDM3B (345 kPa, 0.31 g/cm ³) without prior gravity sedimentation.	126
93.	Filtrate production versus time for run KDM3B without prior gravity sedimentation.	126
94.	Concentration profiles at 30 s intervals under conditions of CHES run PMK10 (520 kPa, 0.31 g/cm ³) without prior gravity sedimentation.	127
95.	Filtrate production versus time for run PMK10 without prior gravity sedimentation.	127
96.	Concentration profiles at 30 s intervals under conditions of CHES run PMK7 (690 kPa, 0.31 g/cm ³) without prior gravity sedimentation.	128
97.	Filtrate production versus time for run PMK7 without prior gravity sedimentation.	128
98.	Specific resistance test apparatus.	130
99.	Semi-log plot of kaolin effective stress versus porosity constitutive relationship calculated from specific resistance tests superimposed over CHES data.	136
100.	Semi-log plot of kaolin permeability versus porosity constitutive relationship calculated from specific resistance tests superimposed over CHES data.	136
101.	Data-model comparison of concentration profiles at 30 s intervals under conditions of CHES run KDMK9 using constitutive relationships calculated from specific resistance tests.	138
102.	Error frequency histogram for calculated constitutive relationship run KDMK9, paired data-model observations of porosity and time as in Figure 3.	138
103.	Data-model comparison of filtrate production with time under conditions of CHES run KDMK9 using constitutive relationships calculated from specific resistance tests.	139
104.	Data-model comparison of concentration profiles at 30 s intervals under conditions of CHES run KDM2 using constitutive relationships calculated from specific resistance tests.	140

105. Error frequency histogram for calculated constitutive relationship run KDM2, paired data-model observations of porosity and time as in Figure 6. 140
106. Data-model comparison of filtrate production with time under conditions of CHESS run KDM2 using constitutive relationships calculated from specific resistance tests. 141
107. Data-model comparison of concentration profiles at 30 s intervals under conditions of CHESS run PMK3 using constitutive relationships calculated from specific resistance tests. . . 142
108. Error frequency histogram for calculated constitutive relationship run PMK3, paired data-model observations of porosity and time as in Figure 9. 142
109. Data-model comparison of filtrate production with time under conditions of CHESS run PMK3 using constitutive relationships calculated from specific resistance tests. 143
110. Data-model comparison of concentration profiles at 30 s intervals under conditions of CHESS run PMK4 using constitutive relationships calculated from specific resistance tests. . . 144
111. Error frequency histogram for calculated constitutive relationship run PMK4, paired data-model observations of porosity and time as in Figure 12. 144
112. Data-model comparison of filtrate production with time under conditions of CHESS run PMK4 using constitutive relationships calculated from specific resistance tests. 145
113. Data-model comparison of concentration profiles at 30 s intervals under conditions of CHESS run PMK5 using constitutive relationships calculated from specific resistance tests. . . 146
114. Error frequency histogram for calculated constitutive relationship run PMK5, paired data-model observations of porosity and time as in Figure 15. 146

115.	Data-model comparison of filtrate production with time under conditions of CHESS run PMK5 using constitutive relationships calculated from specific resistance tests.	147
116.	Data-model comparison of concentration profiles at 30 s intervals under conditions of CHESS run KDMK8 using constitutive relationship calculated from specific resistance tests.	148
117.	Error frequency histogram for calculated constitutive relationship run KDMK8, paired data-model observations of porosity and time as in Figure 18.	148
118.	Data-model comparison of filtrate production with time under conditions of CHESS run KDMK8 using constitutive relationships calculated from specific resistance tests.	149
119.	Data-model comparison of concentration profiles at 30 s intervals under conditions of CHESS run KDM6 using constitutive relationships calculated from specific resistance tests.	150
120.	Error frequency histogram for calculated constitutive relationship run KDM6, paired data-model observations of porosity and time as in Figure 21.	150
121.	Data-model comparison of filtrate production with time under conditions of CHESS run KDM6 using constitutive relationships calculated from specific resistance tests.	151
122.	Data-model comparison of concentration profiles at 30 s intervals under conditions of CHESS run KDM4 using constitutive relationships calculated from specific resistance tests.	152
123.	Error frequency histogram for calculated constitutive relationship run KDM4, paired data-model observations of porosity and time as in Figure 24.	152
124.	Data-model comparison of filtrate production with time under conditions of CHESS run KDM4 using constitutive relationships calculated from specific resistance tests.	153

125. Data-model comparison of concentration profiles at 30 s intervals under conditions of CHESS run PMK9 using constitutive relationships calculated from specific resistance tests. . . . 154
126. Error frequency histogram for calculated constitutive relationship run PMK9, paired data-model observations of porosity and time as in Figure 27. 154
127. Data-model comparison of filtrate production with time under conditions of CHESS run PMK9 using constitutive relationships calculated from specific resistance tests. 155
128. Data-model comparison of concentration profiles at 30 s intervals under conditions of CHESS run KDM7 using constitutive relationships calculated from specific resistance tests. . . . 156
129. Error frequency histogram for calculated constitutive relationship run KDM7, paired data-model observations of porosity and time as in Figure 24. 156
130. Data-model comparison of filtrate production with time under conditions of CHESS run KDM7 using constitutive relationships calculated from specific resistance tests. 157
131. Data-model comparison of concentration profiles at 30 s intervals under conditions of CHESS run KDM5 using constitutive relationships calculated from specific resistance tests. . . . 158
132. Error frequency histogram for calculated constitutive relationship run KDM5, paired data-model observations of porosity and time as in Figure 24. 158
133. Data-model comparison of filtrate production with time under conditions of CHESS run KDM5 using constitutive relationships calculated from specific resistance tests. 159
134. Data-model comparison of concentration profiles at 30 s intervals under conditions of CHESS run KDM3B using constitutive relationships calculated from specific resistance tests. . . . 160

135. Error frequency histogram for calculated constitutive relationship run KDM3B, paired data-model observations of porosity and time as in Figure 24. 160
136. Data-model comparison of filtrate production with time under conditions of Chess run KDM3B using constitutive relationships calculated from specific resistance tests. 161
137. Data-model comparison of concentration profiles at 30 s intervals under conditions of CHESS run PMK10 using constitutive relationships calculated from specific resistance tests. . . 162
138. Error frequency histogram for calculated constitutive relationship run PMK10, paired data-model observations of porosity and time as in Figure 27. 162
139. Data-model comparison of filtrate production with time under conditions of CHESS run PMK10 using constitutive relationships calculated from specific resistance tests. 163
140. Data-model comparison of concentration profiles at 30 s intervals under conditions of CHESS run PMK7 using constitutive relationships calculated from specific resistance tests. . . 164
141. Error frequency histogram for calculated constitutive relationship run PMK7, paired data-model observations of porosity and time as in Figure 30. 164
142. Data-model comparison of filtrate production with time under conditions of CHESS run PMK7 using constitutive relationships calculated from specific resistance tests. 165
143. Plot of porosity gradient versus time for CHESS run PMK6 using constitutive relationships calculated from specific resistance tests. . . 167
144. Plot of suspended solids concentration profiles over time for anaerobic sludge with conditioning predicted by Wells (1990a) ($c_i=0.025 \text{ g/cm}^3$, $P_{app}=69 \text{ kPa}$) dewatering model. 172

145. Filtrate production vs. time as predicted by the Wells (1990a) dewatering model compared to specific resistance test results using anaerobic sludge with conditioner ($c_i=0.025$ g/cm³, $P_{app}=69$ kPa)172
146. Plot of suspended solids concentration profiles over time for anaerobic sludge without conditioning predicted by Wells (1990a) ($c_i=0.022$ g/cm³, $P_{app}=207$ kPa) dewatering model. 173
147. Plot of suspended solids concentration profiles over time for anaerobic sludge with conditioning predicted by Wells (1990a) ($c_i=0.025$ g/cm³, $P_{app}=207$ kPa) dewatering model. 173
148. Filtrate production vs. time as predicted by the Wells (1990a) dewatering model compared to specific resistance test results using anaerobic sludge without conditioner ($c_i=0.022$ g/cm³, $P_{app}=207$ kPa)174
149. Filtrate production vs. time as predicted by the Wells (1990a) dewatering model compared to specific resistance test results using anaerobic sludge with conditioner ($c_i=0.025$ g/cm³, $P_{app}=207$ kPa)174
150. Plot of suspended solids concentration profiles over time for anaerobic sludge without conditioning predicted by Wells (1990a) ($c_i=0.022$ g/cm³, $P_{app}=345$ kPa) dewatering model.175
151. Plot of suspended solids concentration profiles over time for anaerobic sludge with conditioning predicted by Wells (1990a) ($c_i=0.025$ g/cm³, $P_{app}=345$ kPa) dewatering model.175
152. Filtrate production vs. time as predicted by the Wells (1990a) dewatering model compared to specific resistance test results using anaerobic sludge without conditioner ($c_i=0.022$ g/cm³, $P_{app}=345$ kPa)176
153. Filtrate production vs. time as predicted by the Wells (1990a) dewatering model compared to specific resistance test results using anaerobic sludge with conditioner ($c_i=0.025$ g/cm³, $P_{app}=345$ kPa)176

154. Plot of suspended solids concentration profiles over time for anaerobic sludge without conditioning predicted by Wells (1990a) ($c_i=0.022$ g/cm³, $P_{app}=483$ kPa) dewatering model. 177
155. Plot of suspended solids concentration profiles over time for anaerobic sludge with conditioning predicted by Wells (1990a) ($c_i=0.025$ g/cm³, $P_{app}=483$ kPa) dewatering model. 177
156. Filtrate production vs. time as predicted by the Wells (1990a) dewatering model compared to specific resistance test results using anaerobic sludge without conditioner ($c_i=0.022$ g/cm³, $P_{app}=483$ kPa). 178
157. Filtrate production vs. time as predicted by the Wells (1990a) dewatering model compared to specific resistance test results using anaerobic sludge with conditioner ($c_i=0.025$ g/cm³, $P_{app}=483$ kPa). 178
158. Confidence interval estimates for normally distributed, randomly selected values of permeability at various values of porosity. 184
159. Confidence interval estimates for normally distributed, randomly selected values of effective stress at various values of porosity. 184
160. Monte Carlo simulation algorithm. 186
161. Frequency histogram for permeability, k , for 500 runs of parameter picking algorithm using UNIX system pseudo-random number generator at initial porosity of 0.88 g/cm³. 187
162. Frequency histogram for m_v for 500 runs of parameter picking algorithm using UNIX system pseudo-random number generator at initial porosity of 0.88 g/cm³. 188
163. Mean values of suspended solids concentration versus distance from the filter medium with approximate 68% confidence limits as predicted by Wells (1990a) sludge dewatering model for 500 model simulations. 190

164. Mean values of suspended solids concentration versus distance from the filter medium with approximate 68% confidence limits as predicted by Wells (1990a) sludge dewatering model for 500 model simulations. 190
165. Mean values of suspended solids concentration versus distance from the filter medium with approximate 68% confidence limits as predicted by Wells (1990a) sludge dewatering model for 500 model simulations. 191
166. Mean values of suspended solids concentration versus distance from the filter medium with approximate 68% confidence limits as predicted by Wells (1990a) sludge dewatering model for 500 model simulations. 191
167. Mean values of suspended solids concentration versus distance from the filter medium with approximate 68% confidence limits as predicted by Wells (1990a) sludge dewatering model for 500 model simulations. 192
168. Mean values of filtrate volume versus time with approximate 68% confidence limits as predicted by Wells (1990a) sludge dewatering model for 500 model simulations. 193
169. Plot of differences between mean suspended solids concentration obtained after 500 and N model runs at a simulated time of 60 seconds. . . . 194
170. Plot of differences between mean suspended solids concentration obtained after 500 and N model runs at a simulated time of 90 seconds. . . . 195
171. Plot of differences between mean suspended solids concentration obtained after 500 and N model runs at a simulated time of 120 seconds. . . . 195
172. Plot of differences between mean suspended solids concentration obtained after 500 and N model runs at a simulated time of 180 seconds. . . . 196
173. Plot of differences between mean suspended solids concentration obtained after 500 and N model runs at a simulated time of 300 seconds. . . . 196
174. Plot of differences between mean filtrate volume obtained after 500 and N model runs at various times. 197

175. Frequency histogram for permeability, k , for 500 simulations of Wells (1990a) dewatering model at initial porosity of 0.88 g/cm^3 199
176. Frequency histogram for the coefficient of volume compressibility, m_v , for 500 simulations of Wells (1990a) dewatering model at initial porosity of 0.88 g/cm^3 199
177. Plot of data obtained from Bierck, Wells and Dick (1988) versus new constitutive equation for the coefficient of volume compressibility, m_v 202

LIST OF SYMBOLS

a_v	= coefficient of compressibility [LT^2M^{-1}]
A	= area [L^2]
b	= empirical constant [-]
$b_{\#}$	= empirical constant [-]
$b_{\#\#}$	= empirical constant [-]
B	= coefficient used in advective term of consolidation and dewatering models
c	= suspended solids concentration [ML^{-3}]
c_i	= initial suspended solids concentration [ML^{-3}]
c_0	= terminal suspended solids concentration [ML^{-3}]
\bar{c}	= average suspended solids concentration of cake [ML^{-3}]
C	= coefficient used in diffusion term of consolidation and dewatering models [L^2T^{-1}]
C_i	= initial coefficient of consolidation [L^2T^{-1}]
C_0	= value of C at $z=0$ [L^2T^{-1}]
d	= empirical constant [-]
d_f	= number of statistical degrees of freedom
e	= void ratio [-]
e_i	= initial void ratio [-]
e_L	= void ratio at cake surface [-]
e_0^*	= void ratio at stress free state of solids [-]

- e_0 = void ratio at $z=0$ or $m=0$ in coordinate space [-]
- E' = modulus of elasticity of the solid matrix
[$ML^{-1}T^{-2}$]
- F = averaged interfacial interaction term between
the solid and liquid phases [$ML^{-3}T^{-1}$]
- H = length of soil layer [L]
- Δh = change in domain height in one time step [L]
- i = hydraulic gradient [-]
- j = number of a particular node in finite difference
grid [-]
- k = permeability [L^2]
- k_c = permeability in terms of concentration [L^2]
- k_L = permeability at cake surface ($z=L$) [L^2]
- k_0 = initial permeability [L^2]
- K = coefficient of permeability [LT^{-1}]
- K_0 = initial coefficient of permeability [LT^{-1}]
- L = cake length [L]
- L_d = domain length [L]
- m = material coordinate, volume of solids per unit
area [L]
- m_L = material coordinate of cake surface [L]
- m_v = coefficient of volume compressibility [$ML^{-1}T^{-2}$]
- m_{v_c} = coefficient of volume compressibility in terms
of concentration [T^2L^{-2}]
- m_{v_0} = initial coefficient of volume compressibility
[$ML^{-1}T^{-2}$]

M	= total volume of solids per unit area in domain [L]
M_c	= constrained modulus [$ML^{-1}T^{-2}$]
n	= porosity [-]
n_a	= empirical constant [-]
n_b	= breakthrough porosity [-]
n_i	= initial porosity [-]
n_L	= porosity at cake surface [-]
n_0	= porosity at filter medium ($z=0$) [-]
\bar{n}	= average porosity [-]
N	= number of nodes in finite difference grid [-]
N_d	= sample size [-]
$O()$	= order of error of finite difference method
p_a	= empirical constant [$ML^{-1}T^{-2}$]
p_v	= pseudo-viscous pressure [$ML^{-1}T^{-2}$]
P_{app}	= total applied pressure differential [$ML^{-1}T^{-2}$]
ΔP_m	= medium pressure drop [$ML^{-1}T^{-2}$]
r	= coefficient of linear correlation [-]
r_a	= empirical constant [-]
r_s	= specific resistance
R_M	= resistance of filter medium [L^{-1}]
s	= slope of linear portion of t/V versus plot [TL^{-6}]
s_e	= standard deviation of the error
t	= time [T]
T	= time factor [-]

- u = pore water pressure $[ML^{-1}T^{-2}]$
- v_f = vertical component of true fluid velocity $[LT^{-1}]$
- v_r = vertical component of liquid velocity relative to solids $[LT^{-1}]$
- v_s = vertical component of true solid velocity $[LT^{-1}]$
- v_0 = liquid velocity at $z=0$ $[LT^{-1}]$
- V = cumulative volume of filtrate passing the filter medium $[L^3]$
- V_i = initial volume of sludge $[L^3]$
- $V_{\Delta t}$ = volume of filtrate passing the filter medium in one time step $[L^3]$
- w = dry weight of cake deposited per unit volume of filtrate $[MLT^{-2}]$
- \bar{x} = sample mean for abscissa values
- X_1 = slurry pH $[-]$
- X_2 = mixing speed $[T^{-1}]$
- X_3 = flocculant dosage $[-]$
- X_4 = mixing time $[T]$
- X_5 = pressure $[ML^{-1}T^{-2}]$
- X_6 = pressing time $[T]$
- \hat{y} = ordinate value on curve fitted to experimental data
- Y_c = confidence limit for randomly selected ordinate value
- Y_1 = flow time $[T]$
- Y_2 = solid content $[-]$

z	= distance measured from porous medium [L]
α	= empirical constant [L^2]
α'	= empirical constant determined from specific resistance tests [L^2]
α_1	= empirical constant [$ML^{-1}T^{-2}$]
α_2	= empirical constant [LT^{-1}]
β	= empirical constant [-]
β'	= empirical constant determined from specific resistance tests [L^3M^{-1}]
β_1	= empirical constant [$ML^{-1}T^{-2}$]
β_2	= empirical constant [LT^{-1}]
γ	= empirical constant [LT^2M^{-1}]
γ'	= empirical constant determined from specific resistance tests [T^2L^{-2}]
γ_s	= unit weight of solids [$ML^{-2}T^{-2}$]
γ_w	= unit weight of water [$ML^{-2}T^{-2}$]
δ	= empirical constant [-]
δ'	= empirical constant determined from specific resistance tests [$M^{-1}L^3$]
δ_e	= error residual
ϵ	= strain [-]
ζ	= empirical constant [-]
λ	= empirical constant [L^2T^{-1}]
θ	= probability of a Type I error
μ	= dynamic viscosity of pore fluid [$ML^{-1}T^{-1}$]
ν'	= Poisson's ratio for the solid matrix [-]

ξ	= pseudo-viscosity constant [-]
ρ_f	= liquid density [ML ⁻³]
ρ_s	= solids density [ML ⁻³]
ρ_w	= density of water [ML ⁻³]
σ'	= effective stress [ML ⁻¹ T ⁻²]
σ'_b	= breakthrough stress [ML ⁻¹ T ⁻²]
τ	= time level [-]
ϕ	= empirical constant [-]
χ	= stability factor [-]
ψ	= empirical constant [ML ⁻¹ T ⁻²]
ω	= empirical constant [ML ⁻¹ T ⁻²]

CHAPTER I

INTRODUCTION

Treatment of wastewaters produces residual solid/liquid suspensions, or sludges, which must be disposed of into the environment. Separation of water from the sludge solids is necessary to make transportation and ultimate disposal of wastewater sludges more economical. Dewatered sludge takes up less space, thereby decreasing transportation and landfill costs. Sludge must be dewatered before it can be composted. Dewatering is also important to provide shear strength to the soil if placed in landfills, or if it is incinerated, since drier sludges burn more efficiently.

The cost of sludge dewatering is often the biggest fraction of the total expense of sludge management (Evans and Filman 1988). In addition, landfills are filling up, and it has become very difficult, in some areas impossible, to site new landfills. There has also been a trend toward increasing restrictions for sludge disposal on land. The largest amounts of sludge are produced in metropolitan areas, where landfill siting is most difficult, hauling distances are longest, and the potential for beneficial use is limited. Ocean disposal of sludge has now been banned by legislation (Morse 1989). Because of these economic, social and environmental

considerations, there is a growing interest in improving the design, energy efficiency, and performance of sludge dewatering operations.

Dewatering processes include belt filter presses, filter presses, centrifuges, and vacuum filters. Since its first development in the pulp and paper industry, the belt filter press has become one of the most popular methods for dewatering municipal wastewater treatment plant sludges. The belt filter press removes water from sludge by pressing the sludge between porous woven fiber belts.

Despite its widespread use, selection and sizing of sludge dewatering equipment has been based on field experience, trial and error, pilot plant testing, and/or full-scale testing. Laboratory tests, such as the specific resistance test, have been unable to predict full-scale dewatering performance (Dick 1972; EPA 1982) of dewatering processes.

Mathematical models of the physics of the sludge dewatering process would provide the ability to predict dewatering performance and optimize the design and operation of dewatering installations. Empirical models of sludge dewatering processes have the disadvantages of being applicable only to specific sludges; they are only valid within a narrow range of the values of the input variables; and they must be independently verified for each substance, necessitating a relatively large amount of experimental

effort. In contrast, a physically based model applies to the set of all substances that meet the assumptions used to develop the theory (Willis 1983). According to Tiller (1975), the biggest obstacle to the utilization of physically based dewatering models is ignorance of theoretical principles on the part of engineers involved in filtration, as well as the non-analytical approach to filtration generally taken in industry.

This study focuses on a physically-based dewatering model developed by Wells (1990a), driven by an empirical representation of the properties of the sludge. The empirical portion of the model originates from two constitutive relationships needed to solve the model's governing equations. These constitutive relationships were derived by fitting curves to data from one-dimensional pressure filtration experiments. Each of the constitutive equations contains two empirically determined parameters obtained from the slope and ordinate intercept of a regression line through the experimental data. These parameters are related to basic properties which affect sludge dewaterability. Wells (1990b) subsequently presented a method for determining these parameters from specific resistance tests. Results of model runs using these calculated parameter values are presented and compared to data obtained from Bierck, Wells and Dick (1988).

Simulation experiments showed that although the Wells model gives good results for slurries which have undergone

sedimentation prior to filtration, the model can become unstable when predicting the dewatering behavior of a slurry having a uniform concentration throughout the vertical domain. This occurs because of the sharp concentration gradient near the filter medium during the initial stages of filtration, which causes severe dispersive numerical errors. Wells (1991) suggested a method by which the model might be improved to reduce numerical errors that were severe during modeling of initially uniform suspensions. The addition of an "artificial viscosity" term into the original governing equations would, in theory, smooth out the sharp gradient, adding stability to the model without affecting the accuracy of the model results for suspensions which have undergone some sedimentation. The derivation of this term is given, and results of model runs implementing this term are presented.

Because sludge properties which affect the dewatering process are uncertain and highly variable, and the values of these parameters have a great affect on the model's performance, quantifying how model performance was affected by different sets of parameter values was also analyzed. A sensitivity analysis was therefore performed on the dewatering model using stochastic, or Monte Carlo simulation.

Finally, a new constitutive relationship was developed which better fit the experimental data of Bierck, Wells and Dick (1988).

CHAPTER II

BACKGROUND

The basic objectives of modeling any dewatering process are to predict the final porosity (or suspended solids concentration) and the time required to achieve this porosity under various conditions of pressure, temperature, and initial concentration for different material suspensions.

For any modeling effort to be considered complete, it must include the steps of 1) data collection; 2) development of some analytical structure comprising differential equations, empirical relationships and/or experimentation in order to solve the problem; 3) calibration of the various model parameters so that output from the model fits the experimental data; and 4) verification of the model's performance by comparing the output with new data (Thomann 1972).

The problem domain and boundary conditions for modeling constant pressure filtration dewatering are shown in Figure 1. The figure shows a solid-liquid suspension, or slurry, assumed to be of infinite lateral extent with initial porosity $n_i(z)$. Porosity is defined as

$$n = \frac{\text{Volume of voids}}{\text{Total volume}} \quad (1)$$

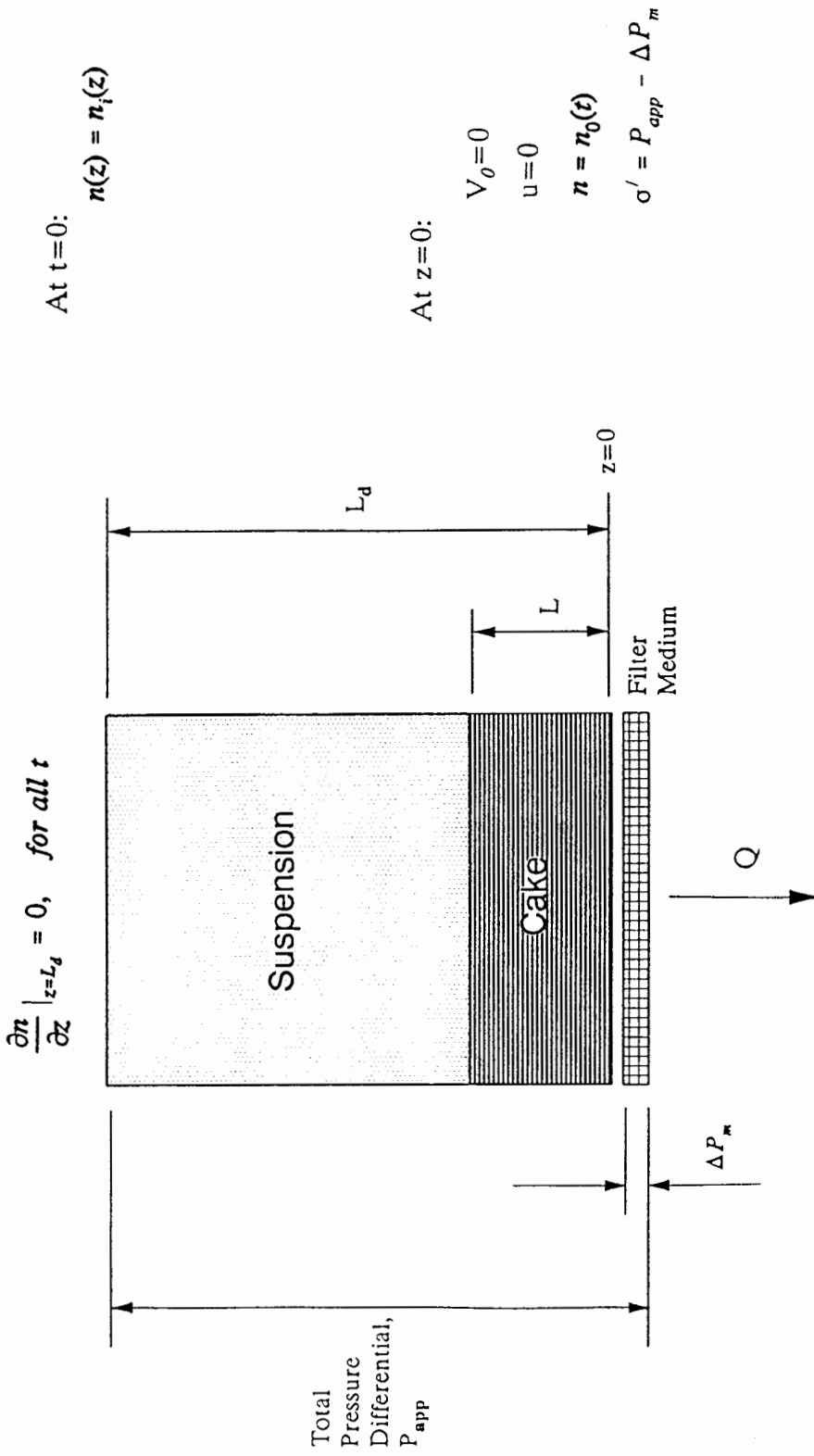


Figure 1. Boundary conditions of compressible cake filtration dewatering, where n_i is the initial porosity, n_0 is the terminal porosity, v_0 is the liquid velocity at $z=0$, and Q is the rate of filtrate production.

The porosity will vary as a function of time and distance from the filter medium during the course of filtration. Drainage and settlement take place in one dimension, coinciding with the direction of the applied pressure and gravity. At $z=0$ the porous medium, or membrane, constitutes a fixed boundary through which liquid may pass, but solid particles may not. Layers of solid particles are deposited at the surface of the membrane, and begin to form the filter cake. The surface layers have a relatively high porosity and liquid content. As more layers are deposited, the surface becomes the cake interior and its porosity begins to decrease as more layers are deposited on top of it. At the point of contact between the cake and filter medium, the porosity takes on its minimum value designated as the terminal porosity, n_0 , which can vary with time. At $z=L_d$ there is a moving boundary across which no liquid flux occurs. The concentration of the suspension at this point does not vary over the time of filtration, if gravity sedimentation is neglected, until surface tension forces act to further consolidate the cake.

Application of a pressure gradient causes a flow of liquid and solid down the pressure gradient. The flow is assumed to obey Darcy's law, with the flow of liquid relative to the flow of solids. For porous media, Darcy's law is valid when flow is well within the laminar range, i.e., viscous forces predominate, and the inertial forces are insignificant (Reynold's number between 1 and 10). At any point in the

solid-liquid domain, the applied pressure is equal to the sum of the solids stress, pore water pressure, and medium pressure drop as

$$P_{app} = \sigma' + u + \Delta P_m \quad (2)$$

where

P_{app} = the applied pressure differential

σ' = the effective stress

u = the porewater pressure

ΔP_m = the medium pressure drop

As the porewater evacuates, stress is transferred from the porewater to the solid-particle framework, causing strain and decreasing the permeability. Both the fluid and solid particle phases are assumed to be incompressible, and all voids are assumed always to be filled with liquid. Since the solid part of the suspension cannot pass the porous membrane, it begins to build up, forming a cake. As the cake thickness, L , increases ($L=0$ at $t=0$), the flow rate decreases. The distance L also defines the cake-slurry interface. Viscous drag at the particle-liquid interfaces within the cake causes some particle rearrangement and packing (strain), such that the cake is compressible (Wakeman 1978; Lee and Sills 1979; Dick and Ball 1983). The weight of the cake is assumed to be negligible compared to the applied stress, and therefore the

applied stress is distributed uniformly within the cake. Also, the filter medium was assumed not to deform during a filtration run, and solid particles were assumed not to penetrate the filter medium to affect its porosity or permeability.

Two types of modeling frames of reference have been used to solve the governing equations: the Lagrangian coordinate system and the Eulerian coordinate system. With the Lagrangian reference the coordinate system moves as it follows a particular amount of mass. Because of this, the governing equation must only be satisfied within boundaries fixed in relation to each other, but not fixed in space. The mathematics of the problem can also be greatly simplified. But since predictions of parameter values are often required relative to fixed points, a transformation of the solution may be required. The choice of the Eulerian reference eliminates this transformation step. With the Eulerian coordinate system the axes are fixed in space, but the boundaries are allowed to move as the dewatering process proceeds (Lee and Sills 1980).

CHAPTER III

MODELING OF ONE-DIMENSIONAL SLUDGE DEWATERING

Dewatering of sludge under constant pressure is similar to the consolidation of a saturated soil. However, review of the available literature shows a lack of information transfer between researchers in the areas of soil mechanics and sludge dewatering. The following review gives the historical development of one-dimensional sludge dewatering modeling.

SMALL STRAIN THEORIES

The first general theory of consolidation, including the concepts of porewater pressure and effective stress, was proposed by Terzaghi in the 1920's. Most published work in the area of soil consolidation is based on the work of Terzaghi (Sills and Lee 1980). Terzaghi derived a linear, diffusion-type equation governing the dissipation of excess porewater pressure as

$$\frac{\partial u}{\partial t} = C \frac{\partial^2 u}{\partial z^2} \quad (3)$$

where

$$C = \frac{K}{\gamma_w m_v} = \text{coefficient of consolidation}$$

$$m_v = \frac{a_v}{1 + e_0} = \text{coef. of volume compressibility}$$

$$a_v = - \frac{\Delta e}{\Delta \sigma'} = \text{coef. of compressibility}$$

K = coefficient of permeability

γ_w = unit weight of water

σ' = effective stress

$$e = \frac{\text{volume of voids}}{\text{volume of solids}} = \text{void ratio}$$

e_i = initial void ratio

z = distance

The relationship between void ratio, e , and porosity, n , is

$$e = \frac{n}{1 - n} \quad \text{or} \quad n = \frac{e}{1 + e}$$

Terzaghi assumed boundaries fixed in space (the thickness of the compressible soil layer remained constant), which meant that his solution was valid only for relatively small strains. There is a fundamental lack of credibility in small strain consolidation theories, particularly for soft soils (or

sludges, e.g., how can there be consolidation when the thickness of the soil layer is constant?). Terzaghi found it convenient to unlink the equations governing stress and porewater pressure by assuming that the total stress at a point in the domain remains constant in time (this can be shown to be untrue). He assumed that permeability remains constant and that the relationship between effective stress and strain was linear, i.e.,

$$\frac{dn}{d\sigma'} = -m_v = \text{constant}$$

It would be considered rare for these latter two assumptions to be valid. In the vast majority of cases, soil and sludge properties vary with position and time of loading. Terzaghi's formulation of Darcy's law as $v = Ki$, where v is the velocity of the liquid relative to fixed spatial coordinates, and i is the hydraulic gradient (head loss per flow length), would therefore be incorrect for most cases. The more correct form is $v_r = Ki$, where v_r is the velocity of liquid relative to the solids. Nevertheless, the Terzaghi model has been found to be useful in practice.

In 1941 Biot presented a three-dimensional consolidation model based on a linearly elastic, stress-strain relationship governed by Hooke's law. This model was an improvement in generality over the Terzaghi model in two ways: 1) The correct form of Darcy's law was used and 2) Biot made no

assumption of constant stress at a point. The assumptions of fixed spatial boundaries and constant permeability still limited Biot's analysis however. In one dimension, Biot's governing equation took the same form as Terzaghi's

$$\frac{\partial \epsilon}{\partial t} = C \frac{\partial^2 \epsilon}{\partial z^2} \quad (4)$$

where

$$C = \frac{K}{\gamma_w} \frac{(1 - \nu') E'}{(1 + \nu') (1 - 2\nu')}$$

ν' = Poisson's ratio for the solid matrix

E' = Young's modulus for the solid matrix

ϵ = vertical strain [-]

Schiffman and Gibson (1964) assumed that K and m_v were independent of time, and therefore were only a function of the spatial coordinate, z . They derived Terzaghi's equation in the following form

$$-m_v(z) \frac{\partial \sigma'}{\partial t} = \frac{\partial}{\partial z} \left[\frac{K(z)}{\gamma_w} \frac{\partial u}{\partial z} \right] \quad (5)$$

which they transformed into an advection-diffusion-type equation

$$\frac{1}{C(z)} \frac{\partial u}{\partial t} = \frac{\partial^2 u}{\partial z^2} + \frac{1}{K} \frac{dK}{dz} \frac{\partial u}{\partial z} \quad (6)$$

where

$$C(z) = \frac{K(z)}{\gamma_w m_v(z)}$$

Lee (1968) also derived this equation using a different method. Schiffman and Gibson (1964) solved Equation 6 using the Crank-Nicholson semi-implicit finite difference method for several functional forms of $K(z)$ and $m_v(z)$, including

$$K(z) = K_0 e^{-\zeta z} \quad (7a)$$

and

$$m_v(z) = m_{v_0} e^{-\zeta z} \quad (7b)$$

where

ζ = an empirically determined constant

They also presented an exhaustive study of the performance of this model as compared to the conventional theory of Terzaghi.

Davis and Raymond (1965) used essentially Equation 6, but allowed K to vary with time as well as depth. However, the solution of their non-linear form of the equation required an approximation with respect to m_v . Since both Schiffman and Gibson's, and Davis and Raymond's consolidation models were based on Terzaghi's consolidation model, they suffered its limitations. Variations in permeability and compressibility

during consolidation are likely to be important only when strains and changes in the porosity (or void ratio) are substantial, but these two models were based on small strain theory (Gibson, England and Hussey 1967).

FINITE STRAIN THEORIES

McNabb (1960) extended the generality of the Terzaghi model by considering a non-constant permeability. He also accounted for the moving boundary, defining the domain in terms of the Lagrangian coordinate system

where

$$m = \int_0^z (1 + e)^{-1} dz \quad (8)$$

and m is the volume of solids per unit area contained in the region between $z=0$ (filter medium) and some arbitrary point in the domain. McNabb used the same form of Darcy's law as Terzaghi to derive a non-linear governing equation which was not limited to small strains

$$\frac{\partial e}{\partial t} = - \frac{\partial}{\partial z} \left[c \frac{\partial u}{\partial z} \right] \quad (9)$$

where

$$c = \frac{K(e)}{1+e}$$

Dimensional analysis of Equation 9 has shown that the

cumulative volume of the liquid displaced from the solid matrix is proportional to the square root of the duration of the consolidation. Numerous studies have verified this result experimentally (Gibson, England, and Hussey 1967; Smiles and Rosenthal 1968; Bierck, Wells and Dick 1988). McNabb used this result to transform Equation 9 via Boltzmann's transformation [$e = f(m/t^{1/2})$] into an ordinary differential equation, which was then solved analytically for the case where K and u are functions of e only. Philip (1955) demonstrated the use of this transformation for the non-linear diffusion equation and solved the resulting ordinary differential equation numerically. McNabb also solved Equation 9 analytically for a finite domain length with boundary conditions

$$\begin{aligned} e &= e_i \text{ for } m \geq 0; t = 0 \\ e &= e_0 \text{ for } m = 0; t > 0 \end{aligned} \tag{10}$$

where

e_i = initial void ratio

m = material coordinate

by linearizing the right hand side and using a Laplace transform and operational calculus techniques. However, no experimental results were presented with which to compare the solutions obtained.

Gibson, England and Hussey (1967) improved upon McNabb's

consolidation model. They changed McNabb's form of Darcy's law to the correct form (using relative liquid velocity), and derived an equation which governs a very general consolidation problem as

$$\frac{\partial e}{\partial t} + B(e) \frac{\partial e}{\partial m} + \frac{\partial}{\partial m} \left[C(e) \frac{\partial e}{\partial m} \right] = 0 \quad (11)$$

where

$$B(e) = \left[\frac{\gamma_s - \gamma_w}{\gamma_w} \right] \left[\frac{d}{de} \left(\frac{K(e)}{1+e} \right) \right]$$

$$C(e) = \frac{1}{\gamma_w} \left[\frac{K(e)}{1+e} \right] \left[\frac{d}{de} (\sigma' (e)) \right]$$

γ_s = unit weight of solids

γ_w = unit weight of water

This model includes the effects of liquid and solid compressibility and self-weight. The functions $B(e)$ and $C(e)$ represent the material properties of the sludge or soil being consolidated. According to Schiffman (1980), all other physically-based one-dimensional consolidation models are special cases of this model. Benson (1987) noted the applicability of this model to sludge dewatering and formulated appropriate boundary conditions (see Figure 1), but he did not offer a solution. Benson (1987) also pointed out that this model includes the phenomenon of filter blinding.

Gibson et al. (1967), modeling one-dimensional consolidation of thin soil layers, simplified the governing equation by neglecting solid and liquid compressibility effects and self-weight to arrive at

$$\frac{\partial e}{\partial t} = \frac{\partial}{\partial m} \left[C \frac{\partial e}{\partial m} \right] \quad (12)$$

where

$$C = - \frac{K(e)}{\rho_f} \frac{(1+e_i)^2}{(1+e)} \frac{d\sigma'}{de}$$

ρ_f = liquid density [ML⁻³]

e_i = initial void ratio

This equation was solved numerically by the Runge-Kutta method for the non-linear case, after assuming that C was related linearly to the void ratio, e as

$$C = C_i + \lambda(e - e_i)$$

The constants C_i and λ were determined experimentally. Still, in order to solve the governing equation, they reverted to fixed spatial coordinates, restricting the analysis to small strains. Results of this model's performance were presented, but were not compared to experimental data or results from other consolidation theories.

Smiles and Rosenthal (1968) seemed to be unaware of McNabb's work, since they derived Equation 9 using a Lagrangian coordinate system, as McNabb had done. Unlike McNabb, however, they did use the correct form of Darcy's law in their analysis. They did not solve the equation. Their focus was the relationships between C and n , K and n , C and e , and K and e .

Philip (1969) derived an equation equivalent to that of Smiles and Rosenthal, but used the Eulerian coordinate system. He demonstrated the application of a numerical solution technique he had devised previously (see Philip, 1955). The solution method assumes small strains however. He also showed how to compute instantaneous values of the most important process variables.

Smiles (1970) made the crossover between soil mechanics consolidation theory and cake filtration theory by presenting the model he had developed (with Rosenthal in 1968)

$$\frac{\partial e}{\partial t} = \frac{\partial}{\partial m} \left[C \frac{\partial e}{\partial m} \right] \quad (13)$$

which is equivalent to Equation 9, with the boundary conditions of Equation 10, (previously presented by McNabb, 1960). He pointed out that the consolidation theory of Philip (1969) was equally applicable to cake filtration and used the numerical procedure of Philip to solve his model.

In 1968 Philip showed that consolidation models based on

a small strain analysis must lead to substantial error. Gibson, Schiffman and Cargill (1981) and Schiffman, Pane and Gibson (1984) have pointed out that field observations show that Terzaghi's linear, small strain theory over-predicts settlement times. Non-linear, large strain theory predicts a faster progression of the consolidation process. In addition, they fail to predict secondary consolidation effects. Secondary consolidation refers to volume changes which are not associated with pore water dissipation.

Smiles and Poulos (1969) developed a consolidation model which was not limited by the magnitude of the strains involved, and included the effects of secondary consolidation. The model consisted of Equation 9 with the boundary conditions of Figure 1, i.e.,

$$\begin{aligned}
 e &= e_i \text{ for } 0 \leq m \leq M; t = 0 \\
 e &= e_0 \text{ for } m = 0; t \geq 0 \\
 \frac{de}{dm} &= 0 \text{ for } m = M; t \geq 0
 \end{aligned}
 \tag{14}$$

where M is the total (constant) volume of solids per unit area in the domain, L_d .

This system was solved using a finite difference technique and also the method of Philip (1969). The $C(e)$ relationship was obtained from earlier experiments (Smiles and Rosenthal 1968). Results of this study included consolidation and void ratio vs. dimensionless time, and e vs. M behavior of

the model. A comparison was also made between this model and one in which C was constant.

Tiller (1975) presented an analytical cake filtration model relating σ' and fractional cake position (z/L) based on the assumption of zero solid velocities

$$\frac{z}{L} = \frac{\int_{\sigma'}^{P_{app}} k d\sigma'}{\int_0^{P_{app}} k d\sigma'} \quad (15)$$

where k is the permeability. Solution of this model required that the relationship between permeability and effective stress was known. Then an equation for the porosity as a function of z/L could be determined. The assumption of zero solids velocities implied the assumption that the average cake porosity was constant.

Tiller and Horng (1983) used the following empirical relationships to solve Equation 15

$$1-n = (1-n_a) \left(1 + \frac{\sigma'}{p_a}\right)^b \quad (16a)$$

and

$$r' = r_a \left(1 + \frac{\sigma'}{p_a}\right)^d \quad (16b)$$

where n_a , p_a , b , r_a and d are empirically determined constants. Willis, Tosun and Collins (1985) used power functions of a simpler form to solve this model.

Wells (1990a) introduced the definition of m_v into Tiller's analysis (Equation 15), and obtained

$$\frac{z}{L} = \frac{\int_n^{n_0} \frac{k}{m_v} dn}{\int_{n_i}^{n_0} \frac{k}{m_v} dn} \quad (17)$$

Known relationships for both permeability and coefficient of volume compressibility versus porosity were required to obtain an equation for porosity as a function of z/L . Wells (1990a) proposed the exponential functions (compare with Equations 7a and 7b)

$$k = \alpha e^{\beta n} \quad (18a)$$

and

$$m_v = \gamma e^{\delta n} \quad (18b)$$

where α , β , γ and δ are empirical constants. Substituting these constitutive relationships into Equation 17 yields

$$n(z/L) = \frac{1}{\beta - \delta} \ln \left[\left(1 - \frac{z}{L} \right) e^{(\beta - \delta)n_0} + \frac{z}{L} e^{(\beta - \delta)n_i} \right] \quad (19)$$

Wells (1990a) also derived equations for porewater pressure, effective stress and permeability as functions of z/L .

Atsumi and Akiyama (1975) stated that Smiles' boundary conditions limit the applicability of his theory, since they imply no liquid flux at the cake-slurry interface. This was not a valid criticism however, since Smiles' assumption (that the void ratio at the cake surface is the same as that of the initial suspension) only implies that the velocity of liquid relative to the solid phase at this point is zero, not that

there was no liquid flow (Wells 1990a). Atsumi and Akiyama derived an additional boundary condition (previously presented by Tiller and Cooper, 1960) applicable at the cake surface

$$C(e) \frac{\partial e}{\partial m} = (e_i - e_L) \frac{dm_L}{dt} \quad \text{at } m = m_L \quad (20)$$

where

e_i = initial void ratio

e_L = void ratio at cake surface

m_L = material coordinate of cake surface

$$C(e) = \frac{k}{\mu(1-e)} \frac{du}{de}$$

The governing equation (Equation 9) and boundary conditions (Equations 10 and 20) were put in non-dimensional form and Boltzmann's similarity transformation was used to convert the governing equation into an ordinary differential equation. In order to make this transformation, the average concentration of the cake was assumed independent of time and the medium resistance was negligible. The governing equation was solved using an approximate $C(e)$ relationship determined experimentally from compression-permeability cell tests and a Runge-Kutta numerical scheme. Model predictions agreed with experimental data from the dewatering of ignition plug slurries.

Kos and Adrian (1975) developed an advective-diffusive-type sludge dewatering model using Lagrangian coordinates and

non-linear, stress-strain relationships. They formulated their governing equation in terms of effective stress as

$$\frac{\partial \sigma'}{\partial t} + c + B \frac{\partial \sigma'}{\partial m} + C \frac{\partial^2 \sigma'}{\partial m^2} = 0 \quad (21)$$

where

c = suspended solids concentration

B = empirical coefficient = $B(m,t)$

C = empirical coefficient = $C(m,t)$

Their analysis showed how the process of dewatering was dependent on two physical properties: permeability and compressibility of the sludge. They also presented data from consolidometer tests using stabilized water treatment plant sludge showing (at least for this particular sludge) that an elastic stress-strain model was clearly not appropriate. No boundary conditions were defined however, nor was a solution given for their governing equation.

Monte and Krizek (1976) followed the procedure of Gibson et al. (1967) in deriving an equation governing large strain consolidation of soils. Monte and Krizek, however, defined a unique reference state (stress-free state) from which any deformation of the solid-liquid system would be measured. This stress-free state was postulated as the state at which the solid-liquid slurry changes from a fluid-like material to one which can withstand some amount of shear stress. Except

for this, though, the governing equation they arrived at was equivalent to that of Gibson et al.

$$\frac{\partial e}{\partial t} = (1+e_0^*) \frac{\partial}{\partial m} \left[\frac{K(e)}{\gamma_w(1+e)} \left(M_c(e) \frac{\partial e}{\partial m} - e\gamma_w - \gamma_s \right) \right] \quad (22)$$

where

$$M_c(e) = \frac{\partial \sigma'}{\partial \epsilon} = \text{constrained modulus}$$

e_0^* = void ratio at the stress free state

ϵ = strain

with initial and boundary conditions equivalent to Smiles and Poulos (1969) (See Equation 14).

The system was solved numerically using a finite element discretization in space and finite difference discretization in time. $M_c(e)$ was assumed to be a linear function of strain (or void ratio)

$$M_c(e) = \alpha_1 + \beta_1 \epsilon$$

with the constants α_1 and β_1 obtained from experimental data. The quantity $K(e)/(1+e)$ was assumed to be a linear function of void ratio also

$$\frac{K(e)}{1+e} = \alpha_2 + \beta_2 e$$

Simulations were performed and compared with four sets of

experimental data. The results, using clay slurries under constant pressure were quite good. The pressure differentials applied were very low (2 psi and 4 psi), but Monte and Krizek state that for effective stresses above about 8 psi the classical (small strain) consolidation theory was a reasonable model, at least for the particular clay they studied.

A sensitivity analysis of the model's performance using different values of e^*_0 showed that the model was very sensitive to the value of this parameter. Since there is no test which would give its value directly for a given soil, this parameter must be determined during the model calibration.

In 1978, Wakeman also presented an advective-diffusive-type model using an Eulerian coordinate system. The governing equation

$$\frac{\partial n}{\partial t} = \frac{\partial}{\partial z} \left[C(n) \frac{\partial n}{\partial z} \right] + \left[\frac{C(n)}{1-n} \frac{\partial n}{\partial z} \right]_{z=0} \frac{\partial n}{\partial z} \quad (23)$$

where

$$C(n) = (1-n) \frac{k}{\mu} \frac{du}{dn}$$

μ = liquid viscosity

was shown to be the same as that of Atsumi and Akiyama (1975) when converted to Lagrangian coordinates. The moving boundary condition was derived as

$$\left. \frac{\partial n}{\partial z} \right|_L = \left[\frac{n_i - n_L}{1 - n_i} \right] \frac{\mu}{k_L} \left. \frac{dn}{du} \right|_L \frac{dL}{dt} \quad (24)$$

with

$$\begin{aligned} n &= n_i & \text{at } t = 0 & \text{ for all } z \\ n &= n_0 & \text{at } z = 0 & \text{ for all } t \\ n &= n_L & \text{at } z = L & \text{ for all } t \end{aligned}$$

where

$$\begin{aligned} n_i &= \text{initial porosity} \\ n_0 &= \text{porosity at } z=0 \text{ (filter medium)} \\ n_L &= \text{porosity at } z=L \text{ (cake surface)} \end{aligned}$$

Wakeman (1978) put the governing equation and boundary conditions in non-dimensional form, then using Boltzmann's similarity transformation and assuming an exponential functional form for $C(n)$ (with the coefficients of the exponential equation determined from CP cell tests), he solved the resulting system using a fourth-order Runge-Kutta numerical scheme as Atsumi and Akiyama (1975) had done. Comparison of the theoretical results with experimental data for ignition plug slurries showed better agreement than the model of Atsumi and Akiyama (1975).

Tosun (1986) rederived the governing equations for cake filtration in both Eulerian and Lagrangian coordinates using the domain and coordinate system of Figure 2 [same as Atsumi

and Akiyama (1975) and Wakeman (1978)]. The governing equations obtained were equivalent to those of Atsumi and Akiyama (1975)

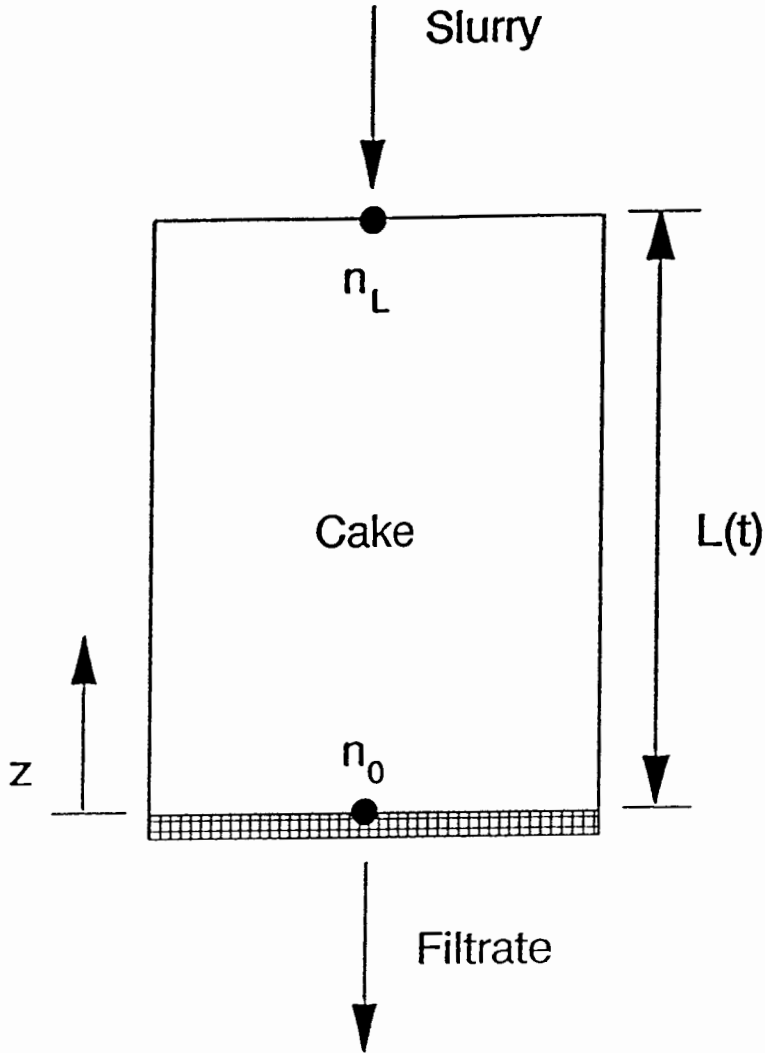


Figure 2. Coordinate system and domain for cake filtration models of Atsumi and Akiyama (1975), Wakeman (1978) and Tosun (1986).

and Wakeman (1978). It should be noted that the models of Atsumi and Akiyama (1975), Wakeman (1978), and Tosun (1986) do not consider the entire problem domain, just the filter cake

(Wells 1990a). An error was noted in Wakeman's formulation of the moving boundary condition by Tosun (1986) and was restated as

$$\frac{\partial n}{\partial z} = \left[\frac{1-\bar{n}}{1-n_i} \right] \left[\frac{n_i - n_L}{1-n_i} \right] \frac{\mu}{k} \frac{dn}{du} \frac{dL}{dt} \quad (25)$$

where

$$\bar{n} = \text{average porosity} = \frac{1}{L} \int_0^L n \, dz$$

(compare with Equation 23). In deriving this boundary condition, the assumption of a constant average porosity was made. Tosun (1986) solved this system using an approximate technique developed by Kehoe (1972), which was simpler and less time consuming than the method of Atsumi and Akiyama (1975). Like Wakeman (1978), an exponential $C(n)$ function was used in the solution. Model results agreed with those of Atsumi and Akiyama (1975).

The governing equation (Equation 11) of Gibson, England and Hussey (1967) was rederived by Lee and Sills (1979), and was shown to apply to situations with drainage at either or both boundaries. This non-linear model was solved using the Crank-Nicholson, semi-implicit finite difference technique. Unlike Gibson, England and Hussey (1967), no simplifying approximations or similarity transformations were used which would have restricted the generality of the solution. The real advantage of this model was the semi-implicit

differencing scheme which eliminated numerical stability problems.

The numerical solution technique used by Lee and Sills was unique in the treatment of the moving boundary. The domain was divided into N equal length segments. At each time step there were $N+1$ unknowns, since the position of the moving boundary (in addition to the porosity at each node) was unknown. Hence, an iterative solution procedure was required. Figure 3 shows how the moving boundary was modeled.

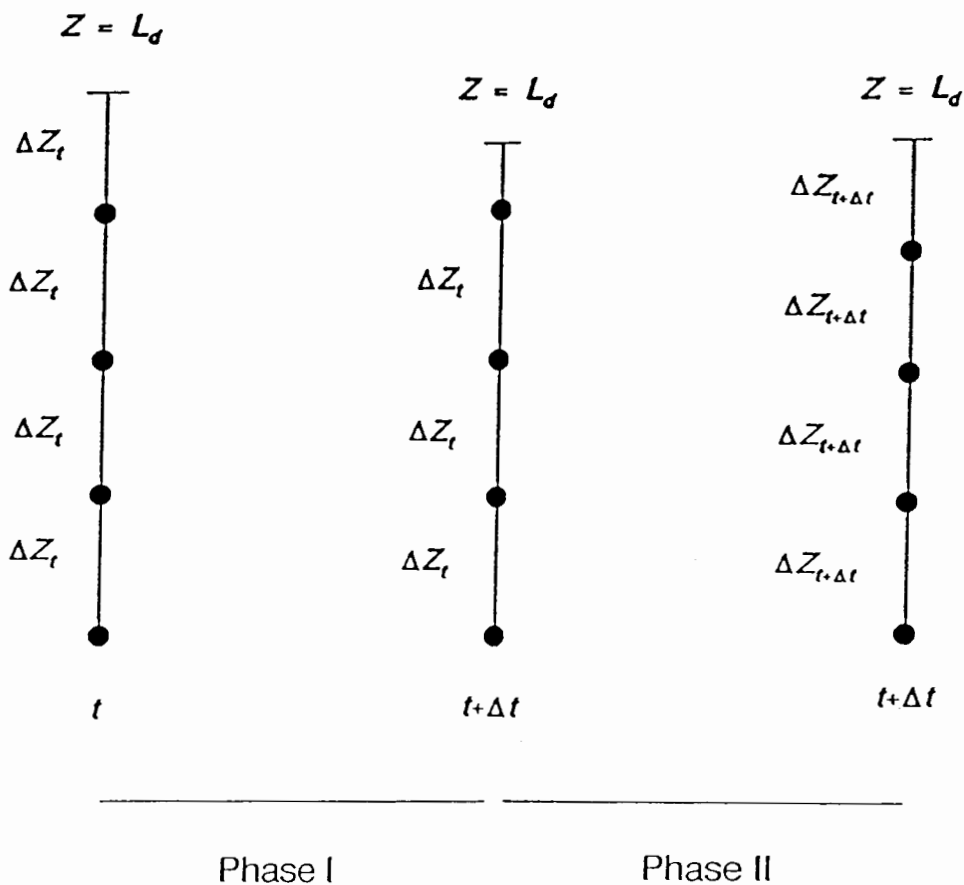


Figure 3. Finite difference grid near moving boundary as treated in the model of Lee and Sills (1979).

After each time step (phase I), the boundary will have moved, so the values of the derivatives at the node next to the moving boundary were approximated using the Lagrangian interpolation formula for unequally spaced grid points. The positions of the grid points were then readjusted to make them equally spaced again (phase II). The number of nodes remained the same. The porosity values at the new grid points were obtained by interpolating from the nodal values just calculated using a cubic spline polynomial as the interpolation function between any two nodes. There was some error introduced at each time step due to this interpolation (two interpolations per time step). To minimize this error, the numerical time step would need to be small. Lee and Sills (1979) used a maximum of 16 time steps in the numerical solutions they presented, where the time step was given in terms of a dimensionless time factor, T , as

$$T = \frac{C(e) t}{H^2}$$

Lee and Sills (1979) did not compare their results to any data. They did compare their numerical solution to the analytical solution of Gibson et al. (1967) for constant C , for which the solutions agreed. Results of model performance using different functional forms for the $C(e)$ relationship were also presented.

Herath, Geladi and Albano (1989) developed an empirical

dewatering model for peat slurries. In vector notation, the model took the following form:

$$\vec{y} = \vec{X}\vec{b} + \vec{\delta}_e \quad (26)$$

where

\vec{y} = one-dimensional matrix of response (dependent) variables

\vec{X} = two-dimensional matrix of design (independent) variables

\vec{b} = one-dimensional matrix of regression coefficients

$\vec{\delta}_e$ = one-dimensional matrix of error residuals

This model was able to predict the rate of filtration and porosity with reasonable accuracy while taking pretreatment conditions (slurry pH, mixing speed, flocculant dosage, mixing time) into account. The empirical model was developed from filtration and compression experiments by performing partial least squares regression analysis on the experimental results to obtain equations of correlation between independent (design) and dependent (response) variables. Two empirical second order polynomial regression equations were presented, one for filtration time

$$Y_1 = b_0 + b_1X_1 + b_2X_2 + b_3X_3 + b_4X_4 + b_{11}X_1^2 + \dots + b_{44}X_4^2 + b_{12}X_1X_2 + b_{13}X_1X_3 + \dots + b_{34}X_3X_4 \quad (27)$$

and one for porosity

$$\begin{aligned}
 Y_2 = & b_0 + b_1X_1 + b_2X_2 + \dots + b_6X_6 + b_{11}X_1^2 + \dots \\
 & + b_{66}X_6^2 + b_{12}X_1X_2 + b_{13}X_1X_3 + \dots + b_{56}X_5X_6
 \end{aligned}
 \tag{28}$$

where

Y_1 = flow time in ln seconds

Y_2 = solid content (%)

X_1 = slurry pH

X_2 = mixing speed

X_3 = flocculant dosage

X_4 = mixing time

X_5 = pressure

X_6 = pressing time

The above equations represent multi-dimensional response surfaces. Theoretically then, it would be a relatively simple matter to optimize the process of dewatering by finding the minima or maxima of the response surfaces. The model was verified by comparing model predictions with additional experimental data from compression dewatering of peat slurries.

Table I summarizes the soil consolidation/sludge dewatering models discussed above.

TABLE I
SUMMARY AND COMPARISON OF DEWATERING MODELS

SMALL STRAIN THEORIES			
Reference	Coord. System	Governing Equation	Solution Method
Terzaghi (1925)	Eulerian	$\frac{\partial u}{\partial t} = c \frac{\partial^2 u}{\partial z^2}$	Analytical Integration
Biot (1941)	Eulerian	$\frac{\partial e}{\partial t} = c \frac{\partial^2 e}{\partial z^2}$	Analytical Integration
Schiffman & Gibson (1964)	Eulerian	$\frac{\partial \sigma'}{\partial t} = -m_v(z) \frac{\partial}{\partial z} \left[\frac{K(z)}{\gamma_v} \frac{\partial u}{\partial z} \right]$	Numerical Integration (FD ¹)
Davis & Raymond (1965)	Eulerian	$\frac{\partial \sigma'}{\partial t} = -m_v(z) \frac{\partial}{\partial z} \left[\frac{K(z, t)}{\gamma_v} \frac{\partial u}{\partial z} \right]$	Analytical Integration
FINITE STRAIN THEORIES			
Reference	Coord. System	Governing Equation	Solution Method
McNabb (1960)	Lagrangian	$\frac{\partial e}{\partial t} = \frac{\partial}{\partial z} \left[C \frac{\partial u}{\partial z} \right]$	Analytical Integration
Gibson et al. (1967)	Lagrangian	$\frac{\partial e}{\partial t} = \frac{\partial}{\partial m} \left[C \frac{\partial e}{\partial m} \right]$	Numerical Integration (FD)
Smiles & Rosenthal (1968)	Lagrangian	$\frac{\partial e}{\partial t} = \frac{\partial}{\partial m} \left[\frac{K}{1+e} \frac{\partial u}{\partial m} \right]$	No Solution Offered
Philip (1970)	Eulerian	$\frac{\partial e}{\partial t} = \frac{\partial}{\partial z} \left[C \frac{\partial u}{\partial z} \right]$	Numerical Integration (FD)
Smiles & Poulos (1969)	Lagrangian	$\frac{\partial e}{\partial t} = \frac{\partial}{\partial z} \left[C \frac{\partial u}{\partial z} \right]$	Numerical Integration (FD)
Tiller (1975)	Eulerian	$\frac{-d\sigma'}{dz} = \frac{\mu n}{k} (v_t - v_s)$	Analytical Integration
Atsumi & Akiyama (1975)	Lagrangian	$\frac{\partial e}{\partial t} = \frac{\partial}{\partial m} \left[C \frac{\partial e}{\partial m} \right]$	Numerical Integration (FD)

TABLE I
SUMMARY AND COMPARISON OF DEWATERING MODELS
(continued)

FINITE STRAIN THEORIES			
Reference	Coord. System	Governing Equation	Solution Method
Kos & Adrian (1975)	Lagrangian	$\frac{\partial \sigma'}{\partial t} + c + B \frac{\partial \sigma'}{\partial m} + C \frac{\partial^2 \sigma'}{\partial m^2} = 0$	No Solution Offered
Monte & Krizek (1976)	Lagrangian	$\frac{\partial e}{\partial t} = (1+e_0^*) \frac{\partial}{\partial m} \left[\frac{K(e)}{\gamma_w (1+e)} \left(M_c(e) \frac{\partial e}{\partial m} - e \gamma_w - \gamma_s \right) \right]$	Numerical Integration (FE ²)
Wakeman (1978)	Eulerian	$\frac{\partial n}{\partial t} = \frac{\partial}{\partial z} \left[C(n) \frac{\partial n}{\partial z} \right] + \left[\frac{C(n)}{1-n} \frac{\partial n}{\partial z} \right]_{z=0} \frac{\partial n}{\partial z}$	Numerical Integration (FD)
Tosun (1986)	Lagrangian/ Eulerian	$\frac{\partial e}{\partial t} = (1+e)^2 \frac{\partial}{\partial z} \left[C(e) \frac{\partial e}{\partial z} \right] = \frac{\partial}{\partial m} \left[C(e) \frac{\partial e}{\partial m} \right]$	Numerical Integration (FD)
Lee & Sills (1979)	Eulerian	$\frac{\partial n}{\partial t} = \frac{\partial}{\partial z} \left[- \frac{K}{\gamma_w} (1+e) \frac{d\sigma'}{de} \right] \frac{\partial n}{\partial z}$	Numerical Integration (FD)
Herath et al. (1989)	Eulerian	$\bar{y} = \bar{X} \bar{b} + \bar{e}$	Partial Least Sqrs. Regression
Wells (1990a)	Eulerian	$\frac{\partial n}{\partial z} = B \frac{\partial n}{\partial z} + \frac{\partial}{\partial z} \left[C(n) \frac{\partial n}{\partial z} \right]$	Numerical Integration (FD)
¹ Finite Difference ² Finite Element			

CHAPTER IV

WELLS MODEL OF CAKE FILTRATION

By applying the principles of conservation of mass and momentum to each phase, Willis (1983) derived a general multiphase filtration theory based on fundamental physical principles for the filtration of a soluble, elastic and non-deformable particulate phase suspended in an incompressible Newtonian fluid (a Newtonian fluid is isotropic, the shear stress is linearly proportional to the rate of strain, and when the strain rate is zero, the stress is hydrostatic). This theory was then used to develop equations describing the filtration of a non-deformable liquid phase through a non-deformable solid phase in one dimension. Wells (1990a) used these governing equations to formulate a one-dimensional, nonlinear, advective-diffusive-type partial differential equation describing changes in porosity in a vertically oriented compressible cake

$$\frac{\partial n}{\partial t} = \underbrace{\frac{\partial}{\partial z} \left[C \frac{\partial n}{\partial z} \right]}_{\text{DIFFUSIVE TERM}} + \underbrace{n_0 v_0}_{\text{ADVECTIVE TERM}} \frac{\partial n}{\partial z} \quad (29)$$

with initial condition

$$n(z, t=0) = n_i(z) \quad (30)$$

and boundary conditions

$$n(z=0, t) = n_0(t) \quad (31)$$

$$\left. \frac{\partial n}{\partial z} \right|_{z=L_d} = 0 \quad (32)$$

where

L_d = domain length

n_0 = porosity at $z=0$ (terminal porosity)

n_i = porosity at $t=0$ (initial porosity)

k = permeability

m_v = coefficient of volume compressibility

v_0 = liquid velocity at $z=0$

μ = dynamic viscosity

$$C = \frac{(1-n)k}{\mu m_v}$$

$$n_0 v_0 = \frac{C_0}{1-n_0} \left. \frac{\partial n}{\partial z} \right|_0$$

C_0 = value of C at $z=0$

$$\left. \frac{\partial n}{\partial z} \right|_0 = \text{porosity gradient at } z=0$$

The initial and boundary conditions are also shown in Figure 1. The boundary condition of Equation 32 is operational when there is no more liquid with initial concentration n_i above the cake, otherwise $n(z=L_d, t)=n_i$.

SOLUTION STRATEGY

The model uses Eulerian coordinates and requires constitutive relationships for k and m_v as functions of porosity, n . These constitutive relationships are models of the behavior of k and m_v . Data from experiments conducted by Bierck, Wells and Dick (1988) with kaolin clay suspensions at the Cornell High Energy Synchrotron Source (CHESS) indicated exponential functions as in Equations 18a and 18b

$$k = \alpha e^{\beta n} \quad (33)$$

$$m_v = \gamma e^{\delta n} = -\frac{\partial n}{\partial \sigma'} \quad (34)$$

where

$$\sigma' = \psi e^{\phi n} \quad (35)$$

with α , β , γ , and δ constants as before. According to Kos and Adrian (1975), sludges and flocculent suspensions are very similar to clays when it comes to dewatering behavior. The highly collimated X-rays at CHESS allowed for precise measurement of the spatial and temporal distribution of suspended solids concentration in a compressible filter cake. Figures 4 and 5 show the data used to determine these constitutive relationships and 'best fit' exponential regression lines through these data.

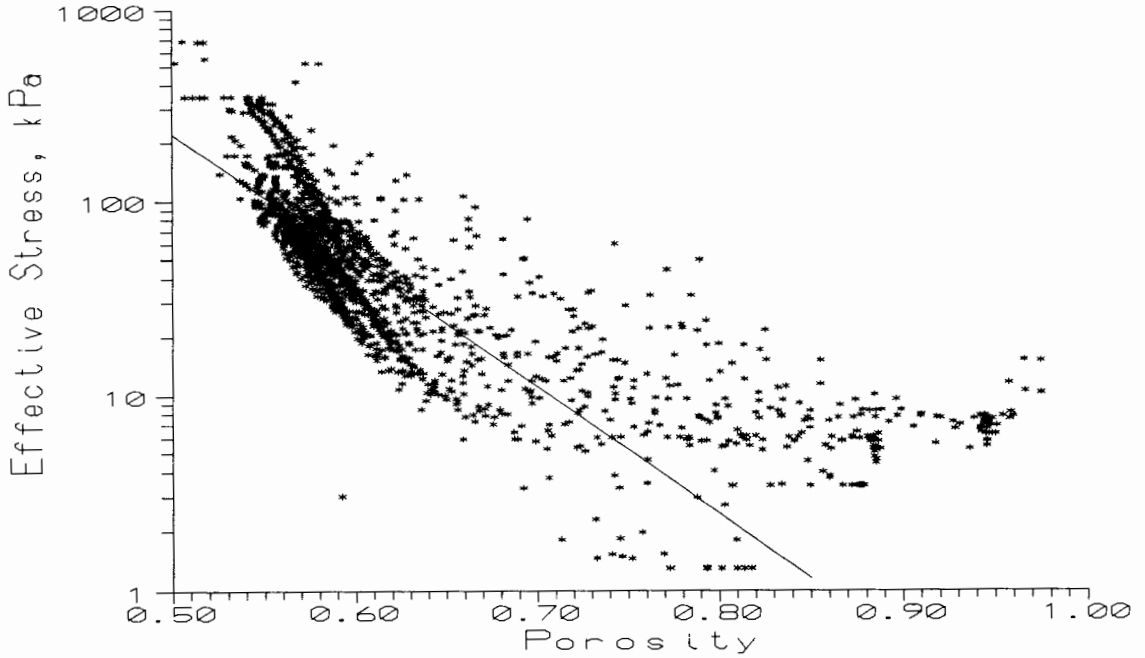


Figure 4. Semi-log plot of effective stress versus porosity data from CHES experiments with exponential best fit of Equation 35.

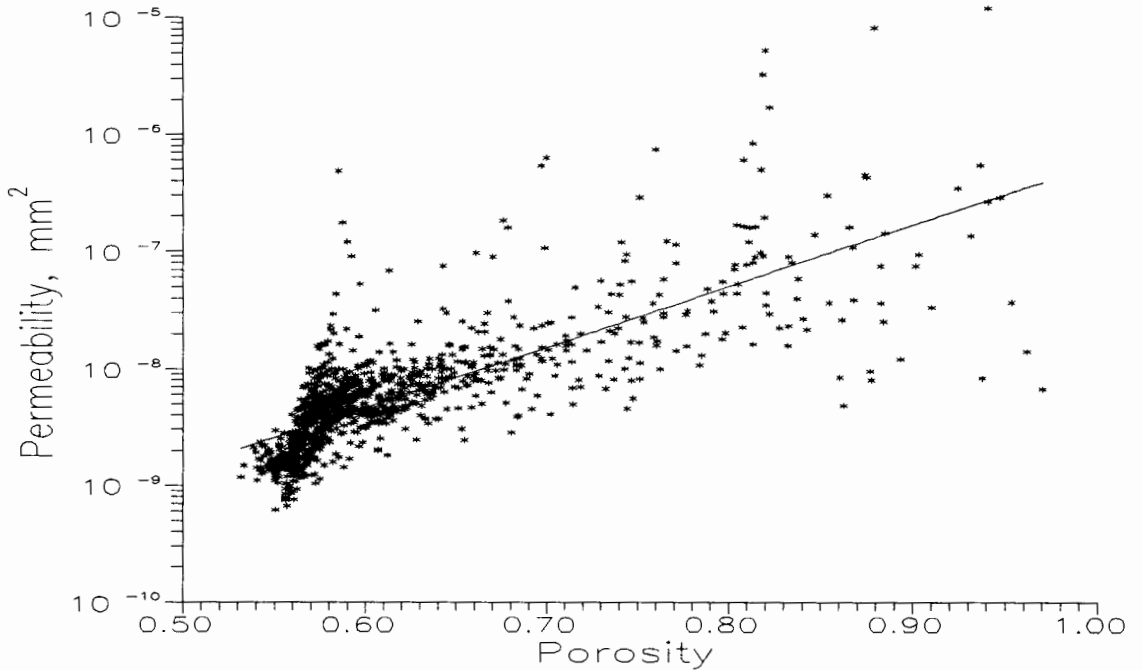


Figure 5. Semi-log plot of permeability versus porosity data from CHES experiments with exponential best fit of Equation 33.

The coefficient of linear correlation, r , between porosity and the log of effective stress is -0.807 . For the porosity versus log of permeability data, r is 0.771 . Both of these correlation coefficients therefore indicate possible linear relationships, as suggested by Wells (1990a).

The model was solved using explicit numerical finite difference techniques. Due to stability problems encountered when using other finite difference methods, an upwind differencing scheme was used to approximate the partial derivative in the advective term. Upwinding is forward spatial differencing applied against the velocity field. This added enough artificial 'diffusion' so that the model would remain stable for a wide range of empirical coefficient (α , β , γ , δ) values.

Centered spatial differencing was used to approximate the partial derivatives of the diffusive term, and forward differencing was used for the time derivative.

In finite difference form, the governing equation becomes

$$\frac{n_j^{\tau+1} - n_j^\tau}{\Delta t} = \frac{1}{\Delta z_j^\tau} \left[C_{j+\frac{1}{2}}^\tau \frac{(n_{j+\frac{1}{2}}^\tau - n_j^\tau)}{\Delta z_{j+\frac{1}{2}}^\tau} - C_{j-\frac{1}{2}}^\tau \frac{(n_j^\tau - n_{j-1}^\tau)}{\Delta z_{j-\frac{1}{2}}^\tau} \right] + \frac{C_0^\tau}{1-n_0} \frac{\partial n}{\partial z} \Big|_{z=0} \frac{1}{\Delta z_{j+\frac{1}{2}}^\tau} (n_{j+1}^\tau - n_j^\tau) \quad (36)$$

where

$$\Delta z^\tau = \frac{1}{2} \left(\Delta z_{j+\frac{1}{2}}^\tau + \Delta z_{j-\frac{1}{2}}^\tau \right)$$

$$\Delta z_{j-\frac{1}{2}}^\tau = z_{j+1}^\tau - z_j^\tau$$

τ = current time level

j = grid point number

z_j = distance from filter medium to grid point j

$$C_j^\tau = \frac{k_j^\tau (1 - n_j^\tau)}{\mu m_{v_0}^\tau}$$

$$C_0^\tau = \frac{k_0^\tau (1 - n_0^\tau)}{\mu m_{v_0}^\tau}$$

Constant grid spacing was used except near the moving boundary ($z=L_d$). The porosity at time level $\tau+1$ was first calculated, then the domain length was adjusted according to the amount of liquid lost during the time step, Δt . The change in the domain length, Δh , was calculated as

$$\Delta h = v_0 n_0 \Delta t \quad (37)$$

The volume of liquid passing through the filter medium in time Δt was then

$$V_{\Delta t} = A \Delta h \quad (38)$$

where A is the cross-sectional area of the filtration cell.

The medium resistance, R_M , was assumed to be constant (no clogging), and was computed from

$$R_M = \frac{P_{app}}{\mu v_0 n_0} \Big|_{t=0} \quad (39)$$

This is an empirical relationship derived from a liquid force balance across the filter medium, assuming that at the beginning of filtration all of the pressure drop is across the filter medium.

The equation for the terminal porosity was developed from the definition of m_v as given in Equation 34 by separating variables and integrating over the length of the filter cake. The terminal porosity was assumed to be constant and was calculated from

$$n_0 = -\frac{1}{\delta} \ln [(e^{-\delta n_i}) + \gamma \delta P_{app}] \quad (40)$$

Another important calculation was the breakthrough stress, σ'_b , of the solid matrix. The breakthrough stress was the stress at which pressurized nitrogen gas broke through the porous matrix of the filter cake in the experiments of Bierck, Wells and Dick (1988). The breakthrough stress was associated with a breakthrough porosity, n_b . At this porosity the solid matrix could not undergo further deformation because the applied pressure differential could not overcome the surface tension force holding liquid in the pores of the solid matrix. The computer model required a value for the breakthrough stress as input, and this value was determined experimentally. Once a value for the breakthrough stress was determined, the

breakthrough porosity was calculated from

$$n_b = -\frac{1}{\delta} \ln[(e^{-\delta n_i}) + \gamma \delta \sigma'_b] \quad (41)$$

Filtration ceased when the porosity reached the breakthrough porosity. In the computer model, this caused the computer simulation to end. The computer simulation will also end if any of the following conditions occurs: 1) the simulated time exceeds some user defined value; 2) the model becomes unstable (usually exhibited by a negative time step); 3) the maximum number of iterations specified by the user is exceeded; 4) the filtrate volume remains constant for two successive iterations, and the simulated time is greater than 90 seconds; or 5) the CPU time of the simulation exceeds a user specified limit.

The liquid velocity at $z=0$, v_0 , was given by

$$v_0 = \frac{k}{\mu n} \frac{du}{dz} \Big|_{z=0} \quad (42)$$

or, since

$$\frac{du}{dz} = \frac{1}{m_v} \frac{\partial n}{\partial z} \quad (43)$$

$$v_0 = \frac{k}{\mu n m_v} \frac{\partial n}{\partial z} \Big|_{z=0} \quad (44)$$

This result has been found to have a very significant influence on the model's performance, and therefore an

accurate calculation was very important. The porosity gradient, $\partial n/\partial z$ at $z=0$ can create problems, especially during the early stages of a simulation, when this porosity gradient was relatively large.

Finite difference representations of $\partial n/\partial z$ at $z=0$ used in the calculation of v_0 having first and second order accuracy in Δz are, respectively

$$\left. \frac{\partial n}{\partial z} \right|_0 = \frac{n_2 - n_1}{\Delta z} + O(\Delta z) \quad (45)$$

and

$$\left. \frac{\partial n}{\partial z} \right|_0 = \frac{-3n_1 + 4n_2 - n_3}{2\Delta z} + O(\Delta z^2) \quad (46)$$

where the subscripts 1, 2, and 3 refer to nodes $j=1, 2,$ and 3.

Wells (1990a) found that although Equation 46 has a higher order of accuracy, it was possible for this derivative to have a negative value, which is physically unrealistic (the porosity must decrease or remain constant as one moves closer to the filter medium, thus a positive gradient). Therefore, in those cases where Equation 46 takes on a negative value, Equation 45 was used to calculate v_0 . Numerical diffusion induced by these upwind differencing schemes was proportional to the grid point spacing, Δz . Numerical accuracy therefore requires a relatively small Δz (simulations of the numerical model showed <1 mm for a domain height of 4 cm). Because the

time step limitation, Δt , for stability was also proportional to Δz , Δt was also relatively small for the numerical scheme.

At the end of each time step, the boundary will have moved an amount Δh . The grid spacing remains constant until the boundary moves past a grid point. When the boundary moves past a grid point, that grid point is removed from the grid, and the total number of grid points is decreased. The new grid spacing remains the same, except in the vicinity of the moving boundary. Figure 6 illustrates the numerical model treatment of the moving boundary and the finite difference grid. This method avoided the errors caused by treating the moving boundary by the method of Lee and Sills (1979).

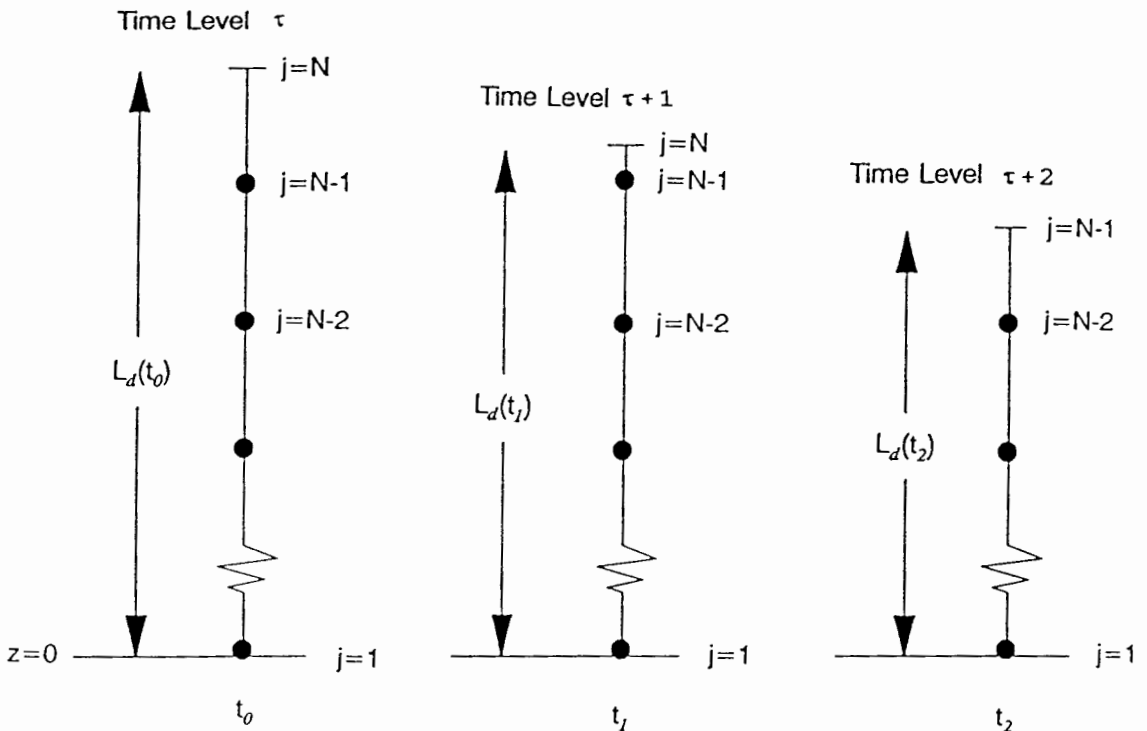


Figure 6. Treatment of moving boundary by Wells (1990a) dewatering model.

The problem of having to know the location of the moving boundary at the $\tau+1$ time level is not encountered with this model due to the explicit differencing scheme. There is also less error induced at each time step with the Wells solution technique because (except at one grid point near the moving boundary) there is no interpolation involved in the porosity calculations. Figure 7 is a flow diagram which illustrates the model's solution procedure.

MODEL CALIBRATION AND VERIFICATION

The model was calibrated by first fitting an exponential curve through the σ' vs. n data (see Figure 8). This curve gave values for the constants γ and δ . This relationship was then kept fixed while the permeability relationship was adjusted. When a reasonable data-model agreement was obtained the model was assumed to be calibrated. This resulted in the values of the constants α and β . Figures 8 and 9 show the final constitutive relationships for the calibrated model superimposed on the CHESS data.

As pointed out by Wells (1990a), the calibrated constitutive relationships will not necessarily coincide with those suggested by the experimental data. The reasons for this include errors in the numerical model, inaccuracies in the measured data, and incorrect functional forms for the constitutive equations themselves.

The calibration was done using data from a CHESS

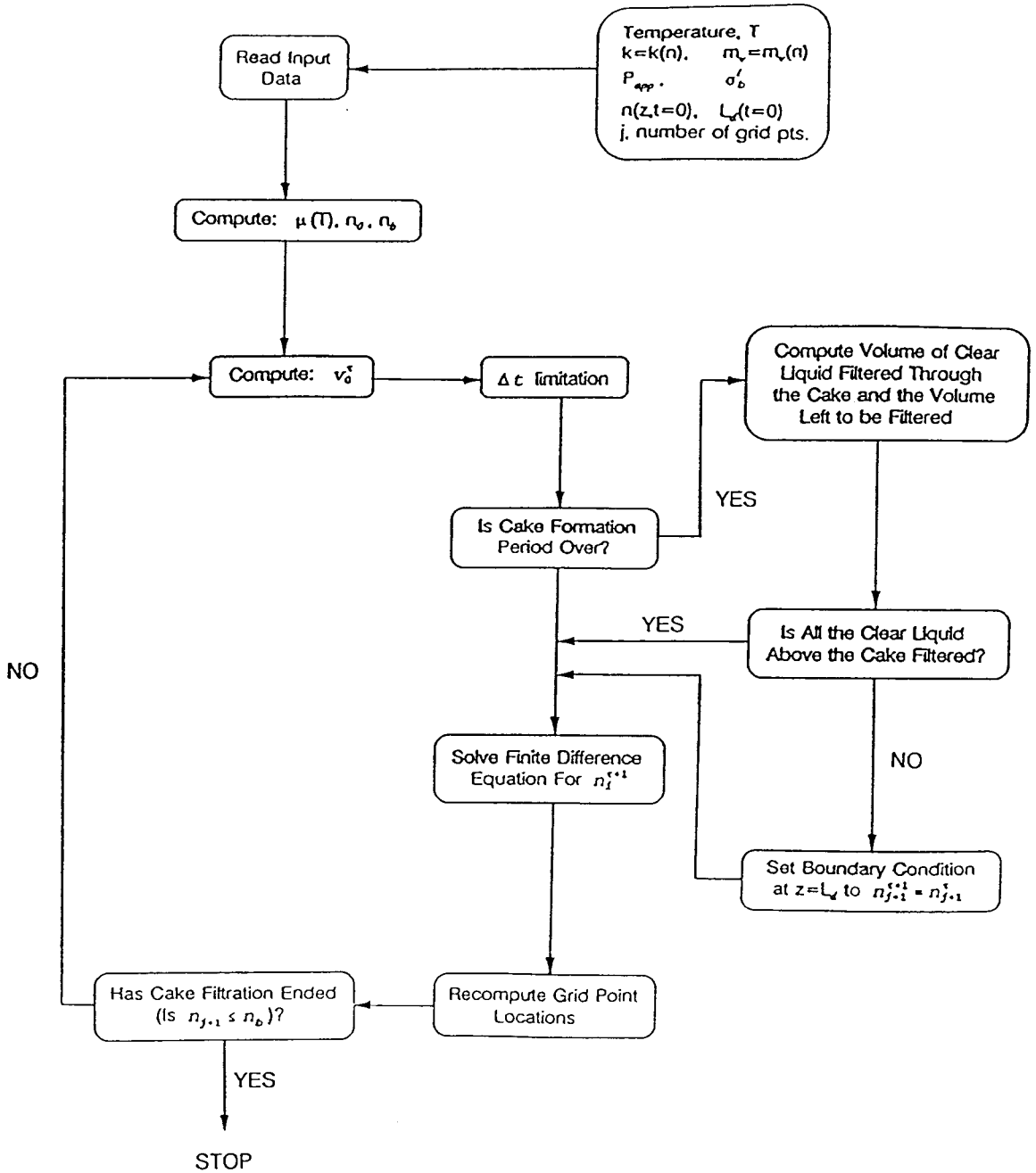


Figure 7. Computation algorithm for Wells (1990) cake filtration dewatering model.

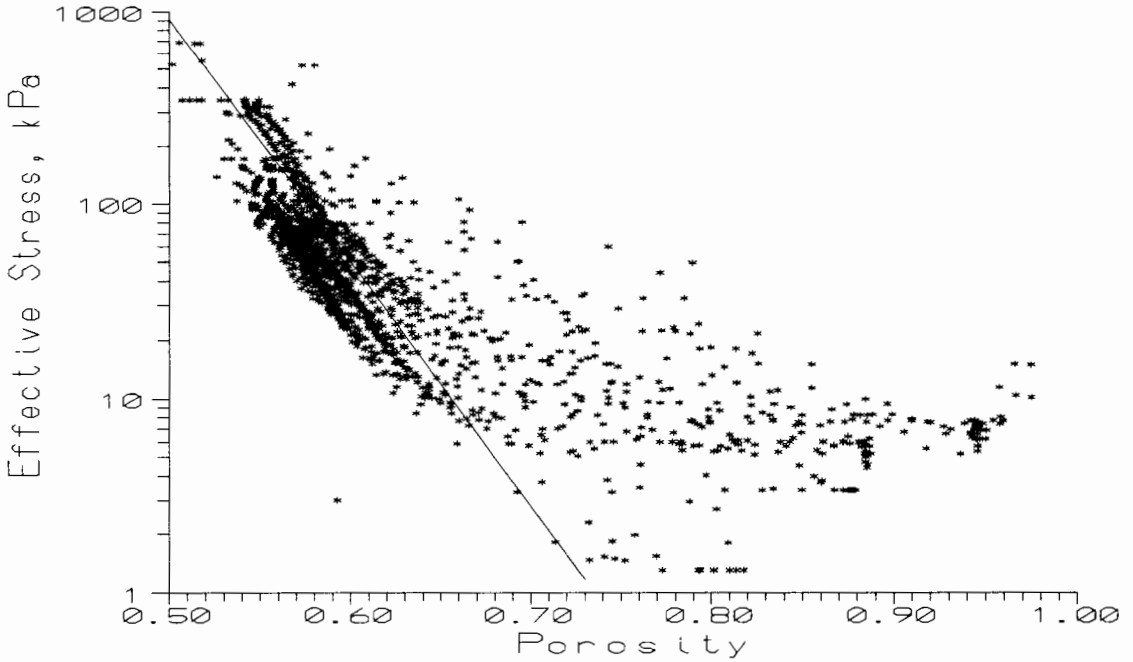


Figure 8. Semi-log plot of calibrated effective stress versus porosity relationship superimposed over CHES data.

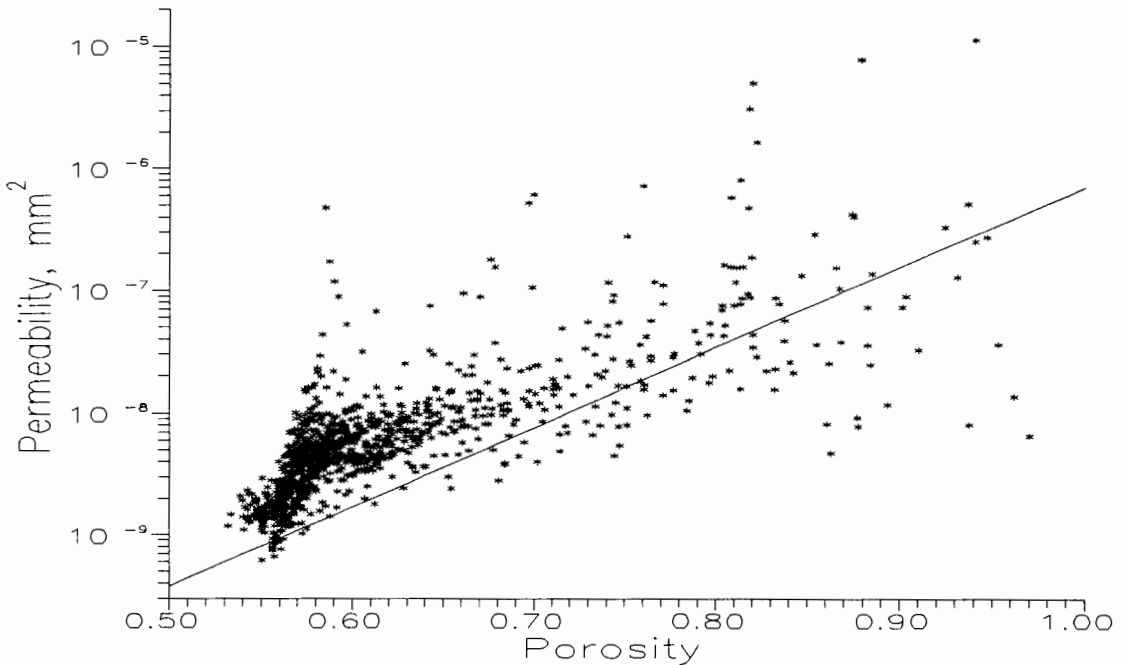


Figure 9. Semi-log plot of calibrated permeability versus porosity constitutive relationship superimposed over CHES data.

experiment with a kaolin clay suspension at an initial concentration of 0.31 g/cm^3 , a constant pressure differential of 103 kPa (15 psi), and a temperature of 25.5° C [labeled KDMK9 by Wells (1990a)]. In the CHESSE experiments three minutes elapsed before pressure was applied to the kaolin suspensions, so some initial sedimentation occurred. Because of this, the porosity was not uniform throughout the domain. Therefore, the porosity profile after three minutes of gravity sedimentation was the initial condition for the computer model during model calibration and verification. The model was verified by performing simulations at 170 kPa (25 psi), 345 kPa (50 psi), 520 kPa (75 psi), and 690 kPa (100 psi), and comparing the simulation results with CHESSE data. The final values of the four parameters used in the calibrated model were

$$\begin{aligned}
 \alpha &= 2.10 \text{ e}^{-15} \text{ cm}^2 \\
 \beta &= 15.0 \\
 \gamma &= 2.04 \text{ e}^{-11} \text{ kPa}^{-1} \\
 \delta &= 28.9
 \end{aligned}
 \tag{47}$$

Table II summarizes the results of computer simulations using this model with these constitutive equations. Results of model simulations as compared with data from the CHESSE experiments are given in Figures 10-24.

TABLE II

SUMMARY OF RESULTS FROM COMPUTER SIMULATIONS USING WELLS
CAKE FILTRATION MODEL ($c_i=0.31 \text{ g/cm}^3$)

CHES RUN	P_{app} (kPa)	Temp. (° C)	CPU* Time (S)	Cake Form. Time (S)	Simula- tion Time (S)	Terminal Porosity
KDMK9	103	25.5	242.8	365.6	900.0	0.5750
KDM2	170	26.0	308.4	334.6	676.8	0.5572
PMK3	345	24.0	229.3	261.2	374.8	0.5332
PMK4	520	24.0	226.1	212.8	296.1	0.5192
PMK5	690	24.0	252.6	185.6	302.4	0.5096

* Using a Tektronix XD88/10 UNIX workstation

In the plots of suspended solids concentration versus height (z distance) above the filter medium, the solid lines are the output from the computer model at each 30 seconds of simulated time. The symbols are the plotted CHES data, which was obtained at 30 second intervals. These plots allow a visual comparison to be made between model predictions at various times with experimental data at the same times. At time $t=0$, the symbols and solid line coincide, since the suspended solids concentration profile at time $t=0$ of the CHES experiments was also used as input for the computer model.

The plots of error versus frequency are the result of a point by point comparison of model output at each data point from the CHES experiments.

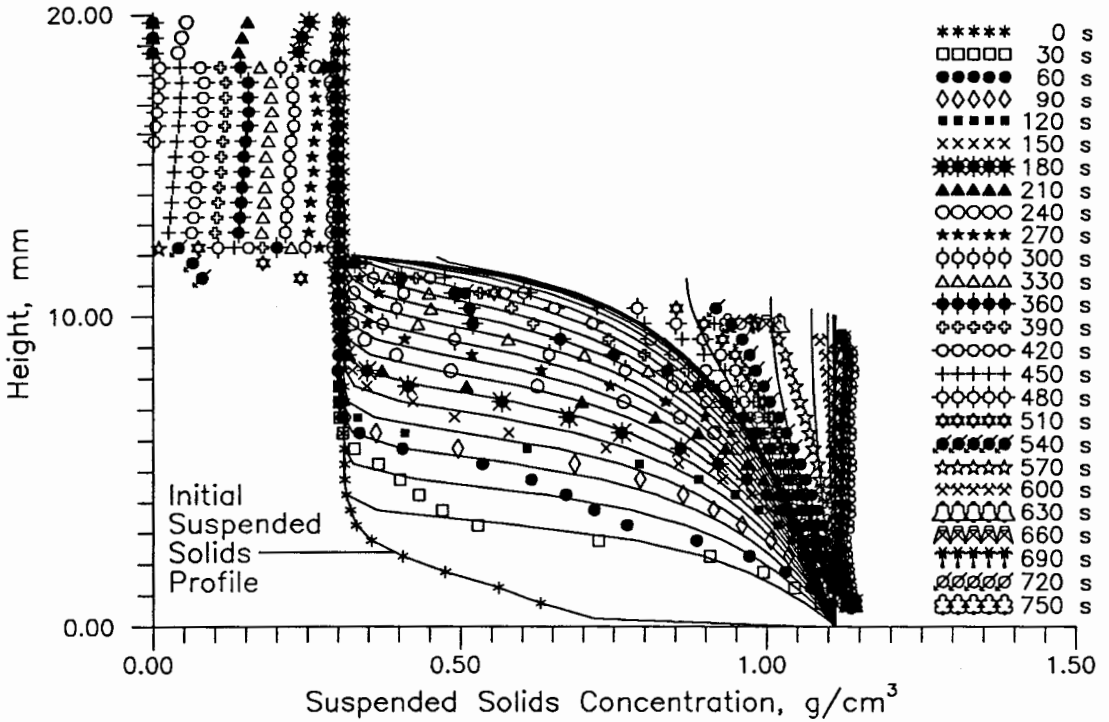


Figure 10. Data-model comparison of concentration profiles at 30 s intervals under conditions of CHES run KDMK9 (100 kPa, 0.31 g/cm³).

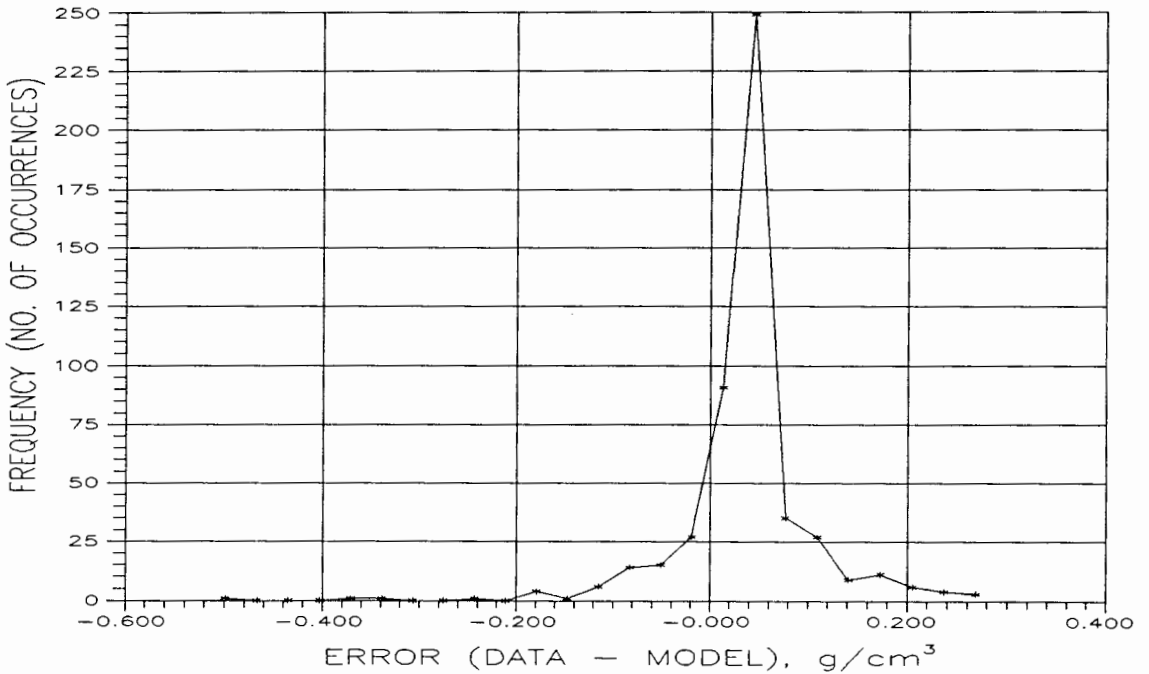


Figure 11. Error frequency histogram for run KDMK9, paired data-model observations of porosity and time as in Figure 10.

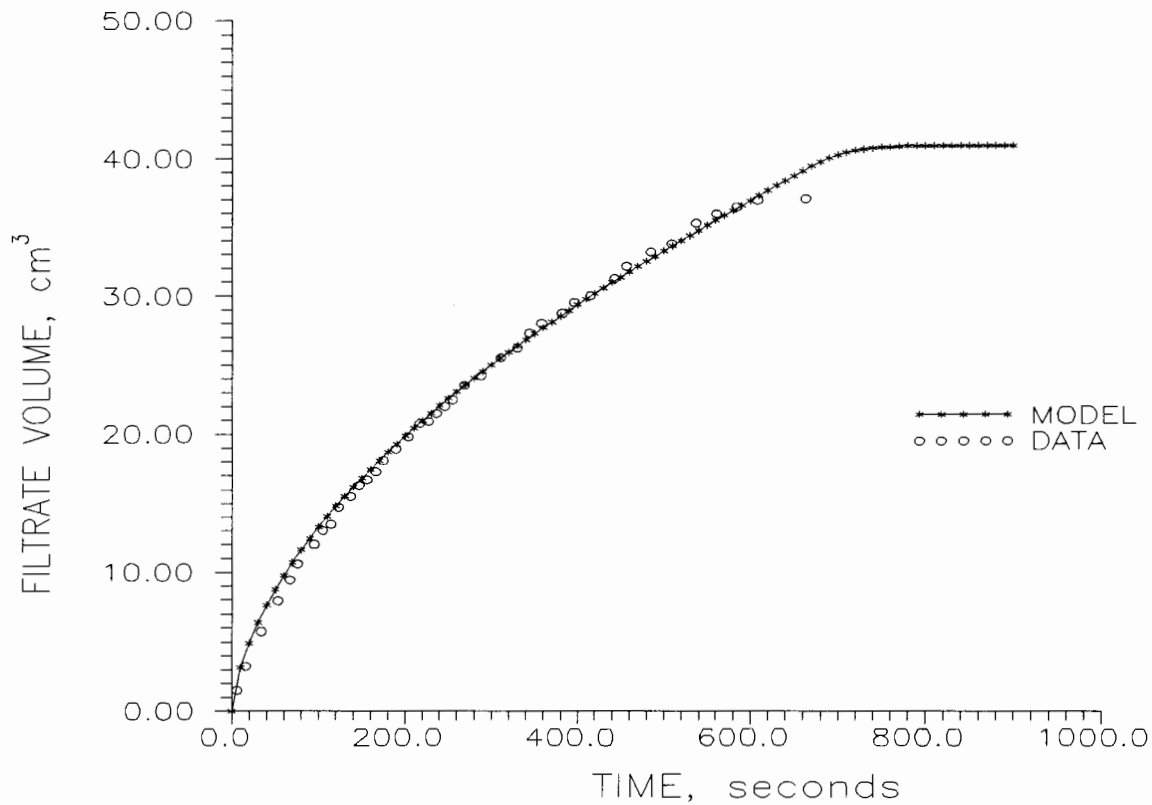


Figure 12. Data-model comparison of filtrate production with time under conditions of CHES run KDMK9 (103 kPa, 0.31 g/cm³).

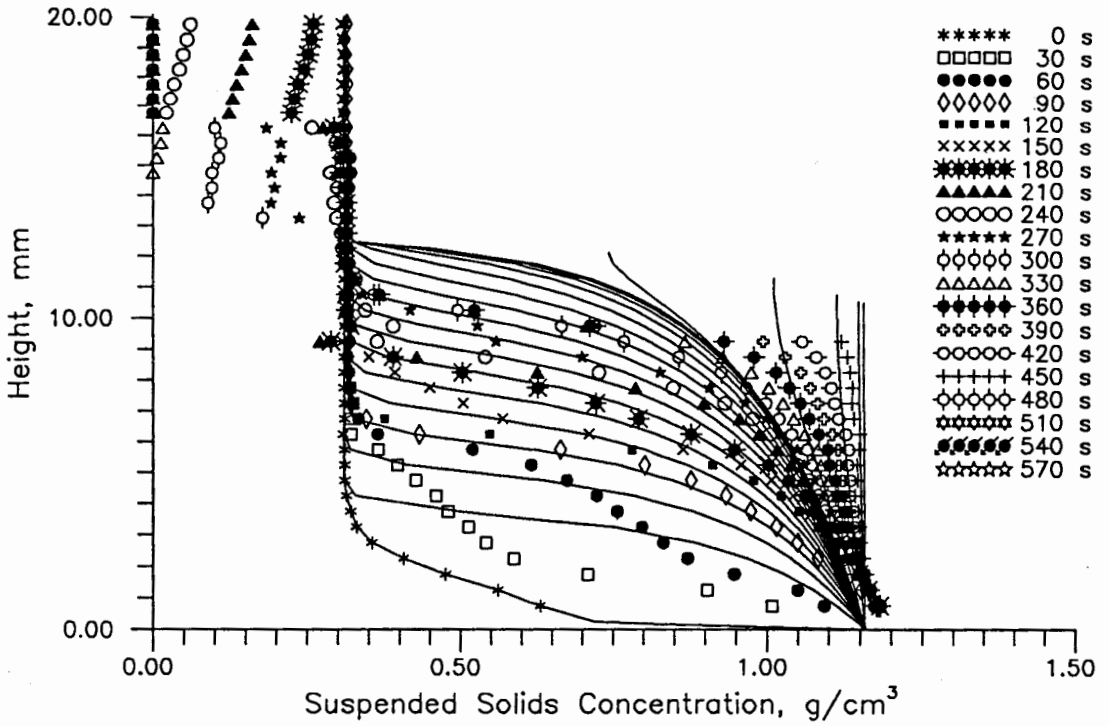


Figure 13. Data-model comparison of concentration profiles at 30 s intervals under conditions of CHES run KDM2 (172 kPa, 0.31 g/cm³).

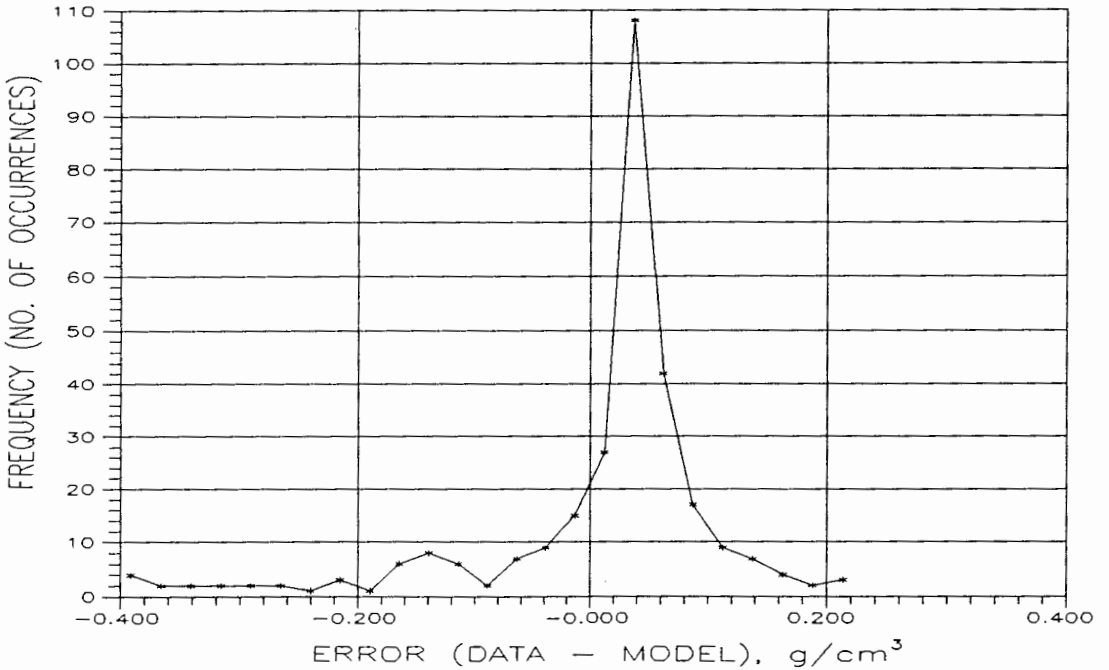


Figure 14. Error frequency histogram for run KDM2, paired data-model observations of porosity and time as in Figure 13.

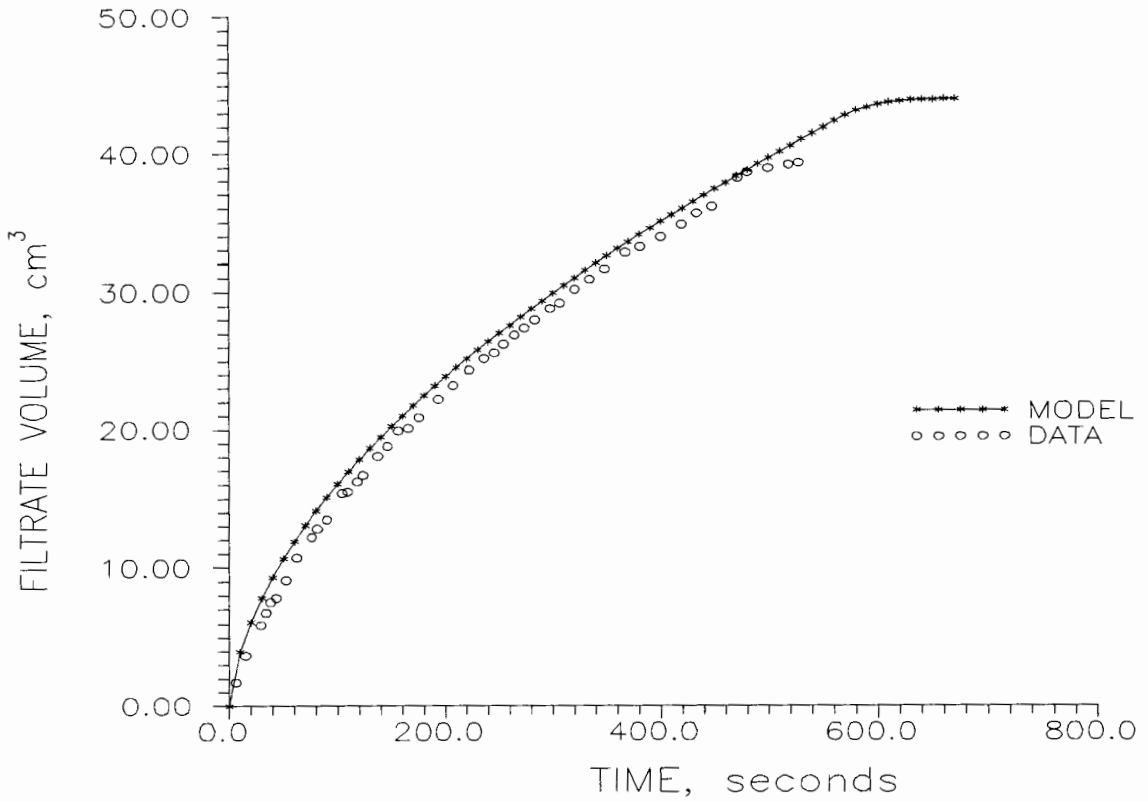


Figure 15. Data-model comparison of filtrate production with time under conditions of CHES run KDM2 (172 kPa, 0.31 g/cm³).

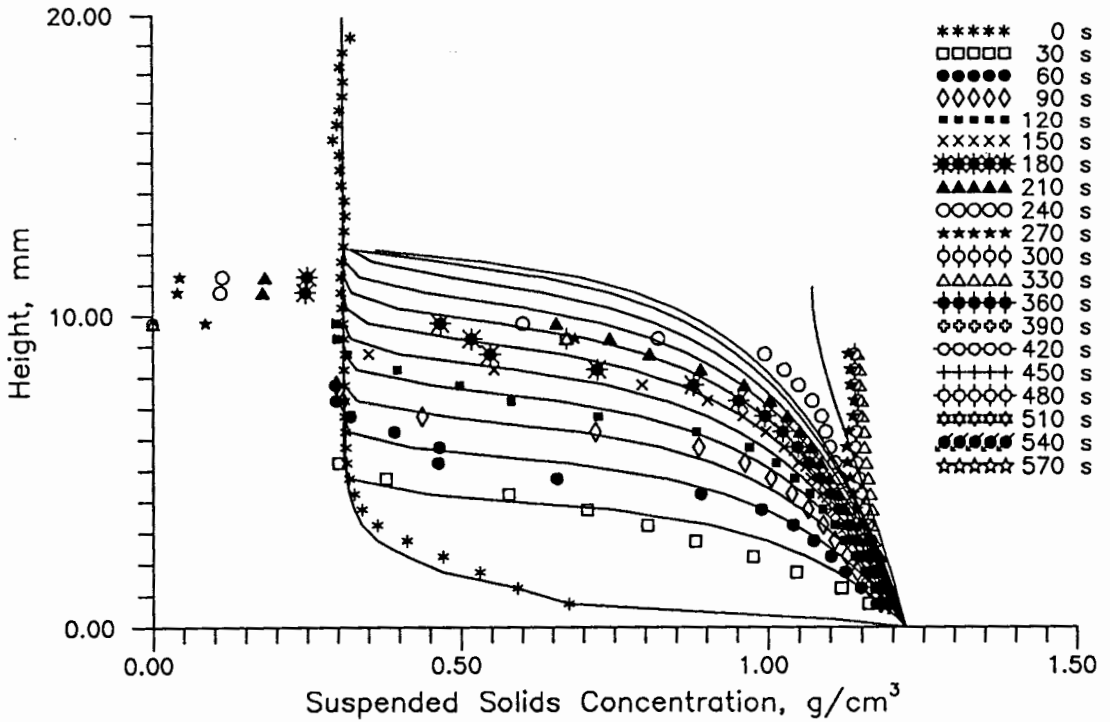


Figure 16. Data-model comparison of concentration profiles at 30 s intervals under conditions of CHES run PMK3 (345 kPa, 0.31 g/cm³).

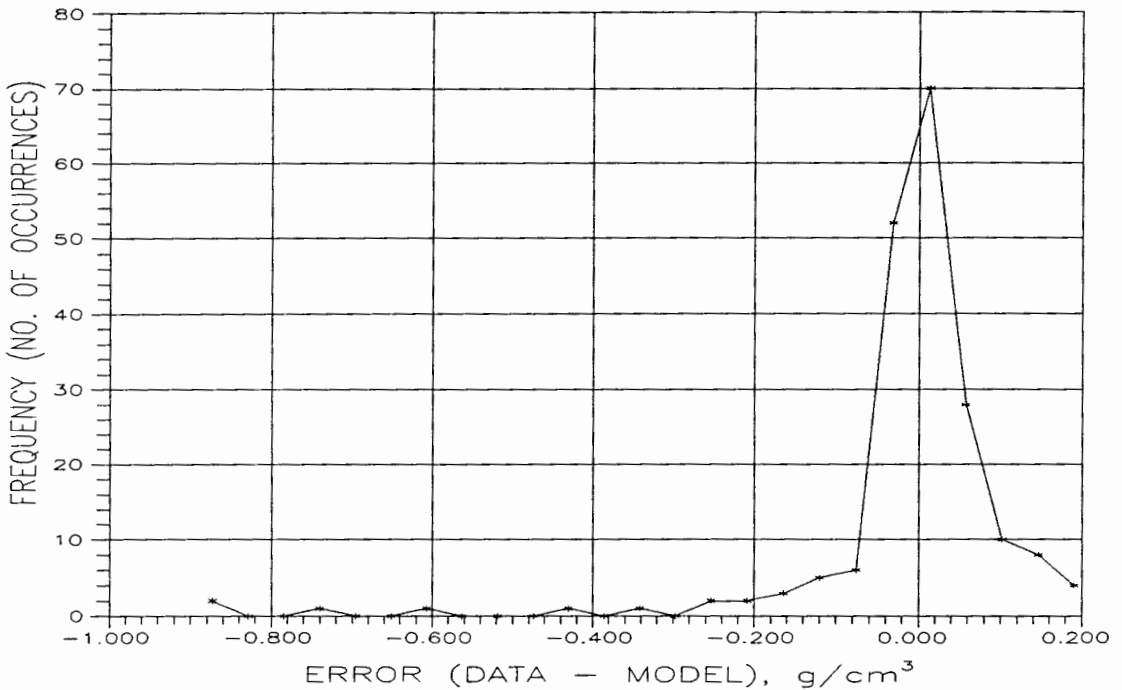


Figure 17. Error frequency histogram for run PMK3, paired data-model observations of porosity and time as in Figure 16.

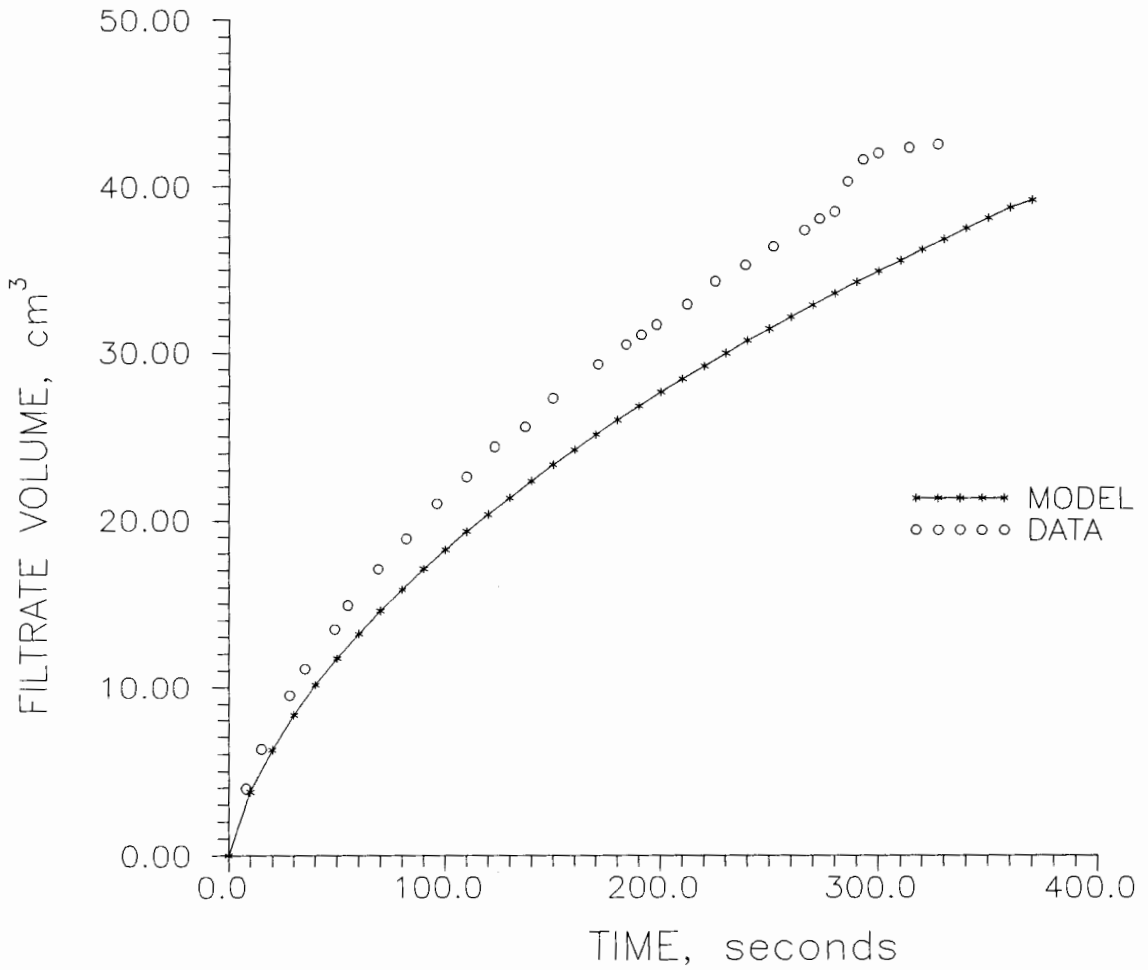


Figure 18. Data-model comparison of filtrate production with time under conditions of CHES run PMK3 (345 kPa, 0.31 g/cm³).

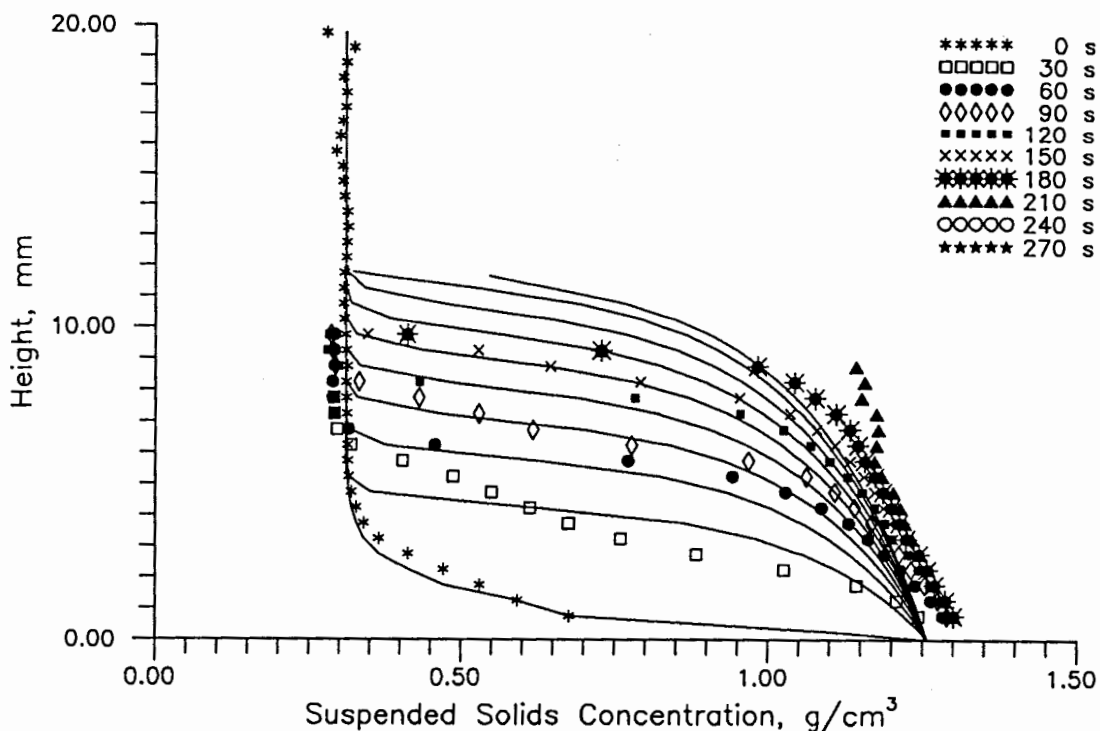


Figure 19. Data-model comparison of concentration profiles at 30 s intervals under conditions of CHES run PMK4 (517 kPa, 0.31 g/cm^3).

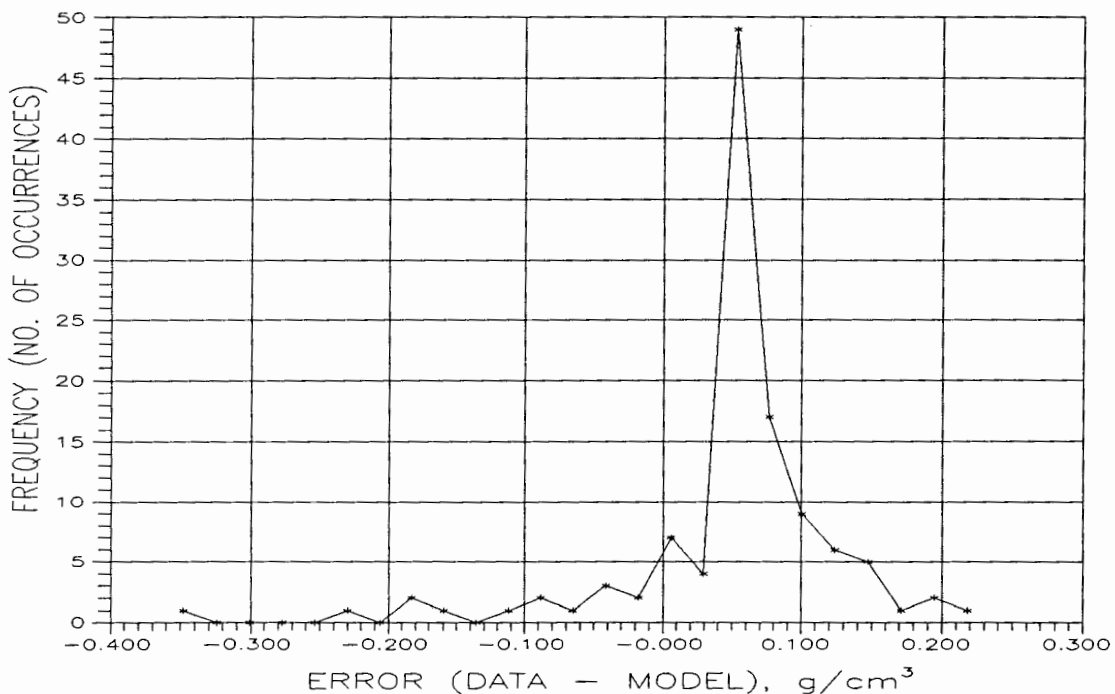


Figure 20. Error frequency histogram for run PMK4, paired data-model observations of porosity and time as in Figure 19.

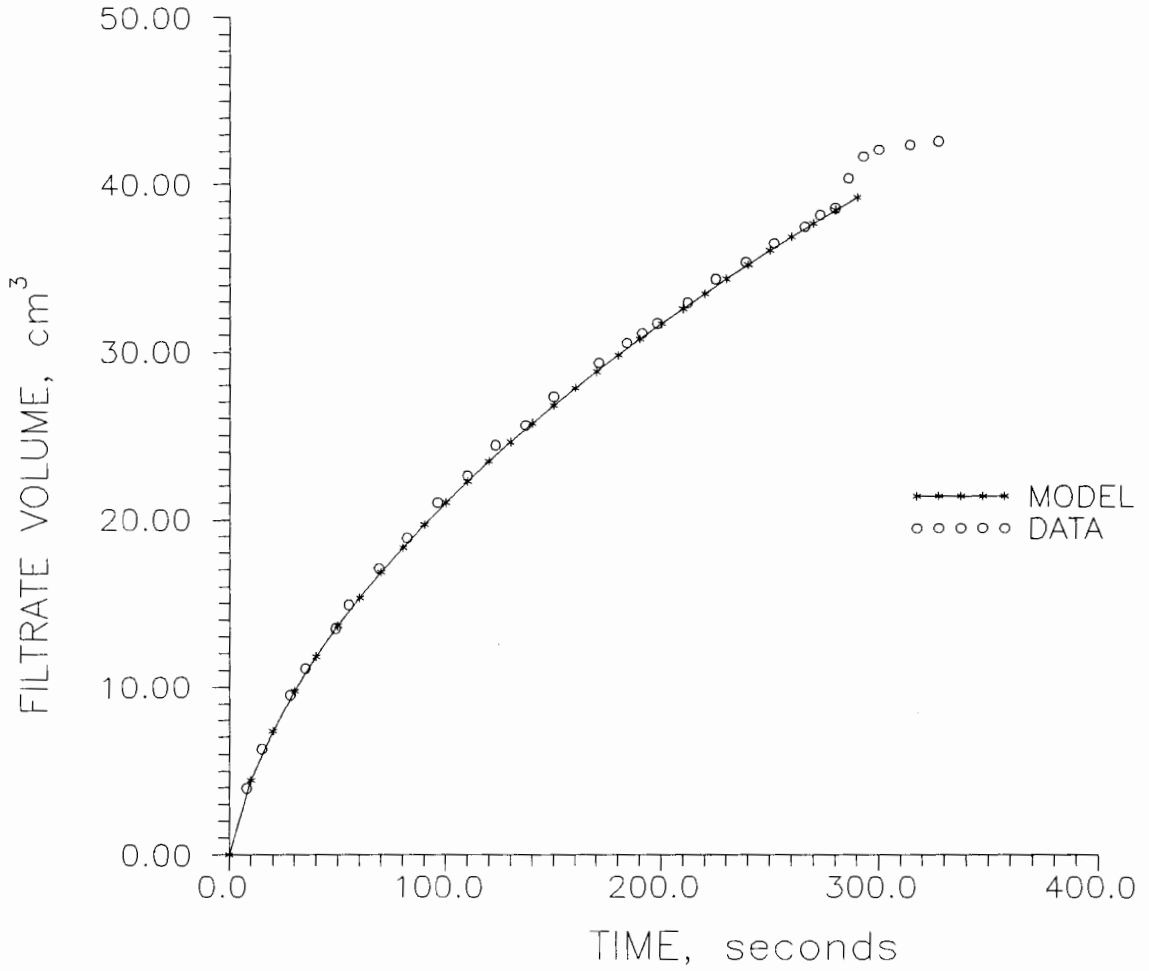


Figure 21. Data-model comparison of filtrate production with time under conditions of CHES run PMK4 (517 kPa, 0.31 g/cm³).

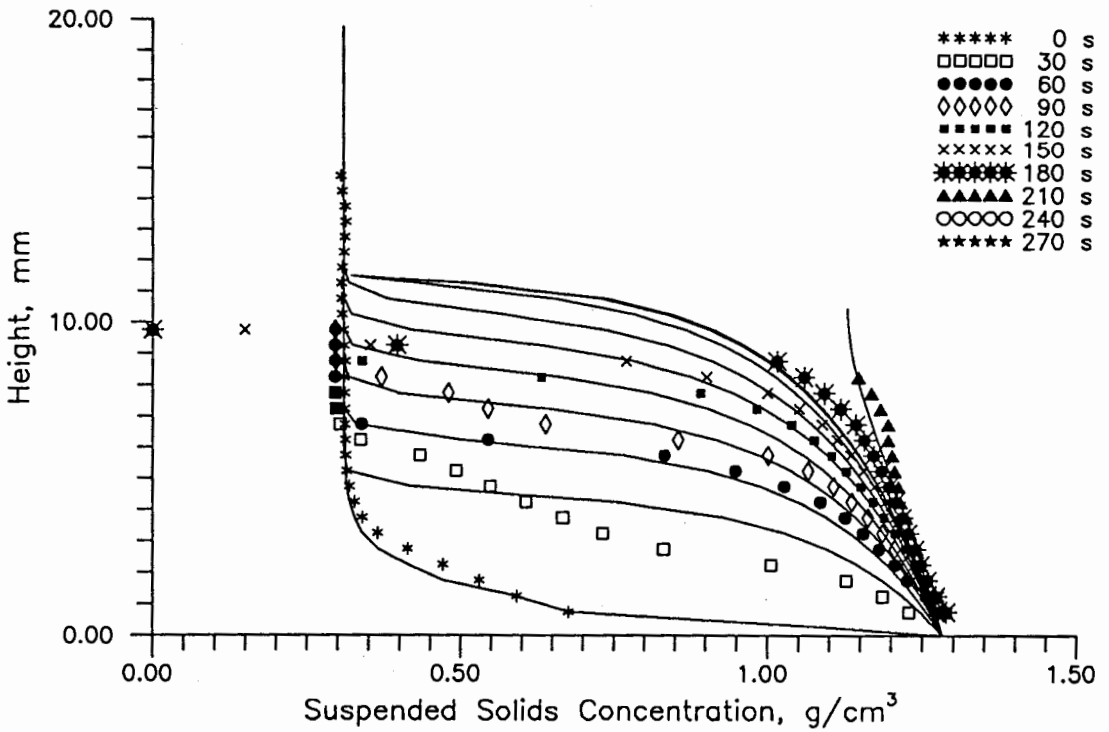


Figure 22. Data-model comparison of concentration profiles at 30 s intervals under conditions of CHES run PMK5 (682 kPa, 0.31 g/cm³).

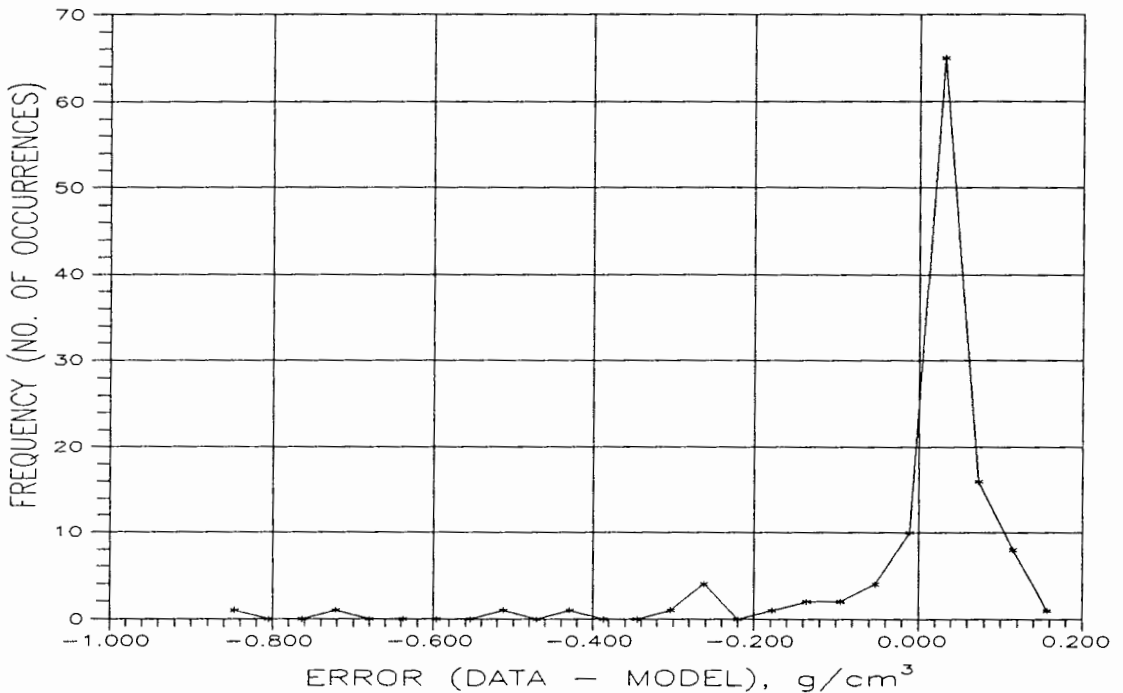


Figure 23. Error frequency histogram for run PMK5, paired data-model observations of porosity and time as in Figure 22.

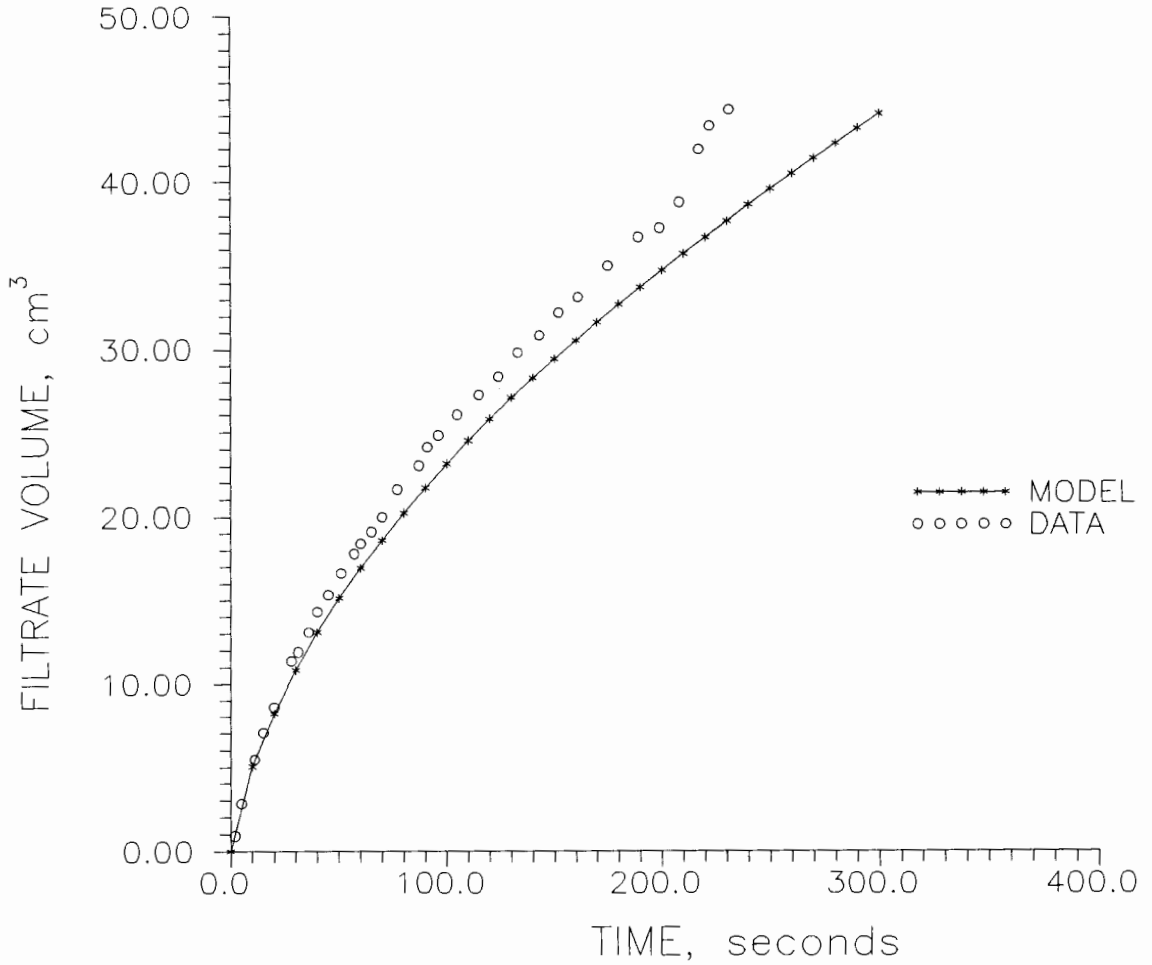


Figure 24. Data-model comparison of filtrate production with time under conditions of CHES run PMK5 (682 kPa, 0.31 g/cm³).

As can be seen, the agreement between the model and experimental data is quite good, and would seem to validate the appropriateness of the assumptions made in the model's development. Table III gives statistical information for each run.

TABLE III

STATISTICS FROM DATA-MODEL COMPARISON OF POROSITY AND DISTANCE OVER TIME ($c_i=0.31 \text{ g/cm}^3$)

CHESS RUN	Number of Comparisons	Mean Error	Standard Deviation of Error	Skewness	Coef. of Variation
KDMK9	506	0.037	0.071	-1.581	1.925
KDM2	291	0.081	0.107	-1.804	13.17
PMK3	196	0.011	0.137	-3.985	12.29
PMK4	115	0.049	0.080	-1.930	1.63
PMK5	118	-0.008	0.146	-3.607	-16.79

CHAPTER V

FURTHER EXPERIMENTS WITH THE WELLS MODEL

As part of the present study, additional experiments using the Wells (1990a) sludge dewatering model were conducted with two different initial suspended solids concentrations. These experiments showed how the model's performance was affected by changes in the initial slurry concentration. Changing the initial suspended solids concentration revealed that the model has a limited range of predictive capability for a given set of constitutive equations. The results of simulation experiments and model-data comparisons for a suspension with an initial concentration of 0.47 g/cm^3 are shown in Tables IV and V and Figures 25-39. As with the experiments done by Wells (1990a), the suspended solids profile used as input to the model included a period of gravity sedimentation. More detailed summaries of simulation results can be found in Appendix B.

TABLE IV

SUMMARY OF RESULTS FROM COMPUTER SIMULATIONS USING WELLS
CAKE FILTRATION MODEL ($c_i=0.47 \text{ g/cm}^3$)

CHESS RUN	P_{app} (kPa)	Temp. (° C)	CPU* Time (Sec.)	Cake Form. Time (Sec.)	Simula- tion Time (Sec.)	Terminal Porosity
KDMK8	103	26.0	325.5	404.1	900.0	0.5750
KDM6	172	26.0	344.7	301.2	771.0	0.5572
KDM4	345	26.0	328.6	224.6	498.6	0.5331
PMK9	517	24.0	296.9	165.1	421.5	0.5192
PMK6	682	24.0	162.3	76.6	284.6	0.5096

* Using a Tektronix XD88/10 UNIX workstation

The results are quite good, except in the case of the data-model comparison of porosity versus distance at various times for run PMK9. The wide discrepancy is believed to be a result of comparing the model output to the wrong experimental data. Although the data was labeled as coming from a test at a pressure of 517 kPa, it is believed that it is more likely from a test at a lower pressure. The data set is seen to be obviously out of place when it is compared with the other experimental data sets from tests at this concentration. The terminal concentration for the data of run PMK9 is lower than for experiments using much lower pressures. This is also verified by noting the good agreement of the model in Figure 36 with filtrate production data from an independent experiment (CHESS run PMK9).

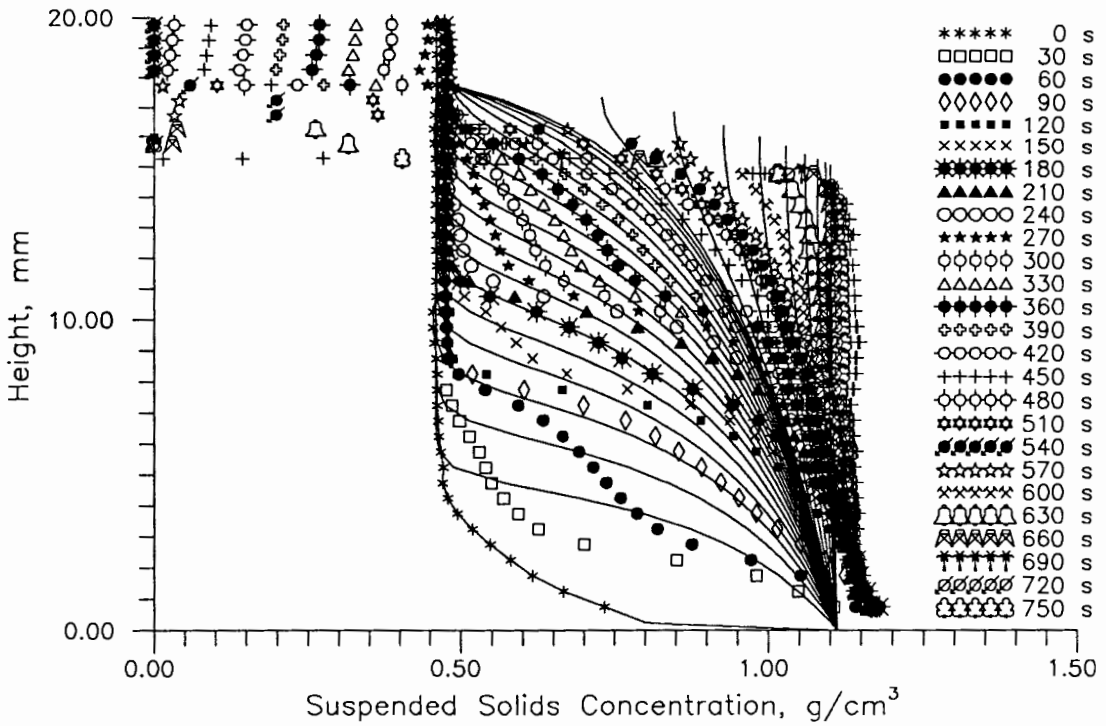


Figure 25. Data-model comparison of concentration profiles at 30 s intervals under conditions of CHES run KDMK8 (103 kPa, 0.47 g/cm³).

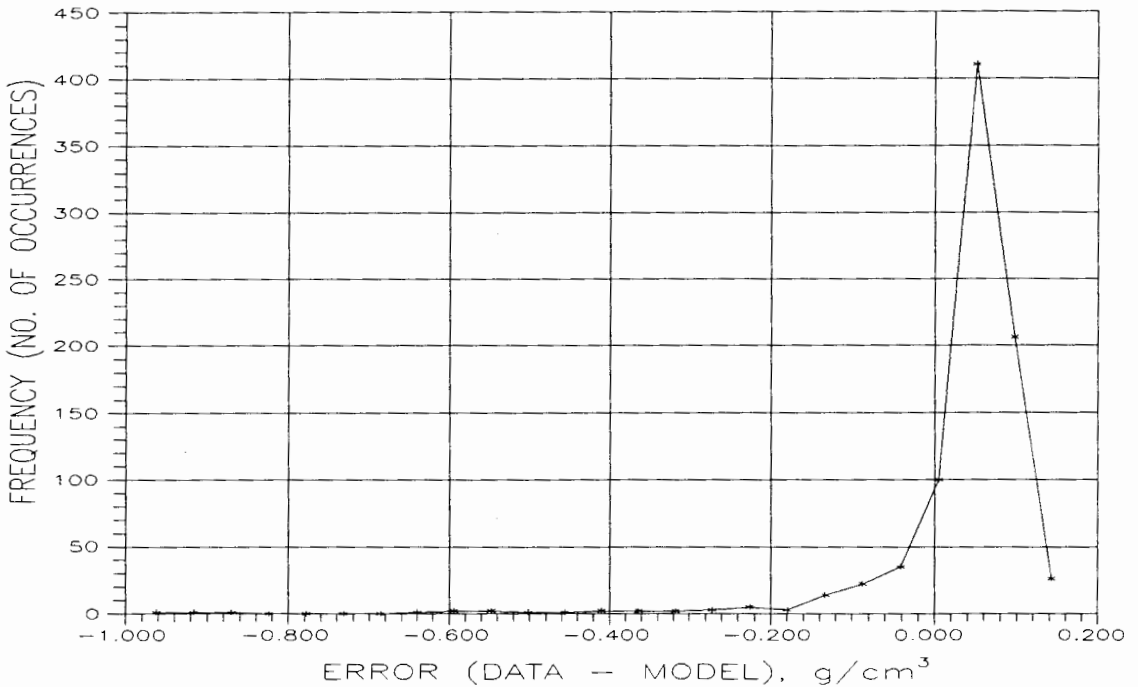


Figure 26. Error frequency histogram for run KDMK8, from paired data-model observations of porosity and time as in Figure 25.

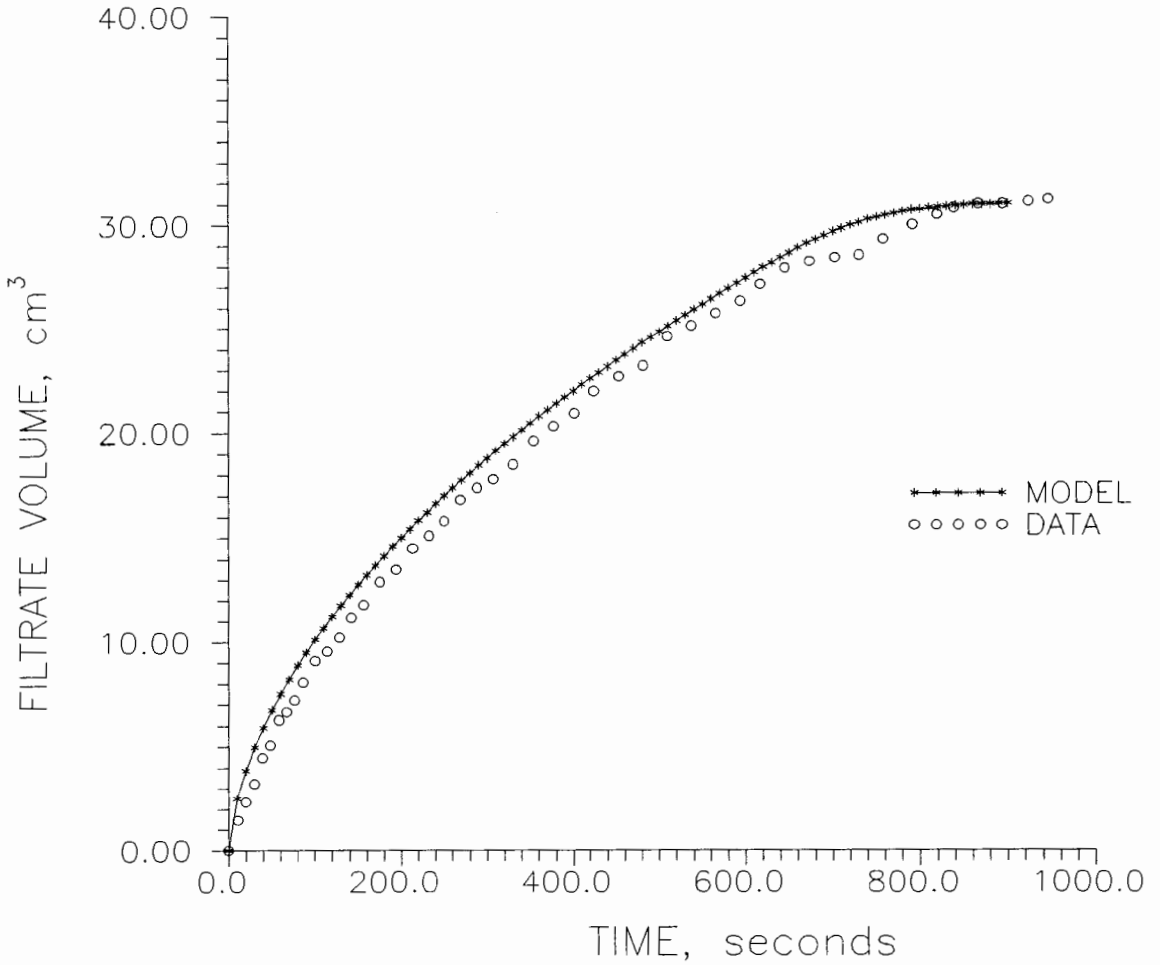


Figure 27. Data-model comparison of filtrate production with time under conditions of CHES run KDMK8 (103 kPa, 0.47 g/cm³).

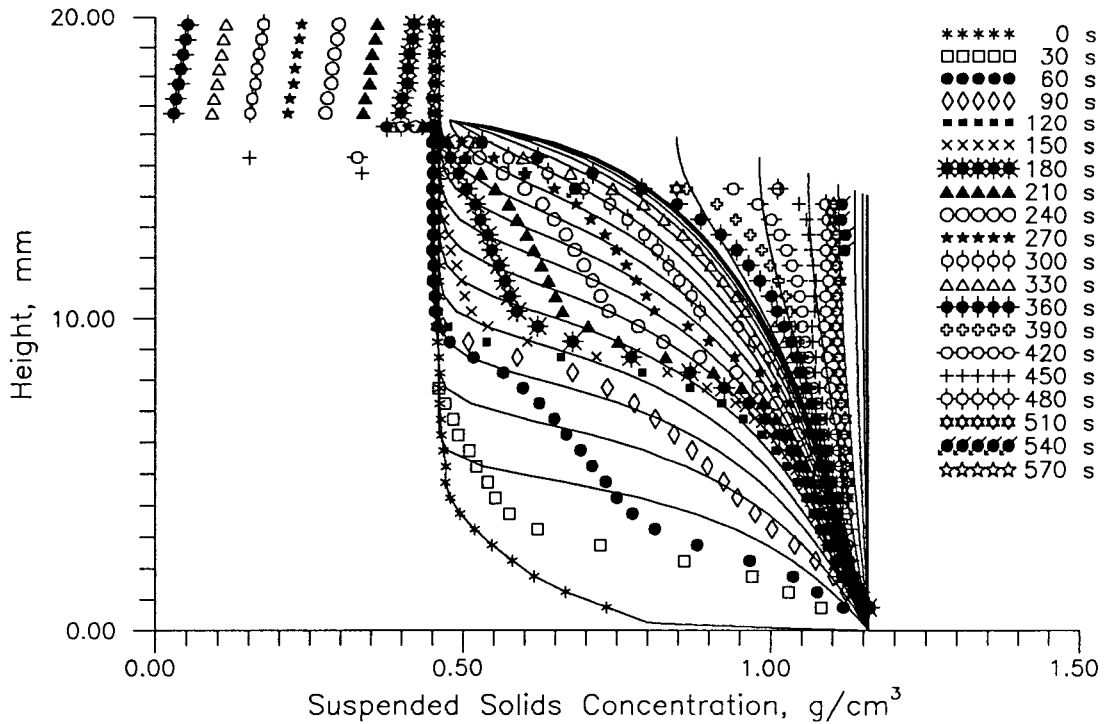


Figure 28. Data-model comparison of concentration profiles at 30 s intervals under conditions of CHES run KDM6 (172 kPa, 0.47 g/cm^3).

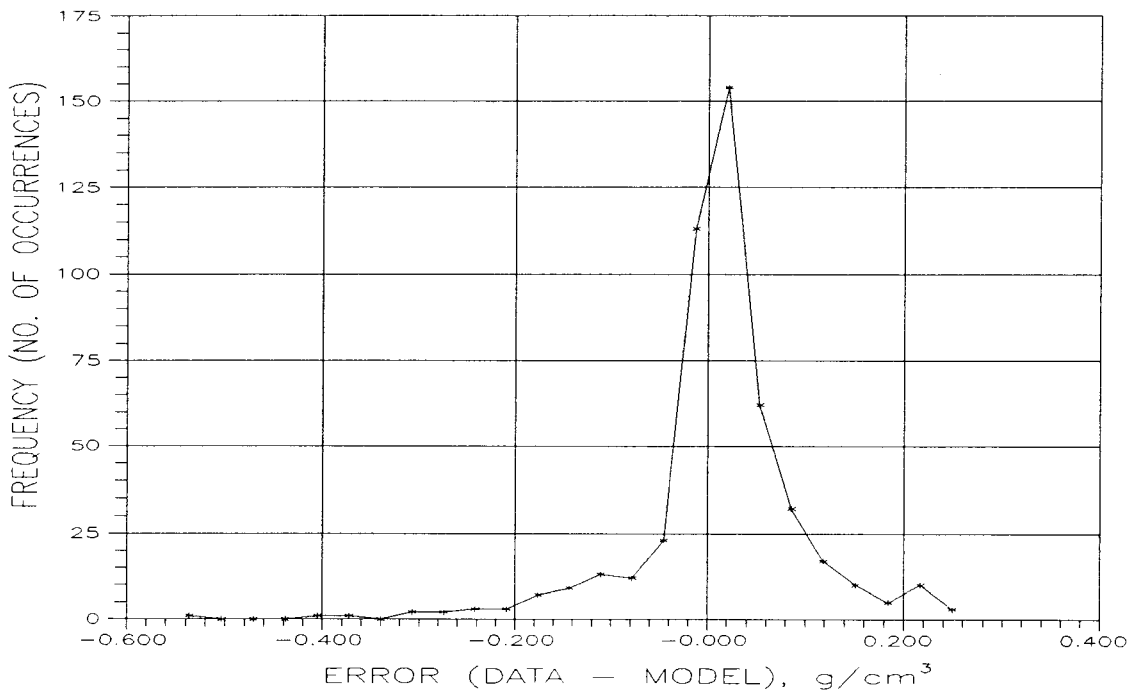


Figure 29. Error frequency histogram for run KDM6, from paired data-model observations of porosity and time as in Figure 28.

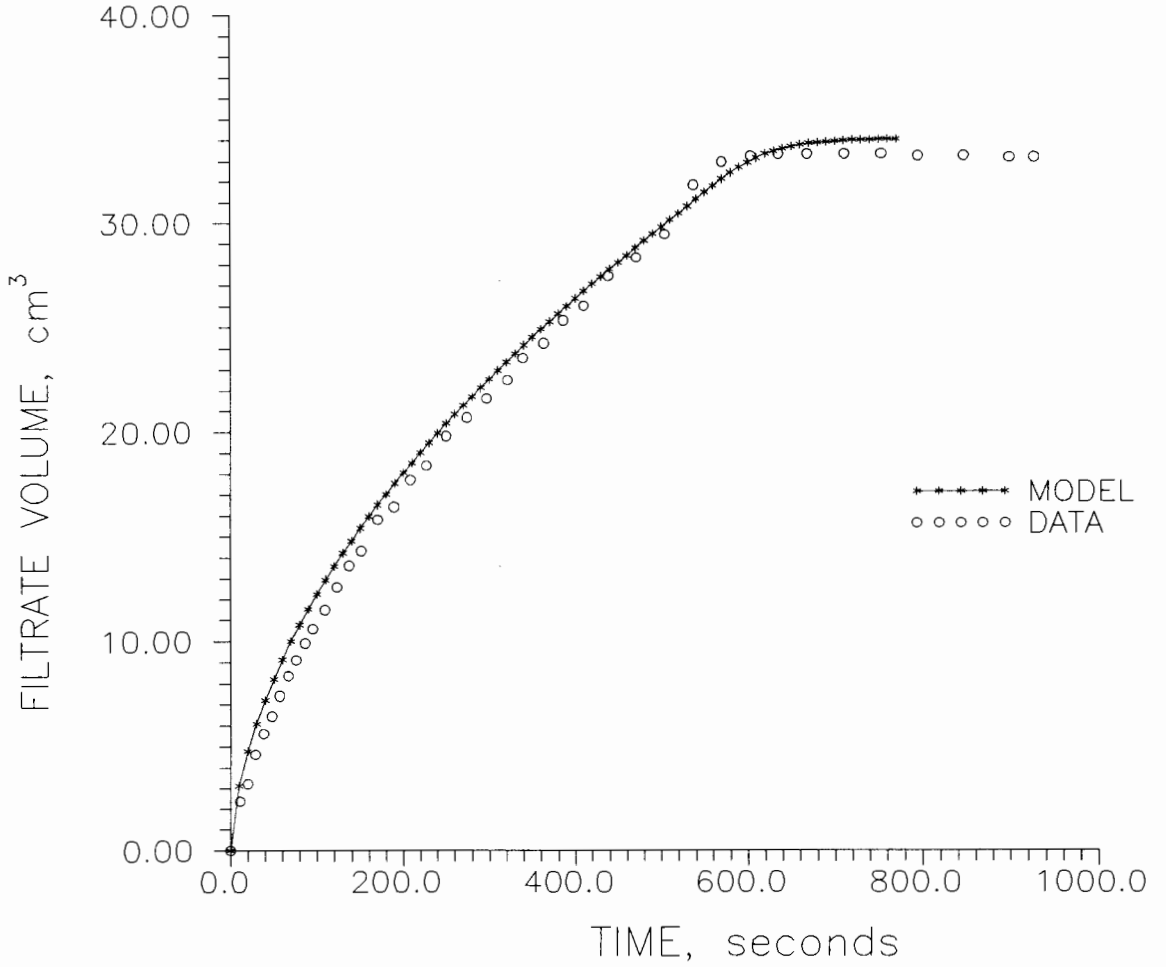


Figure 30. Data-model comparison of filtrate production with time under conditions of CHES run KDM6 (172 kPa, 0.47 g/cm³).

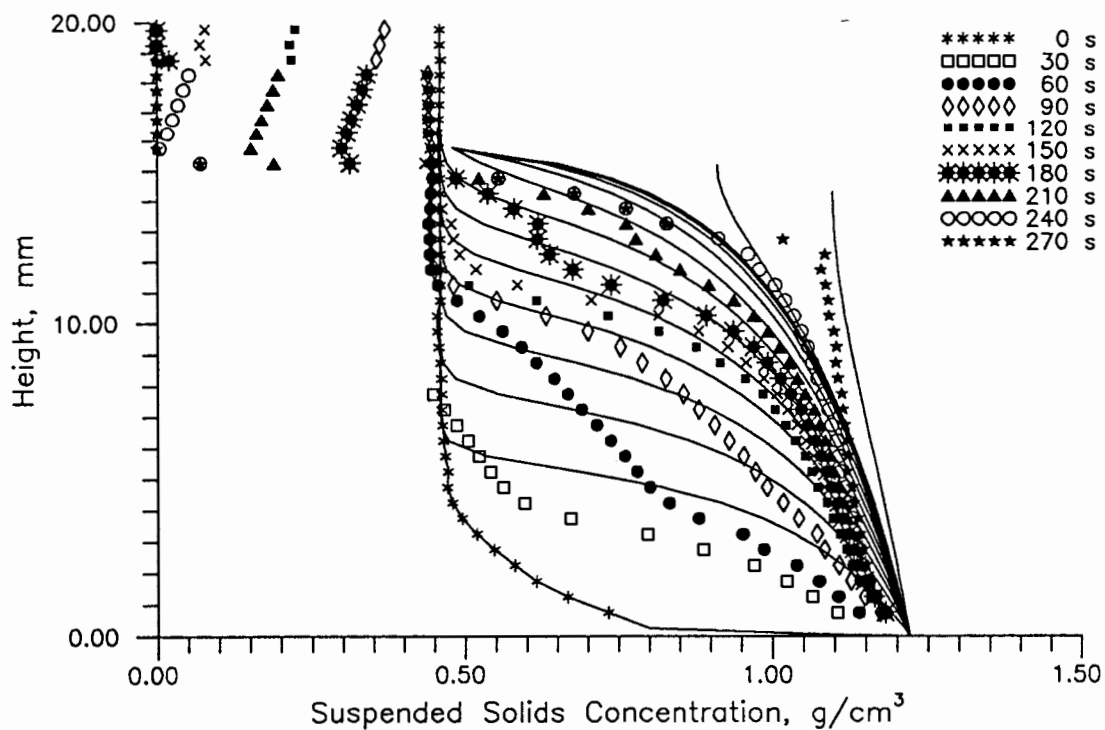


Figure 31. Data-model comparison of concentration profiles at 30 s intervals under conditions of CHES run KDM4 (345 kPa, 0.47 g/cm³).

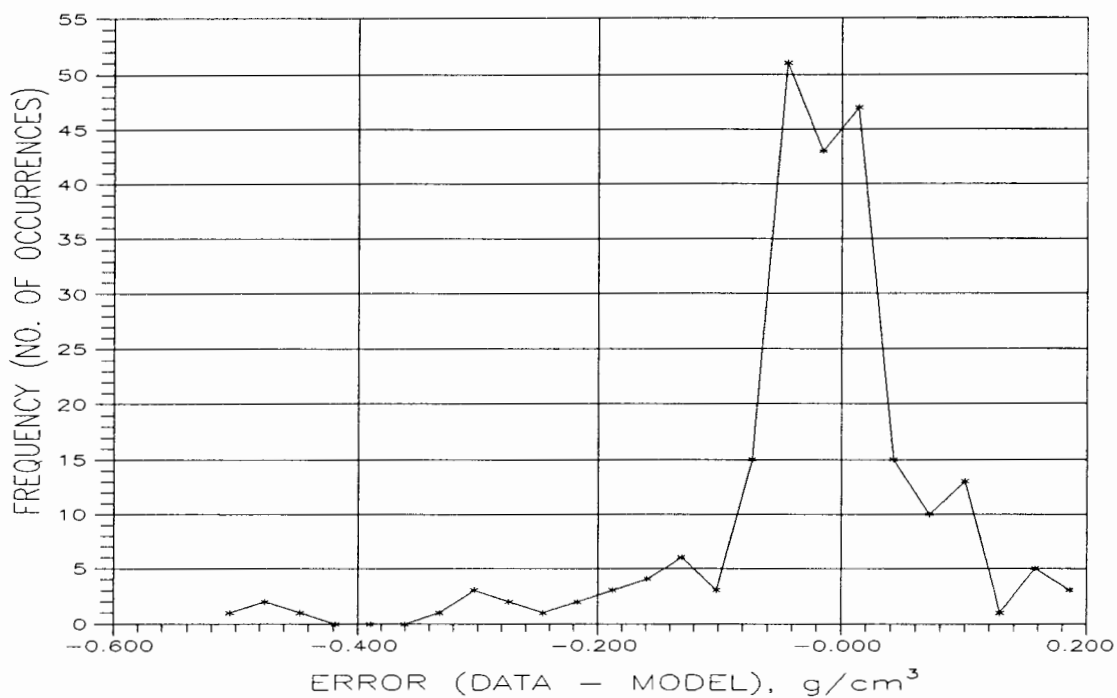


Figure 32. Error frequency histogram for run KDM4, from paired data-model observations of porosity and time as in Figure 31.

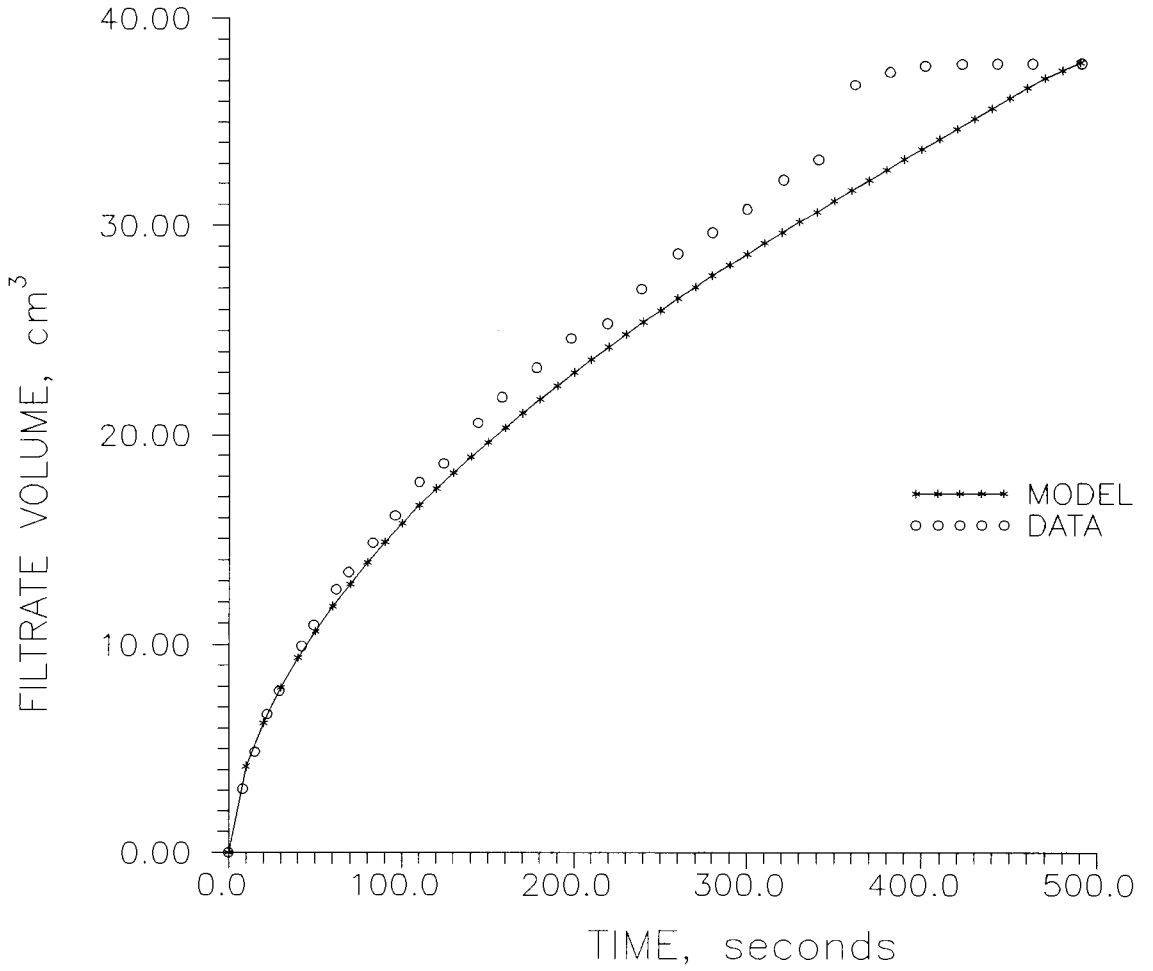


Figure 33. Data-model comparison of filtrate production with time under conditions of CHES run KDM4 (345 kPa, 0.47 g/cm³).

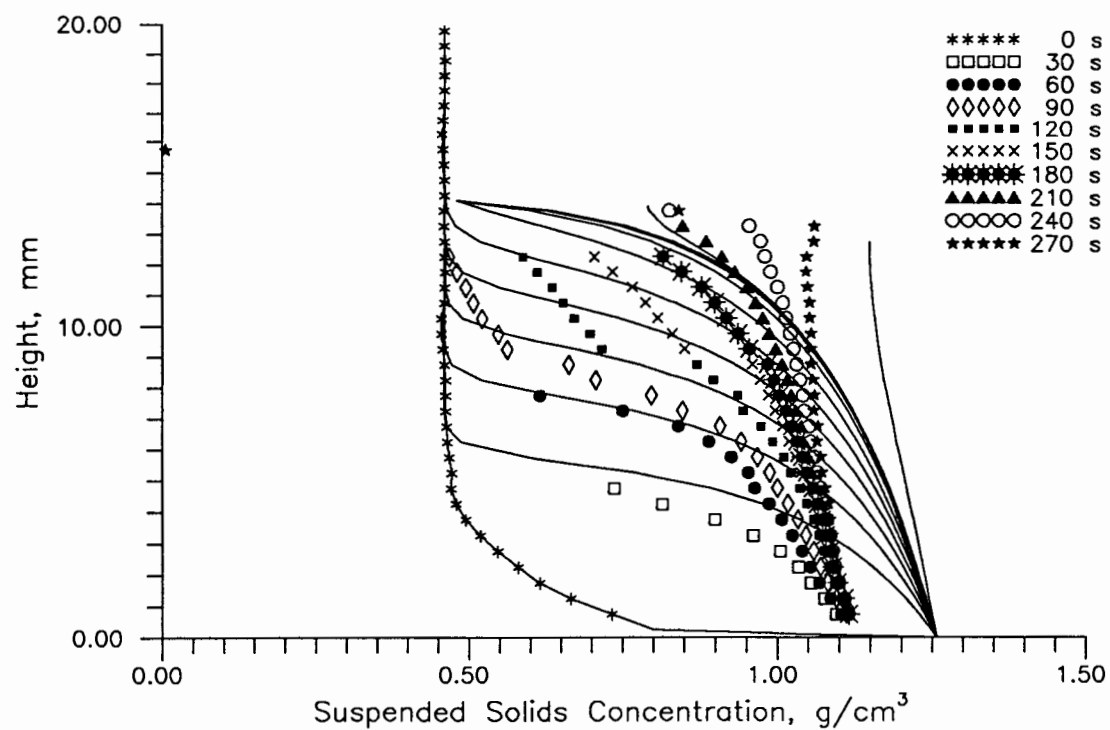


Figure 34. Data-model comparison of concentration profiles at 30 s intervals under conditions of CHES run PMK9 (517 kPa, 0.47 g/cm³).

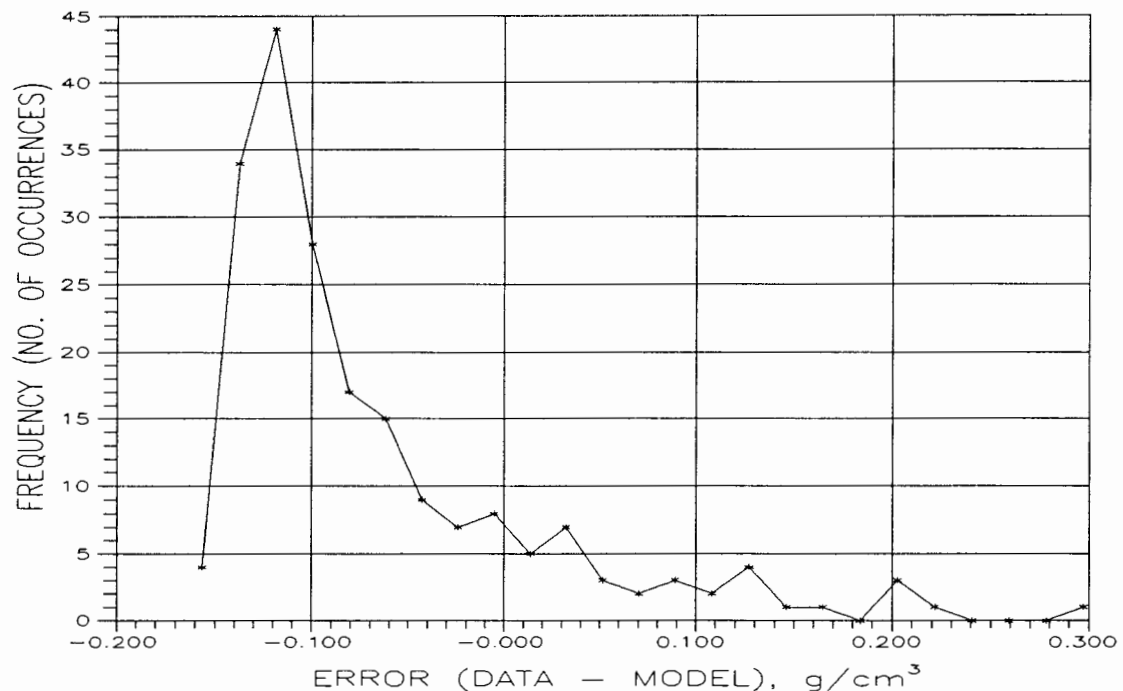


Figure 35. Error frequency histogram for run PMK9, from paired data-model observations of porosity and time as in Figure 34.

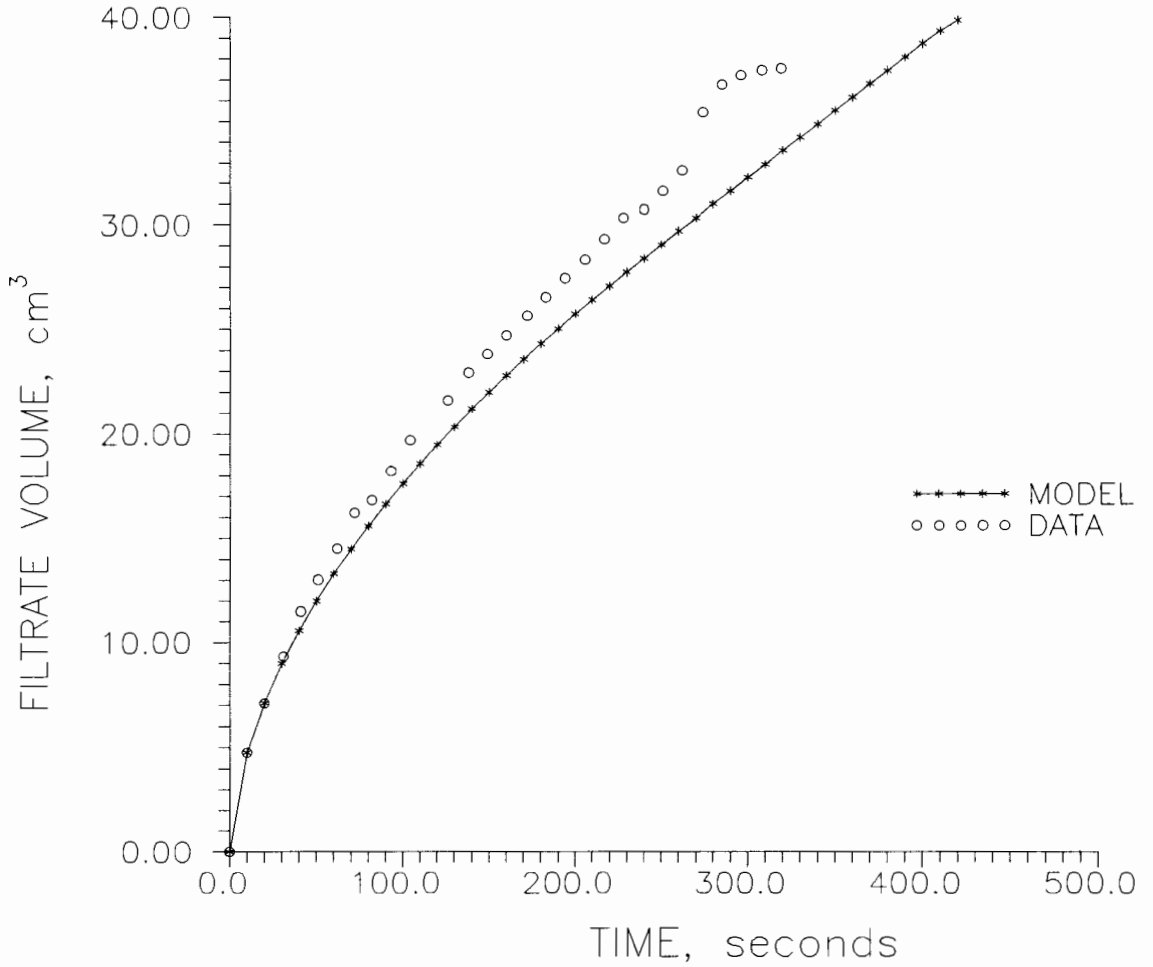


Figure 36. Data-model comparison of filtrate production with time under conditions of CHES run PMK9 (517 kPa, 0.47 g/cm³).

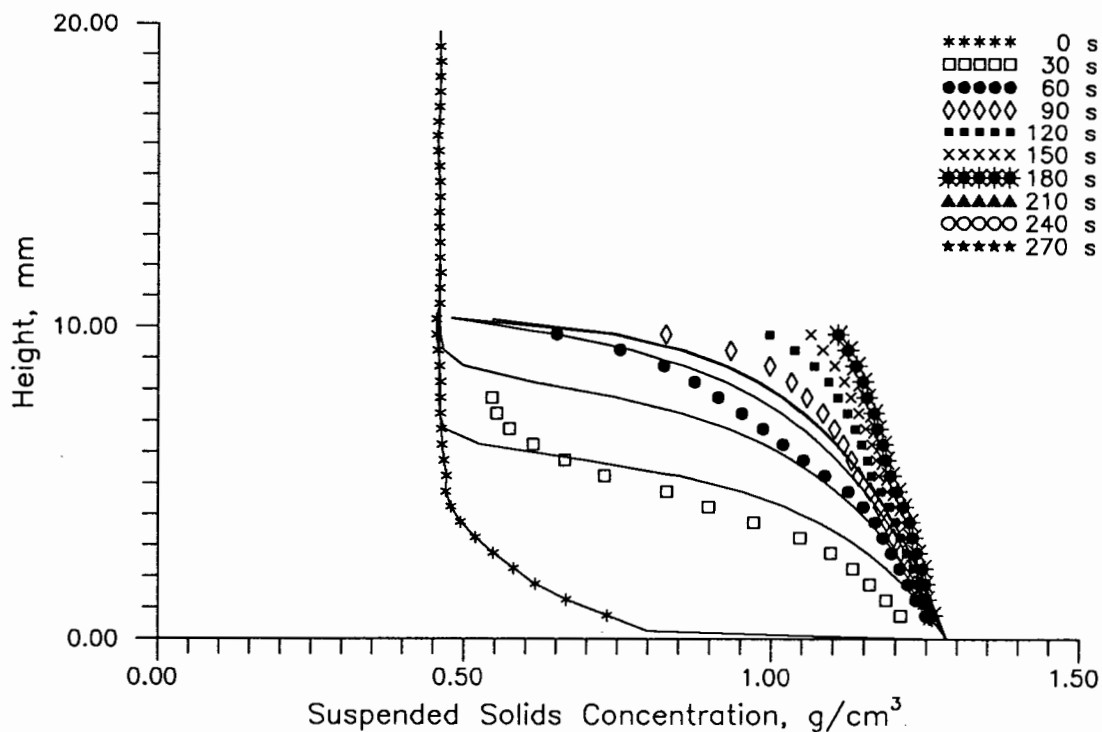


Figure 37. Data-model comparison of concentration profiles at 30 s intervals under conditions of CHES run PMK6 (682 kPa, $0.47 \text{ g}/\text{cm}^3$).

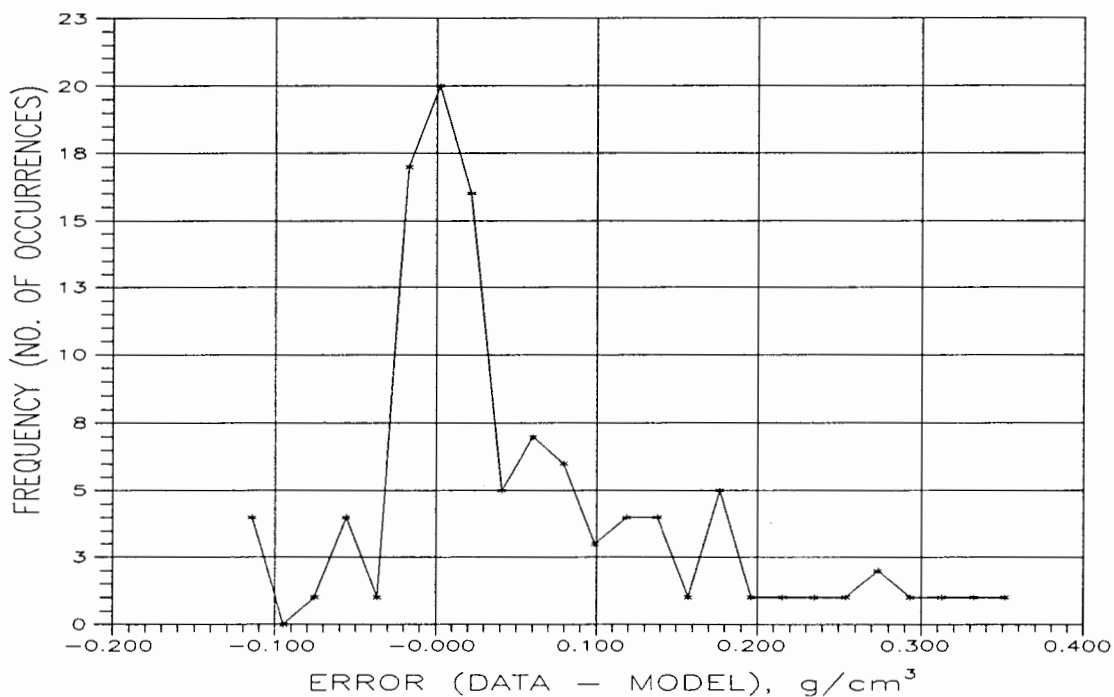


Figure 38. Error frequency histogram for run PMK6, from paired data-model observations of porosity and time as in Figure 37.

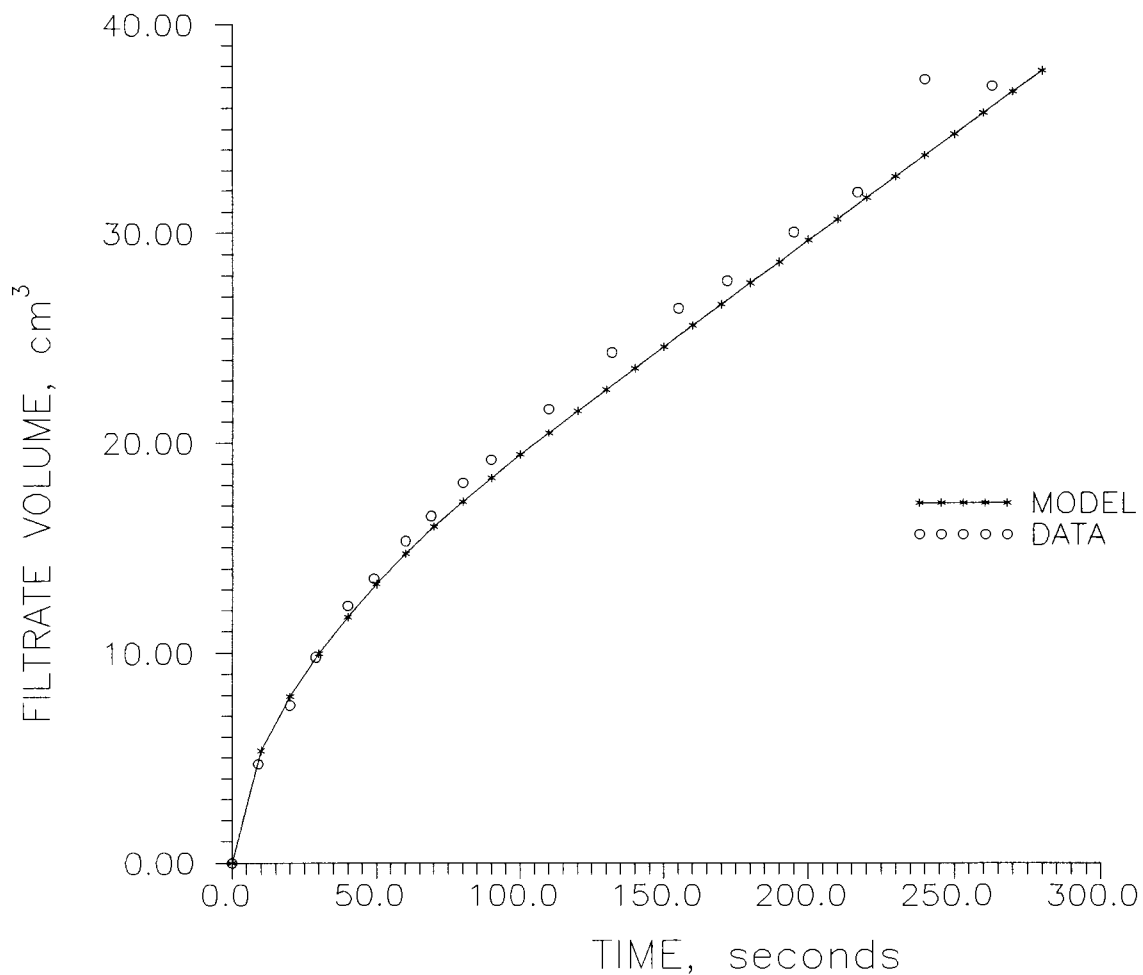


Figure 39. Data-model comparison of filtrate production with time under conditions of CHES run PMK6 (682 kPa, 0.47 g/cm³).

TABLE V

STATISTICS FROM DATA-MODEL COMPARISON OF POROSITY AND
DISTANCE OVER TIME ($c_i=0.47 \text{ g/cm}^3$)

CHESS RUN	Number of Comparisons	Mean Error	Standard Deviation of Error	Skewness	Coef. of Variation
KDMK8	866	0.031	0.148	-3.540	4.745
KDM6	496	-0.001	0.104	-2.105	-88.52
KDM4	232	-0.025	0.103	-1.859	-4.075
PMK9	199	-0.066	0.084	1.779	-1.279
PMK6	108	0.036	0.078	1.122	2.140

The model also slightly underpredicted the final suspended solids concentration for run KDMK8. Comparing this result to the results of run KDM6 reveals an apparent inconsistency in the data. The CHESS data show that the final suspended solids concentration of the lower pressure experiment (KDMK8) is higher than the final concentration for run KDM6 (higher pressure), which doesn't make sense physically, unless the sludge has a preferred pressure for best dewaterability. It is therefore possible that this inconsistency is due to experimental and not model error.

The results of simulation experiments and model-data comparisons for a suspension with an initial concentration of 0.14 g/cm^3 are shown in Tables VI and VII and Figures 40-54. As before, input to the model includes a porosity profile resulting from a period of gravity sedimentation. Again, more detailed summaries of the simulation results can be found in

Appendix B.

TABLE VI

SUMMARY OF RESULTS FROM COMPUTER SIMULATIONS USING WELLS
CAKE FILTRATION MODEL ($c_i=0.14 \text{ g/cm}^3$)

CHESS RUN	P_{app} (kPa)	Temp. (° C)	CPU* Time (Sec.)	Cake Form. Time (Sec.)	Simula- tion Time (Sec.)	Terminal Porosity
KDM7	103	26.0	63.5	131.4	517.0	0.5750
KDM5	172	26.0	63.0	101.4	382.5	0.5572
KDM3B	345	26.0	60.7	71.5	255.2	0.5331
PMK10	517	24.0	63.6	60.0	214.7	0.5192
PMK7	682	24.0	67.1	51.6	184.2	0.5096

* Using a Tektronix XD88/10 UNIX workstation

The results of simulations at the initial suspended solids concentration of 0.14 g/cm^3 are somewhat mixed. The experimental data of CHESS run PMK10 seems to be from an experiment conducted at a lower pressure than 517 kPa, since the final suspended solids concentration is lower than that for the experiment run at 103 kPa (KDM7). The model consistently predicts a slower rate of filtrate production, although it does a very good job of predicting the total amount of filtrate produced. The filtrate production rate is related to v_0 , Equation , which is calculated from the ratio of k/m_v and the porosity gradient at $z=0$. Because the k/m_v ratio is involved in the calculation, the deviation of model predictions of filtrate volume versus time from experimental

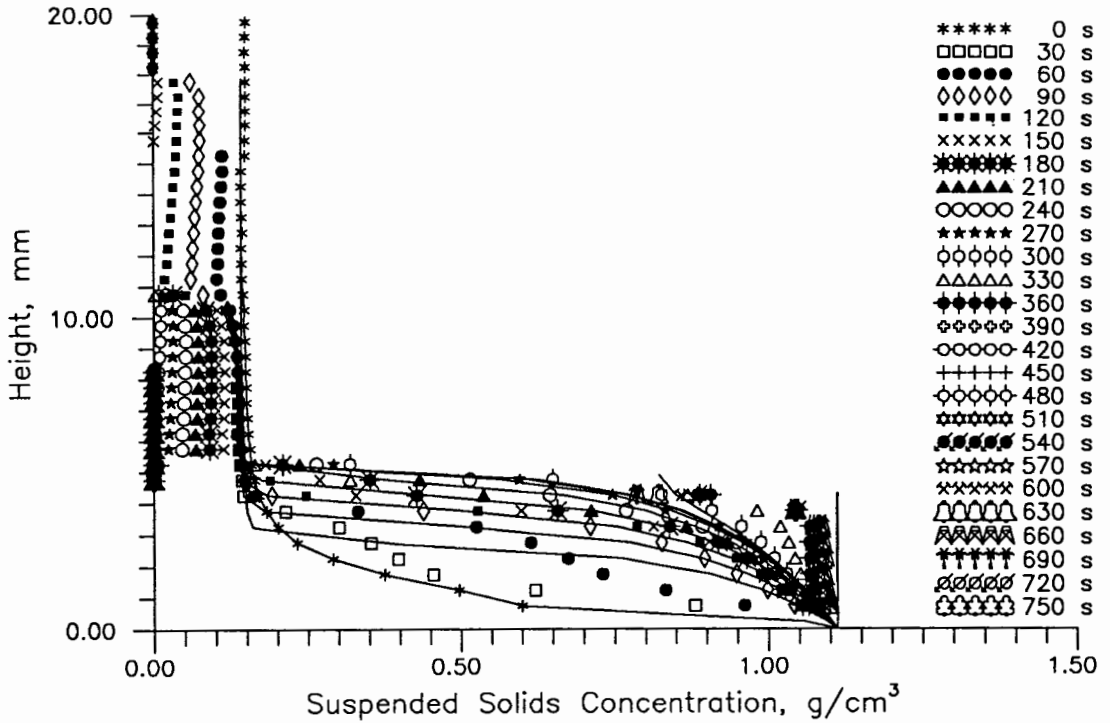


Figure 40. Data-model comparison of concentration profiles at 30 s intervals under conditions of CHES run KDM7 (103 kPa, 0.14 g/cm³).

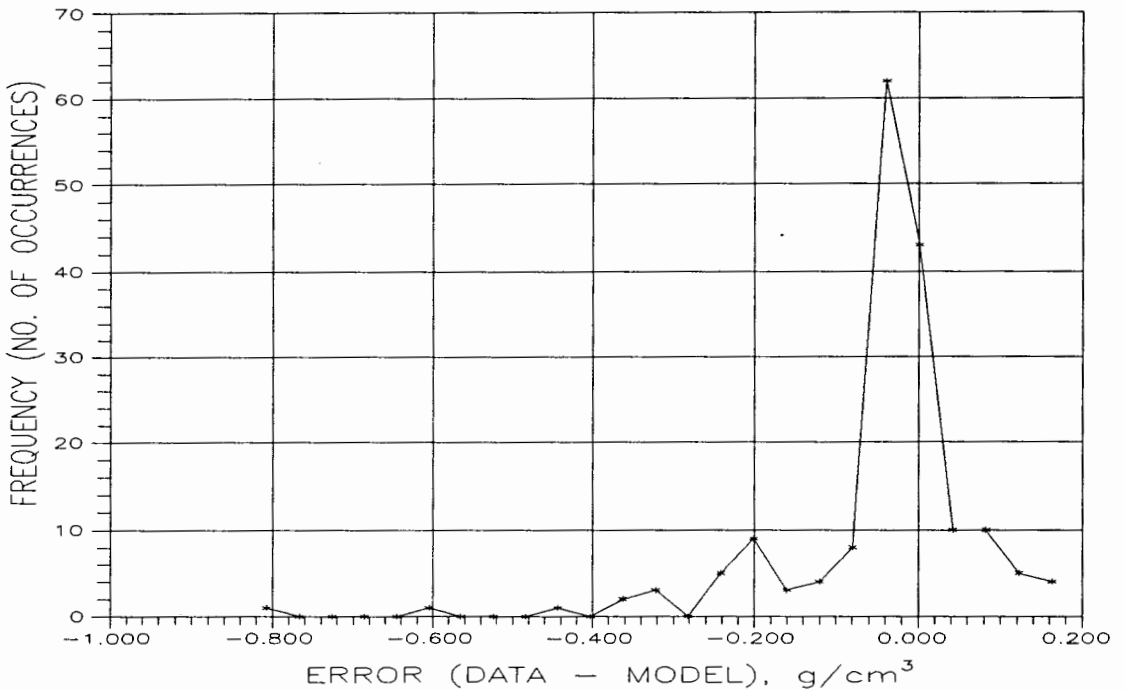


Figure 41. Error frequency histogram for run KDM7, paired data-model observations of porosity and time as in Figure 40.

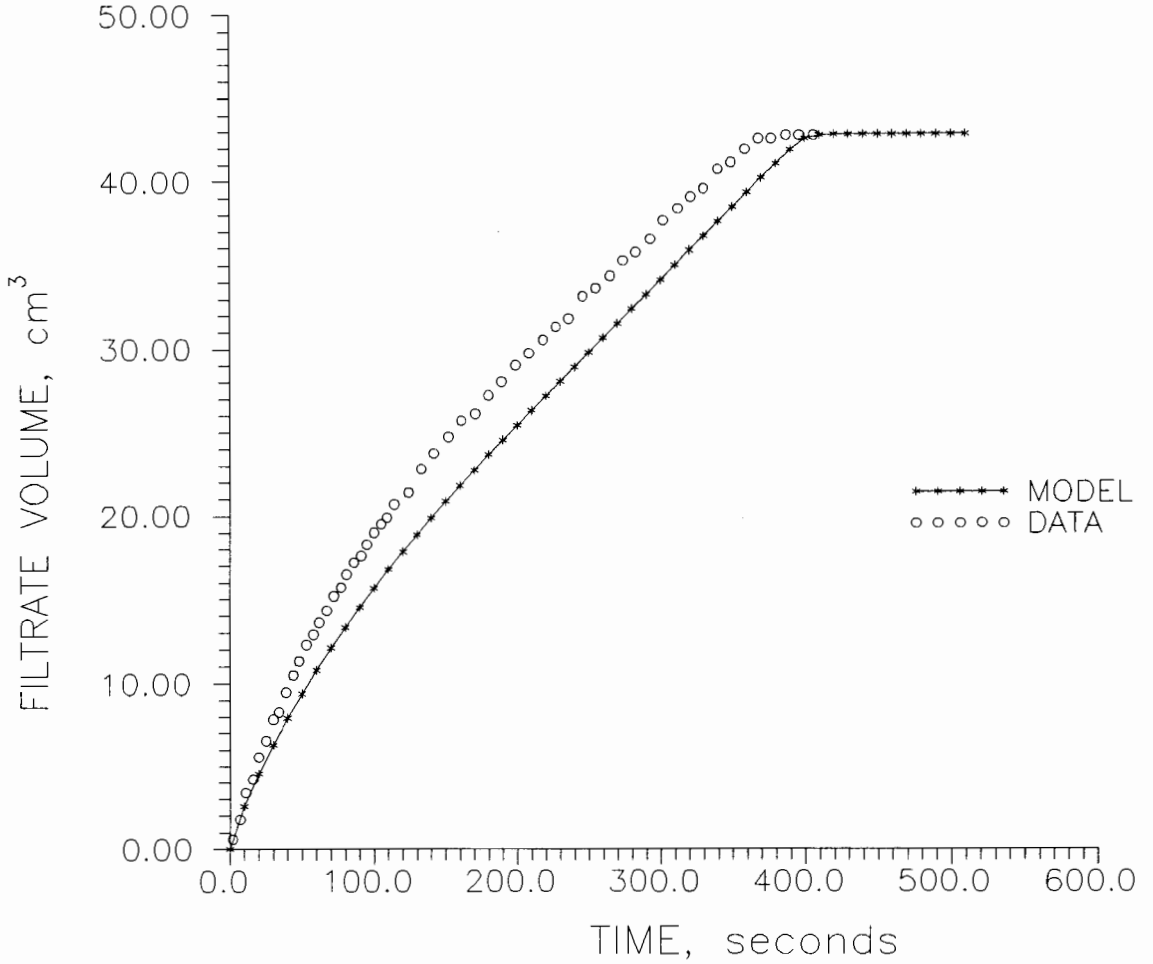


Figure 42. Data-model comparison of filtrate production with time under conditions of CHES run KDM7 (103 kPa, 0.14 g/cm³).

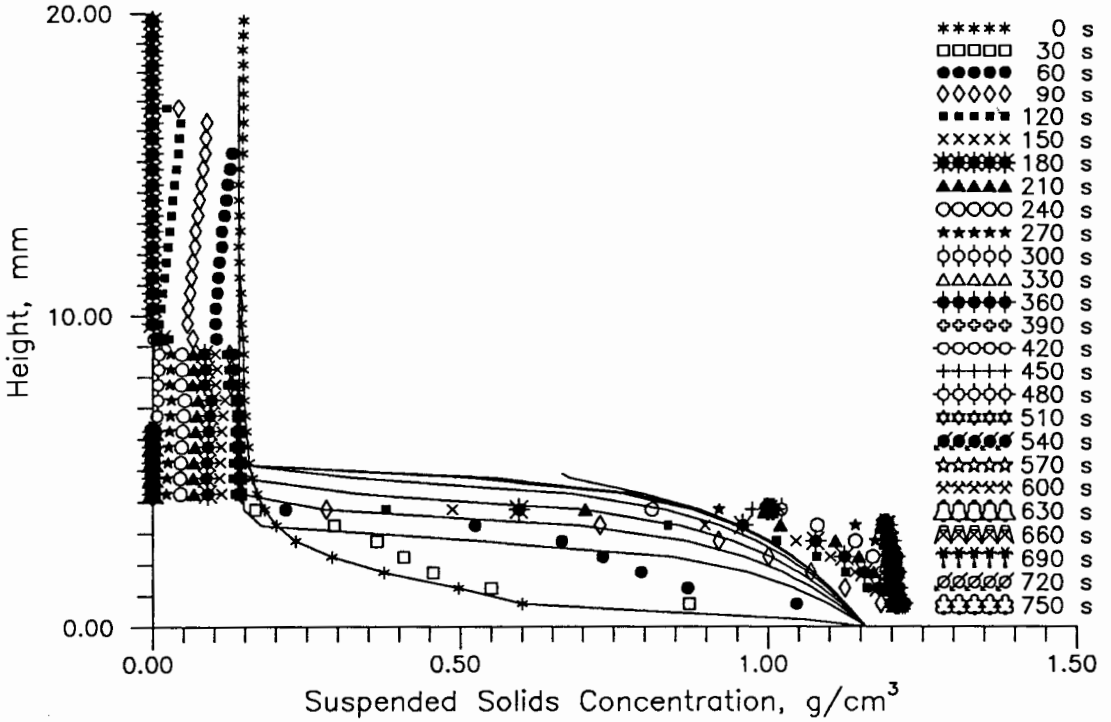


Figure 43. Data-model comparison of concentration profiles at 30 s intervals under conditions of CHES run KDM5 (172 kPa, 0.14 g/cm³).

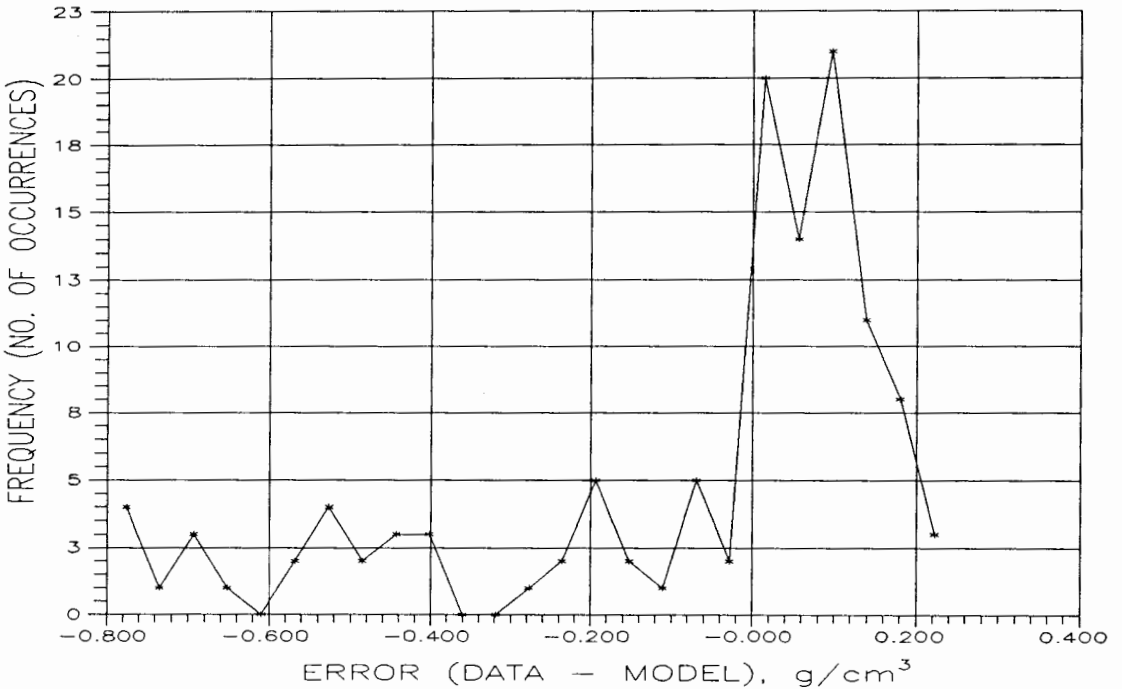


Figure 44. Error frequency histogram for run KDM5, paired data-model observations of porosity and time as in Figure 43.

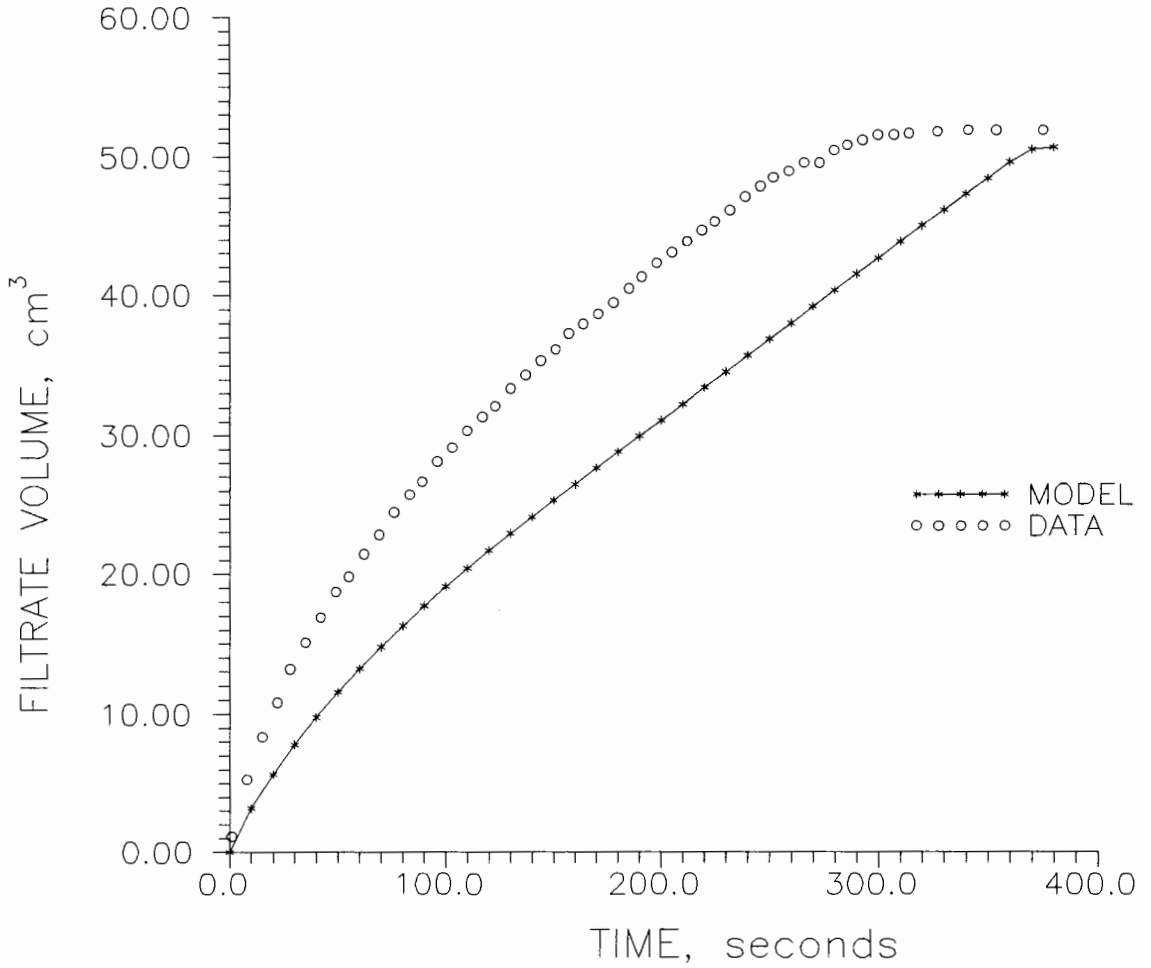


Figure 45. Data-model comparison of filtrate production with time under conditions of CHES run KDM5 (172 kPa, 0.14 g/cm³).

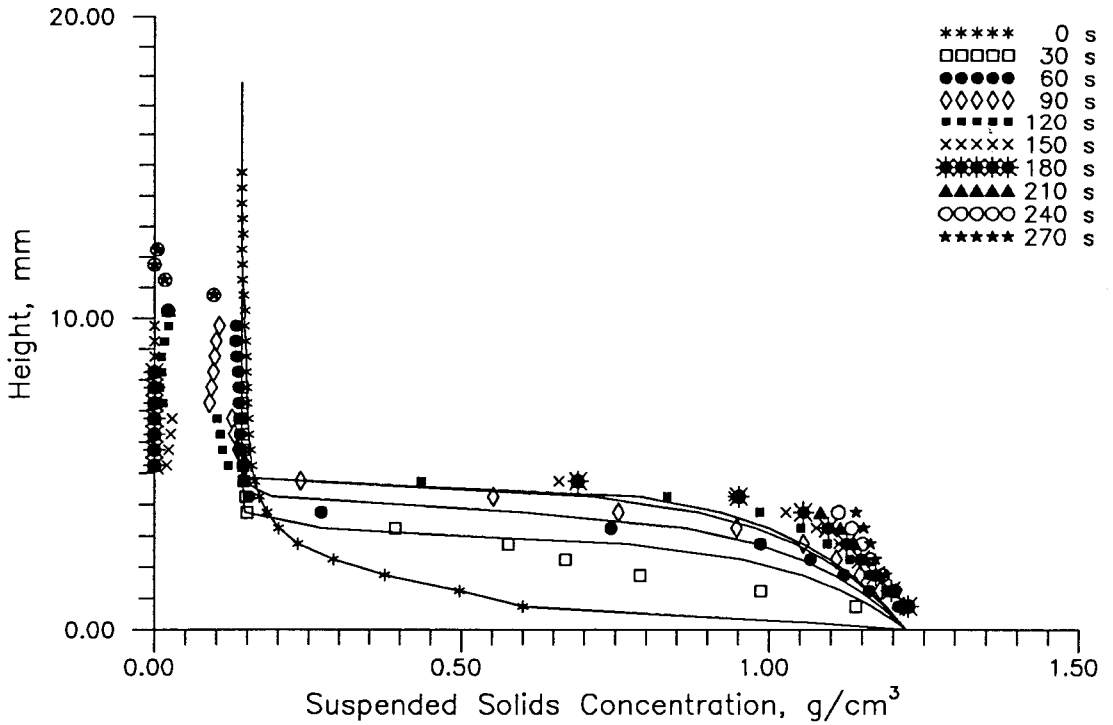


Figure 46. Data-model comparison of concentration profiles at 30 s intervals under conditions of CHES run KDM3B (345 kPa, 0.14 g/cm³).

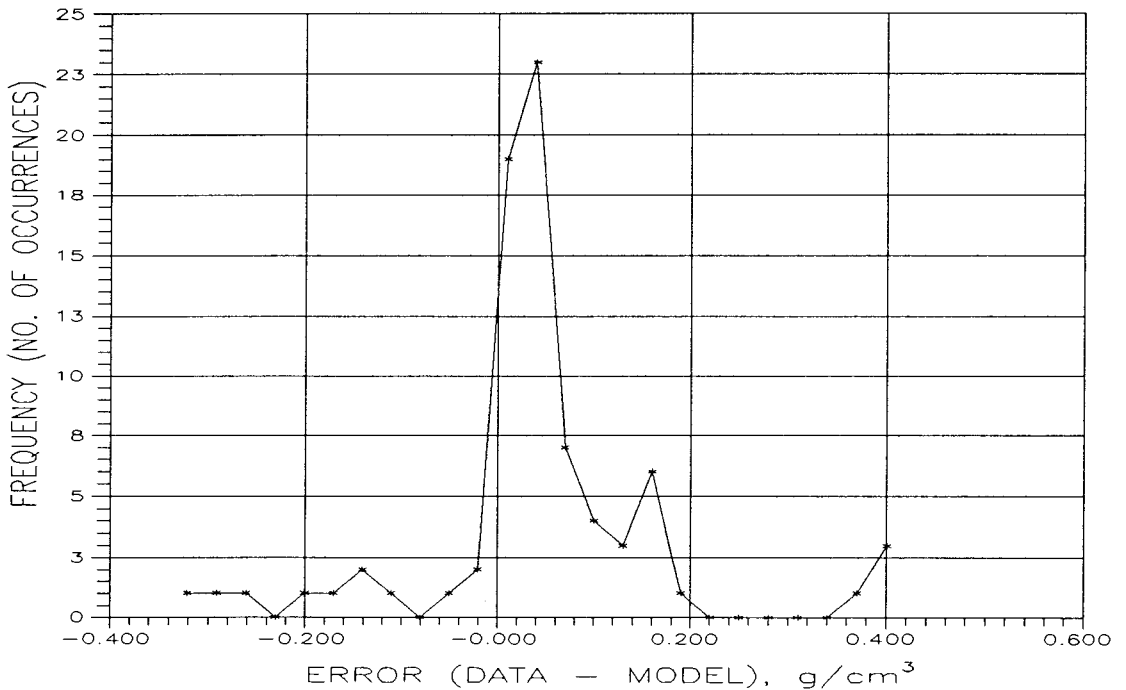


Figure 47. Error frequency histogram for run KDM3B, paired data-model observations of porosity and time as in Figure 46.

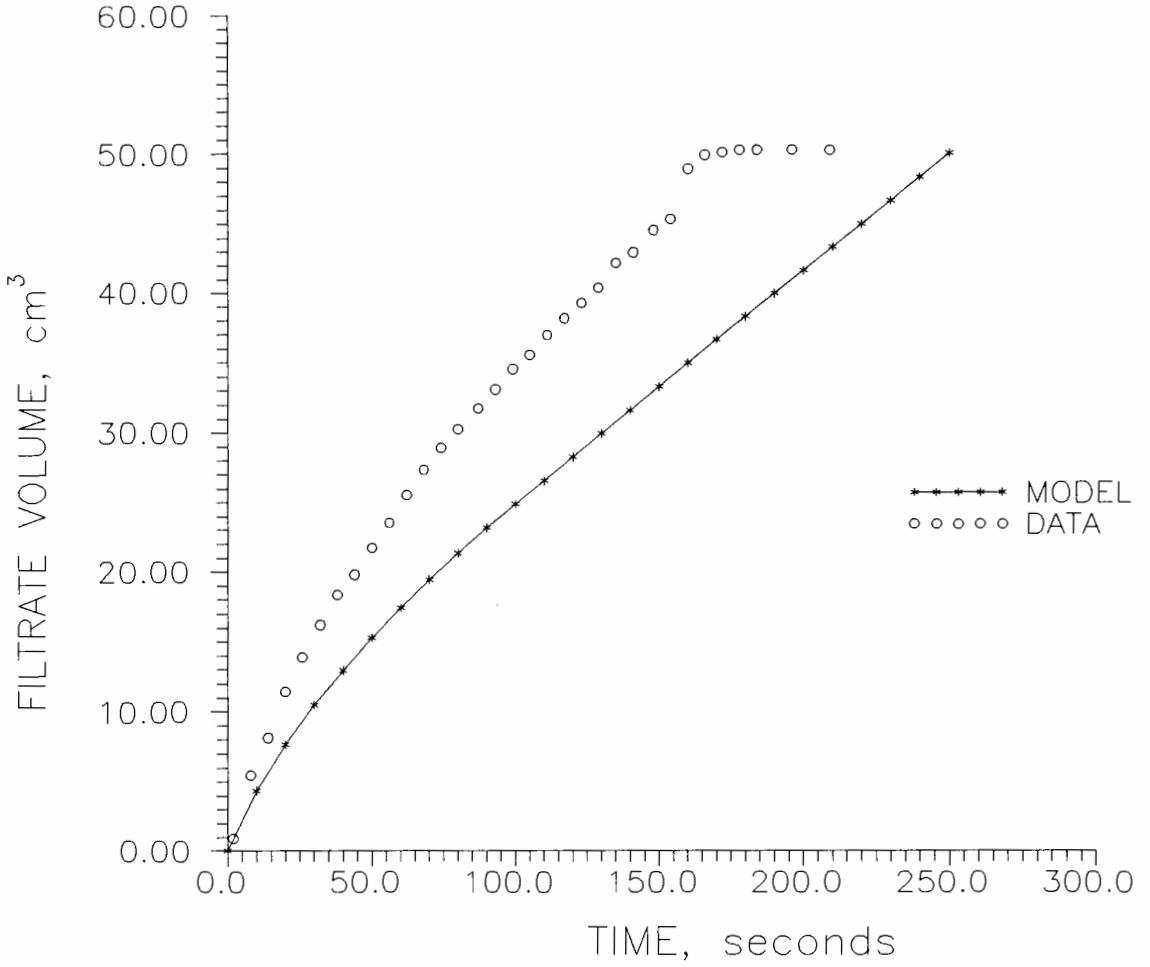


Figure 48. Data-model comparison of filtrate production with time under conditions of CHES run KDM3B (345 kPa, 0.14 g/cm³).

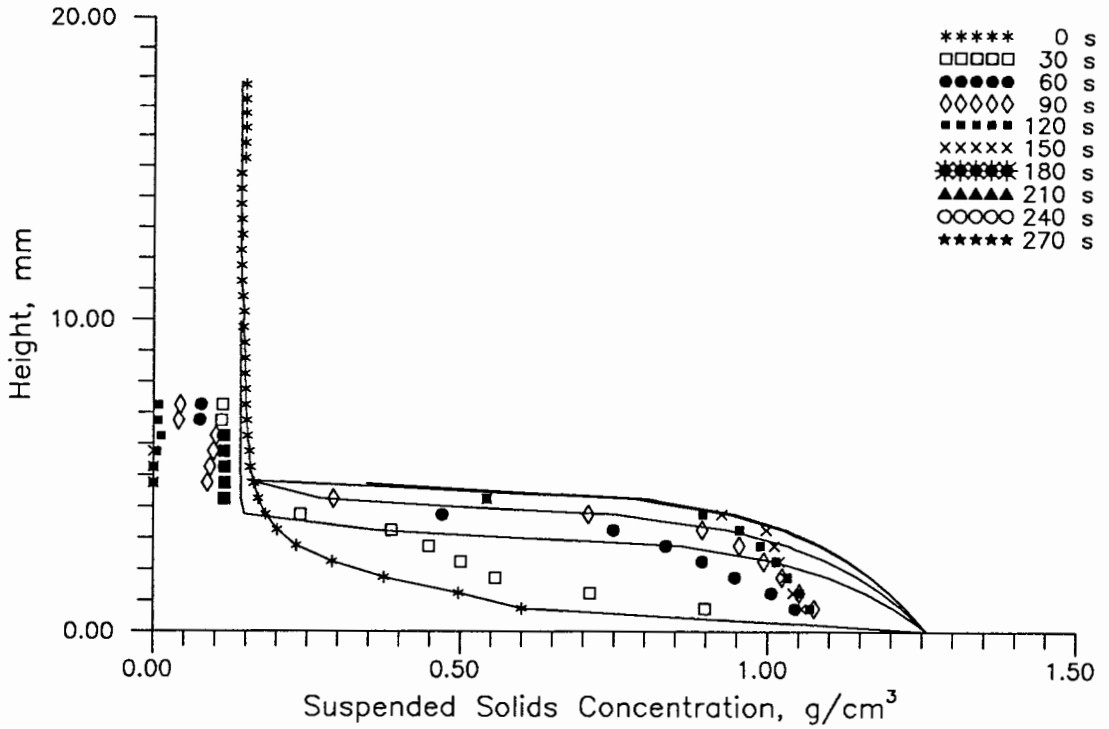


Figure 49. Data model comparison of concentration profiles at 30 s intervals under conditions of CHES run PMK10 (517 kPa, 0.14 g/cm³).

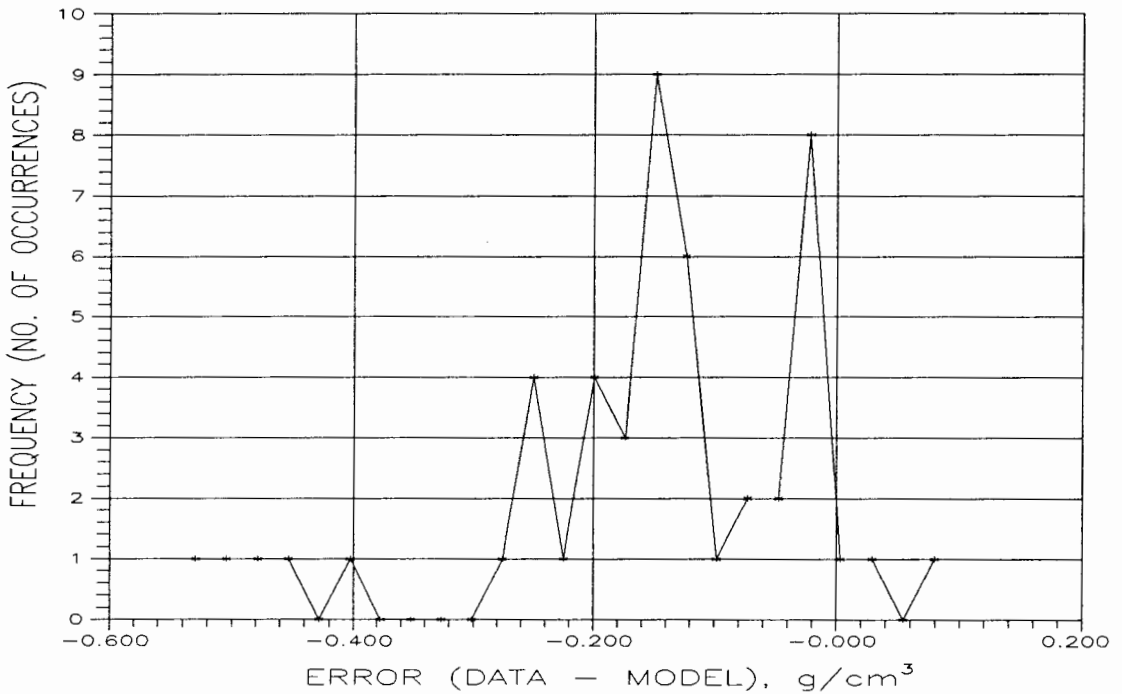


Figure 50. Error frequency histogram for run PMK10, paired data-model observations of porosity and time as in Figure 49.

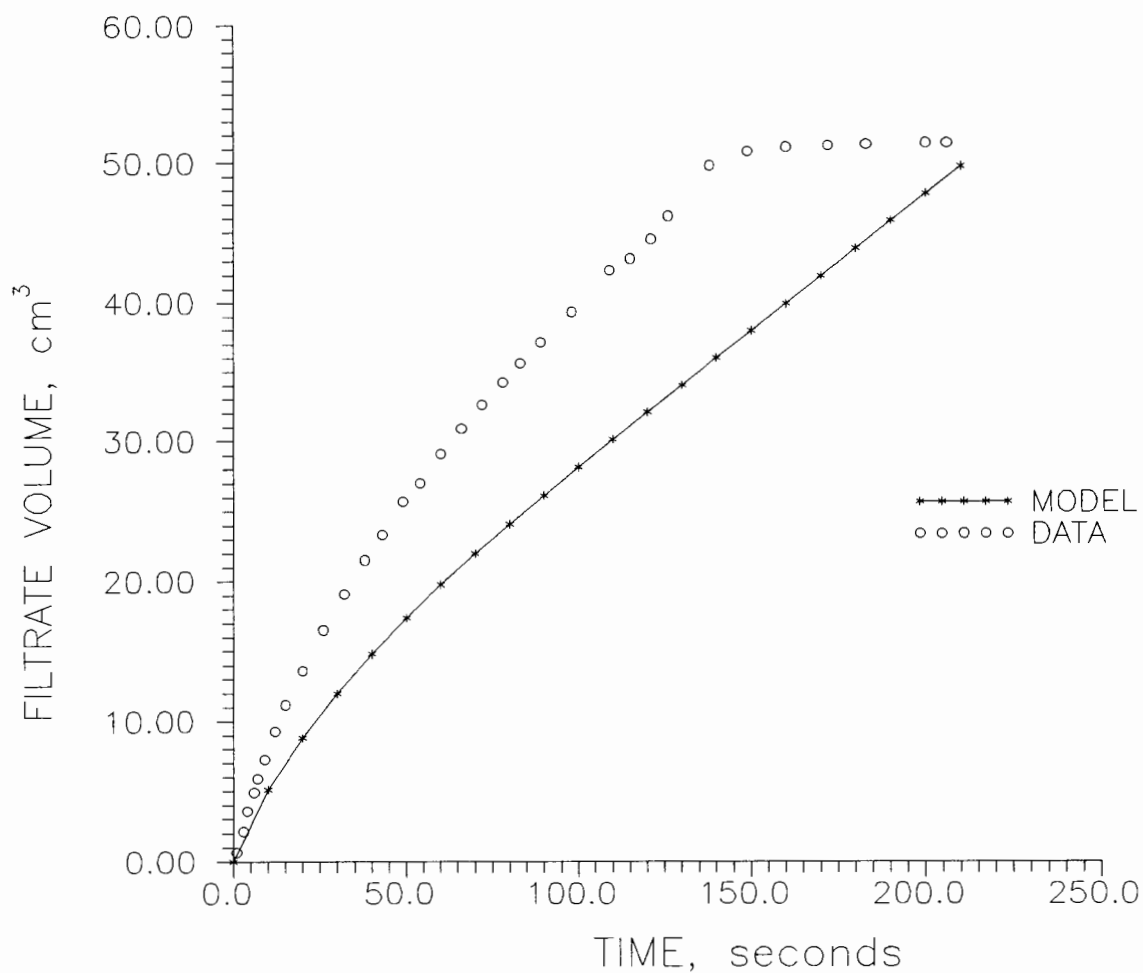


Figure 51. Data-model comparison of filtrate production with time under conditions of CHES run PMK10 (517 kPa, 0.14 g/cm³).

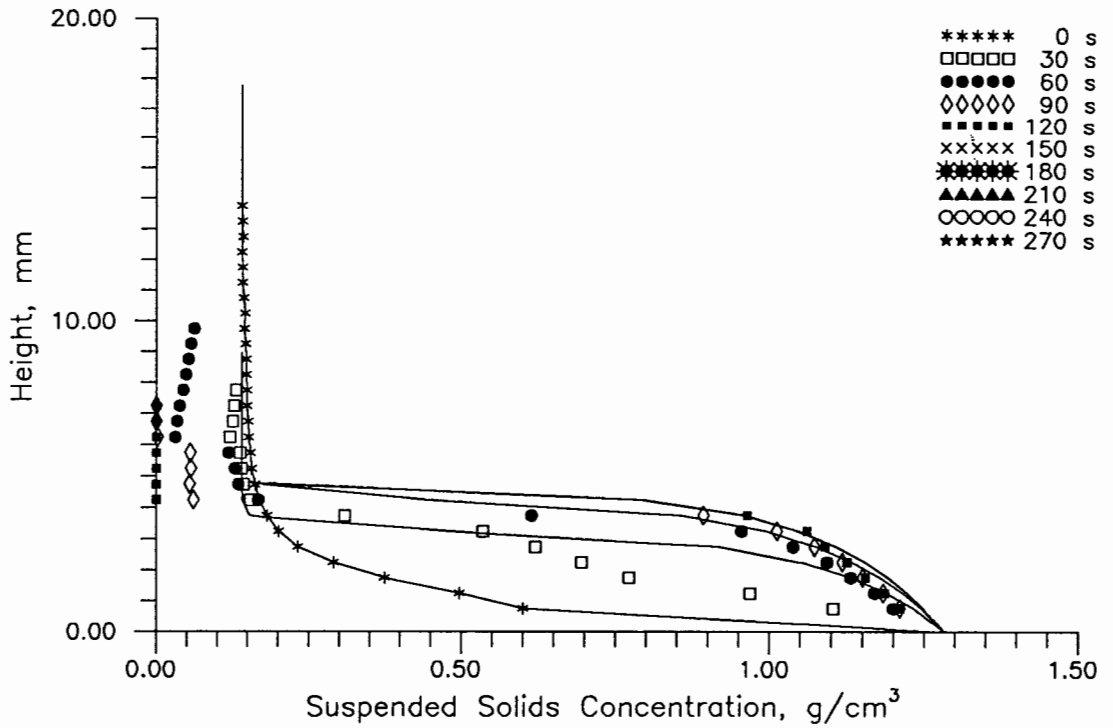


Figure 52. Data-model comparison of concentration profiles at 30 s intervals under conditions of CHES run PMK7 (682 kPa, 0.14 g/cm³).

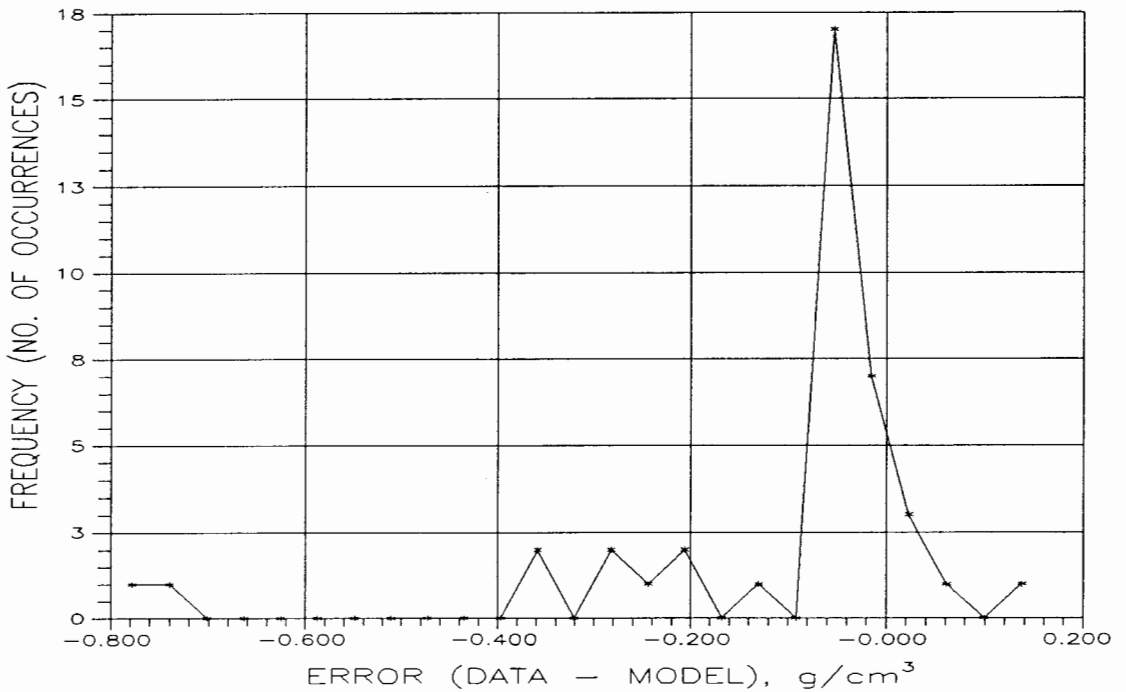


Figure 53. Error frequency histogram for run PMK7, paired data-model observations of porosity and time as in Figure 52.

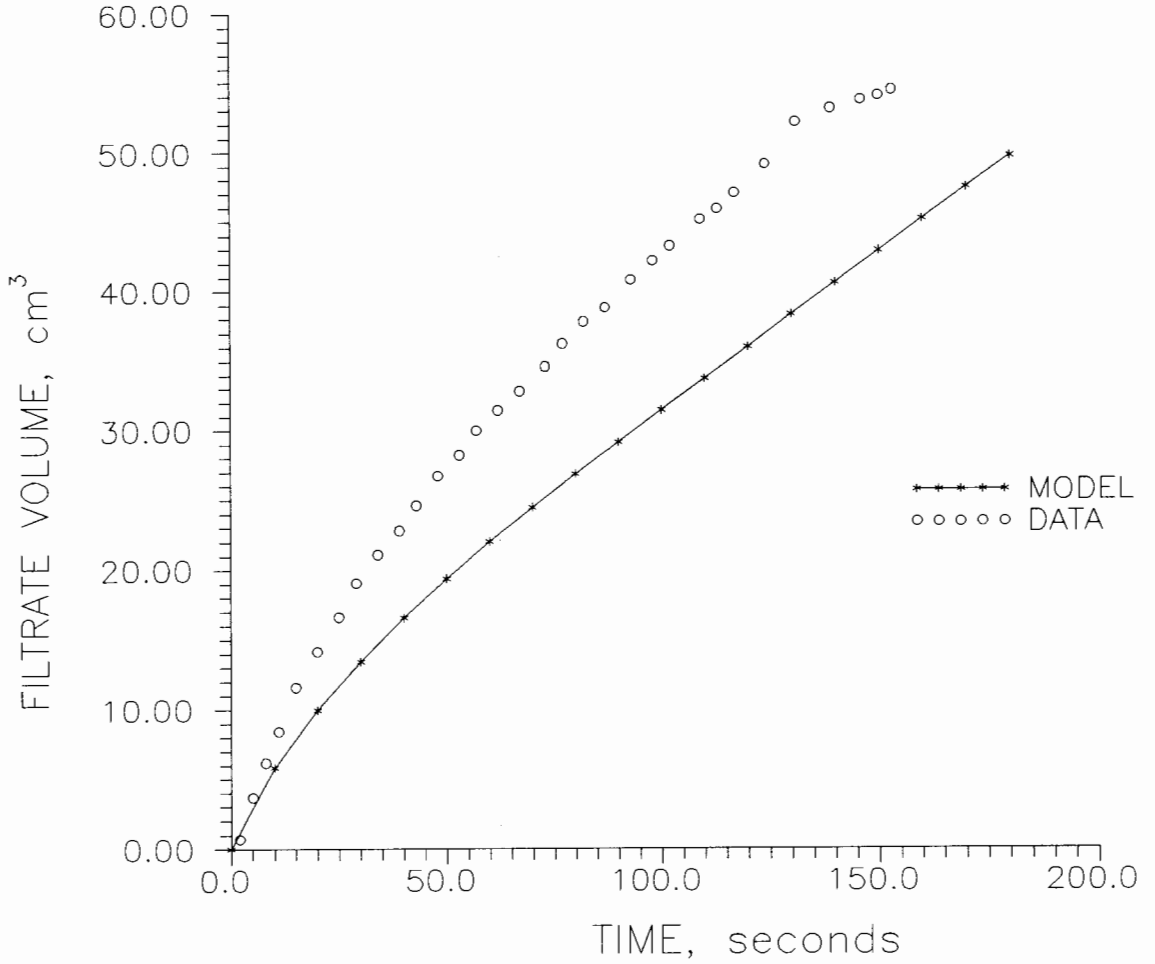


Figure 54. Data-model comparison of filtrate production with time under conditions of CHES run PMK7 (682 kPa, 0.14 g/cm³).

TABLE VII

STATISTICS FROM DATA-MODEL COMPARISON OF POROSITY AND
DISTANCE OVER TIME ($c_i=0.14 \text{ g/cm}^3$)

CHESS RUN	Number of Comparisons	Mean Error	Standard Deviation of Error	Skewness	Coef. of Variation
KDM7	171	-0.045	0.125	-2.579	-2.794
KDM5	118	-0.079	0.274	-1.264	-3.457
KDM3B	78	0.043	0.127	0.333	2.982
PMK10	49	-0.159	0.137	-1.086	-0.859
PMK7	44	-0.106	0.190	-2.265	-1.796

data indicates that the constitutive relationships may be inaccurate at this concentration. The suspended solids concentration of 0.14 g/cm^3 equates to a porosity of 0.946. The plot of σ' versus porosity (Figure 4) shows that the constitutive equation deviates significantly from the CHESS data at this porosity. This may explain the decreased accuracy. The data-model comparison of filtrate volume versus time indicates that the ratio of k/m_v predicted by the model at this initial concentration should be higher.

The CHESS data show some inconsistencies in the final suspended solids concentrations. For example, the final suspended solids concentration of run PMK7 (highest pressure) does not vary significantly from two tests using lower pressures (KDM3B and KDM5), but there is a big jump in the final suspended solids concentration for run KDM7. The model predicts a more consistent change in the final concentration

with changing pressure. The discrepancy between the model's prediction and the experimental data is most evident (discounting the CHESS data for run PMK10) for run KDM5. The model does, however, predict that the final suspended solids concentration for the highest and lowest pressure runs rather closely. More experimental testing would have to be conducted at the same pressures and initial suspended solids concentration to be able to conclude that either the data or the model are incorrect.

SIMULATIONS WITH UNIFORM INITIAL POROSITY PROFILES

Simulations were also conducted using constant initial porosity profiles as input to the mathematical model as opposed to previous runs in which the porosity profiles were the result of a period of gravity sedimentation.

Since it is not always possible to obtain an accurate sedimentation profile at the time pressure is applied to the solid-liquid suspension, it would be good if the model could give accurate results for a constant initial porosity profile.

Table VIII gives a summary of model output for simulations in which the initial porosity was constant. Realistic results were only obtained for CHESS run KDMK8, therefore figures are presented for this run only. The conditions under which the simulations were performed were the same as those of the CHESS experiments except for the initial uniform porosity profile.

TABLE VIII

SUMMARY OF RESULTS FROM COMPUTER SIMULATIONS USING WELLS
CAKE FILTRATION MODEL WITH UNIFORM INITIAL POROSITY
DISTRIBUTIONS

CHESS RUN	P_{app} (kPa)	CPU* TIME (S)	CAKE FORM. TIME (S)	END OF RUN (S)	FILT. VOL. (cm ³)	Δt_{ave} (S)
$c_i=0.47$						
KDMK8	103	115	387.7	900.0	37.5	4.8×10^{-2}
KDM6	172	34	13.5	13.8	58.8	2.9×10^{-3}
KDM4	345	64	7.7	7.9	58.8	8.5×10^{-4}
PMK9	517	89	6.1	6.2	58.9	4.8×10^{-4}
PMK6	682	112	5.0	5.1	58.8	3.2×10^{-4}
$c_i=0.31$						
KDMK9	103	134	11.4	11.8	56.7	5.7×10^{-4}
KDM2	172	255	8.6	8.8	59.8	2.7×10^{-4}
PMK3	345	323	5.3	5.5	55.1	1.1×10^{-4}
PMK4	517	436	4.2	4.3	55.1	6.4×10^{-5}
PMK5	682	625	3.8	3.9	59.7	4.4×10^{-5}
$c_i=0.14$						
KDM7	103	858	10.6	10.9	59.0	7.3×10^{-5}
KDM5	172	1629	6.8	7.0	59.0	2.8×10^{-5}
KDM3B	345	2663	4.6	4.7	59.0	1.2×10^{-5}
PMK10	517	3542	3.8	3.9	59.0	7.2×10^{-6}
PMK7	682	4302	3.2	3.3	59.0	5.1×10^{-6}

* Using a Tektronix XD88/10 UNIX workstation

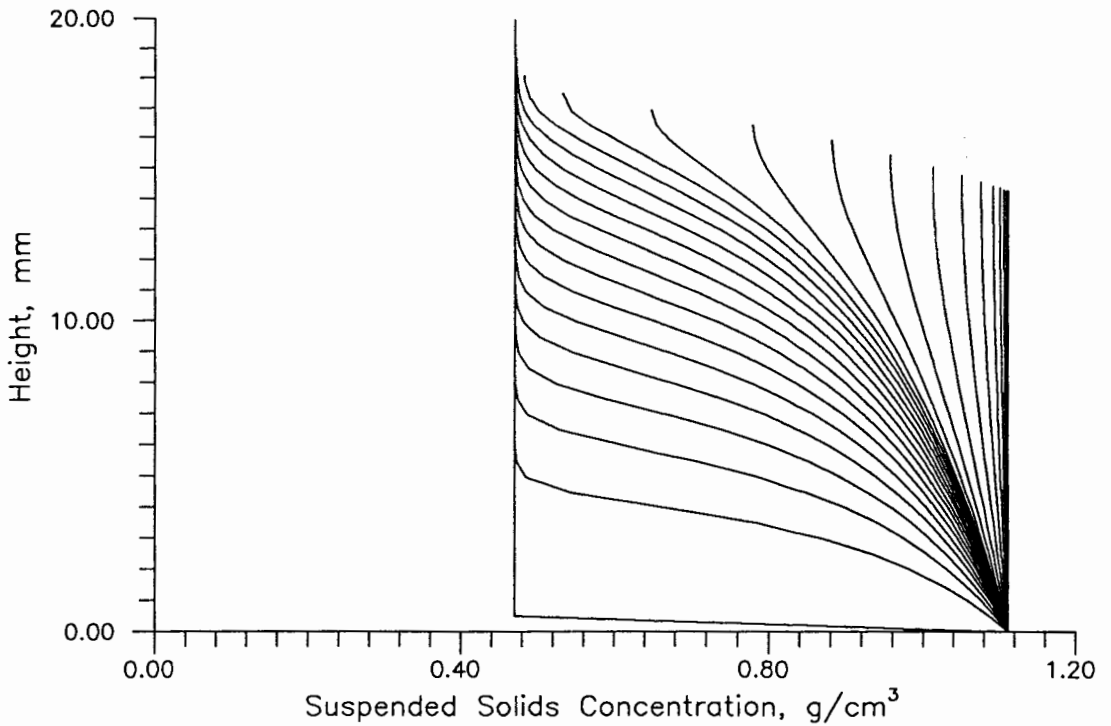


Figure 55. Concentration profiles at 30 s intervals under conditions of CHES run KDMK8 with uniform initial porosity profile as predicted by Wells (1990a) dewatering model.

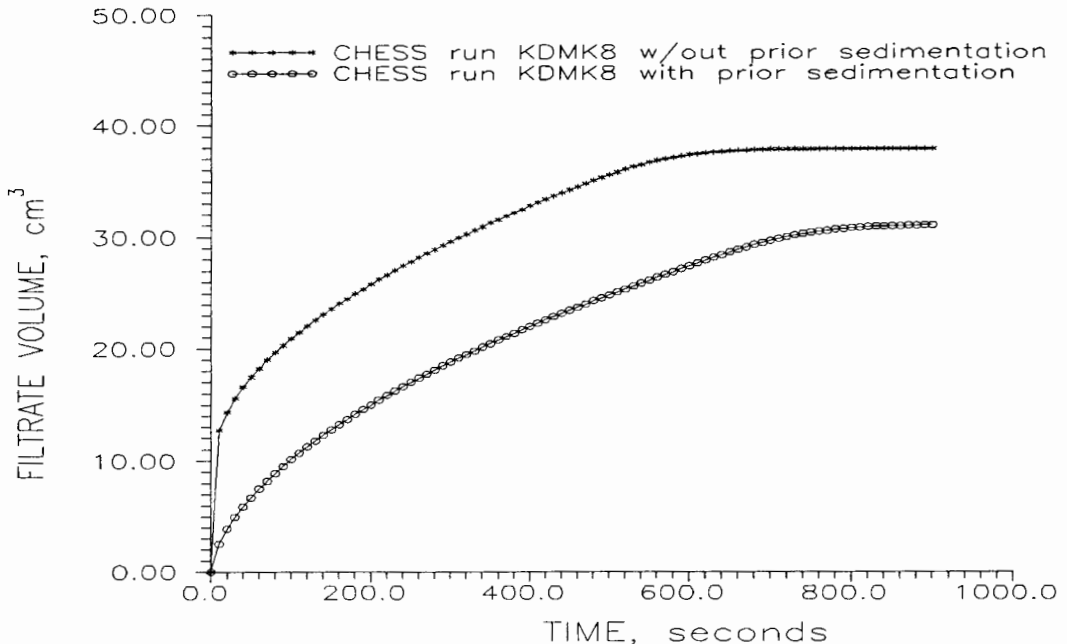


Figure 56. Filtrate production versus time for conditions of CHES run KDMK8 with and without prior gravity sedimentation as predicted by Wells (1990a) dewatering model.

Use of a constant initial porosity as input to the dewatering model results in a large initial porosity gradient, $\partial n/\partial z$. Table VIII shows the effect of a high porosity gradient on the model's performance. Comparing these results to those of the previous section, three significant changes can be observed: 1) The runs end after a very short simulation time; 2) The total filtrate volume is greatly increased; and 3) The time step is much smaller. All three results can be traced to the high porosity gradient.

During each iteration, the time step, Δt , required to maintain stability is calculated. The time step used in the numerical scheme is taken as the minimum value obtained from

$$\Delta t \leq \frac{\phi \Delta z^2}{2\chi} \quad (48)$$

$$\Delta t \leq \frac{\phi \Delta z^2}{n_0 v_0 \Delta z + 2\chi} \quad (49)$$

and

$$\Delta t \leq \frac{\phi 2\chi}{(n_0 v_0)^2} \quad (50)$$

where

ϕ = numerical stability factor between 0 and 1

$$\chi = \frac{k_{j+\frac{1}{2}}(1-n_{j+\frac{1}{2}})}{m_{v_{j+\frac{1}{2}}}\mu}$$

$k_{j+\frac{1}{2}}$ = permeability at node $j+\frac{1}{2}$

$$m_{v_{j+\frac{1}{2}}} = \text{coefficient of volume compressibility at } j+\frac{1}{2}$$

$$n_{j+\frac{1}{2}} = \text{porosity at node } j+\frac{1}{2}$$

As stated previously the grid spacing Δz was reduced to decrease numerical diffusion and increase numerical accuracy, therefore Δt tends to be small. Also, v_0 is linearly proportional to the porosity gradient, so a large porosity gradient will result in a smaller time step.

In addition, the larger value of v_0 causes the value of the filtrate production rate to increase. More filtrate is produced per unit of time. The run ends early because all of the liquid is filtered in a much shorter period of time, and the breakthrough porosity is reached sooner. The higher filtrate production rate is an expected result for filtration runs with an initially uniform porosity since there is initially less resistance to filtration due to the lower initial suspended solids concentration near the filter medium. The total filtrate produced should not change much, if at all, given the same initial amount of liquid. The total filtration time would be expected to be somewhat shorter, but not to the extent predicted by the Wells (1990a) model in every case except CHES run KDMK8. For a uniform initial concentration, run KDMK8 had the lowest initial porosity gradient of all the simulations tested, and probably represents a border line of numerical stability and accuracy for the model, given the initial concentration, applied pressure, and constitutive

relationships.

The larger porosity gradient for these runs would magnify somewhat the effects of any errors in the constitutive equations. Also, since numerical errors are proportional to the porosity gradient, the larger porosity gradient may also be responsible for larger numerical errors.

Figures 57-60 compare the behavior of the porosity gradient for simulations at two different pressures for model runs with, and without prior sedimentation.

Figure 57 shows run KDMK8 with a nonuniform (prior sedimentation) initial porosity. The porosity gradient is initially large, but decreases very rapidly and the results of the model run as given in Figures 55 and 56 are good. Figure 59 shows the same run with a constant initial porosity. The initial porosity is again large to begin with, but not much higher than the simulation with prior gravity sedimentation. The gradient decreases, but not so rapidly as before. As mentioned before, the results of model runs for CHES run KDMK8 with a uniform initial porosity profile are reasonable.

Figure 59 shows the model calibration run, KDMK9, with prior sedimentation. The results for this run were given in Figures 10-12. Again, the gradient is large initially but drops off rapidly. Figure 60 shows the same run with a uniform initial porosity profile. The initial gradient is quite high again. The rate of decrease of the value of the porosity gradient is much slower though, and it levels off at

a high value. The results of model runs for KDMK9 without prior sedimentation are correspondingly inaccurate. The inaccuracy of the other model runs can similarly be traced to this behavior of the porosity gradient over time.

The effect of the porosity gradient on the advective and diffusive terms (see Equation 29) of the governing equation is shown in Figures 61 and 62. The two terms have opposite signs, and realistic results are obtained only as long as the negative diffusive term dominates, as in Figure 61, resulting in a decreasing porosity with time. When the porosity gradient is large, as in the case of an initially uniform porosity profile, the advective term may become equal to or greater than the diffusive term, as in Figure 62. When this happens, the porosity stops decreasing and may actually increase (which is physically impossible).

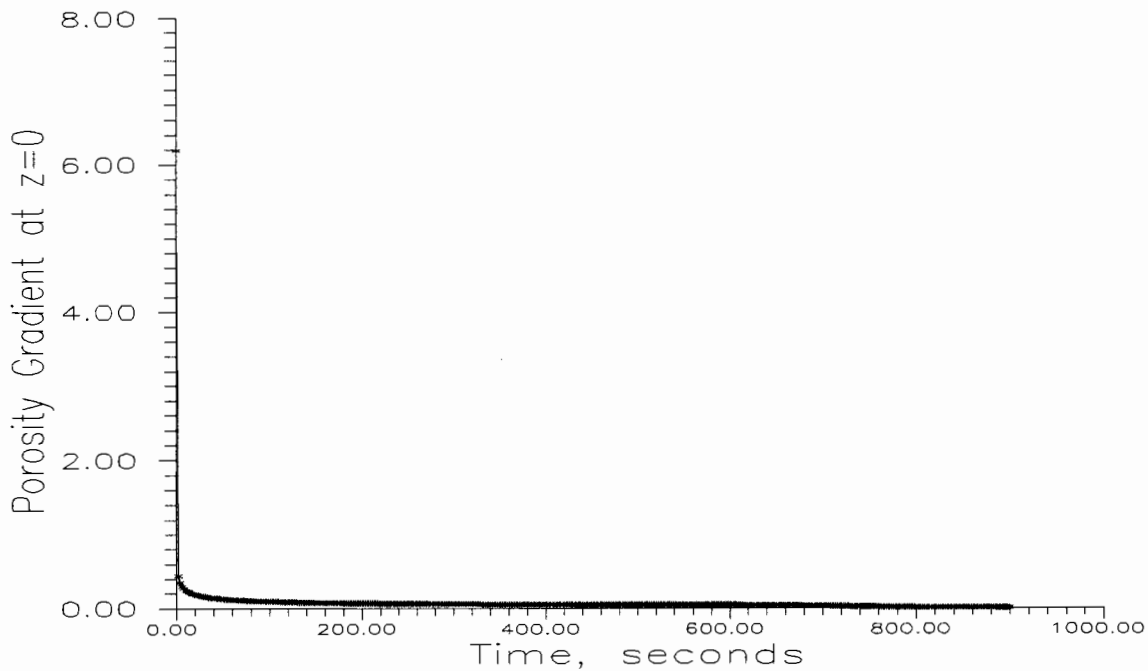


Figure 57. Plot of porosity gradient versus time for CHESS run KDMK8 with prior sedimentation.

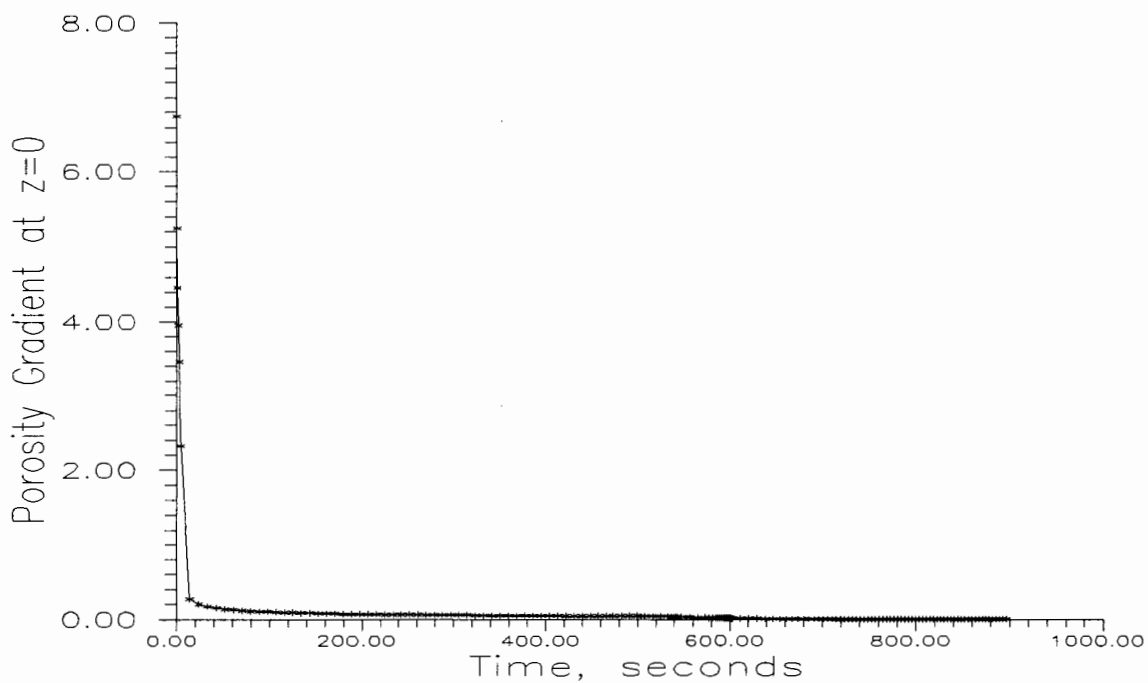


Figure 58. Plot of porosity gradient versus time for CHESS run KDMK8 without prior sedimentation.

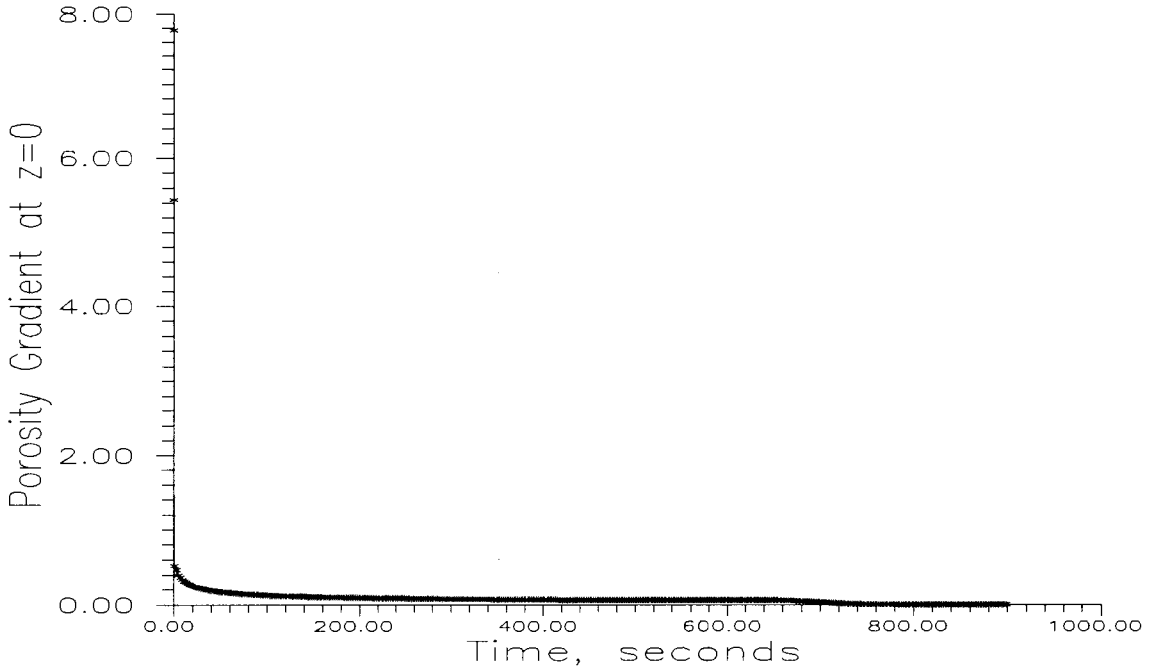


Figure 59. Plot of porosity gradient versus time for CHES run KDMK9 with prior sedimentation.

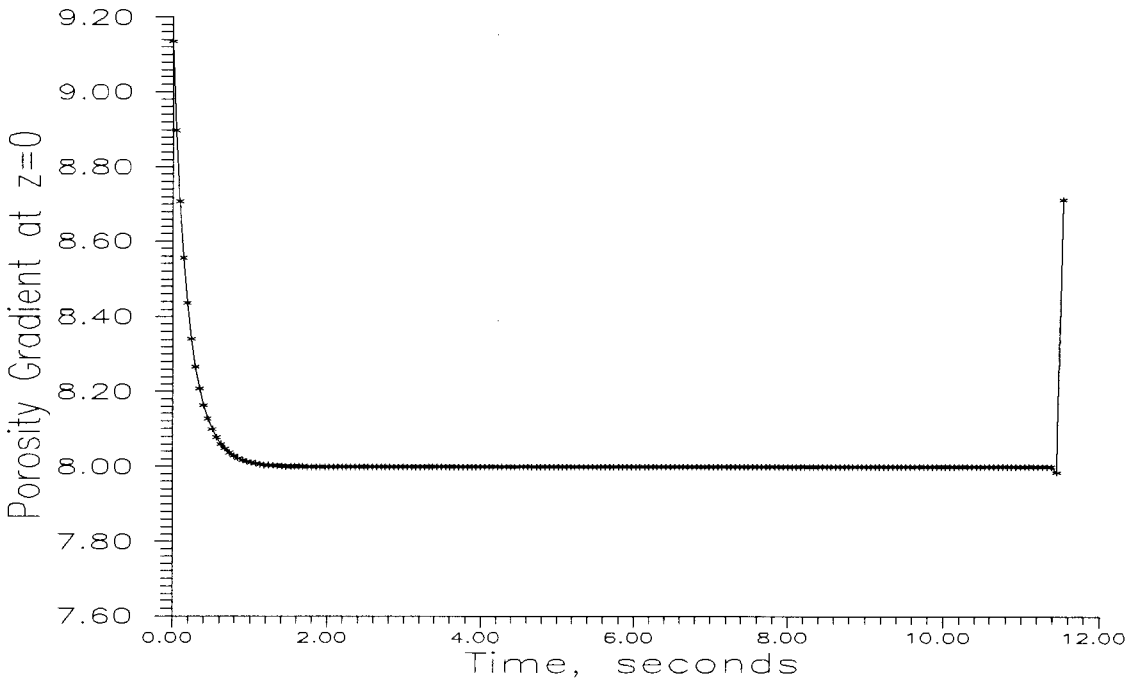


Figure 60. Plot of porosity gradient versus time for CHES run KDMK9 without prior sedimentation.

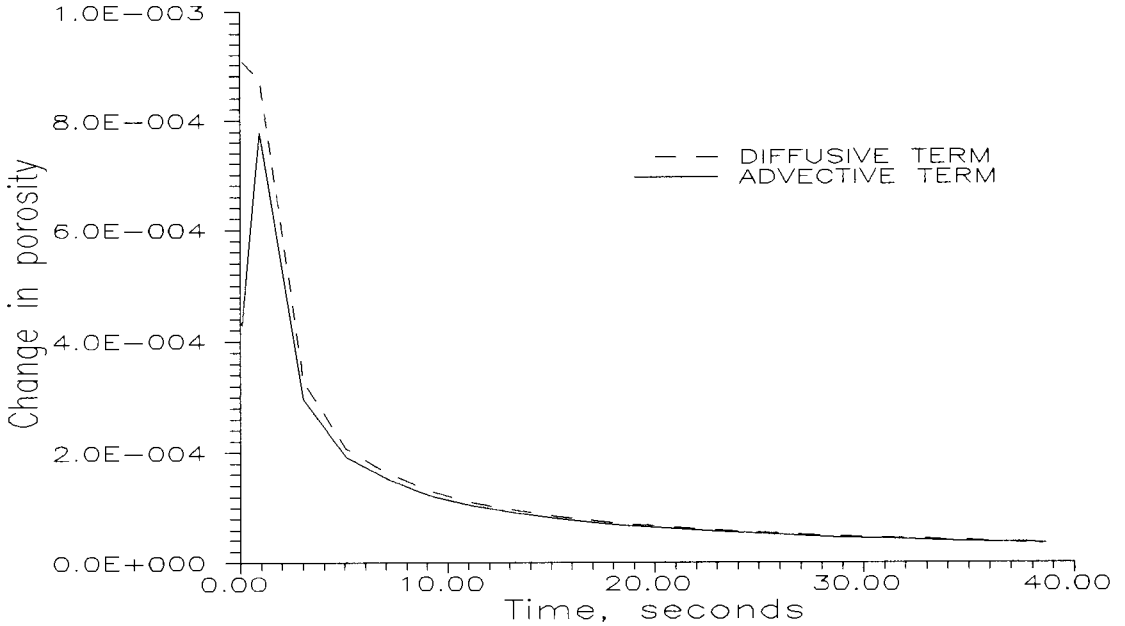


Figure 61. Plot of diffusive and convective terms of governing equation versus time for CHESS run KDMK8 with prior sedimentation at grid point number 2.

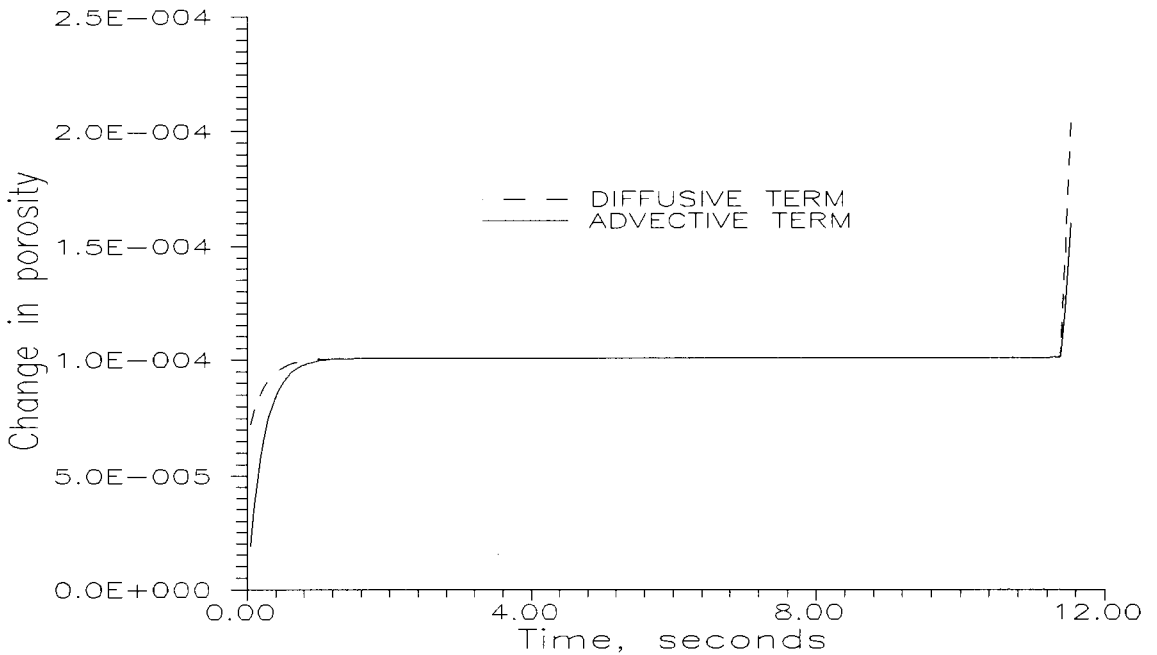


Figure 62. Plot of diffusive and convective terms of governing equation over time for CHESS run KDMK9 without prior sedimentation at grid point number 2.

CHAPTER VI

WELLS MODEL WITH ARTIFICIAL VISCOSITY

As observed in the previous chapter, the numerical solution technique outlined by Wells (1990a) can give inaccurate results when the initial porosity is uniform throughout the problem domain. The reason for this is the initial discontinuity in the porosity profile at $z=0$. Upon application of the external pressure gradient the porosity at the filter medium instantaneously changes from the initial porosity, n_i , to the terminal porosity, n_0 . This is shown in Figure 63.

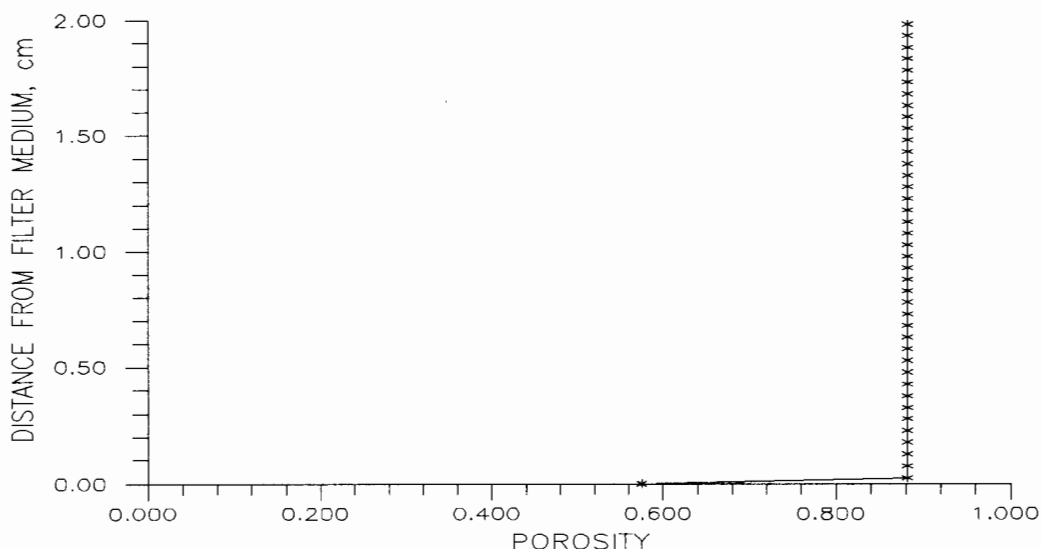


Figure 63. Porosity profile immediately after application of the external pressure gradient ($P_{app}=103$ kPa), for a slurry with an initially uniform porosity of 0.88.

The pore water pressure undergoes a similar change. Initially at zero, the pore water pressure immediately increases to the value of the applied pressure, P_{app} . Such rapid changes occurring across a very narrow region in space are termed shocks. They are manifested mathematically as discontinuities in the variables which describe the flow.

The discontinuity in the porosity results in a very large porosity gradient, $\partial n/\partial z$, at the filter medium. Depending upon the porosity gradient and the applied pressure, this may cause the numerical scheme to be unstable, or if stable, the time step may be very small, or numerical errors may cause the results to be inaccurate.

To effectively and accurately deal with shocks additional physical conditions need to be specified. Boundary conditions obtained from the Rankine-Hugoniot equations are one way to deal with shocks. They are difficult to apply in practice, however. Von Neumann and Richtmeyer (1950) developed a much simpler technique in which a dissipative mechanism is introduced into the governing equations upon which the numerical model is based. They called this technique the artificial viscosity, or pseudo-viscosity method. This method eliminates the need for boundary conditions on each side of the discontinuity. The shocks are smoothed out internally, automatically, whenever and wherever they occur, without unduly affecting the accuracy of the numerical scheme.

The dissipative mechanism takes the form of a nonlinear

pressure term, p_v , which is introduced entirely for mathematical, not physical, reasons. Therefore, p_v can be any convenient function, provided that certain requirements are satisfied [see von Neumann and Richtmeyer (1950)]. Von Neumann and Richtmeyer (1950), and Richtmeyer and Morton (1967) applied this concept to a compressible fluid in which the inertial terms of the one-dimensional fluid flow were significant. In the present study, the fluid is assumed to be incompressible and inertial terms are neglected, thus the form of the pseudo-viscous pressure equation is not the same as in their study. The pseudo-viscous pressure, p_v , is introduced directly into the equations governing the flow to dissipate the porewater pressure shock.

DERIVATION OF WELLS COMPRESSIBLE CAKE FILTRATION MODEL WITH ARTIFICIAL VISCOSITY

From Willis (1983) and Wells (1990a) the continuity equation for the liquid phase is

$$\frac{\partial n}{\partial t} - \frac{\partial}{\partial z}(nv_f) = 0 \quad (51)$$

where v_f is the vertical component of the true fluid velocity. Equivalently, the equation for continuity of the solid phase is

$$\frac{\partial n}{\partial t} + \frac{\partial}{\partial z}[(1-n)v_s] = 0 \quad (52)$$

where v_s is the vertical component of the true solid velocity. Combining Equations 51 and 52, integrating, and applying the boundary conditions of Figure 1 Wells (1990a) obtained a relationship between v_s and v_f as

$$v_s = \frac{n_0 v_0 - n v_f}{1-n} \quad (53)$$

The liquid momentum equation derived by Wells (1990a) is

$$F(v_f - v_s) = \frac{du}{dz} \quad (54)$$

where $F = \frac{n\mu}{k}$

Substituting Equation 53 into Equation 54 and solving for v_f

$$v_f = \frac{1-n}{F} \frac{du}{dz} + n_0 v_0 \quad (55)$$

Substituting Equation 55 into Equation 51 results in

$$\frac{\partial n}{\partial t} = \frac{\partial}{\partial z} \left[\frac{n(1-n)}{F} \frac{du}{dz} + n_0 v_0 \frac{\partial n}{\partial z} \right] \quad (56)$$

Again, from Wells (1990a)

$$\frac{du}{dz} = -\frac{d\sigma'}{dn} \frac{dn}{dz} \quad (57)$$

Adding the pseudo-viscous pressure and substituting the

definition of m_v from Equation 34 gives

$$\frac{d(u+p_v)}{dz} = \frac{1}{m_v} \frac{\partial n}{\partial z} \quad (58)$$

or

$$\frac{du}{dz} = \frac{1}{m_v} \frac{\partial n}{\partial z} - \frac{dp_v}{dz} \quad (59)$$

In the present study, p_v was obtained from the liquid momentum balance equation in the following form

$$\frac{d^2u}{dz^2} = \mu \frac{\partial}{\partial z} \left[\frac{n}{k} (v_f - v_s) \right] \quad (60)$$

as

$$p_v = (\xi \Delta z)^2 \mu \frac{\partial}{\partial z} \left[\frac{n}{k} (v_f - v_s) \right] \quad (61)$$

where ξ is a constant. This equation defines the pseudo-viscous pressure as a fractional porewater pressure. This was chosen because the porewater pressure gradient is one of the driving forces for dewatering, and therefore, if the problems associated with the discontinuity in the porewater pressure during the early stages of dewatering could be corrected, the problem of obtaining realistic results with an initially uniform porosity profile would be solved. It was predicted that this function would respond to porosity and porewater

pressure changes in such a manner that it could be used to offset numerical difficulties associated with the large initial porosity and porewater pressure gradients.

Substituting Equation 59 into Equation 56 gives

$$\frac{\partial n}{\partial t} = \frac{\partial}{\partial z} \left[\frac{n(1-n)}{F} \left(\frac{1}{m_v} \frac{\partial n}{\partial z} - \frac{dp_v}{dz} \right) \right] + n_0 v_0 \frac{\partial n}{\partial z} \quad (62)$$

or

$$\frac{\partial n}{\partial t} = B \frac{\partial n}{\partial z} + \frac{\partial}{\partial z} \left[C \frac{\partial n}{\partial z} - D \frac{dp_v}{dz} \right] \quad (63)$$

where

$$B = n_0 v_0$$

$$C = \frac{k(1-n)}{\mu m_v} = \frac{n(1-n)}{F m_v}$$

$$D = \frac{n(1-n)}{F} = C m_v$$

Simplifying again gives the governing equation including artificial viscosity

$$\frac{\partial n}{\partial t} = B \frac{\partial n}{\partial z} + \frac{\partial}{\partial z} \left[C \frac{\partial n}{\partial z} - C m_v \frac{dp_v}{dz} \right] \quad (64)$$

Substituting Equation 59 into the equation for v_0 (Equation 42) results in

$$v_0 = \frac{k}{\mu m_v n} \frac{\partial n}{\partial z} \Big|_{z=0} - \frac{k}{\mu n} \frac{dp_v}{dz} \Big|_{z=0} \quad (65)$$

then

$$B = n_0 v_0 = \frac{C_0}{1-n_0} \frac{\partial n}{\partial z} \Big|_{z=0} - \frac{C_0 m_v}{1-n_0} \frac{dp_v}{dz} \Big|_{z=0} \quad (66)$$

FINITE DIFFERENCE FORM OF GOVERNING EQUATION WITH ARTIFICIAL VISCOSITY

The numerical scheme is identical to that of Wells (1990a), forward differencing in time, upwinding in the advective terms and centered differencing for the diffusive terms. In finite difference form the governing equation becomes

$$\begin{aligned} \frac{n_j^{\tau+1} - n_j^\tau}{\Delta t} = & \frac{1}{\Delta z_j^\tau} \left[\frac{C_{j+\frac{1}{2}}^\tau (n_{j+1}^\tau - n_j^\tau)}{\Delta z_{j+\frac{1}{2}}^\tau} - \frac{C_{j-\frac{1}{2}}^\tau (n_j^\tau - n_{j-1}^\tau)}{\Delta z_{j-\frac{1}{2}}^\tau} \right] \\ & - \frac{1}{\Delta z_j^\tau} \left[\frac{C_{j+\frac{1}{2}}^\tau m_{v,j+\frac{1}{2}}^\tau (p_{v,j+1}^\tau - p_{v,j}^\tau)}{\Delta z_{j+\frac{1}{2}}^\tau} - \frac{C_{j-\frac{1}{2}}^\tau m_{v,j-\frac{1}{2}}^\tau (p_{v,j}^\tau - p_{v,j-1}^\tau)}{\Delta z_{j-\frac{1}{2}}^\tau} \right] \\ & + n_0 v_0 \left(\frac{n_{j+1}^\tau - n_j^\tau}{\Delta z_j^\tau} \right) \end{aligned} \quad (67)$$

where

$$\begin{aligned}
 p_{v_j} = & \frac{\mu n_{j+\frac{1}{2}}^\tau}{\Delta z_j^\tau} \frac{\left(\xi \Delta z_{j+\frac{1}{2}}^\tau\right)^2}{k_{j+\frac{1}{2}}^\tau} \left(v_{f_{j+\frac{1}{2}}}^\tau - \frac{n_0 v_0^\tau - n_{j+\frac{1}{2}}^\tau v_{f_{j+\frac{1}{2}}}^\tau}{1 - n_{j+1}^\tau} \right) \\
 & - \frac{\mu n_{j-\frac{1}{2}}^\tau}{\Delta z_j^\tau} \frac{\left(\xi \Delta z_{j-\frac{1}{2}}^\tau\right)^2}{k_{j-\frac{1}{2}}^\tau} \left(v_{f_{j-\frac{1}{2}}}^\tau - \frac{n_0 v_0^\tau - n_{j-\frac{1}{2}}^\tau v_{f_{j-\frac{1}{2}}}^\tau}{1 - n_{j-\frac{1}{2}}^\tau} \right)
 \end{aligned} \tag{68}$$

in the diffusive term, and

$$\begin{aligned}
 p_{v_j} = & \frac{\mu n_{j+1}^\tau}{\Delta z_j^\tau} \frac{\left(\xi \Delta z_{j+1}^\tau\right)^2}{k_{j+1}^\tau} \left(v_{f_{j+1}}^\tau - \frac{n_0 v_0^\tau - n_{j+1}^\tau v_{f_{j+1}}^\tau}{1 - n_{j+1}^\tau} \right) \\
 & - \frac{\mu n_j^\tau}{\Delta z_j^\tau} \frac{\left(\xi \Delta z_j^\tau\right)^2}{k_j^\tau} \left(v_{f_j}^\tau - \frac{n_0 v_0^\tau - n_j^\tau v_{f_j}^\tau}{1 - n_j^\tau} \right)
 \end{aligned} \tag{69}$$

in the calculation of v_0 . The finite difference form of v_0 then becomes

$$v_0 = \frac{k}{\mu m_\nu n} \Big|_{z=0} \left(\frac{n_2^\tau - n_1^\tau}{\Delta z_1^\tau} \right) - \frac{k}{\mu n} \Big|_{z=0} \left(\frac{p_{v_2}^\tau - p_{v_1}^\tau}{\Delta z_1^\tau} \right) \tag{70}$$

CALIBRATION OF THE ARTIFICIAL VISCOSITY CONSTANT

The modified finite difference forms of the governing equation and the equation for v_0 were incorporated into the computer model and simulation experiments were performed using input data corresponding to the CHESS experiments. Tests were conducted using both uniform initial porosity profiles and initial porosity profiles resulting from prior gravity sedimentation in order to calibrate the artificial viscosity constant ξ .

The constant, ξ , allows some control over the amount of additional viscosity added to the model's numerical scheme. It was calibrated to the minimum value necessary for model accuracy and numerical stability using uniform initial porosity profiles.

Two boundaries on the value of ξ were observed. At lower values of ξ the model was stable, but not accurate, because the large initial porosity gradient caused the sum of the convective terms to be greater than the sum of the diffusive terms. A physically unrealistic situation occurred where the porosity stopped decreasing while the pore liquid evacuated. The model output in these cases was similar to that of Table VIII. At higher values of ξ the model was not stable, and simulations ended when the computer model detected a negative time step. It was also observed that the larger the initial porosity gradient, the more distinct these boundaries were (i.e., the boundaries for the conditions of CHESS run KDMK8

without prior gravity sedimentation were much less sharply defined than those for the conditions of CHESS run PMK7 without prior gravity sedimentation). The width between the boundaries was also affected by the magnitude of the initial porosity gradient at the filter medium. The distance between the boundaries on ξ were seen to vary inversely with the magnitude of the initial porosity gradient at $z=0$. Within these boundaries, the model results seemed to be accurate (no data were available with which to compare results from initially uniform porosity profiles) when compared with model output from simulations with an initial porosity profile resulting from prior sedimentation. The model results were better than results obtained without the addition of the pseudo-viscous pressure terms. The calibrated value of ξ (the value used to produce the results presented in this study) was assumed to lie just above the lower ξ boundary.

The artificial viscosity constant was calibrated by simple trial and error for the conditions of each CHESS run using uniform initial porosity profiles as input, and was found to vary between 0 and 0.096. Figure 64 shows how the addition of artificial viscosity improved the behavior of the porosity gradient for the model calibration run with a uniform initial porosity (compare to Figure 60). As was stated previously, this was necessary in order to obtain realistic results from the computer model for suspensions with a uniform initial porosity.

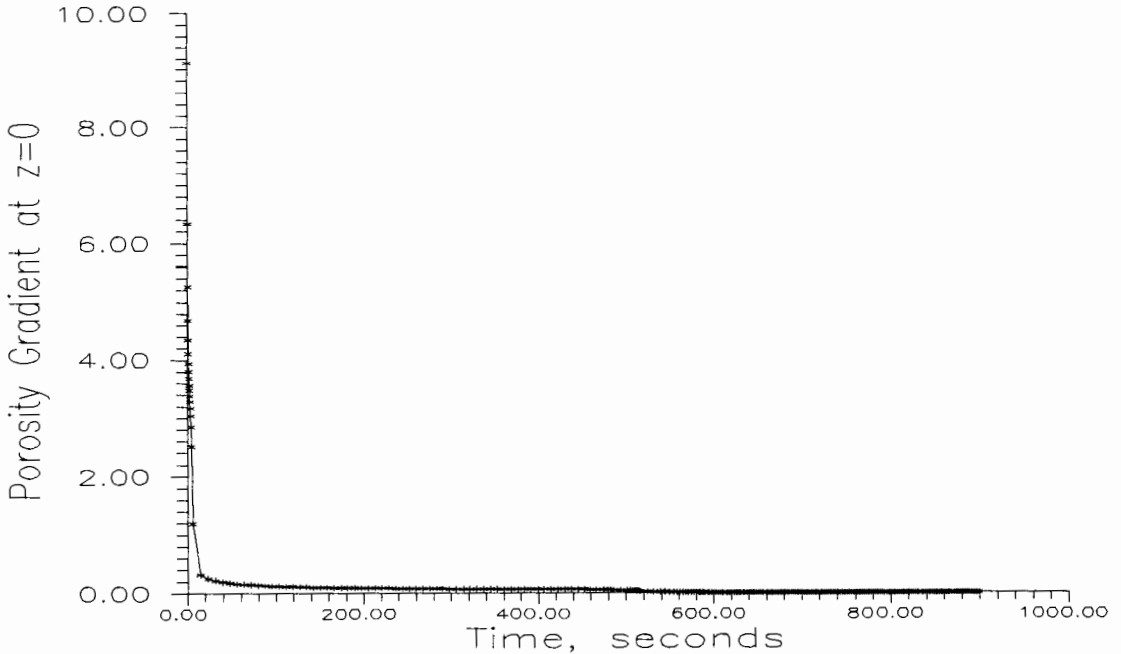


Figure 64. Plot of porosity gradient versus time for CHESS run KDMK9 without prior gravity sedimentation using artificial viscosity at node 2.

Figures 65-67 show the propagation of the porosity shock wave at nodes 2, 5 and 10 of the finite difference grid over time. The terms of the governing equation resulting from the introduction of artificial viscosity are labeled as 'DIFFUSIVE 2' and 'CONVECTIVE 2' in these figures. The sum of the diffusive terms must be greater than the sum of the convective terms in order for the porosity to decrease with time. The additional diffusive term obtained from the introduction of the artificial viscosity assured that this criterion was met. These figures also show that artificial viscosity was not significant at nodes 5 ($z=2.0$ mm) and 10 ($z=4.5$ mm). The discontinuity in the shock front had already been smoothed

out. However, addition of artificial viscosity was found to be crucial at node 2 ($z=0.5$ mm) during the very early stages of filtration as the sharp front of the shock wave moves away from the boundary at $z=0$.

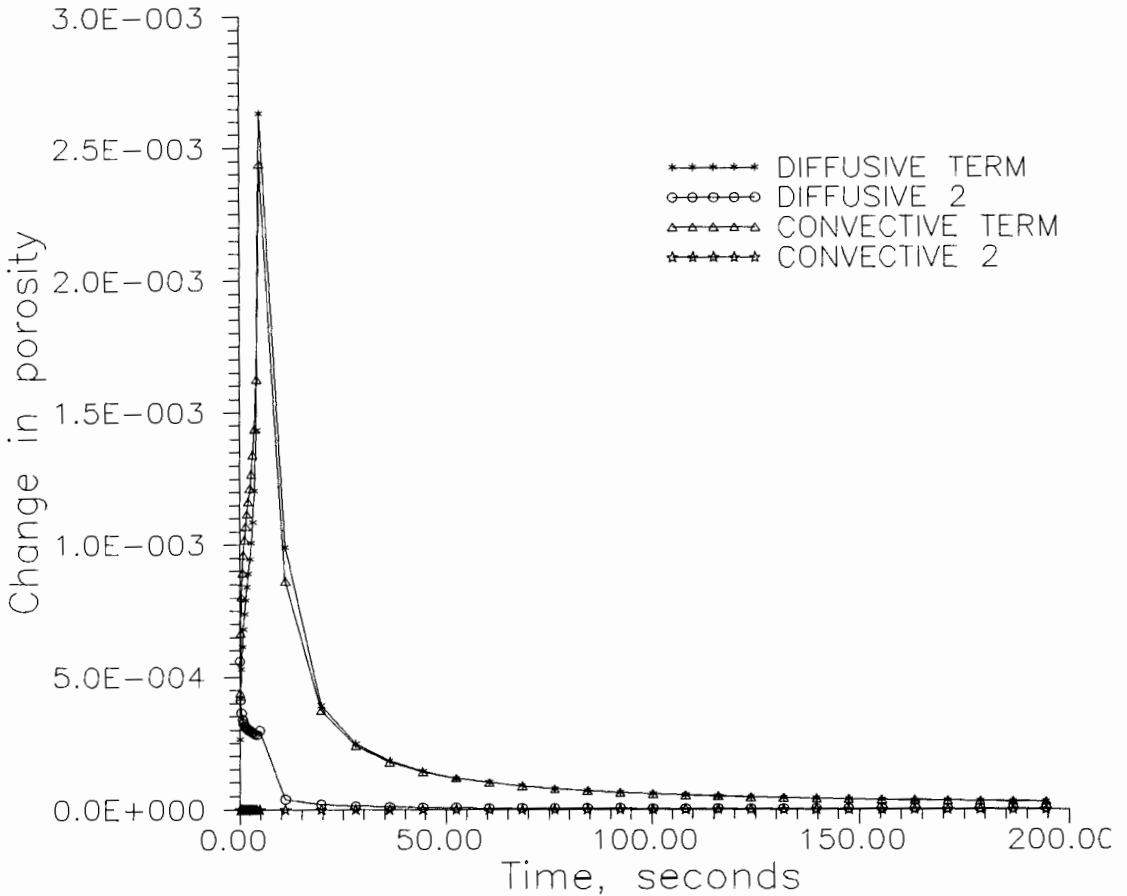


Figure 65. Plot of diffusive and convective terms of governing equation versus time with artificial viscosity for CHES run KDMK9 without prior gravity sedimentation at grid point 2.

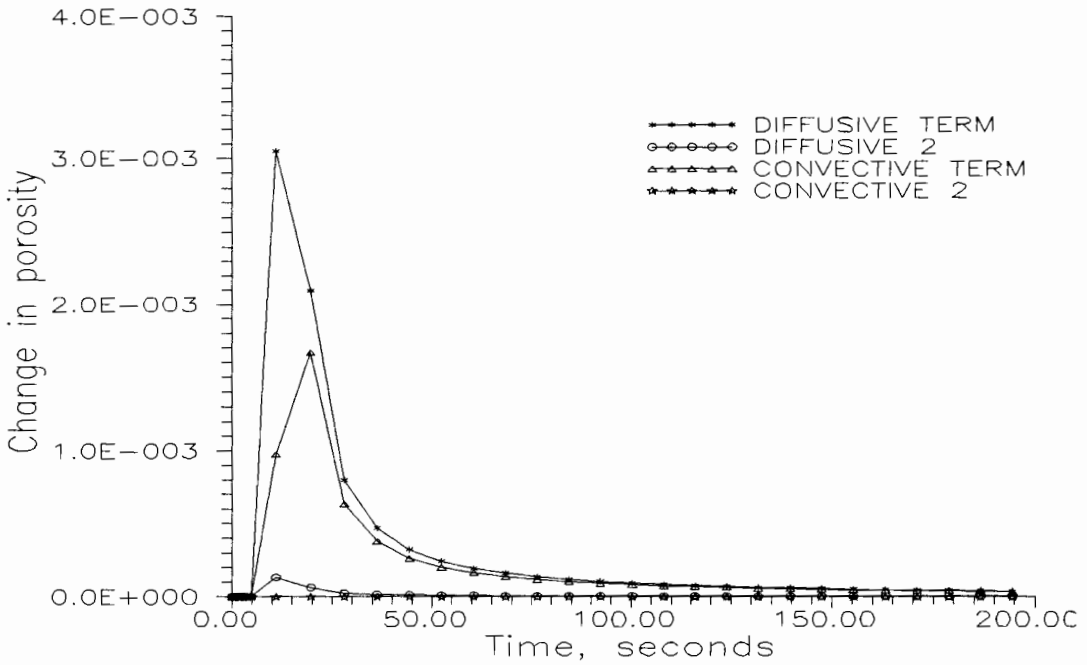


Figure 66. Plot of diffusive and convective terms of governing equation versus time with artificial viscosity for CHES run KDMK9 without prior gravity sedimentation at grid point 5.

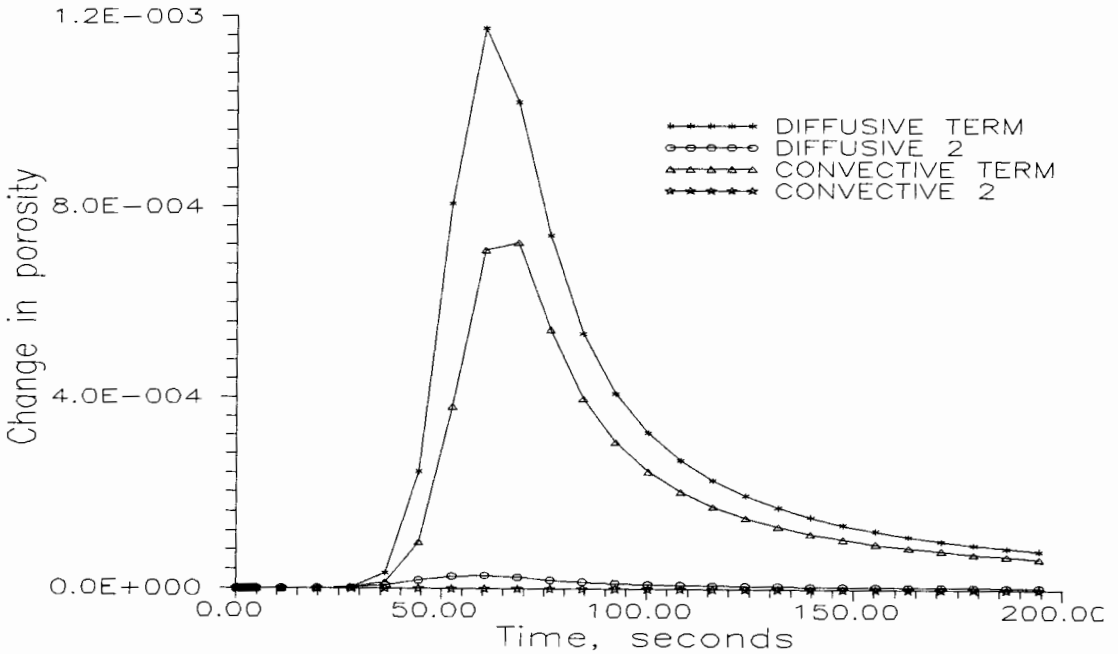


Figure 67. Plot of diffusive and convective terms of governing equation versus time with artificial viscosity for CHES run KDMK9 without prior gravity sedimentation at grid point 10.

Table IX is a summary of the results of these model runs and the calibrated ξ values.

TABLE IX

SUMMARY OF RESULTS OF SIMULATIONS USING THE WELLS (1990a) SLUDGE DEWATERING MODEL WITH ARTIFICIAL VISCOSITY

CHESS Run	ξ	Cake Form. Time (S)	Simulation Time (S)	Cum. Filt. Volume (cm ³)	CPU* Time (S)	$\frac{\partial n}{\partial z} \Big _{z=0, t=0}$ (cm ⁻¹)
$c_i = 0.47 \text{ g/cm}^3$						
KDMK8	0.000	520.7	900.0	33.75	325.5	7.36
KDM6	0.037	287.5	563.8	34.25	314.5	7.89
KDM4	0.055	279.9	395.0	35.81	187.1	8.62
PMK9	0.055	232.0	307.6	36.59	173.6	9.03
PMK6	0.055	186.0	239.4	37.70	118.3	9.32
$c_i = 0.31 \text{ g/cm}^3$						
KDMK9	0.073	399.7	900.0	41.16	253.7	9.20
KDM2	0.074	327.7	493.8	44.19	185.4	9.73
PMK3	0.077	239.6	295.6	39.63	160.0	10.45
PMK4	0.078	201.0	239.6	39.45	172.0	10.87
PMK5	0.076	187.1	218.4	43.67	235.5	11.16
$c_i = 0.14 \text{ g/cm}^3$						
KDM7	0.096	350.1	729.3	48.46	292.5	11.14
KDM5	0.096	280.3	358.4	49.26	358.6	11.68
KDM3B	0.094	218.7	248.8	47.84	445.0	12.40
PMK10	0.095	168.5	189.6	48.21	562.5	12.82
PMK7	0.090	139.5	155.1	48.59	754.5	13.11

* Using a Tektronix XD88/10 UNIX workstation

It can be seen that the calibrated ξ values vary with the initial suspended solids concentration. As was desired, the added terms had little or no effect on the model except in the vicinity of the shock. Only the additional diffusive term, DIFFUSIVE 2, was ever important.

It was also desired that the effect of adding artificial viscosity to the numerical scheme have a minimal effect on model runs in which the initial porosity profile was not uniform (i.e., prior gravity sedimentation). To see if this was the case, model simulations using artificial viscosity were performed with initial porosity profiles resulting from prior gravity sedimentation.

Table X shows the effect of adding artificial viscosity to CHESSE runs with prior gravity sedimentation.

As can be seen, the addition of artificial viscosity did affect the results. For simulations at initial concentrations of 0.47 and 0.31 g/cm³, the effect was minimal. The larger changes at the 0.14 g/cm³ initial concentration may have been a result of the inaccuracy of one or both of the constitutive equations in the higher porosity regions. The computer CPU time change was a result of the additional calculations involved when artificial viscosity was introduced, as well as the small time step calculated by the computer model as a consequence of the large initial porosity gradient. Even so, no simulation took more than 10 minutes on a Tektronix XD88 UNIX workstation. Table X also shows that if artificial

viscosity is used for simulations with initial porosity profiles resulting from prior gravity sedimentation, it is probably not necessary to recalibrate the model with the additional parameter ξ . Provided that the initial calibration is good, and the constitutive equations are accurate, the effect of adding artificial viscosity to simulations with initial porosity profiles resulting from prior gravity sedimentation is small. There is, however, a provision in the computer model for the user to turn the addition of artificial viscosity on or off.

Figures 68-97 show the results of simulations using initially uniform porosity profiles as input to the computer model graphically. No data were available with which to compare these results.

The important result demonstrated here has been the significant improvement in the performance of the Wells (1990a) sludge dewatering model, such that reasonable results were obtained for a class of problems which the model could not solve accurately before.

TABLE X

EFFECT OF ARTIFICIAL VISCOSITY ON CHESS RUNS WITH PRIOR GRAVITY SEDIMENTATION

CHESS Run	ξ	CPU Time % Change	Cake Formation Time % Change	Simulated Time % Change	Filtrate Volume % Change
$c_i = 0.47 \text{ g/cm}^3$					
KDMK8	0.0	0.0	0.0	0.0	0.0
KDM6	0.037	+110.4	+0.1	+0.9	-0.7
KDM4	0.055	+113.7	+0.7	+2.2	-1.6
PMK9	0.055	+114.2	+1.1	+2.8	-1.6
PMK6	0.055	+119.6	+1.7	+3.5	-1.3
$c_i = 0.31 \text{ g/cm}^3$					
KDMK9	0.073	+114.5	+2.7	0.0	-2.9
KDM2	0.074	+123.6	+4.2	+8.2	-3.1
PMK3	0.077	+124.8	+3.8	+6.6	-4.2
PMK4	0.078	+127.5	+5.0	+7.3	-4.5
PMK5	0.075	+130.0	+4.5	+8.0	-4.3
$c_i = 0.14 \text{ g/cm}^3$					
KDM7	0.096	+180.5	+7.8	+26.0	-2.6
KDM5	0.096	+181.0	+8.2	+24.8	-3.3
KDM3B	0.094	+192.7	+8.2	+24.9	-3.7
PMK10	0.095	+189.9	+10.4	+26.9	-3.9
PMK7	0.090	+176.2	+11.9	+24.7	-3.5

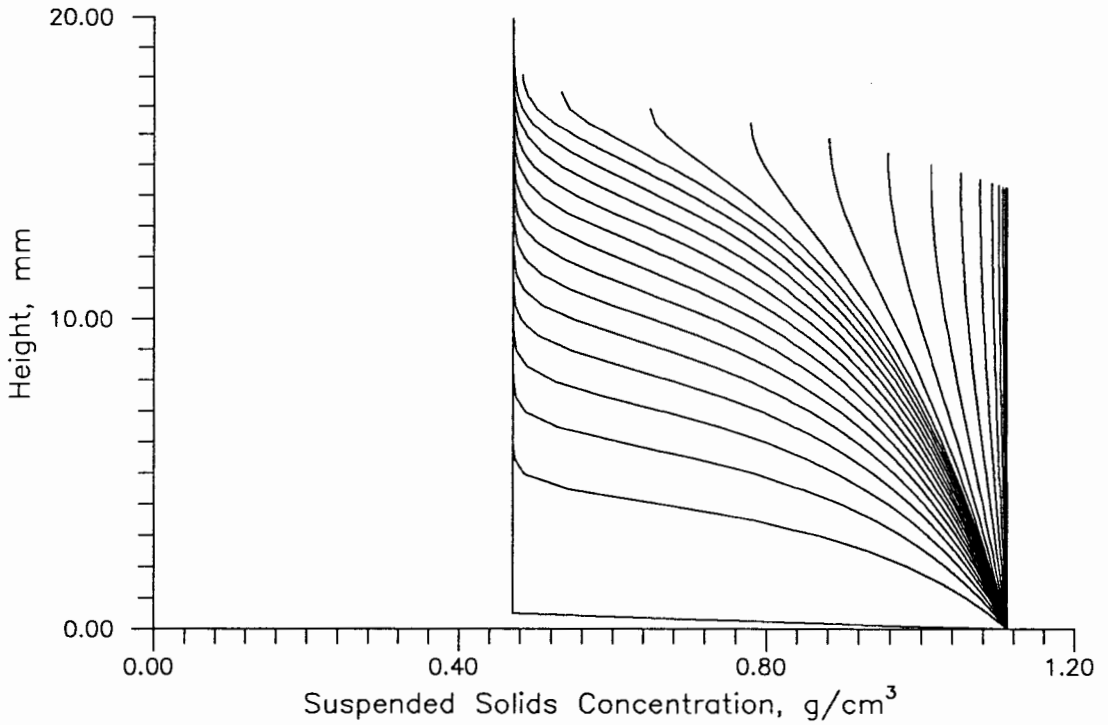


Figure 68. Concentration profiles at 30 s intervals under conditions of CHES run KDMK8 (103 kPa, 0.47 g/cm³) without prior gravity sedimentation.

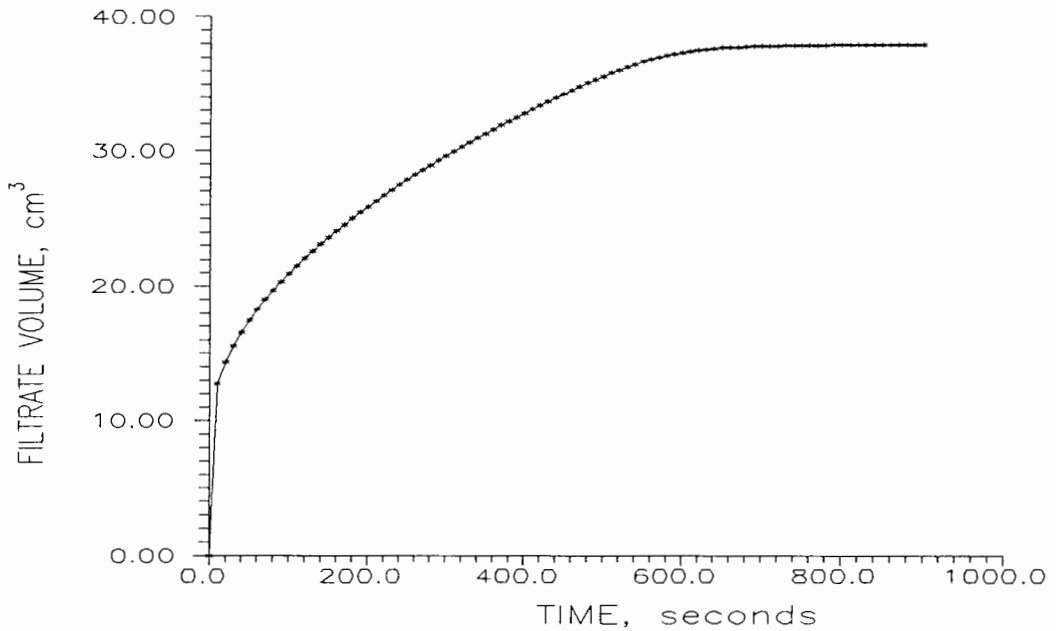


Figure 69. Filtrate production versus time for run KDMK8 without prior gravity sedimentation.

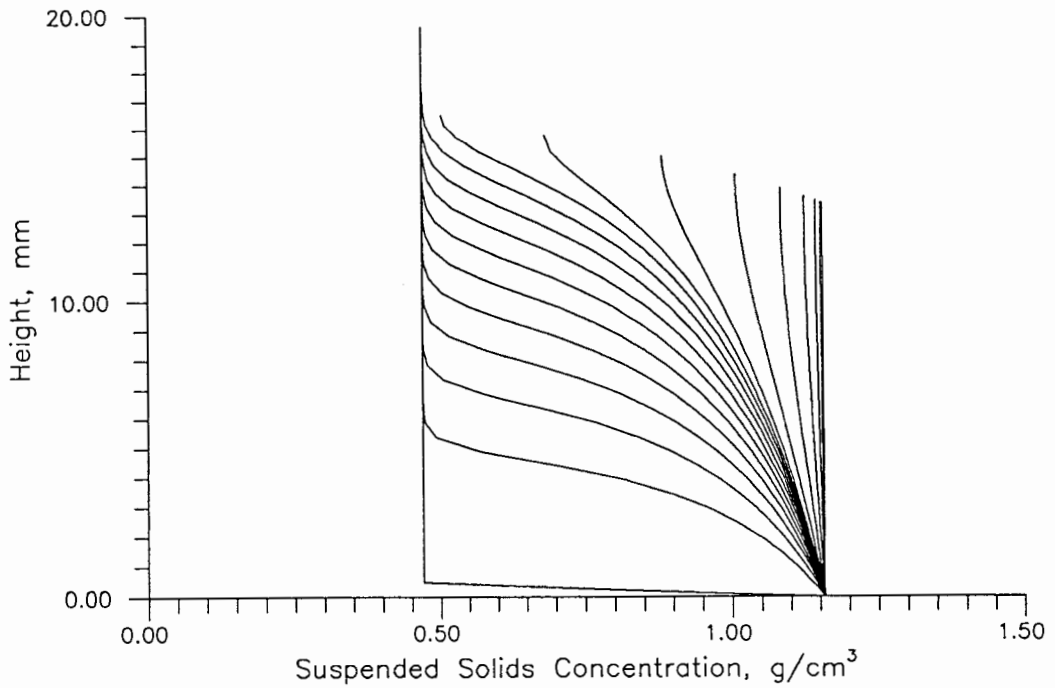


Figure 70. Concentration profiles at 30 s intervals under conditions of CHES run KDM6 (170 kPa, 0.47 g/cm³) without prior gravity sedimentation.

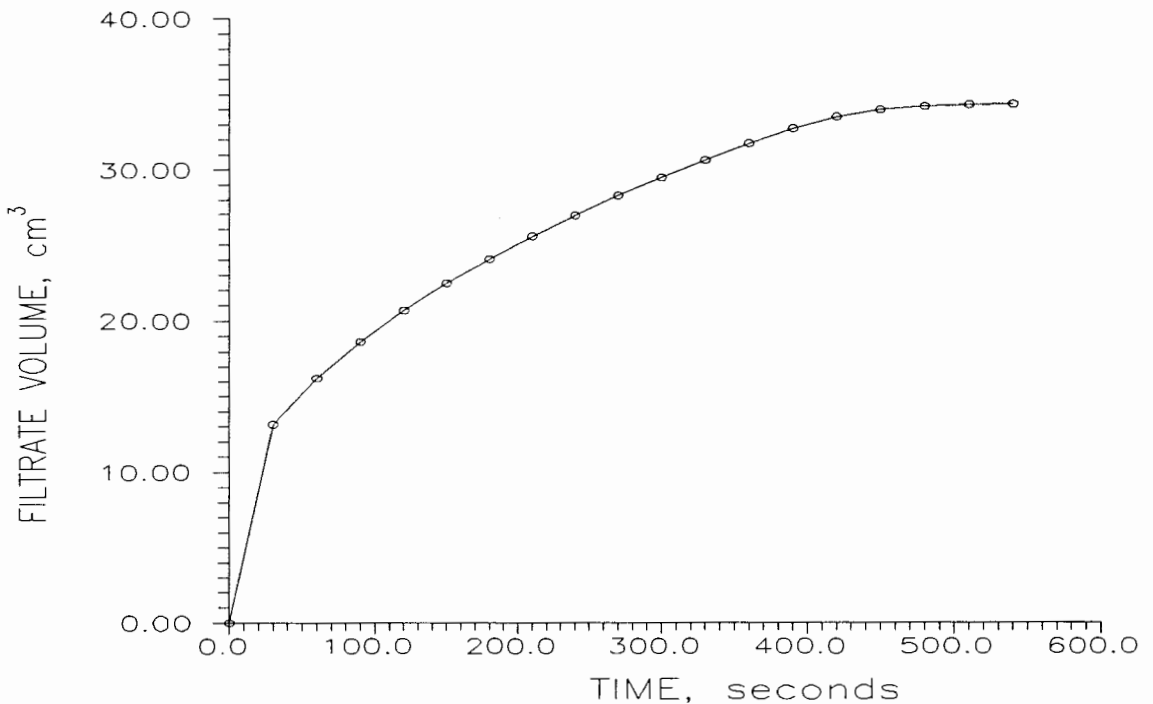


Figure 71. Filtrate production versus time for run KDM6 without prior gravity sedimentation.

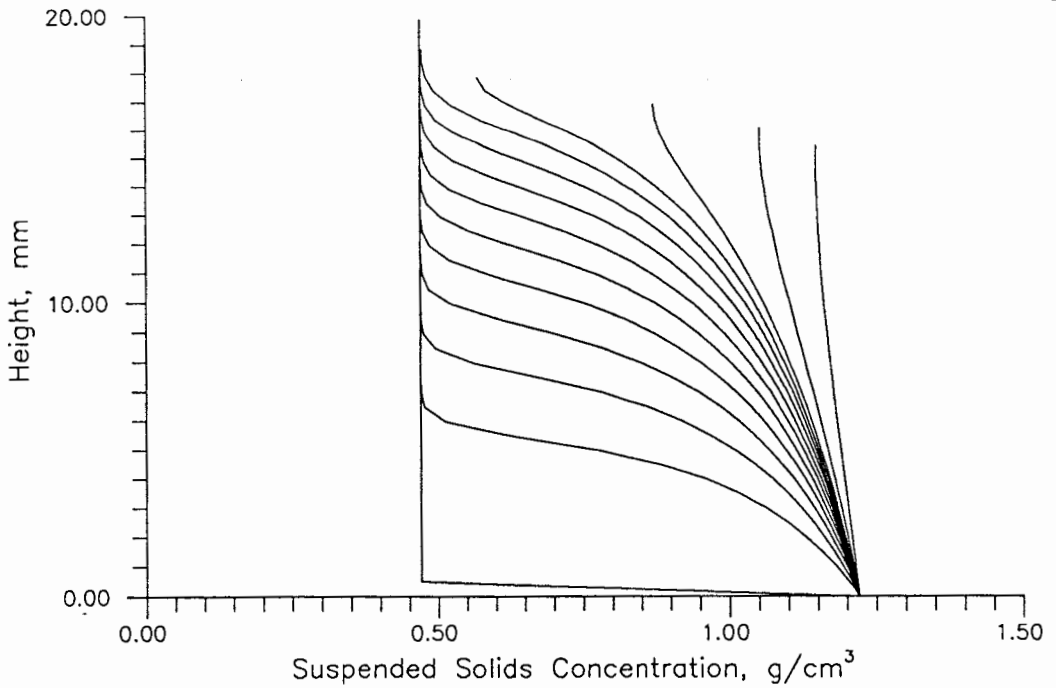


Figure 72. Concentration profiles at 30 s intervals under conditions of CHES run KDM4 (345 kPa, 0.47 g/cm³) without prior gravity sedimentation.

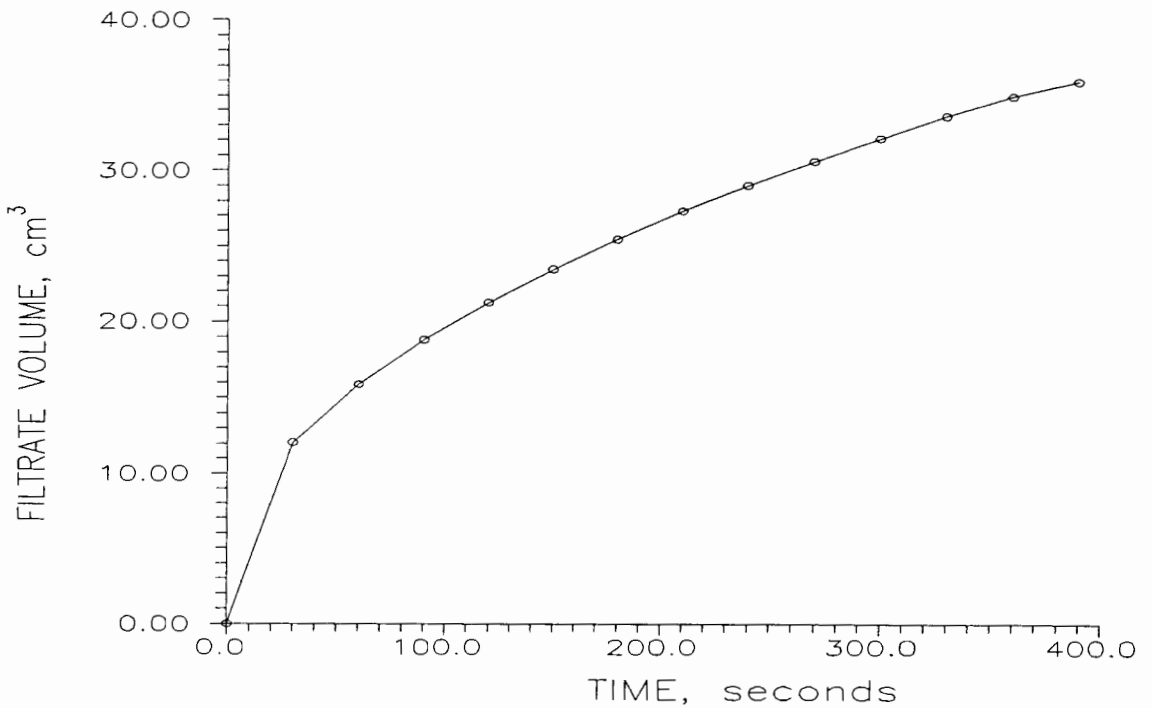


Figure 73. Filtrate production versus time for run KDM4 without prior gravity sedimentation.

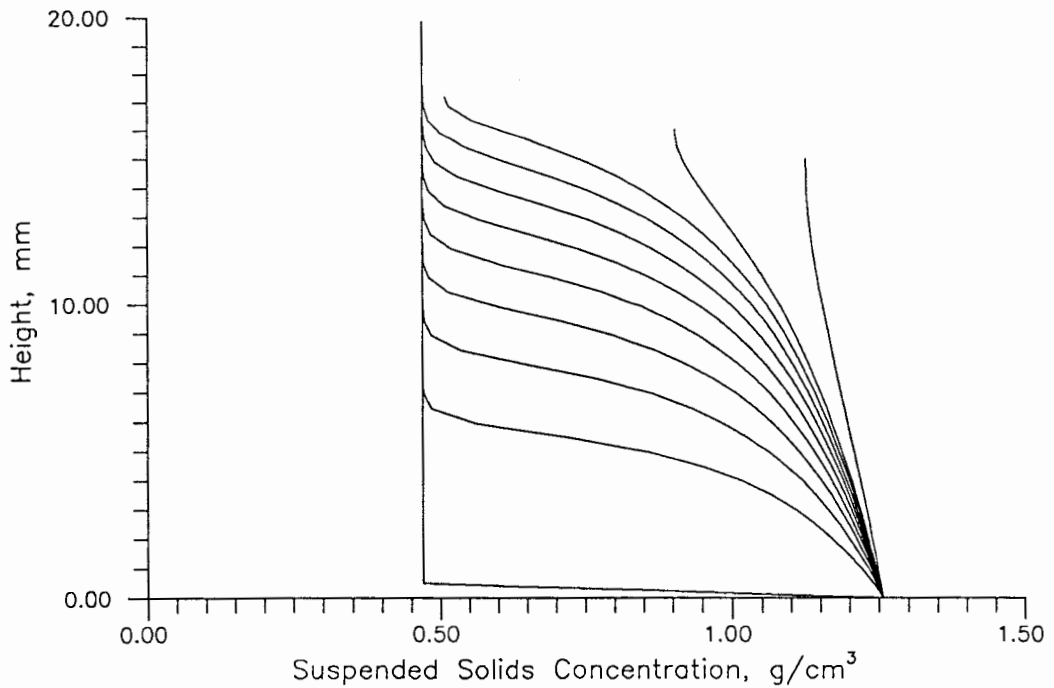


Figure 74. Concentration profiles at 30 s intervals under conditions of CHES run PMK9 (520 kPa, 0.47 g/cm³) without prior gravity sedimentation.

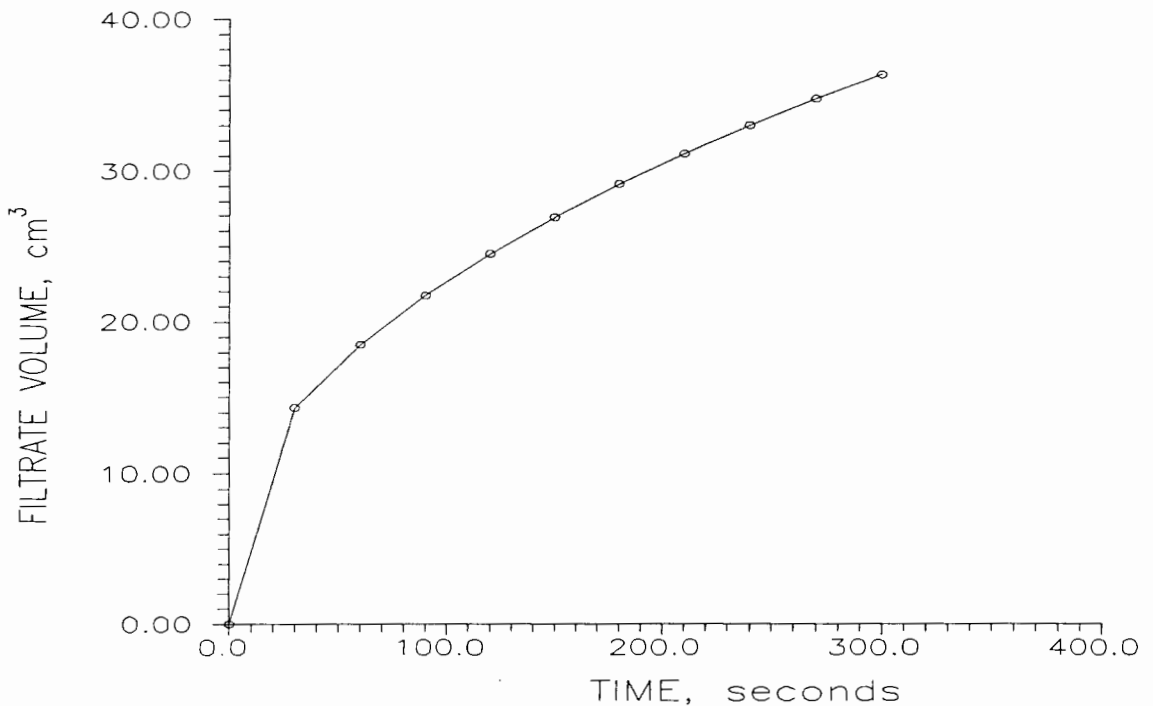


Figure 75. Filtrate production versus time for run PMK9 without prior gravity sedimentation.

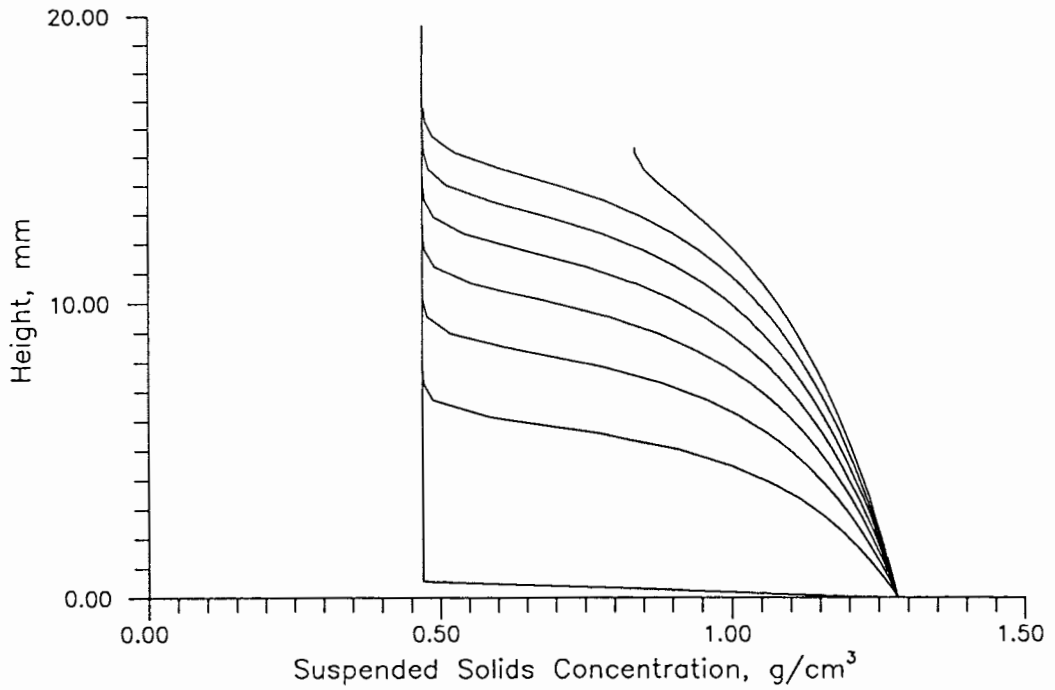


Figure 76. Concentration profiles at 30 s intervals under conditions of CHES run PMK6 (690 kPa, 0.47 g/cm³) without prior gravity sedimentation.

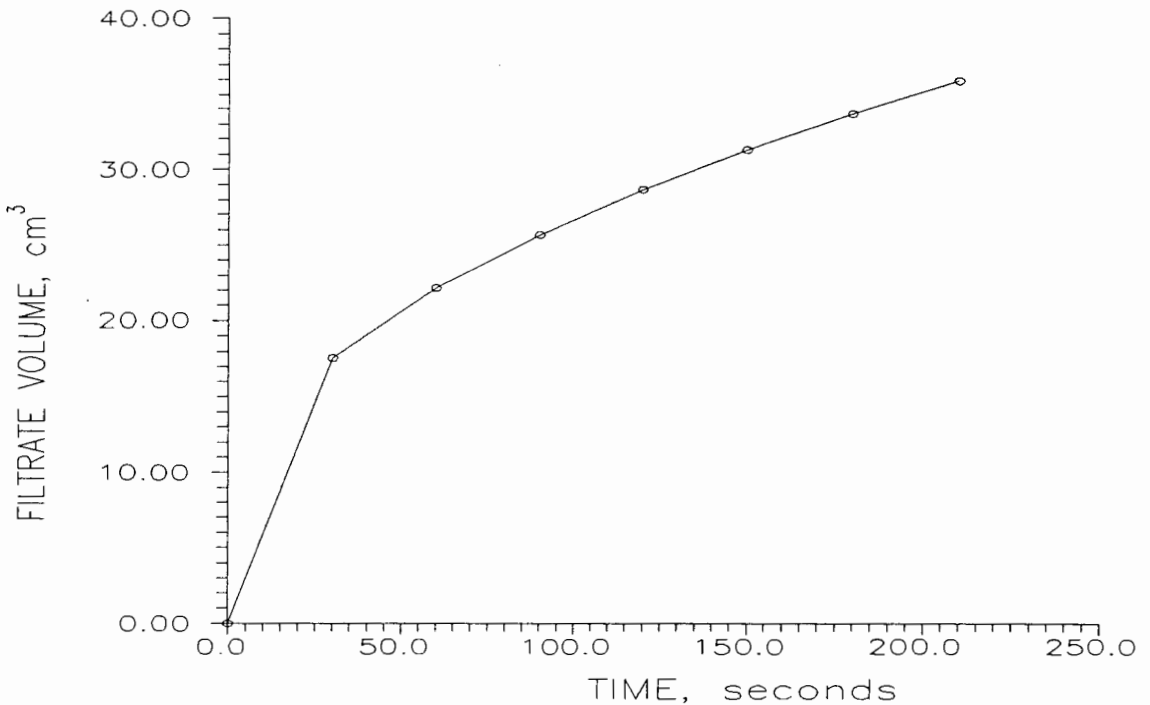


Figure 77. Filtrate production versus time for run PMK6 without prior gravity sedimentation.

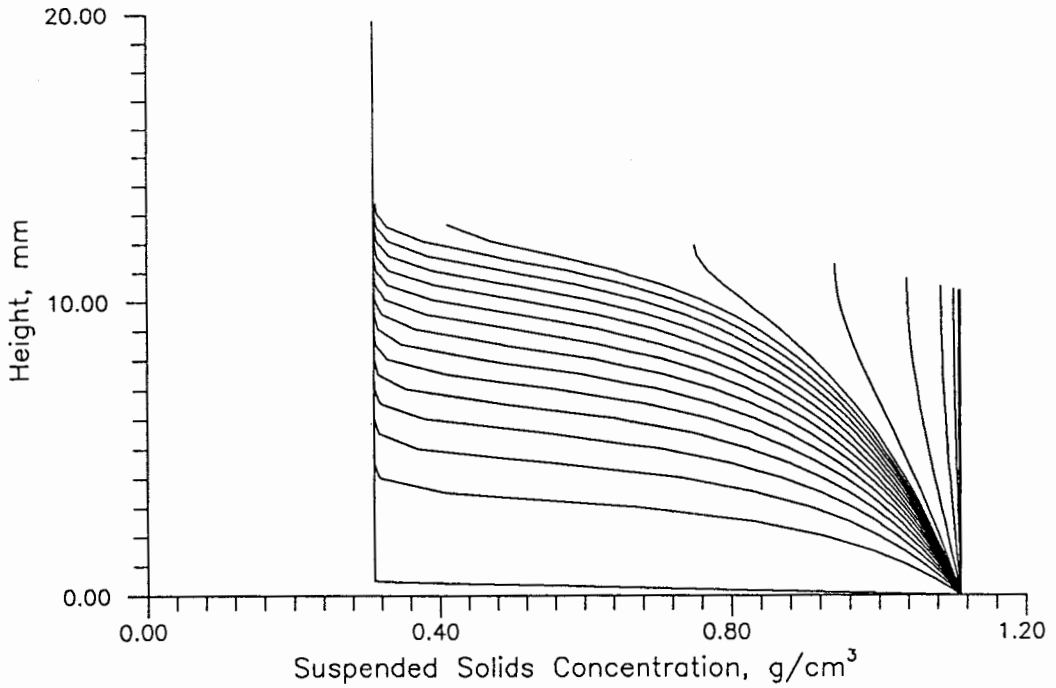


Figure 78. Concentration profiles at 30 s intervals under conditions of CHES run KDMK9 (103 kPa, 0.31 g/cm³) without prior gravity sedimentation.

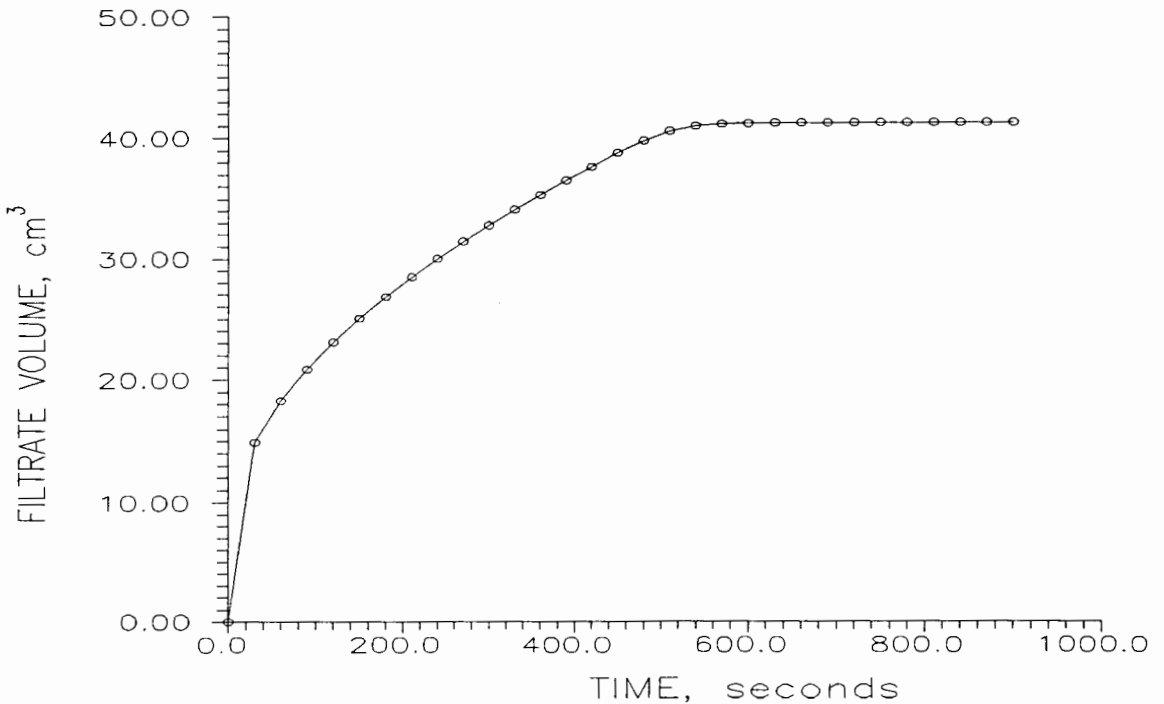


Figure 79. Filtrate production versus time for run KDMK9 without prior gravity sedimentation.

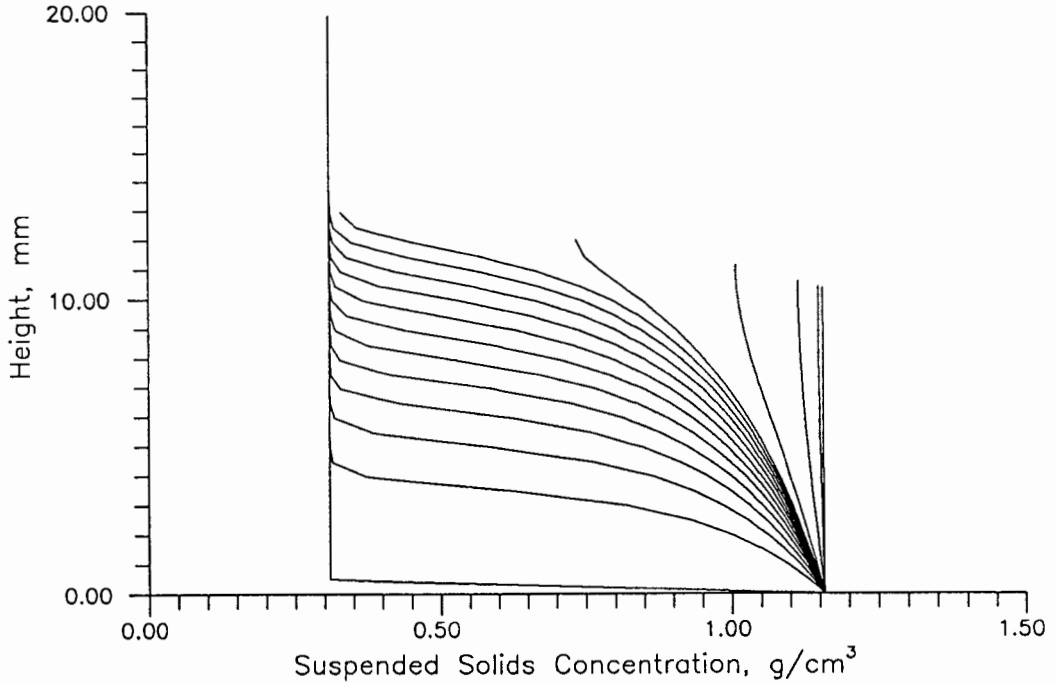


Figure 80. Concentration profiles at 30 s intervals under conditions of CHES run KDM2 (170 kPa, 0.31 g/cm³) without prior gravity sedimentation.

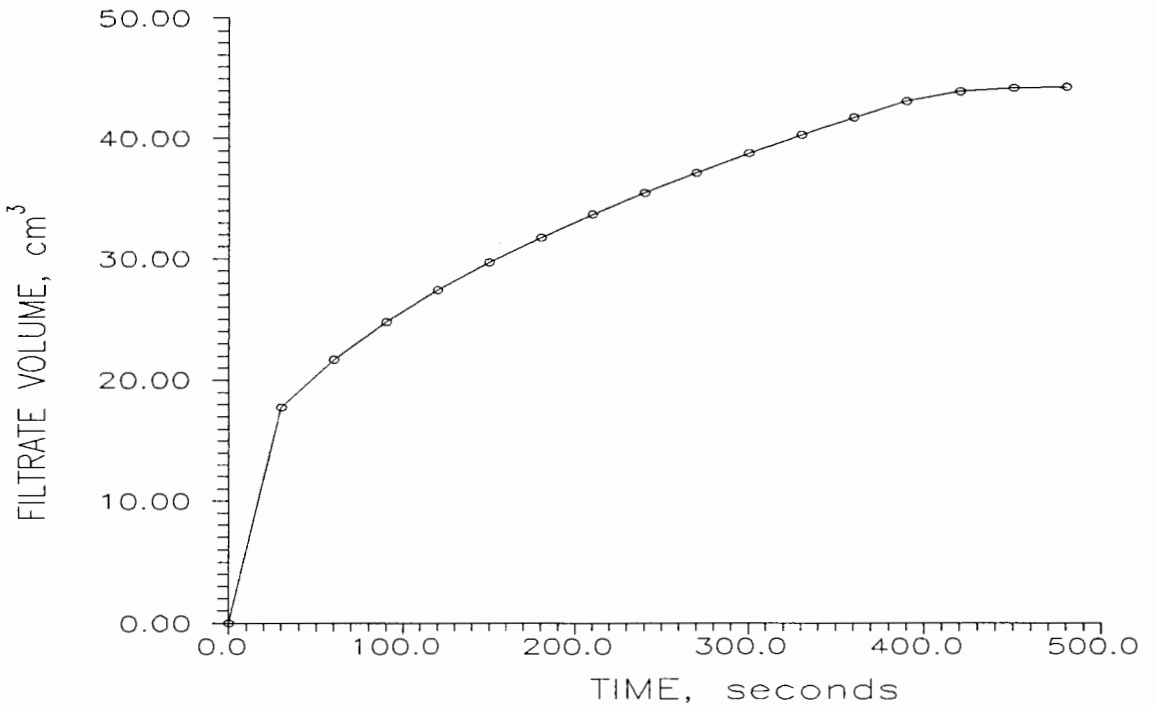


Figure 81. Filtrate production versus time for run KDM2 without prior gravity sedimentation.

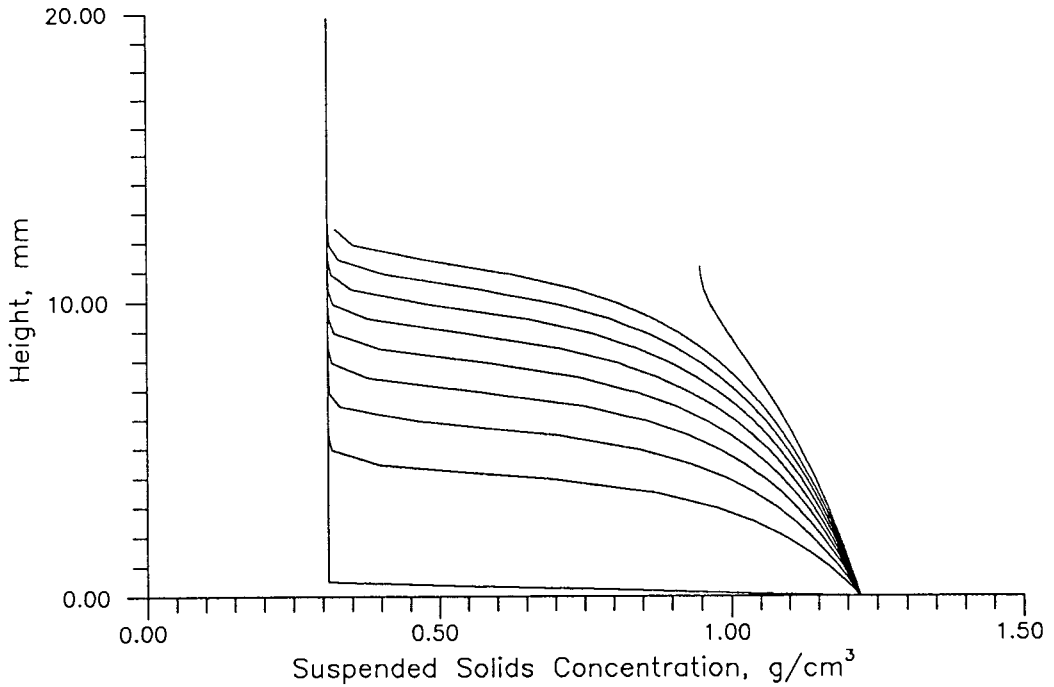


Figure 82. Concentration profiles at 30 s intervals under conditions of CHES run PMK3 (345 kPa, 0.31 g/cm³) without prior gravity sedimentation.

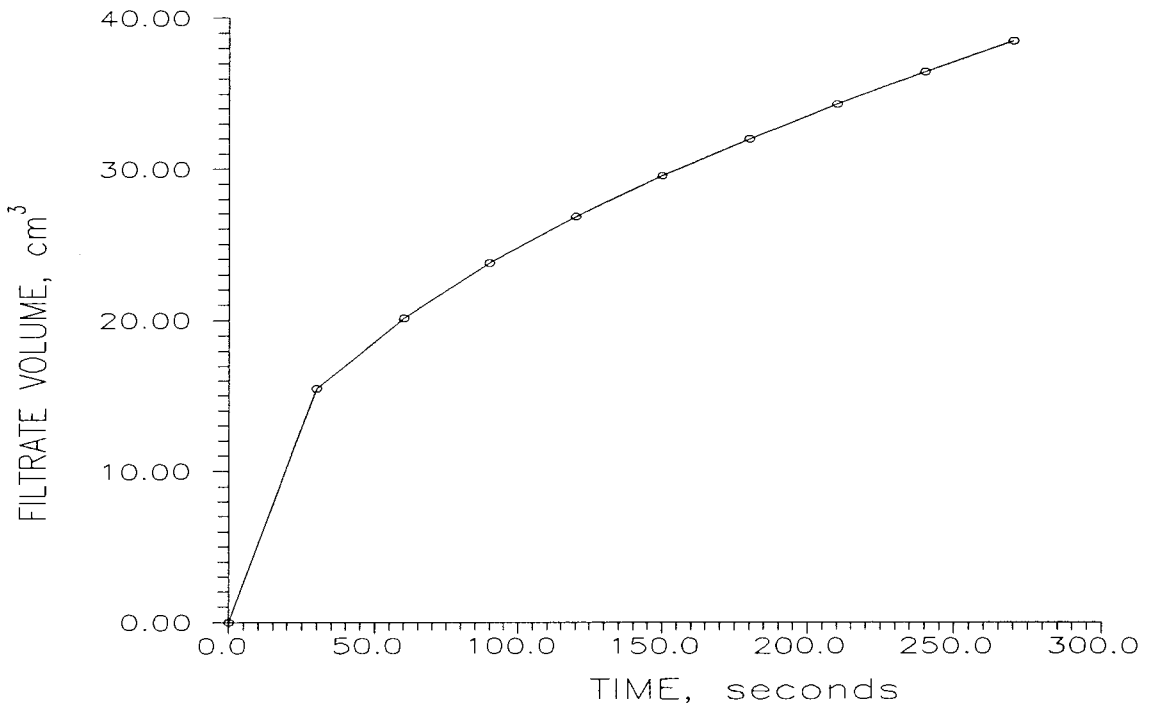


Figure 83. Filtrate production versus time for run PMK3 without prior gravity sedimentation.

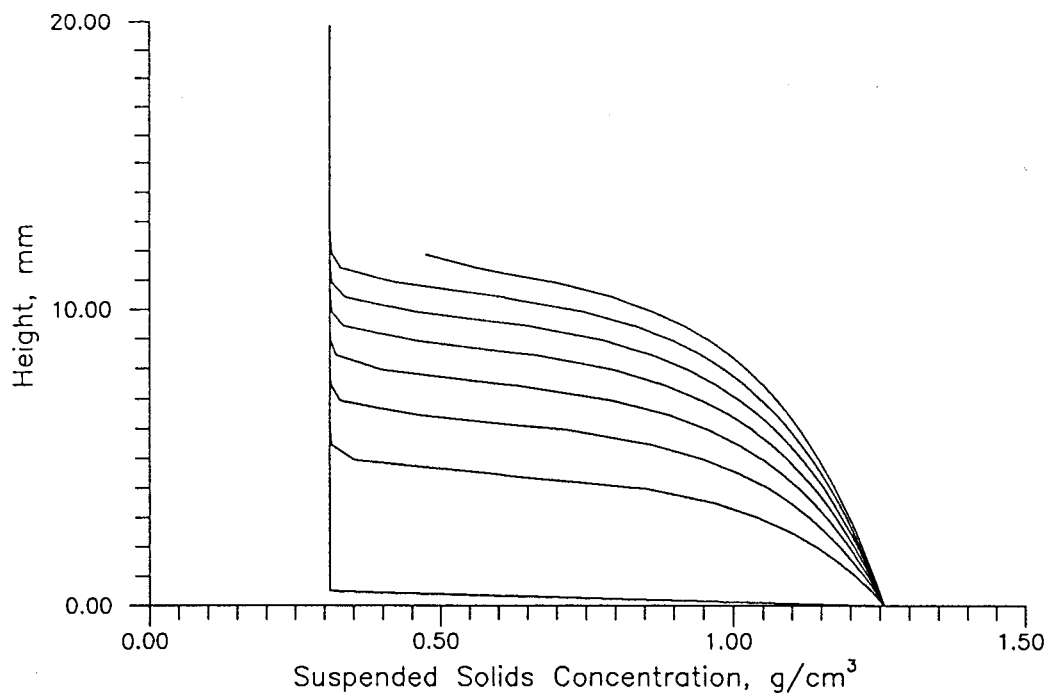


Figure 84. Concentration profiles at 30 s intervals under conditions of CHES run PMK4 (520 kPa, 0.31 g/cm³) without prior gravity sedimentation.

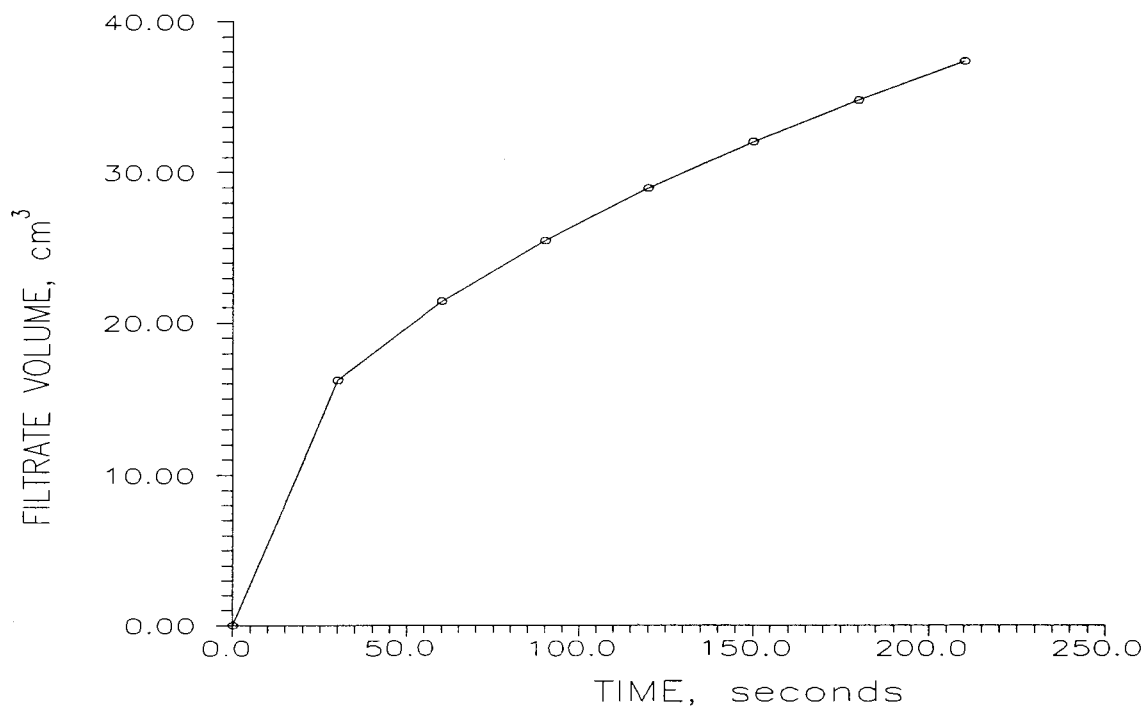


Figure 85. Filtrate production versus time for run PMK4 without prior gravity sedimentation.

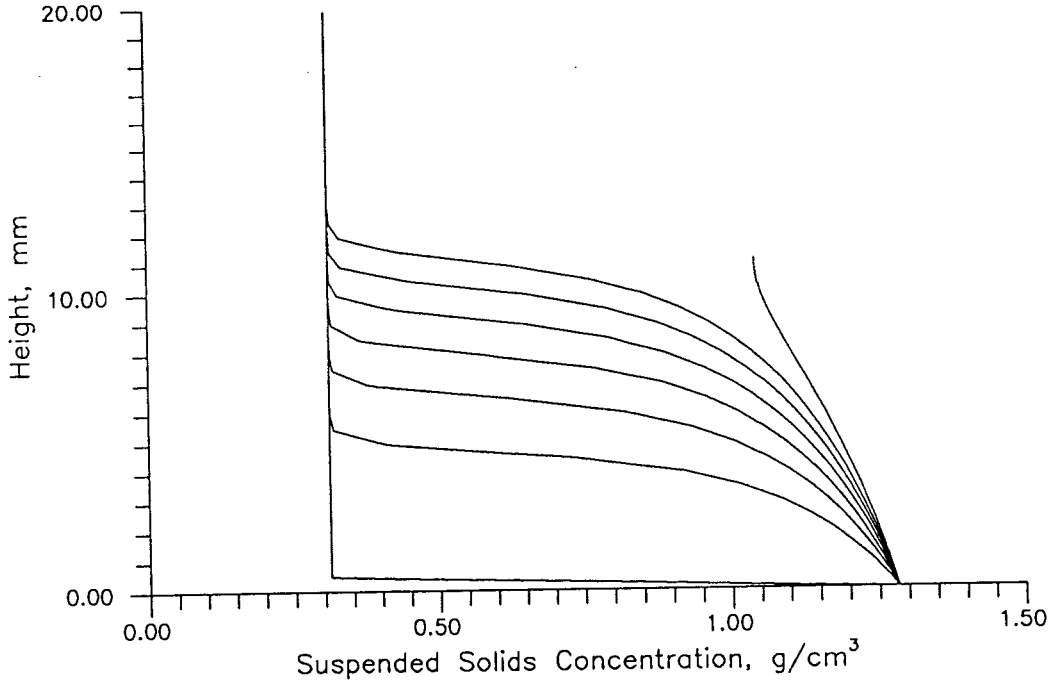


Figure 86. Concentration profiles at 30 s intervals under conditions of CHES run PMK5 (690 kPa, 0.31 g/cm³) without prior gravity sedimentation.

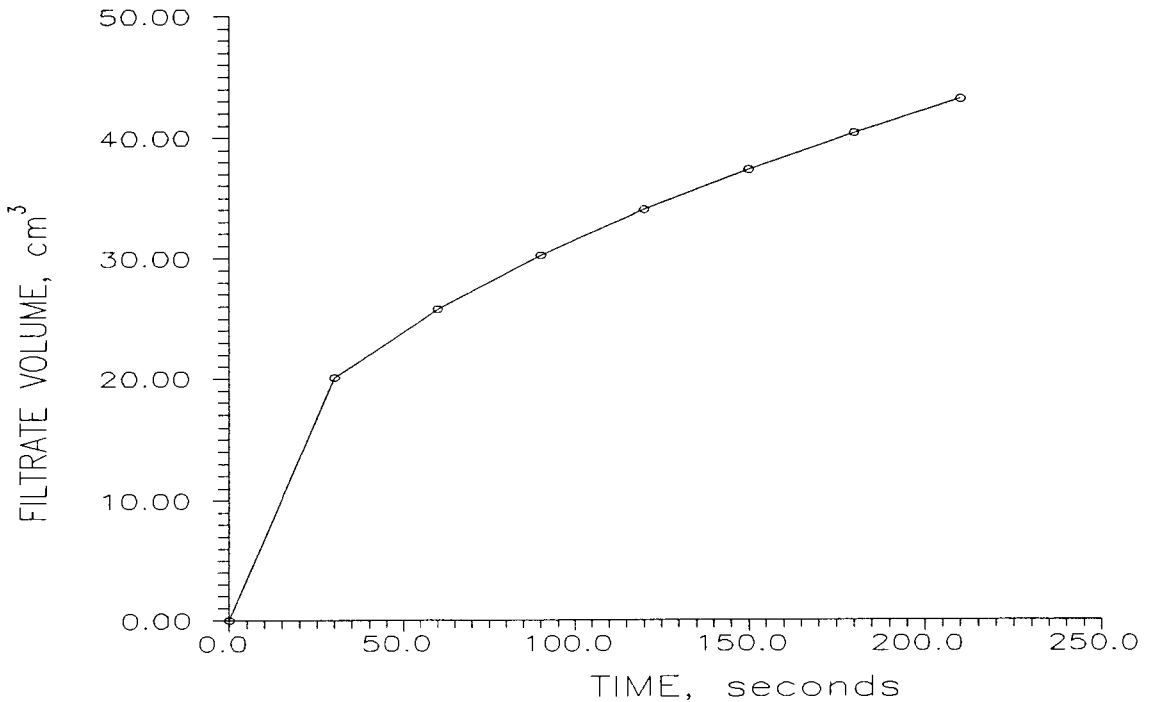


Figure 87. Filtrate production versus time for run PMK5 without prior gravity sedimentation.

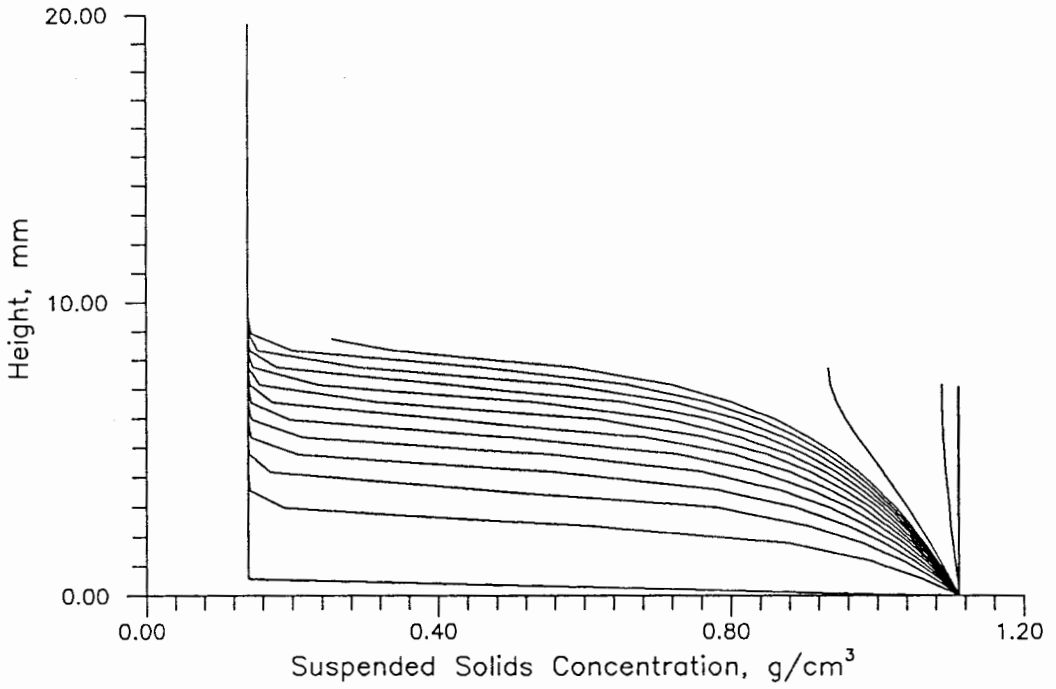


Figure 88. Concentration profiles at 30 s intervals under conditions of CHES run KDM7 (103 kPa, 0.14 g/cm³) without prior gravity sedimentation.

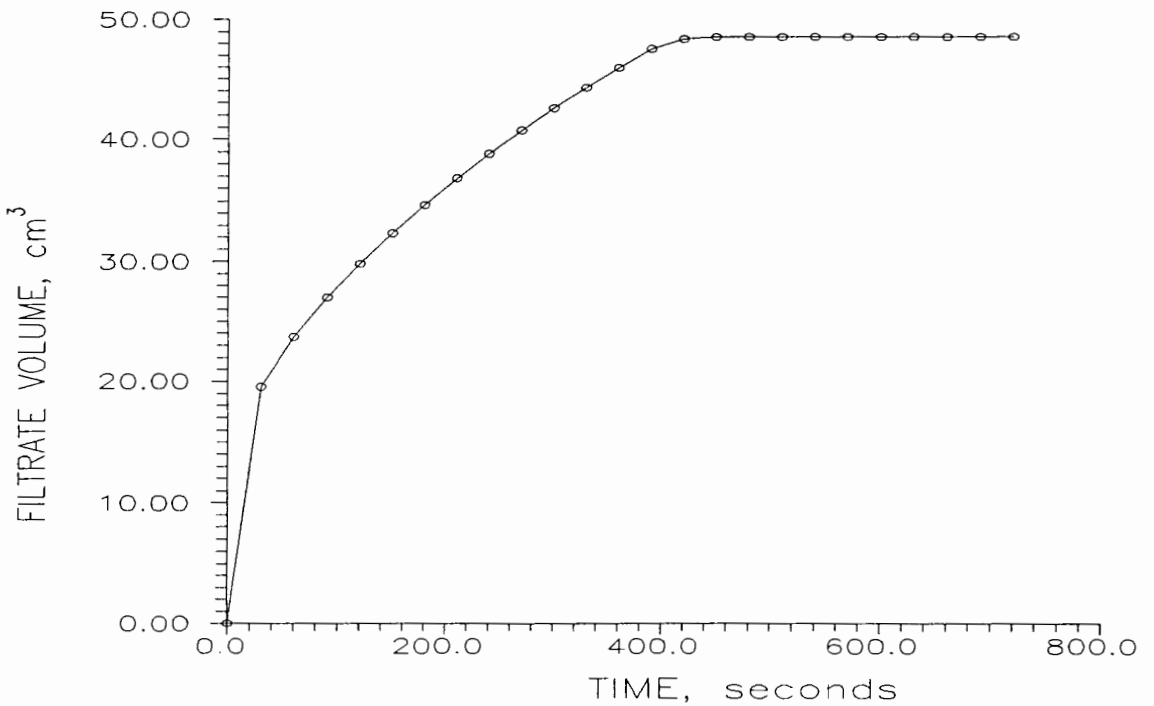


Figure 89. Filtrate production versus time for run KDM7 without prior gravity sedimentation.

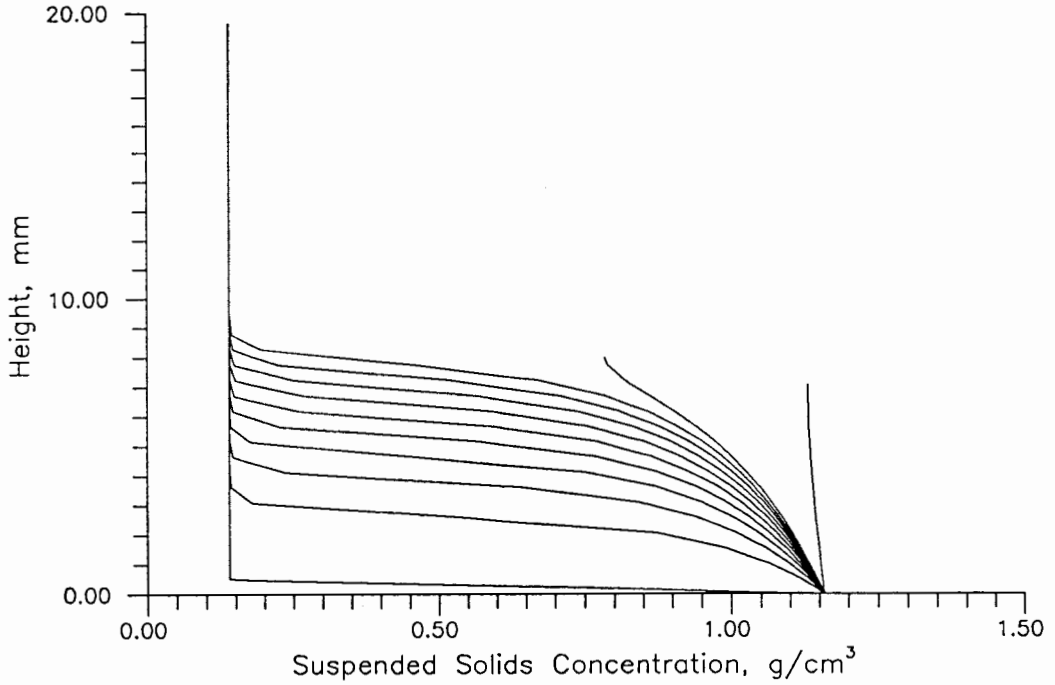


Figure 90. Concentration profiles at 30 s intervals under conditions of CHES run KDM5 (170 kPa, 0.31 g/cm³) without prior gravity sedimentation.

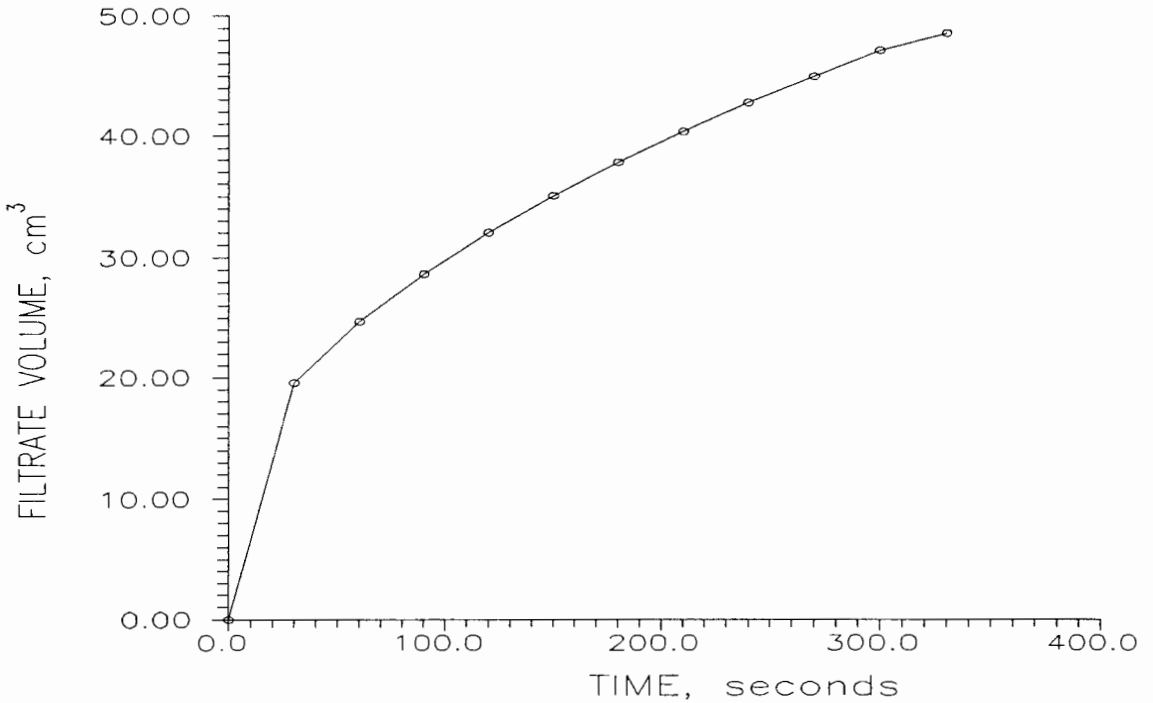


Figure 91. Filtrate production versus time for run KDM5 without prior gravity sedimentation.

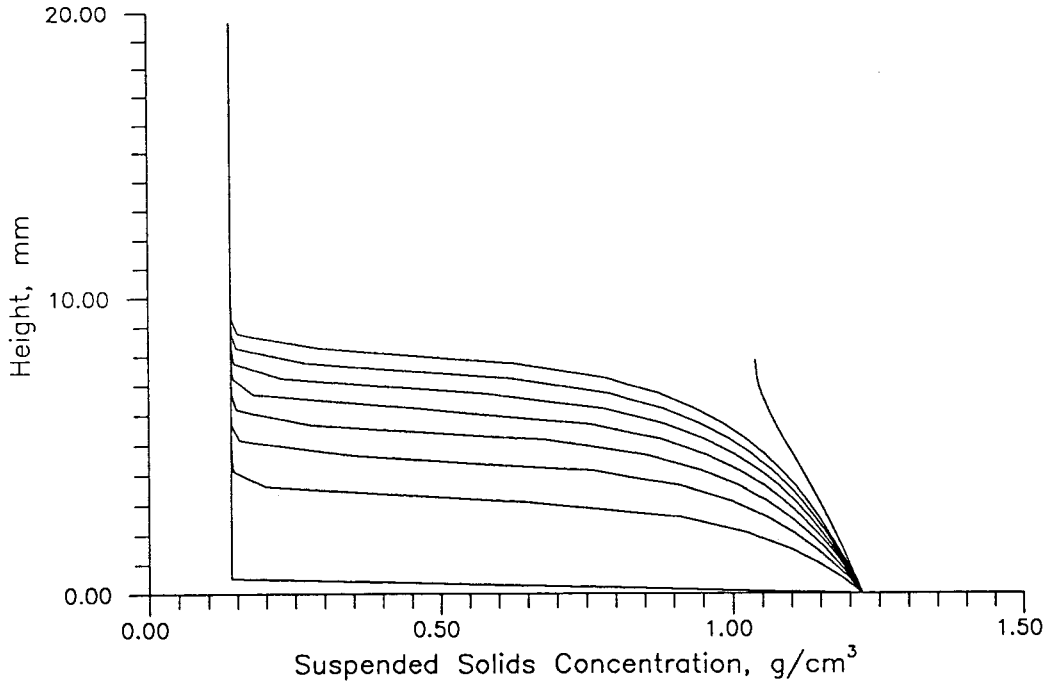


Figure 92. Concentration profiles at 30 s intervals under conditions of CHES run KDM3B (345 kPa, 0.31 g/cm³) without prior gravity sedimentation.

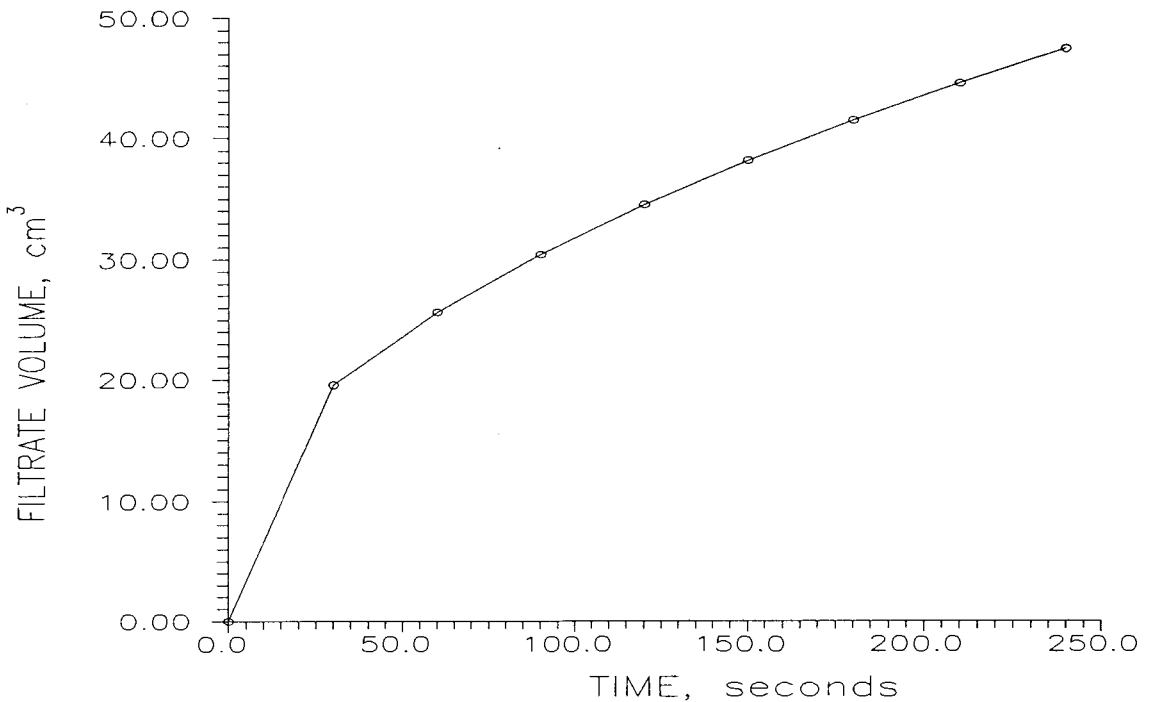


Figure 93. Filtrate production versus time for run KDM3B without prior gravity sedimentation.

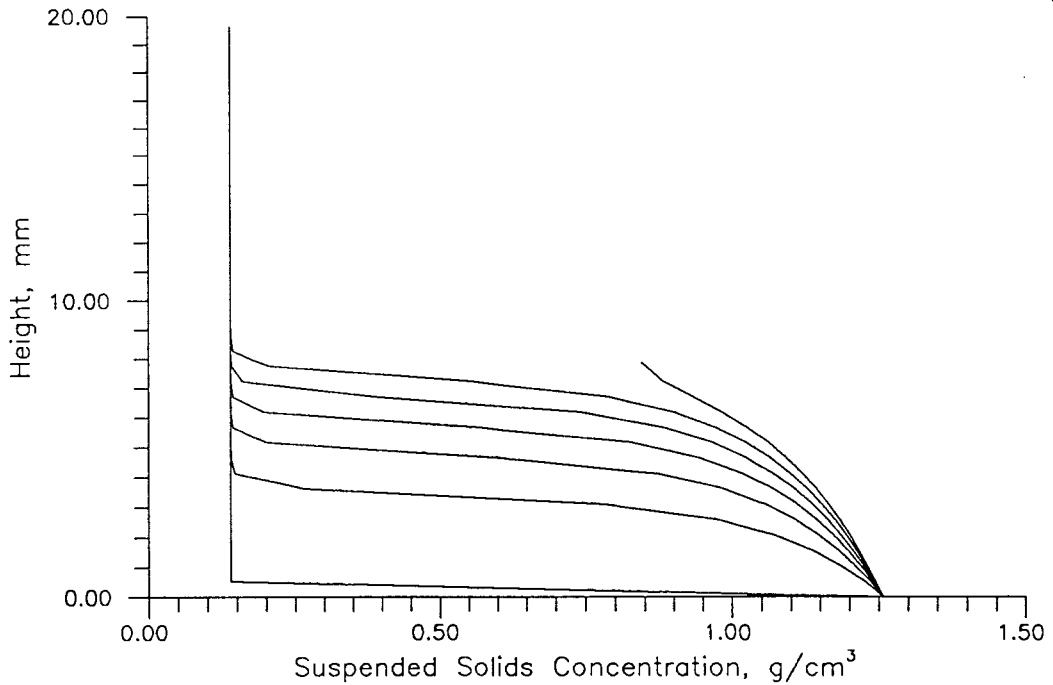


Figure 94. Concentration profiles at 30 s intervals under conditions of CHES run PMK10 (520 kPa, 0.31 g/cm³) without prior gravity sedimentation.

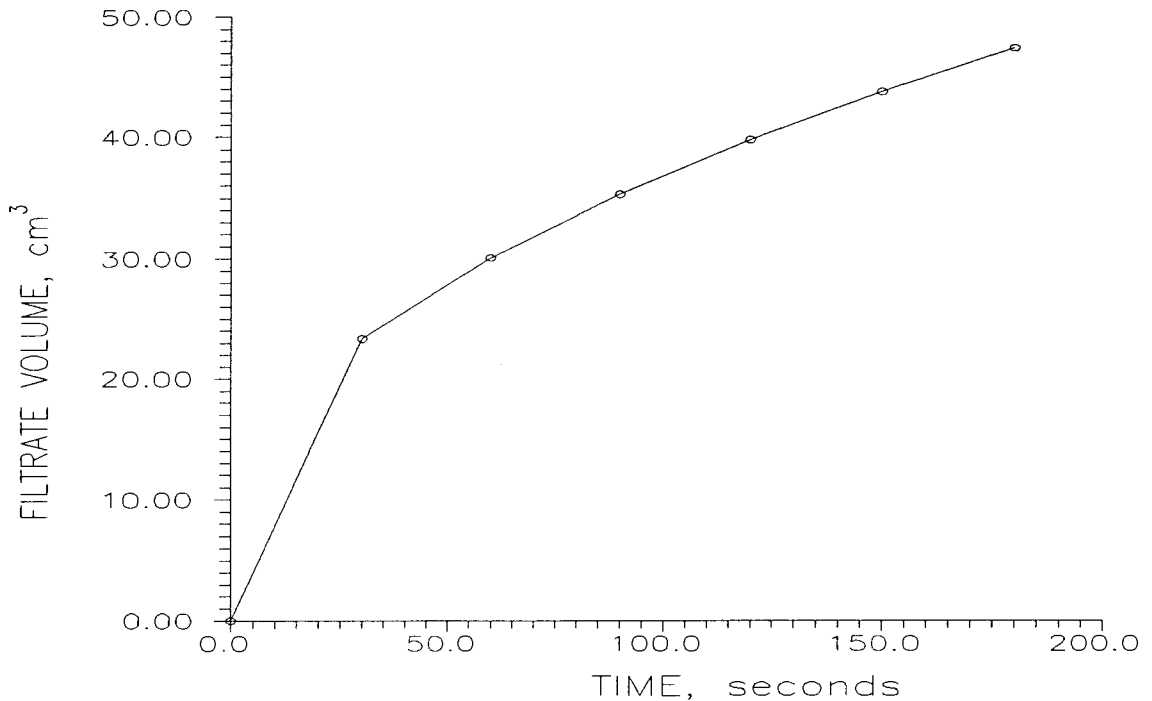


Figure 95. Filtrate production versus time for run PMK10 without prior gravity sedimentation.

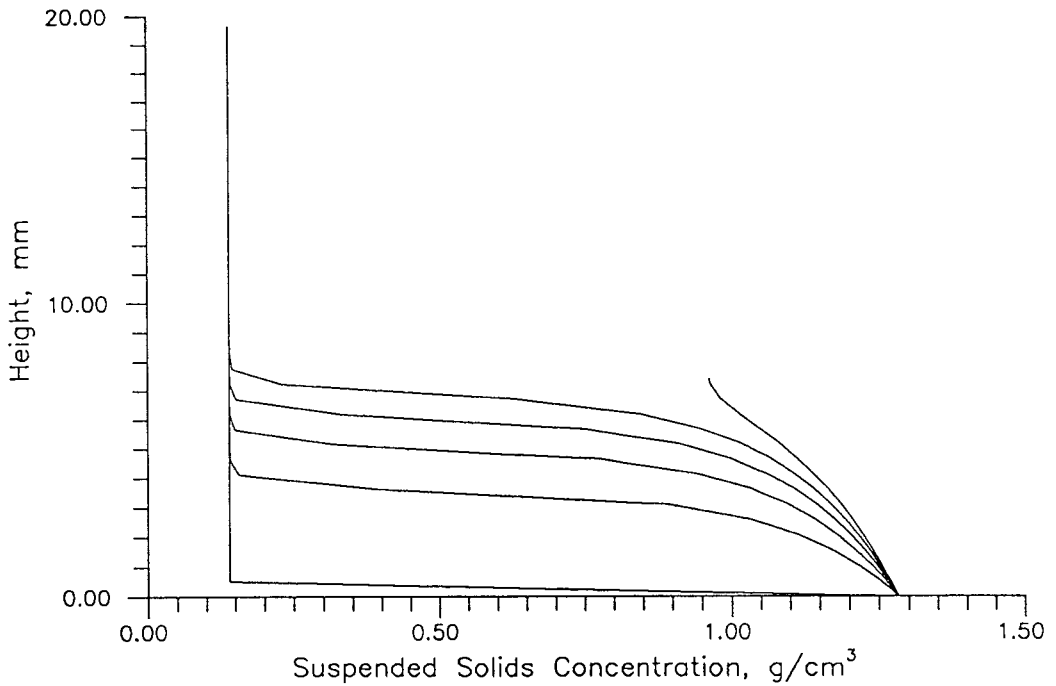


Figure 96. Concentration profiles at 30 s intervals under conditions of CHES run PMK7 (690 kPa, 0.31 g/cm³) without prior gravity sedimentation.

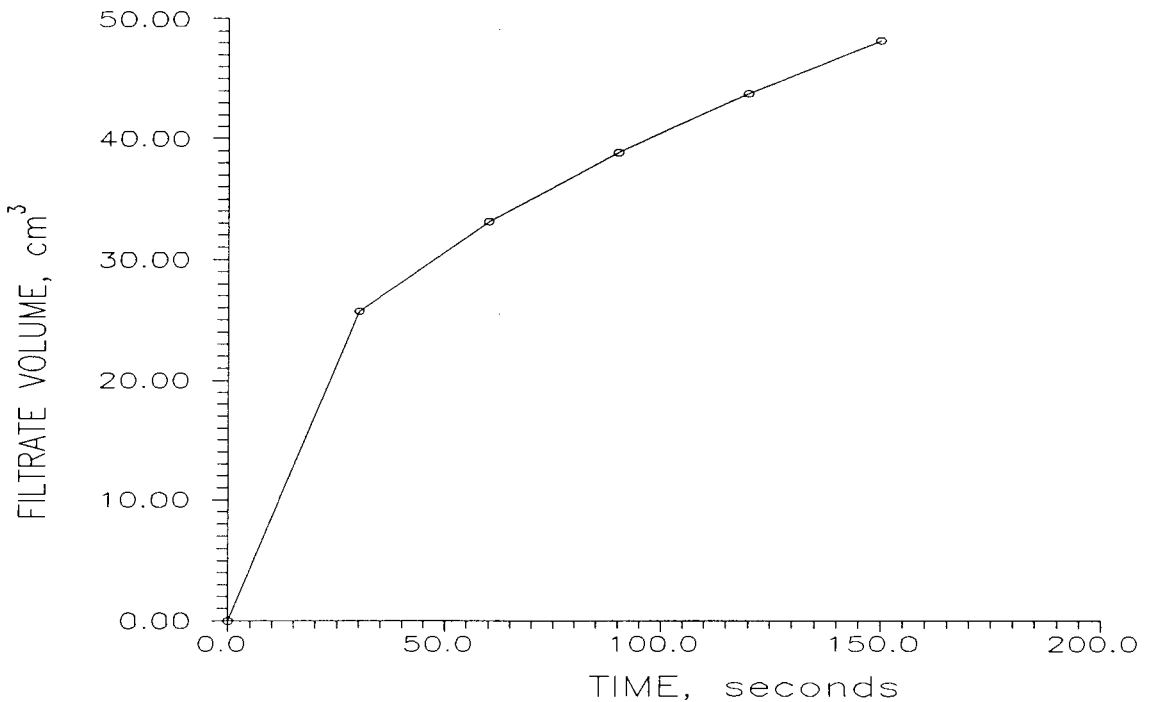


Figure 97. Filtrate production versus time for run PMK7 without prior gravity sedimentation.

CHAPTER VII

DETERMINATION OF CONSTITUTIVE RELATIONSHIPS FROM SPECIFIC RESISTANCE TESTS

Because the method of Bierck, Wells, and Dick (1988) cannot routinely be used to determine the sludge dewaterability parameters α , β , γ , and δ , a simple, reproducible and readily available method is needed for determining these parameters if the Wells dewatering model is to be a useful tool for the design of sludge dewatering equipment. Wells (1990b) proposed a methodology for determining these parameters from specific resistance tests. The specific resistance test apparatus is shown in Figure 98. A known volume of sludge is poured into the filtration cell at time zero and a constant pressure is applied, either in the form of pressure or vacuum. Filtrate volume is then measured as time proceeds. The specific resistance is calculated from

$$r_s = \frac{2P_{app} A^2 s}{\mu w} \quad (71)$$

where

w = dry weight of cake deposited per unit volume of
filtrate

s = slope of linear portion of a plot of t/V

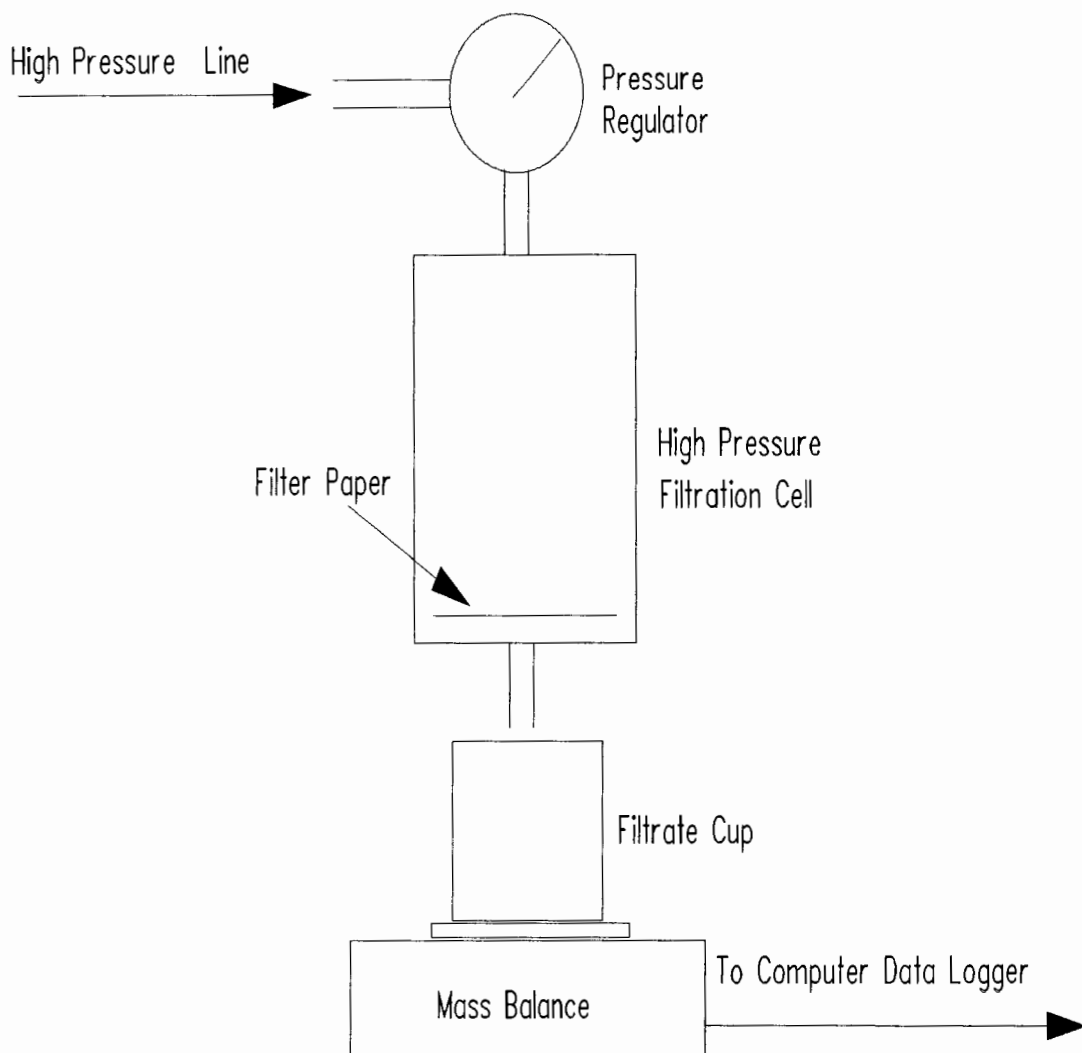


Figure 98. Specific resistance test apparatus.

versus V from the data of the specific resistance test

A = area of filtration cell

V_i = volume of sludge added

The following is an outline of the method for determining sludge dewaterability parameters proposed by Wells (1990b).

Assuming exponential forms for permeability, k and the

coefficient of volume compressibility, m_v , as functions of suspended solids concentration, c , the constitutive equations can be formulated as

$$k_c = \alpha' e^{\beta' c} \quad (72)$$

and

$$m_{v_c} = \gamma' e^{\delta' c} \quad (73)$$

where α' , β' , γ' , and δ' are constants determined from specific resistance tests. The definition of specific resistance, r_s , (assuming that the porewater pressure is a function only of suspended solids concentration) is

$$r_s = \frac{P_{app}}{\bar{c}} \left[\int_{c_0}^{c_i} \frac{-k_c}{m_v} dc \right]^{-1} \quad (74)$$

where

\bar{c} = average suspended solids concentration of cake

c_i = initial suspended solids concentration of
slurry

c_0 = terminal suspended solids concentration (c at
 $z=0$)

The four unknown parameters α' , β' , γ' , and δ' can be determined by applying a non-linear least squares curve fitting technique developed by Wells (1990b). Values of the four parameters are assumed, and using Equation 71, the specific resistance, r_s , is calculated and plotted as a

function of the applied pressure differential, P_{app} . The values of specific resistance at each pressure differential are compared to data from actual specific resistance tests and the error between Equation 71 and the experimental data is calculated. By judicious choice of the dewaterability parameters α' , β' , γ' , and δ' the error between Equation 71 and the experimental data can be minimized.

Since the parameters α' , β' , γ' and δ' were derived in terms of suspended solids concentration rather than porosity, a conversion must be made before the parameters can be used in the dewatering model. Knowing that

$$k_c = k$$

and

$$c = \rho_s(1-n) \quad (75)$$

then from Equations 72 and 75

$$k = \alpha' e^{\rho_s \beta' (1-n)}$$

or

$$k = \alpha' e^{\rho_s \beta'} e^{-\rho_s \beta' n}$$

So, the first two parameters needed for the dewatering model can be calculated from

$$\alpha = \alpha' e^{\rho_s \beta'}$$

and

$$\beta = -\rho_s \beta'$$

Similarly, knowing that

$$m_{v_c} = \rho_s m_v$$

then from Equations 73 and 75

$$m_v = \frac{1}{\rho_s} \gamma' e^{\rho_s \delta' (1-n)}$$

or

$$m_v = \frac{1}{\rho_s} \gamma' e^{\rho_s \delta'} e^{-\rho_s \delta' n}$$

which yields the last two parameters needed

$$\gamma = \frac{1}{\rho_s} \gamma' e^{\rho_s \delta'}$$

and

$$\delta = -\rho_s \delta'$$

Wells (1990b) conducted specific resistance experiments using suspensions of synthetic kaolin sludge, a polymer-dosed anaerobic sludge, and an anaerobic sludge without conditioning. Using the methodology outlined above, dewaterability parameters were determined for each sludge. Table XI summarizes the parameters obtained by Wells from this procedure. Table XII gives the converted parameters that were later used as input to the dewatering model.

TABLE XI

SUMMARY OF DEWATERABILITY PARAMETERS OBTAINED FROM SPECIFIC RESISTANCE TESTS

Sludge	α' [cm ²]	β' [cm ³ /g]	γ' [s ² /cm ²]	δ' [cm ³ /g]
Kaolin Flat-D with distilled water. ($c_i=0.31$ g/cm ³)	4.5×10^{-9}	-4.7	2.3×10^{-2}	-10.1
Anaerobic di- gested combined primary + waste activated sludge w/o conditioner ($c_i=0.022$ g/cm ³)	5.0×10^{-10}	-100.0	3.42×10^{-5}	-91.5
Anaerobic di- gested combined primary + waste activated sludge w/o conditioner ($c_i=0.025$ g/cm ³)	1.0×10^{-8}	-33.7	2.0×10^{-4}	-34.4

TABLE XII

SUMMARY OF CONVERTED DEWATERABILITY PARAMETERS TO BE USED IN DEWATERING MODEL

Sludge	α [cm ²]	β [-]	γ [cm-s ² /g]	δ [-]
Kaolin Flat-D with distilled water. ($c_i=0.31$ g/cm ³)	2.1×10^{-14}	12.3	2.83×10^{-14}	26.5
Anaerobic di- gested combined primary + waste activated sludge w/o conditioner ($c_i=0.022$ g/cm ³)	7.9×10^{-71}	140.0	5.69×10^{-61}	128.1
Anaerobic di- gested combined primary + waste activated sludge with conditioner ($c_i=0.025$ g/cm ³)	3.24×10^{-29}	47.2	1.73×10^{-25}	48.2

Figures 99 and 100 show the calculated constitutive relationships for kaolin suspensions superimposed over CHES data. The calculated constitutive equations are seen to be very close to the calibrated constitutive equations used in chapters 4 and 5. Results of computer simulations using these constitutive relationships under the conditions of CHES runs are summarized in Table XIII, and are shown graphically in Figures 101-142. Table XV presents the results of statistical comparisons between CHES data and model output for the constitutive relationships calculated for kaolin sludge.

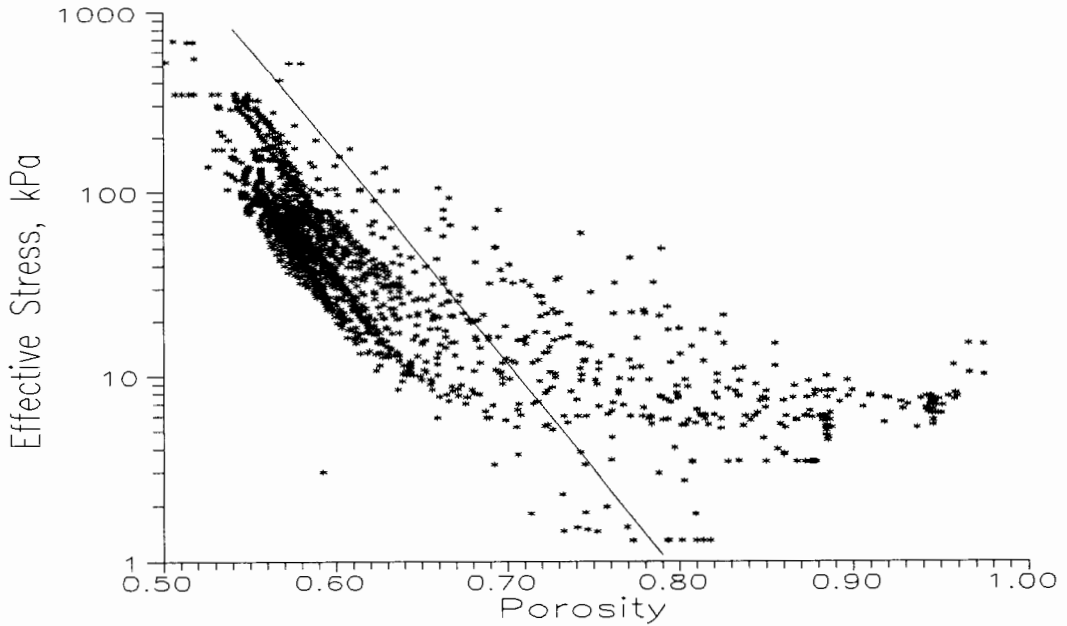


Figure 99. Semi-log plot of kaolin effective stress versus porosity constitutive relationship calculated from specific resistance tests superimposed over CHES data.

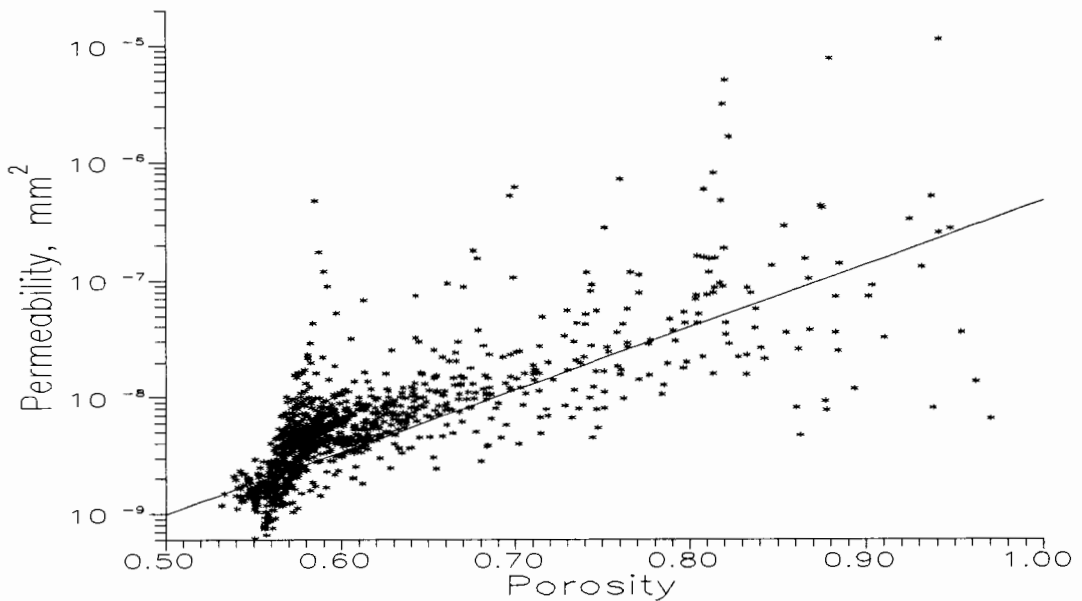


Figure 100. Semi-log plot of kaolin permeability versus porosity constitutive relationship calculated from specific resistance tests superimposed over CHES data.

TABLE XIII

SUMMARY OF RESULTS FROM COMPUTER SIMULATIONS USING
CONSTITUTIVE RELATIONSHIPS FOR KAOLIN SLUDGE CALCULATED FROM
SPECIFIC RESISTANCE TESTS

Run	P_{app} (kPa)	Temp. (° C)	CPU* Time (S)	Form. Time (S)	Simu- lated Time (S)	Term. Porosity
$c_i = 0.47 \text{ cm}^3$						
KDMK8	103	26.0	369.0	375.2	900.0	0.5311
KDM6	172	26.0	325.3	267.4	595.2	0.5117
KDM4	345	26.0	310.9	185.6	378.6	0.4855
PMK9	517	24.0	271.3	127.2	303.5	0.4702
PMK6	682	24.0	180.3	1.3	2.0	0.4598
$c_i = 0.31 \text{ cm}^3$						
KDMK9	103	25.5	275.4	306.1	900.0	0.5311
KDM2	172	26.0	298.7	265.2	502.6	0.5117
PMK3	345	26.0	227.0	212.7	291.7	0.4855
PMK4	517	24.0	225.9	168.3	225.3	0.4702
PMK5	682	24.0	230.4	142.6	224.7	0.4598
$c_i = 0.14 \text{ cm}^3$						
KDM7	103	26.0	63.1	114.6	418.1	0.5311
KDM5	172	26.0	69.2	83.9	310.4	0.5117
KDM3B	345	26.0	86.3	56.2	197.6	0.4855
PMK10	517	24.0	118.5	45.2	161.6	0.4702
PMK7	682	24.0	166.6	36.8	133.0	0.4598

* Using a Tektronix XD88/10 UNIX workstation

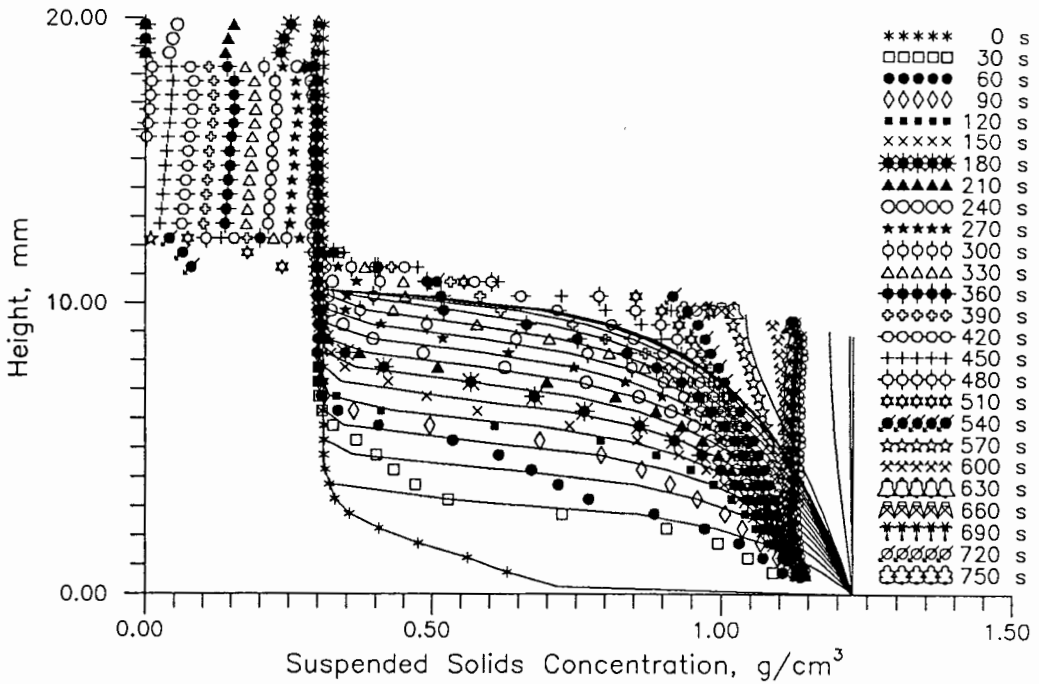


Figure 101. Data-model comparison of concentration profiles at 30 s intervals under conditions of CHES run KDMK9 using constitutive relationships calculated from specific resistance tests.

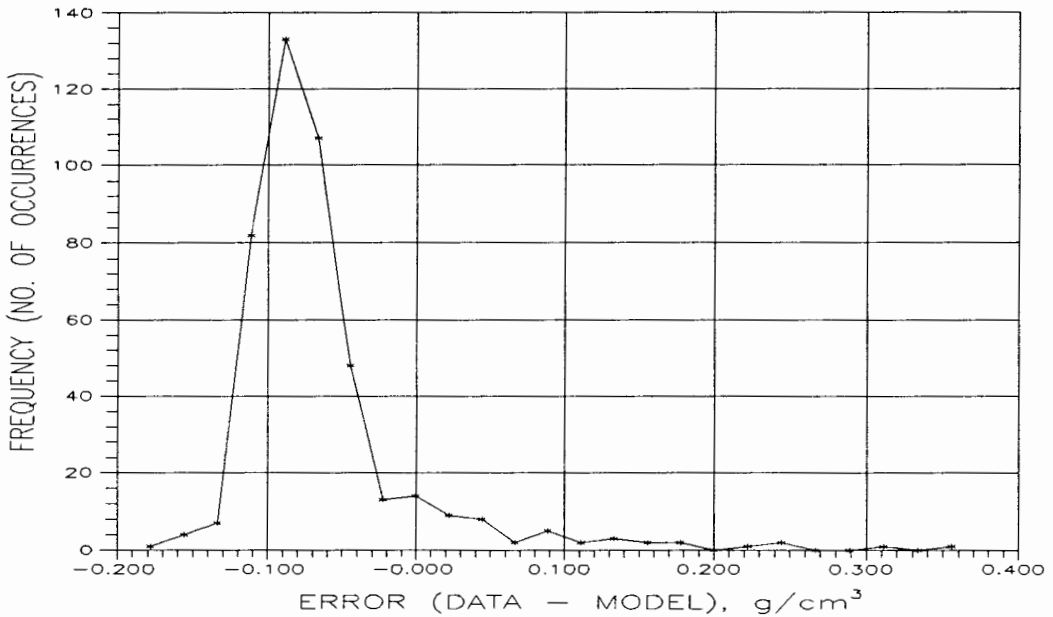


Figure 102. Error frequency histogram for calculated constitutive relationship run KDMK9, paired data-model observations of porosity and time as in Figure 101.

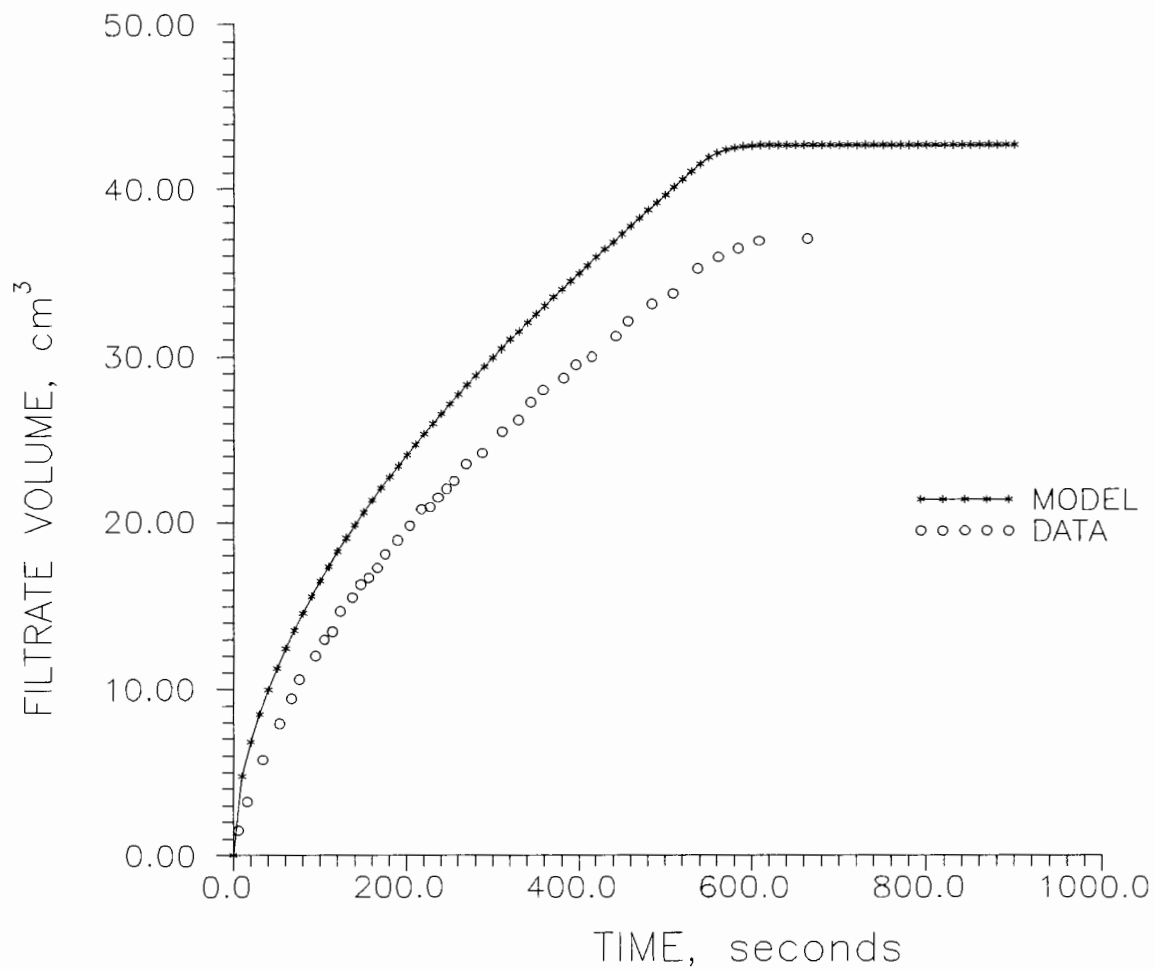


Figure 103. Data-model comparison of filtrate production with time under conditions of CHES run KDMK9 using constitutive relationships calculated from specific resistance tests.

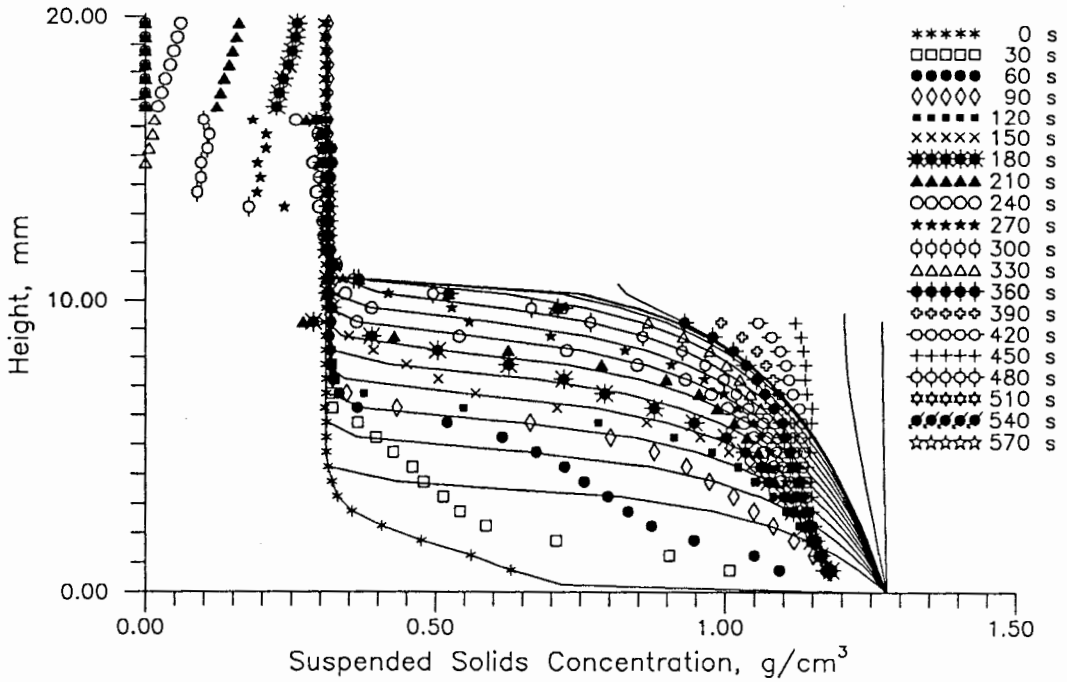


Figure 104. Data-model comparison of concentration profiles at 30 s intervals under conditions of CHES run KDM2 using constitutive relationships calculated from specific resistance tests.

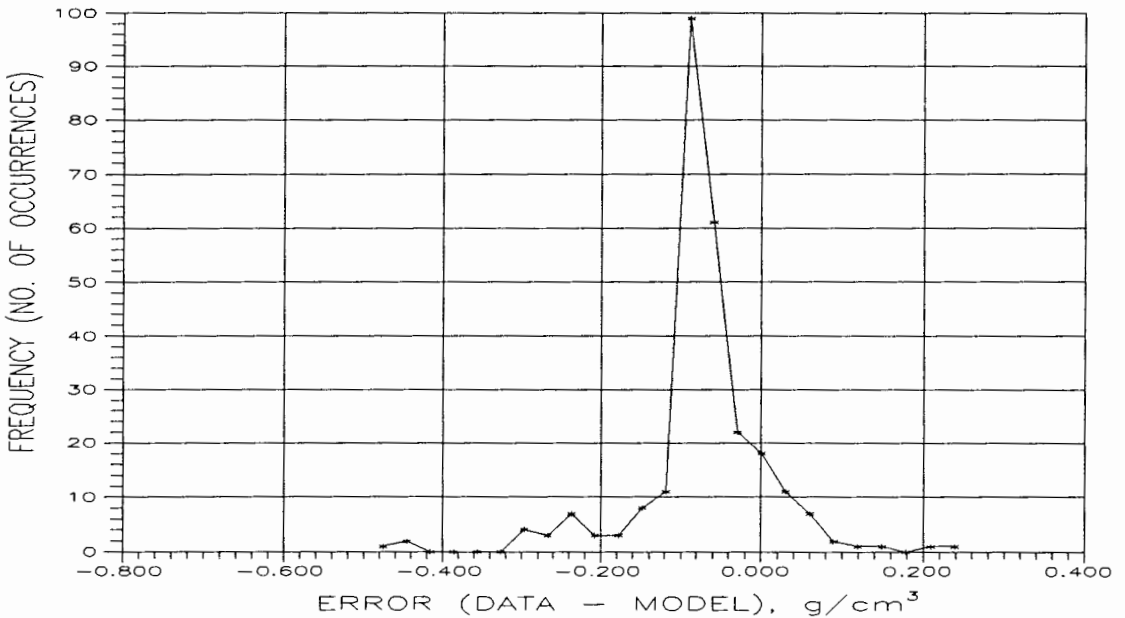


Figure 105. Error frequency histogram for calculated constitutive relationship run KDM2, paired data-model observations of porosity and time as in Figure 104.

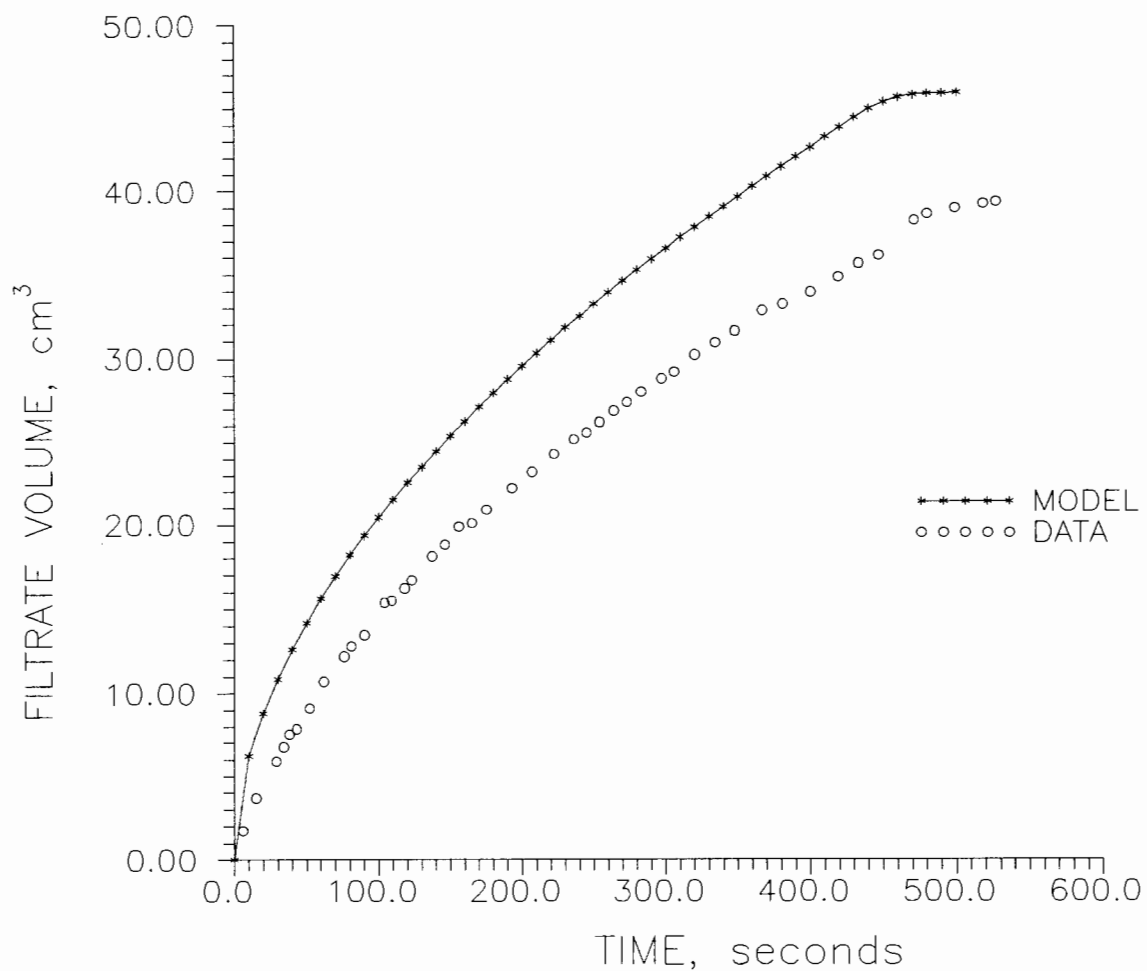


Figure 106. Data-model comparison of filtrate production with time under conditions of CHES run KDM2 using constitutive relationships calculated from specific resistance tests.

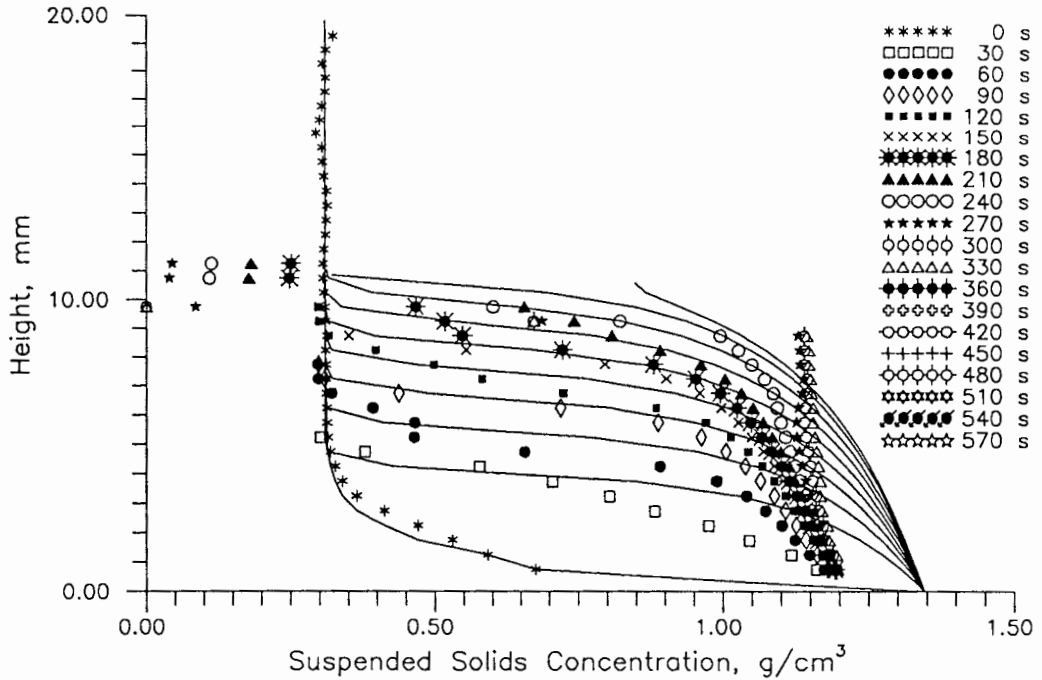


Figure 107. Data-model comparison of concentration profiles at 30 s intervals under conditions of CHES run PMK3 using constitutive relationships calculated from specific resistance tests.

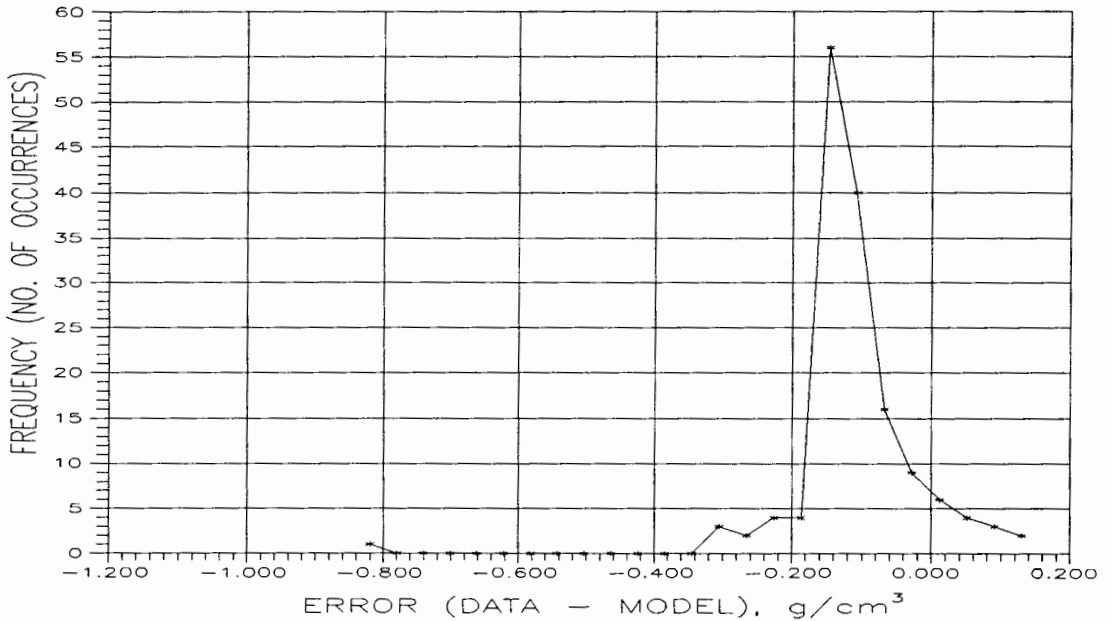


Figure 108. Error frequency histogram for calculated constitutive relationship run PMK3, paired data-model observations of porosity and time as in Figure 107.

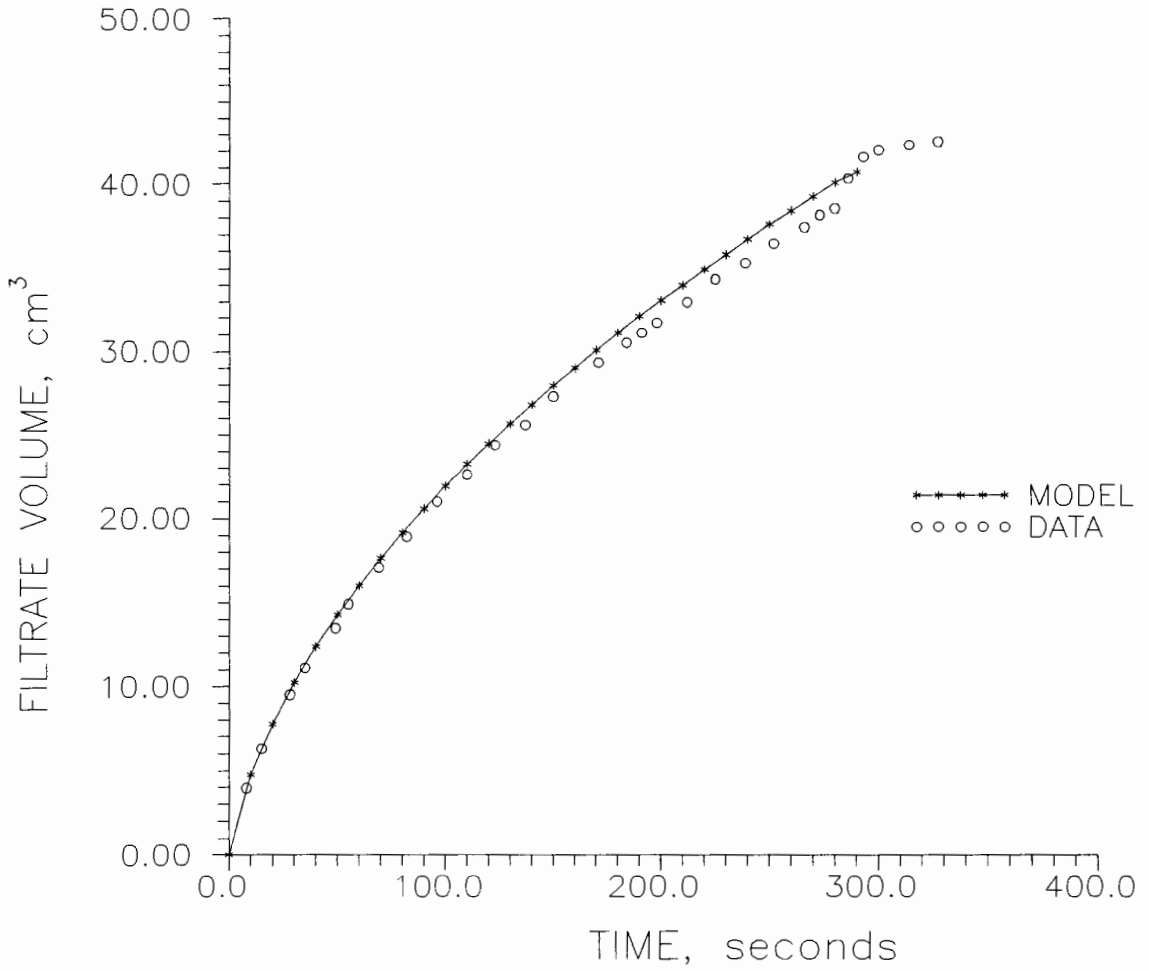


Figure 109. Data-model comparison of filtrate production with time under conditions of CHES run PMK3 using constitutive relationships calculated from specific resistance tests.

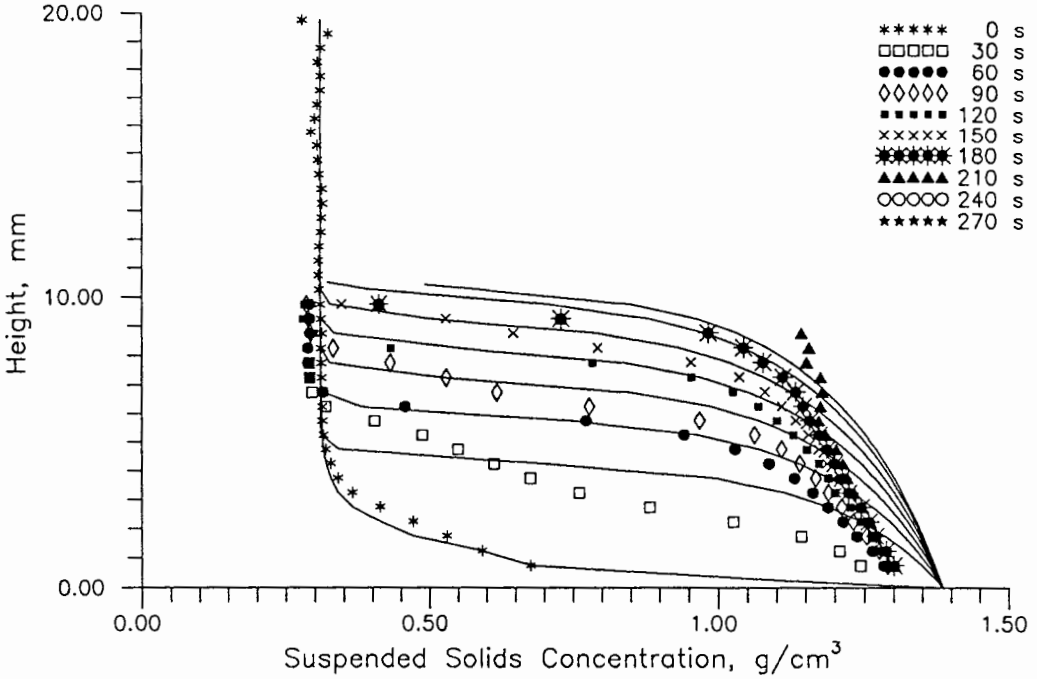


Figure 110. Data-model comparison of concentration profiles at 30 s intervals under conditions of CHES run PMK4 using constitutive relationships calculated from specific resistance tests.

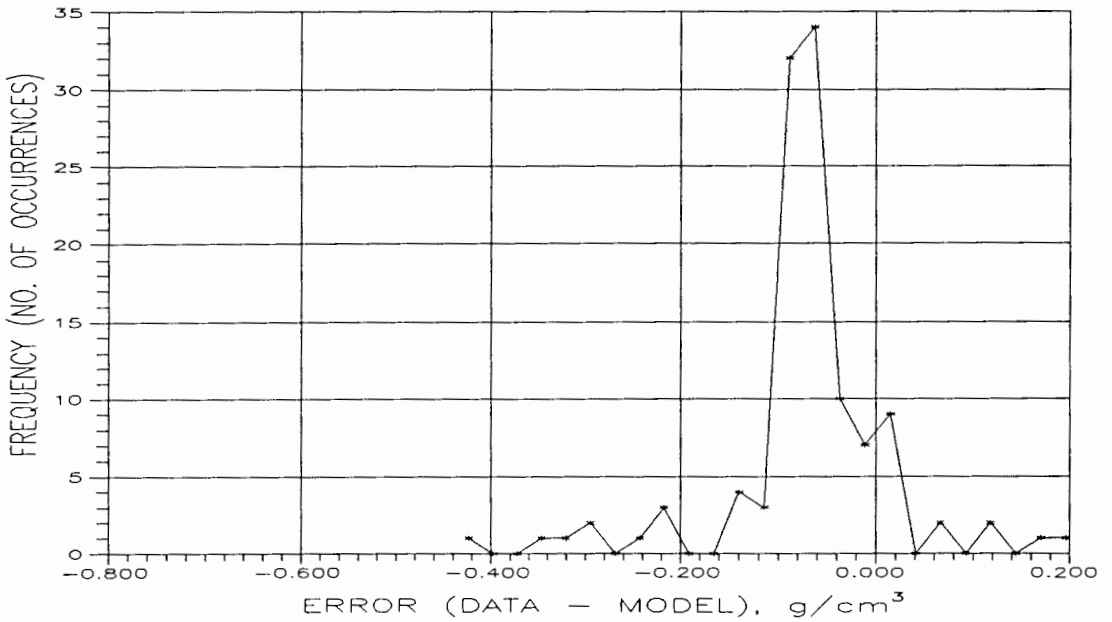


Figure 111. Error frequency histogram for calculated constitutive relationship run PMK4, paired data-model observations of porosity and time as in Figure 110.

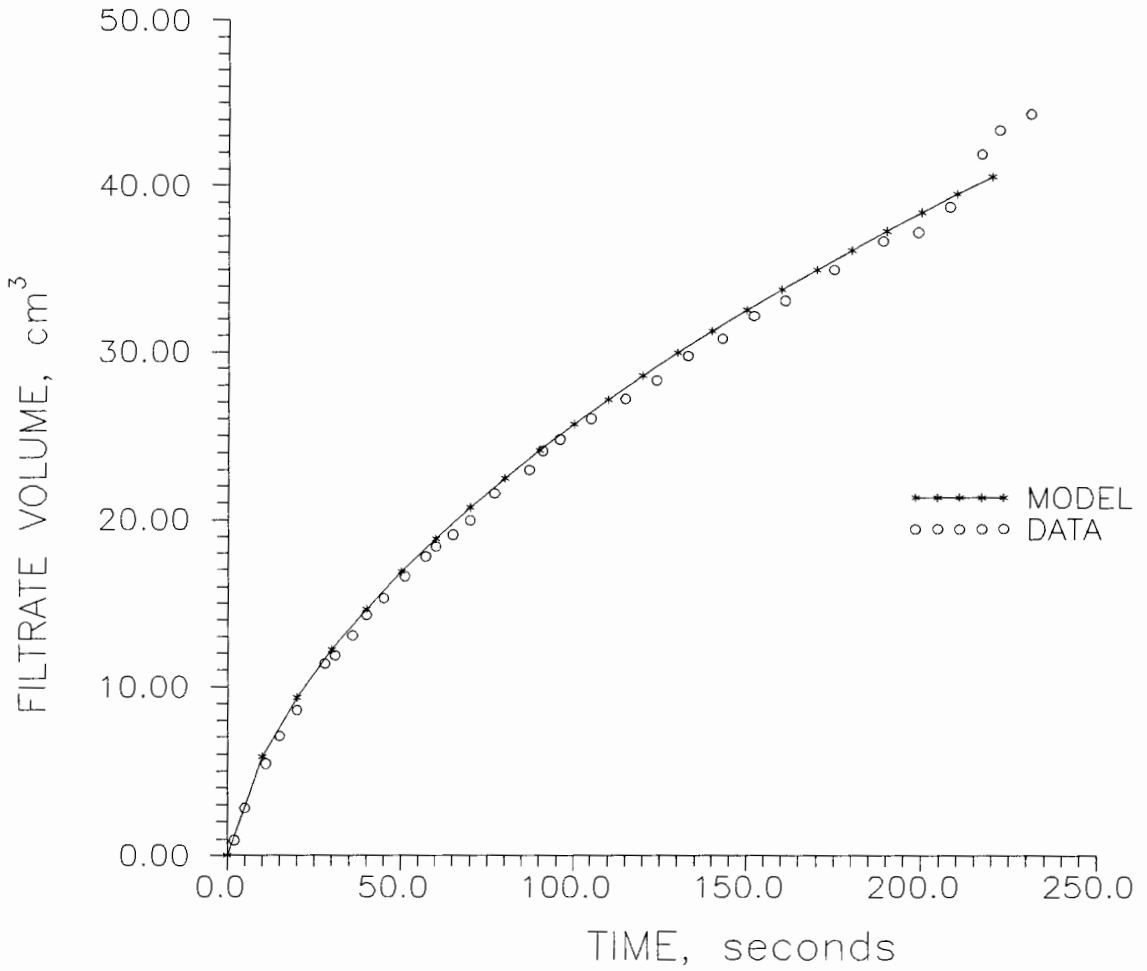


Figure 112. Data-model comparison of filtrate production with time under conditions of CHES run PMK4 using constitutive relationships calculated from specific resistance tests.

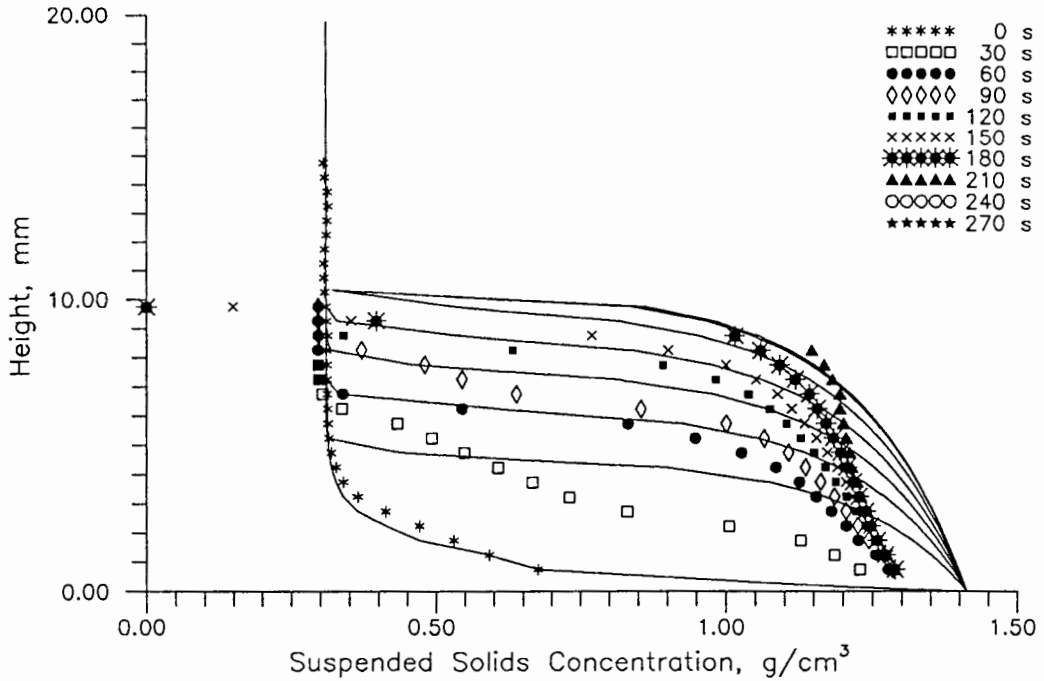


Figure 113. Data-model comparison of concentration profiles at 30 s intervals under conditions of CHES run PMK5 using constitutive relationships calculated from specific resistance tests.

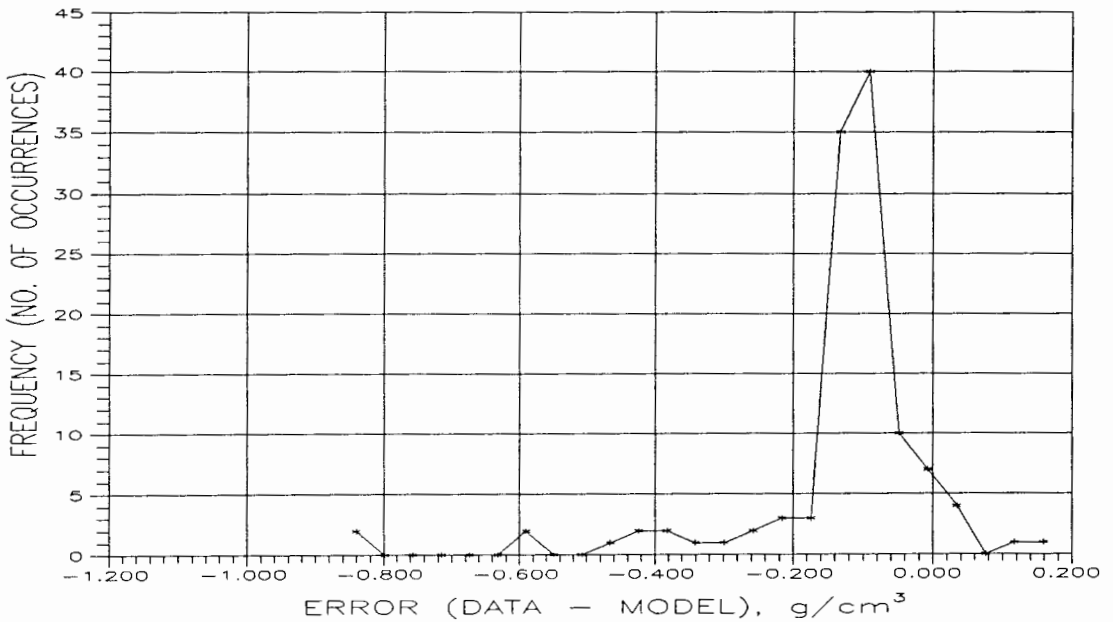


Figure 114. Error frequency histogram for calculated constitutive relationship run PMK5, paired data-model observations of porosity and time as in Figure 113.

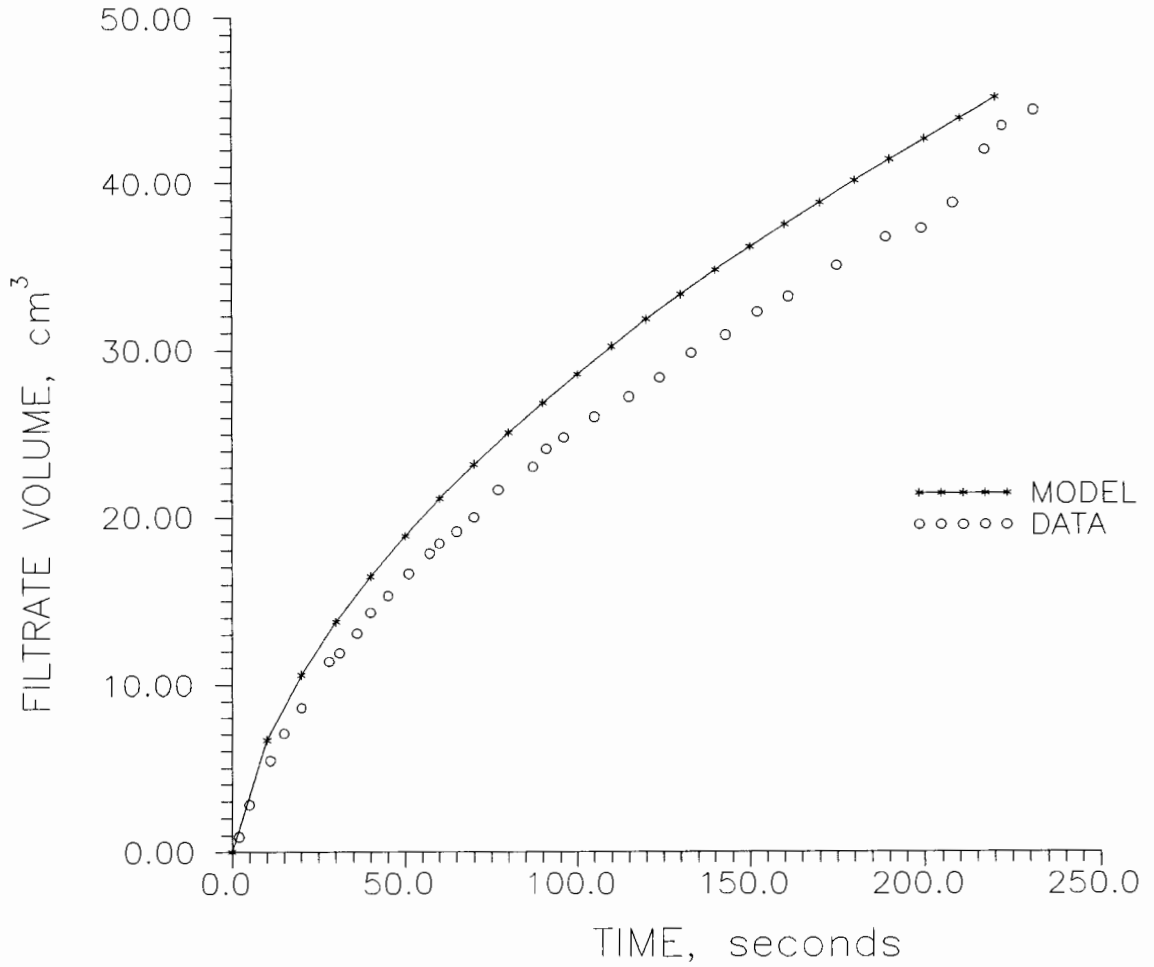


Figure 115. Data-model comparison of filtrate production with time under conditions of CHES run PMK5 using constitutive relationships calculated from specific resistance tests.

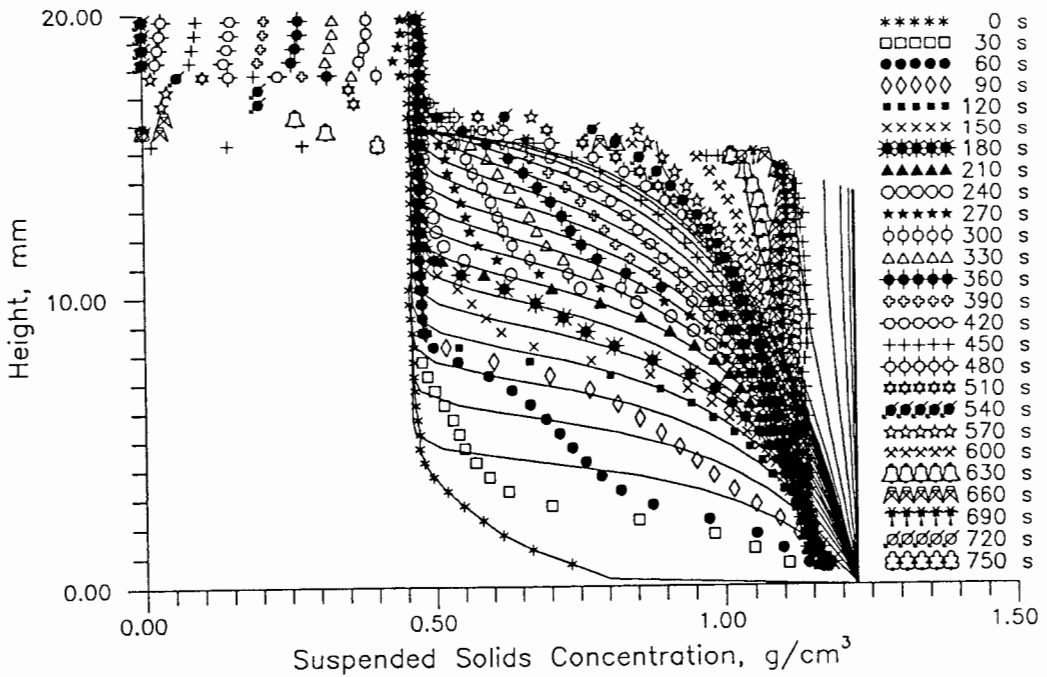


Figure 116. Data-model comparison of concentration profiles at 30 s intervals under conditions of CHES run KDMK8 using constitutive relationship calculated from specific resistance tests.

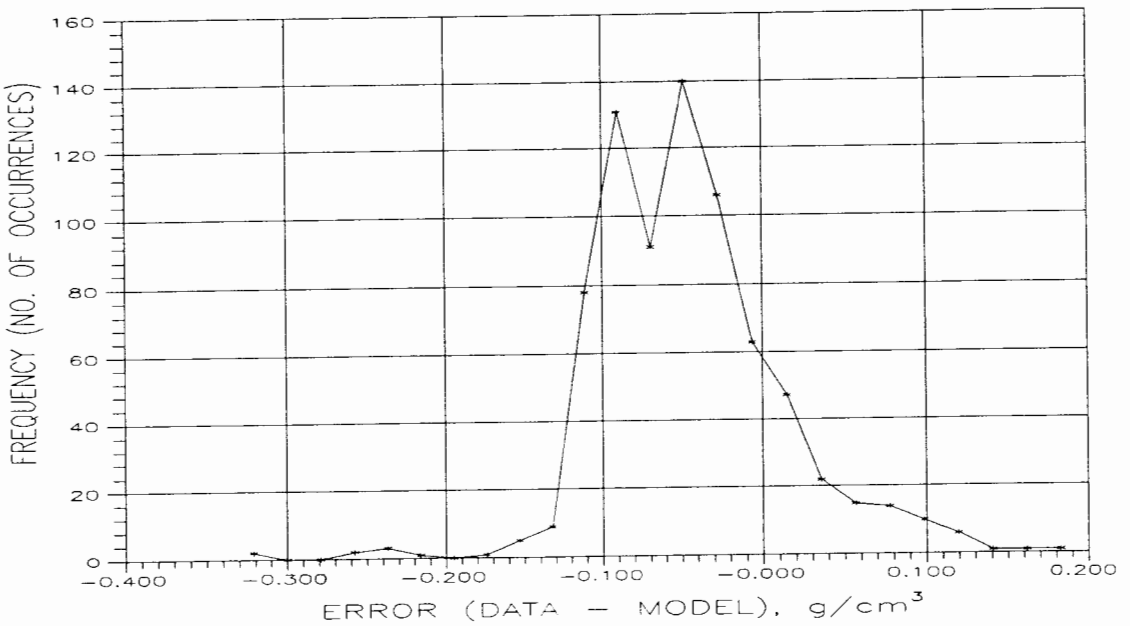


Figure 117. Error frequency histogram for calculated constitutive relationship run KDMK8, paired data-model observations of porosity and time as in Figure 116.

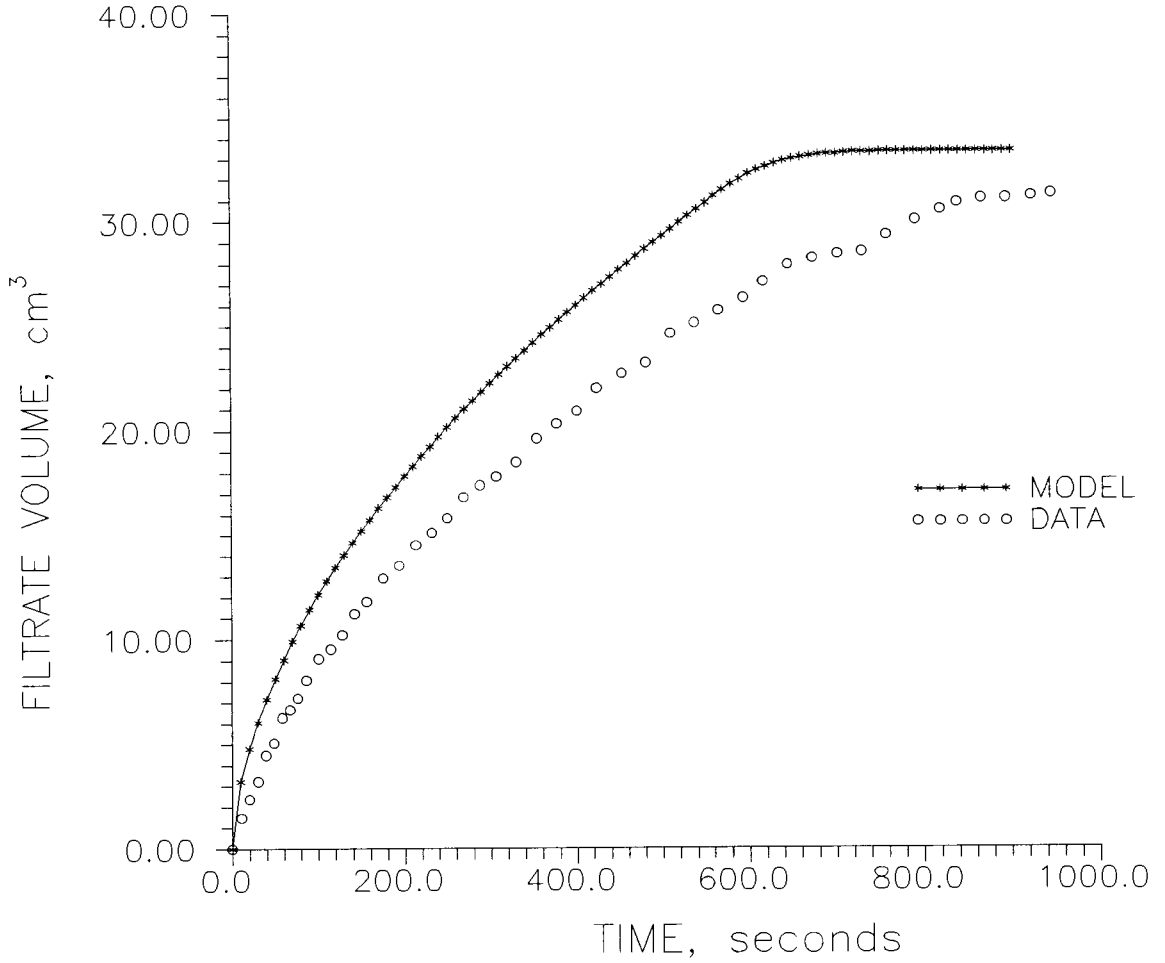


Figure 118. Data-model comparison of filtrate production with time under conditions of CHES run KDMK8 using constitutive relationships calculated from specific resistance tests.

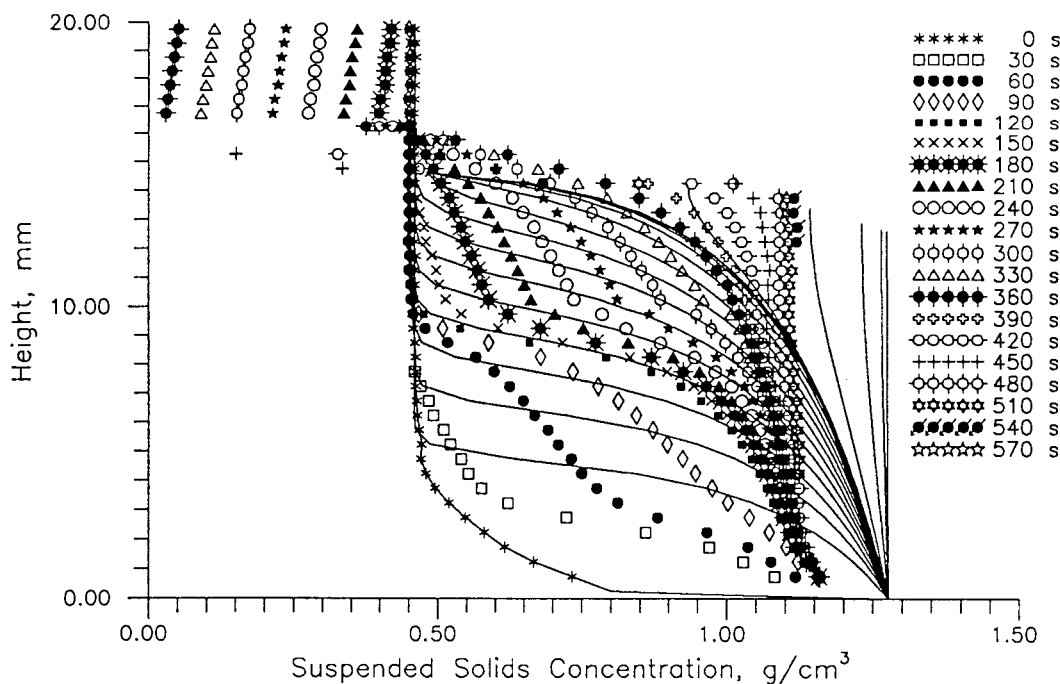


Figure 119. Data-model comparison of concentration profiles at 30 s intervals under conditions of CHES run KDM6 using constitutive relationships calculated from specific resistance tests.

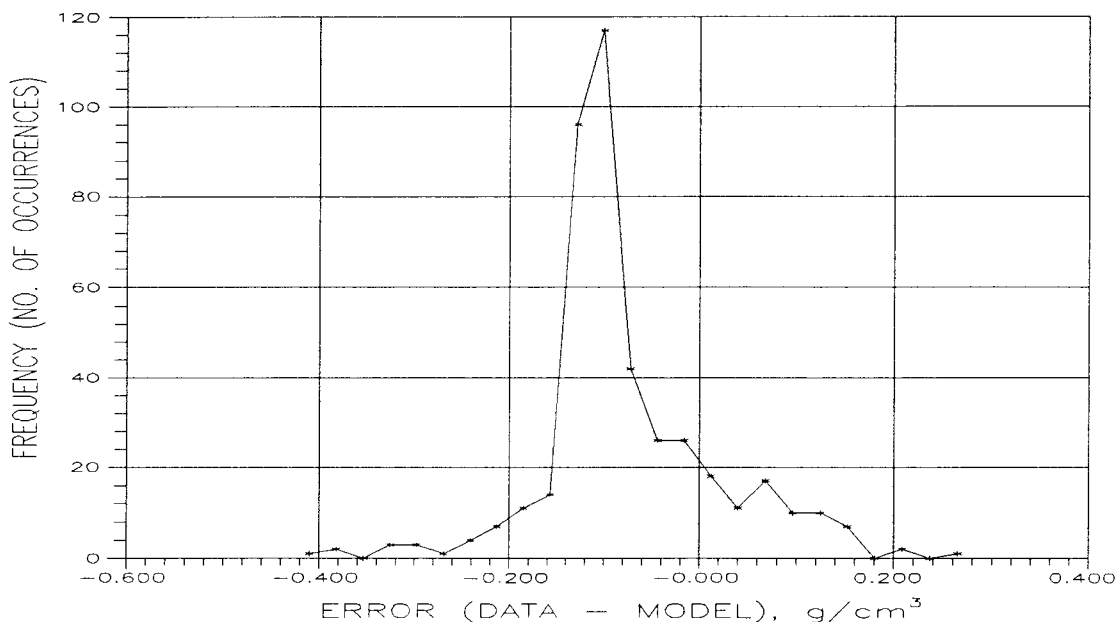


Figure 120. Error frequency histogram for calculated constitutive relationship run KDM6, paired data-model observations of porosity and time as in Figure 119.

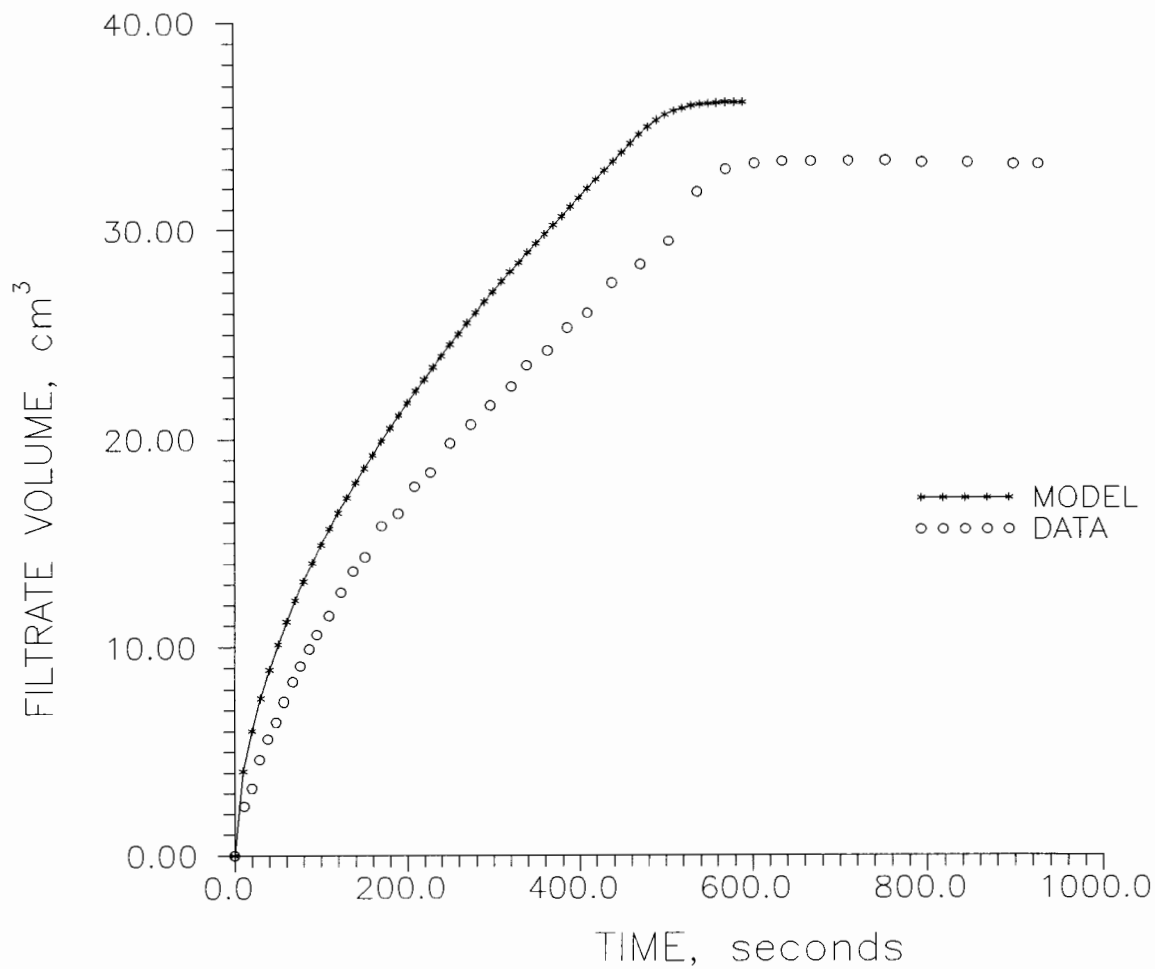


Figure 121. Data-model comparison of filtrate production with time under conditions of CHES run KDM6 using constitutive relationships calculated from specific resistance tests.

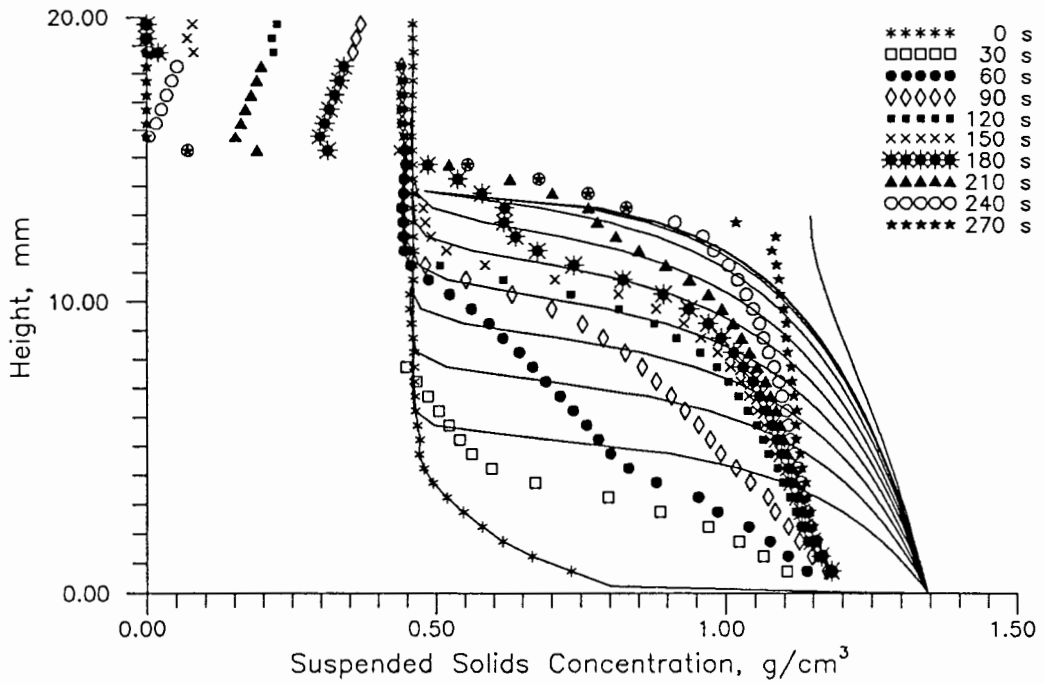


Figure 122. Data-model comparison of concentration profiles at 30 s intervals under conditions of CHES run KDM4 using constitutive relationships calculated from specific resistance tests.

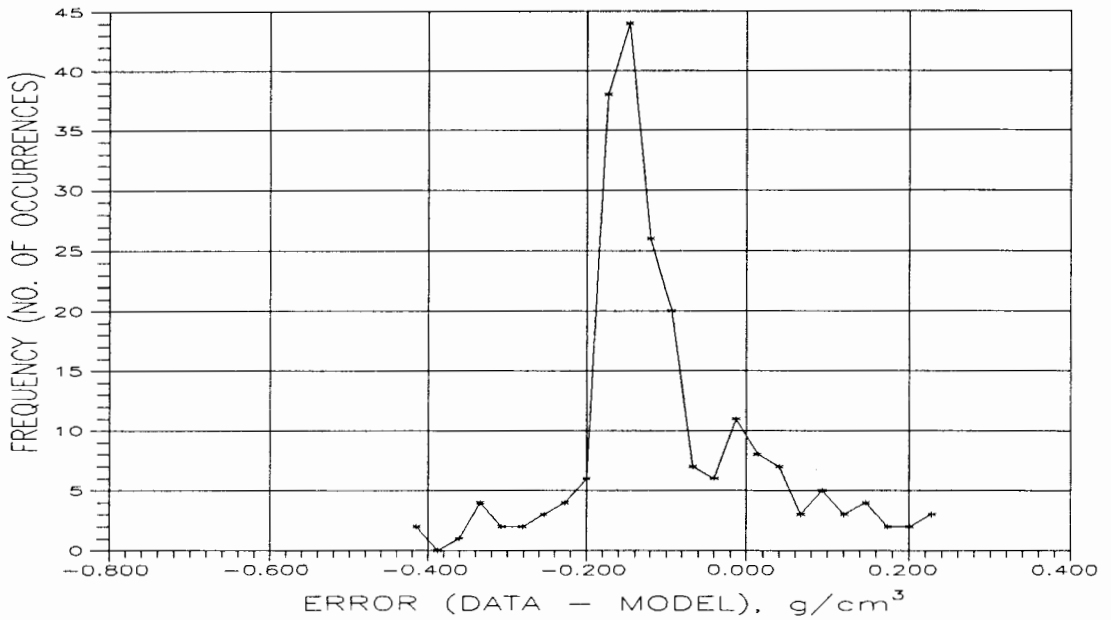


Figure 123. Error frequency histogram for calculated constitutive relationship run KDM4, paired data-model observations of porosity and time as in Figure 122.

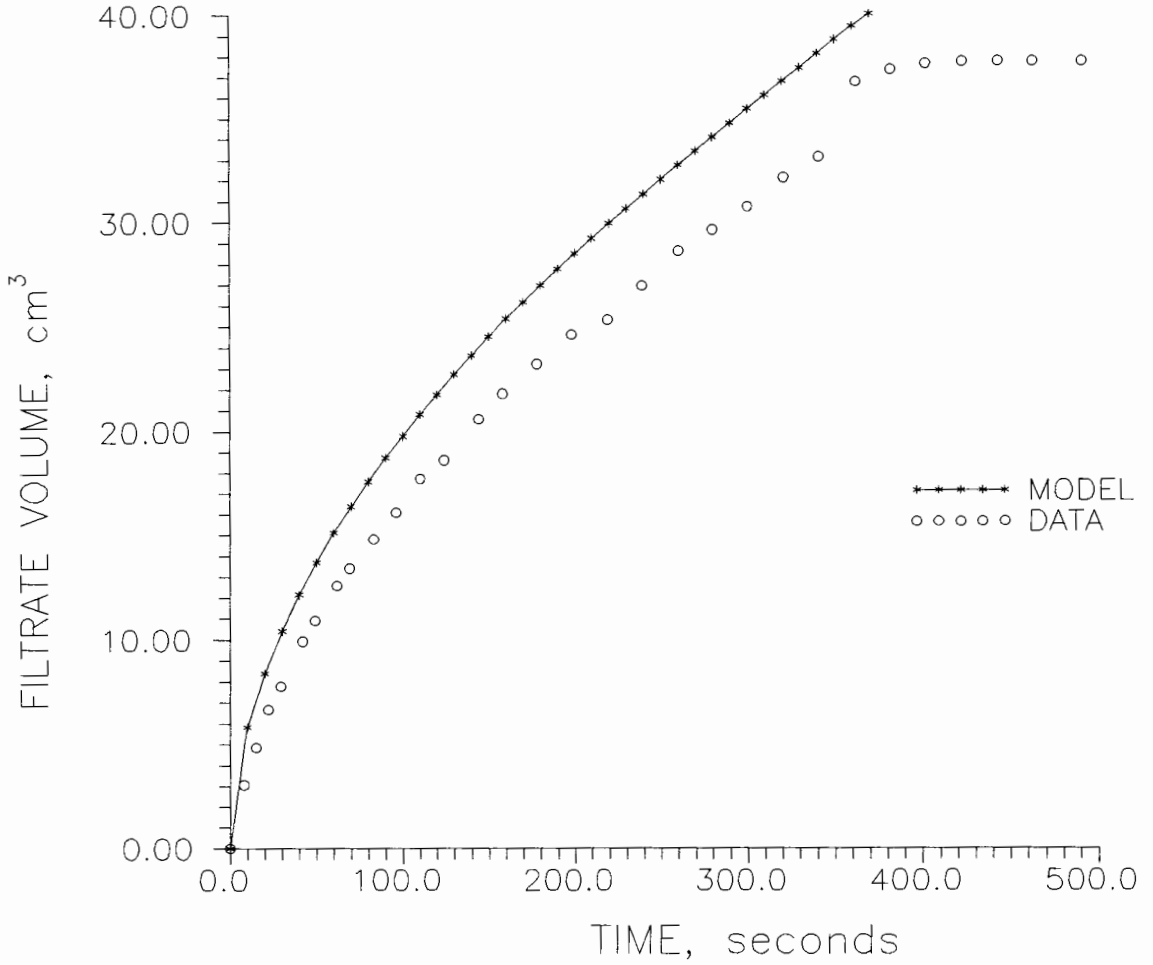


Figure 124. Data-model comparison of filtrate production with time under conditions of CHES run KDM4 using constitutive relationships calculated from specific resistance tests.

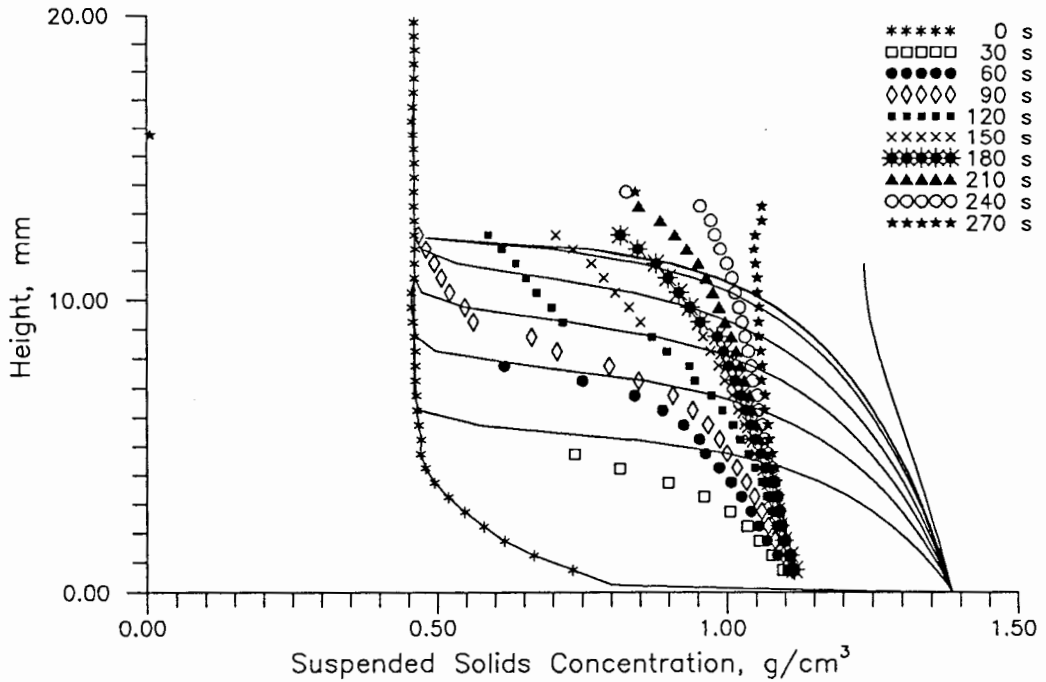


Figure 125. Data-model comparison of concentration profiles at 30 s intervals under conditions of CHES run PMK9 using constitutive relationships calculated from specific resistance tests.

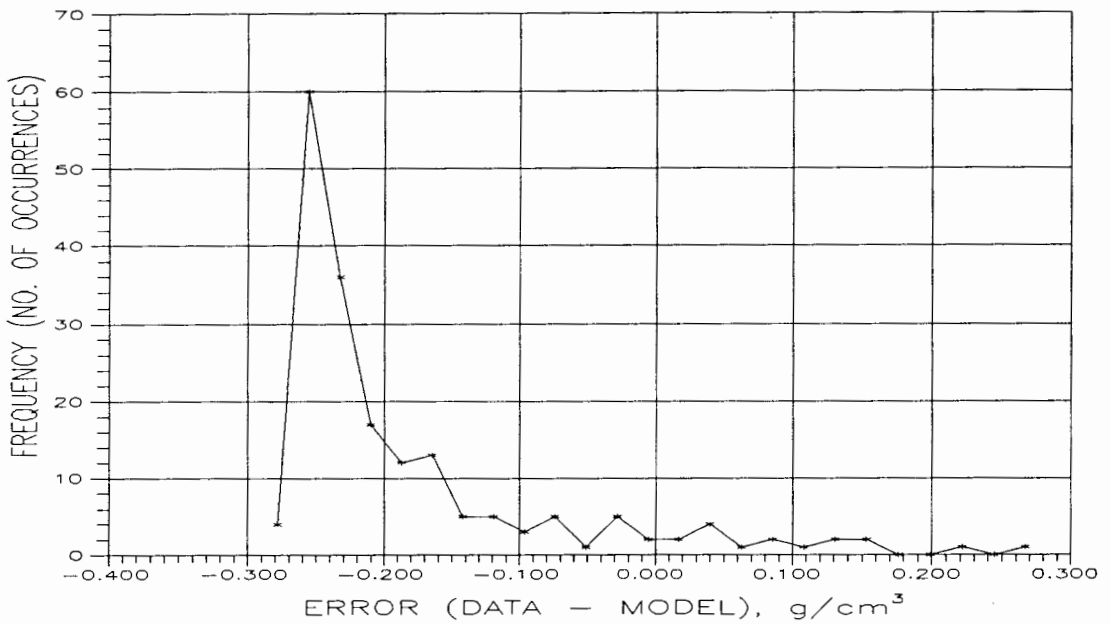


Figure 126. Error frequency histogram for calculated constitutive relationship run PMK9, paired data-model observations of porosity and time as in Figure 125.

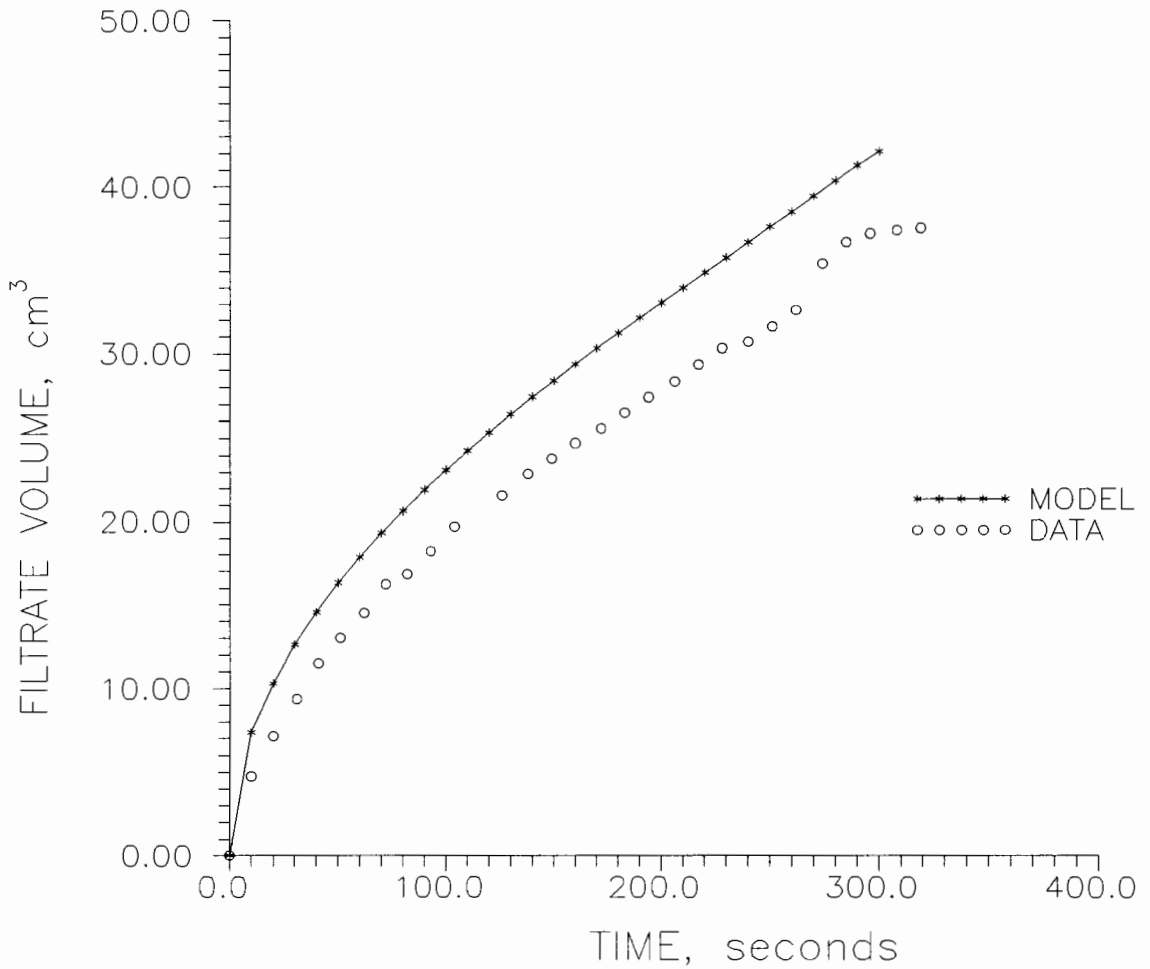


Figure 127. Data-model comparison of filtrate production with time under conditions of CHES run PMK9 using constitutive relationships calculated from specific resistance tests.

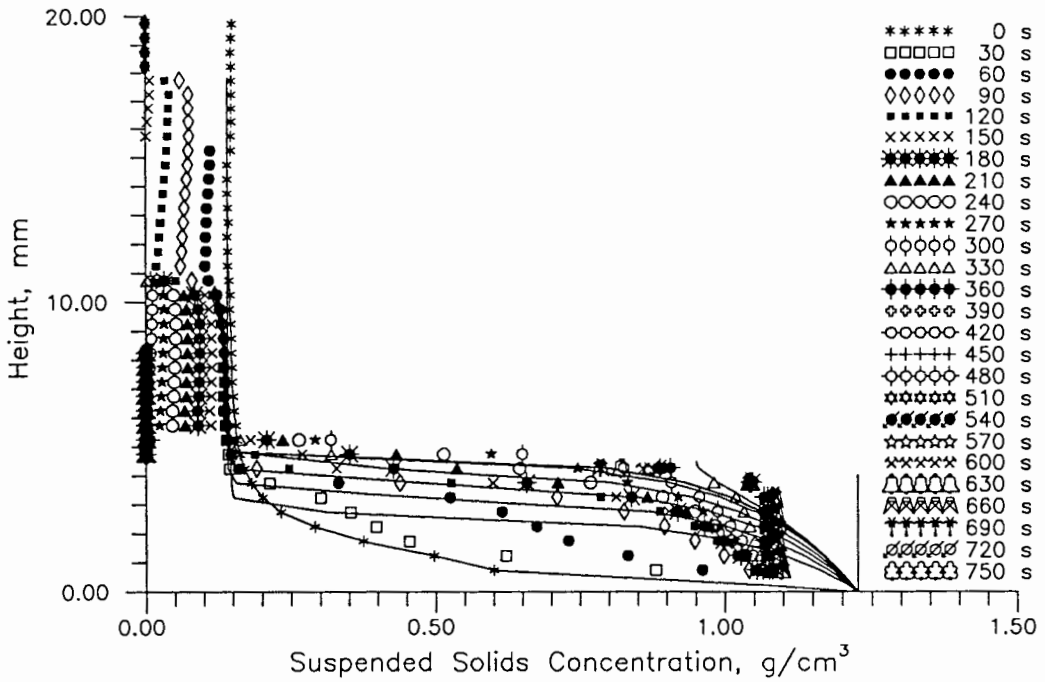


Figure 128. Data-model comparison of concentration profiles at 30 s intervals under conditions of CHES run KDM7 using constitutive relationships calculated from specific resistance tests.

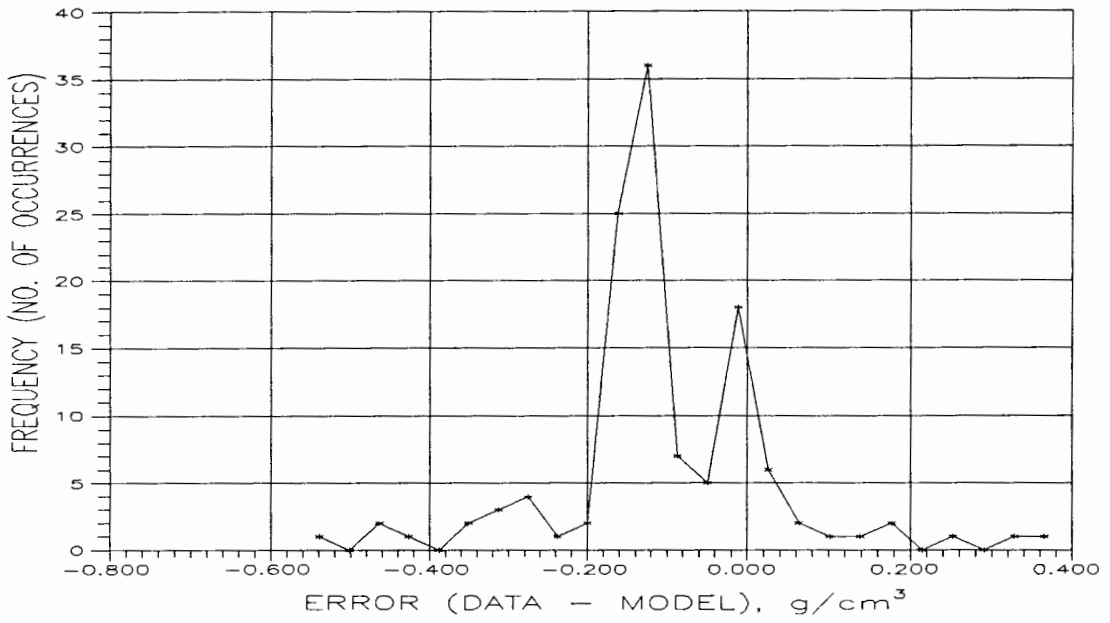


Figure 129. Error frequency histogram for calculated constitutive relationship run KDM7, paired data-model observations of porosity and time as in Figure 128.

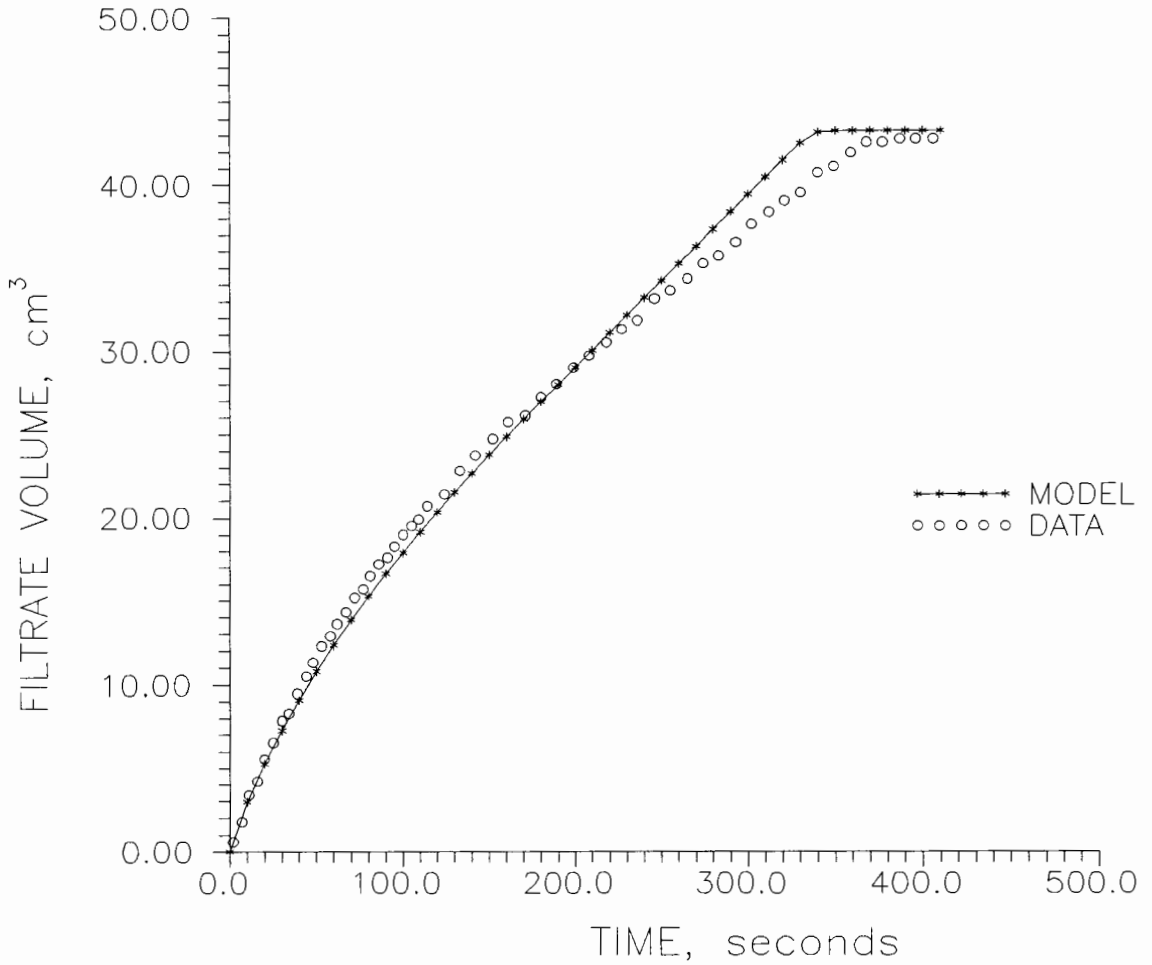


Figure 130. Data-model comparison of filtrate production with time under conditions of CHES run KDM7 using constitutive relationships calculated from specific resistance tests.

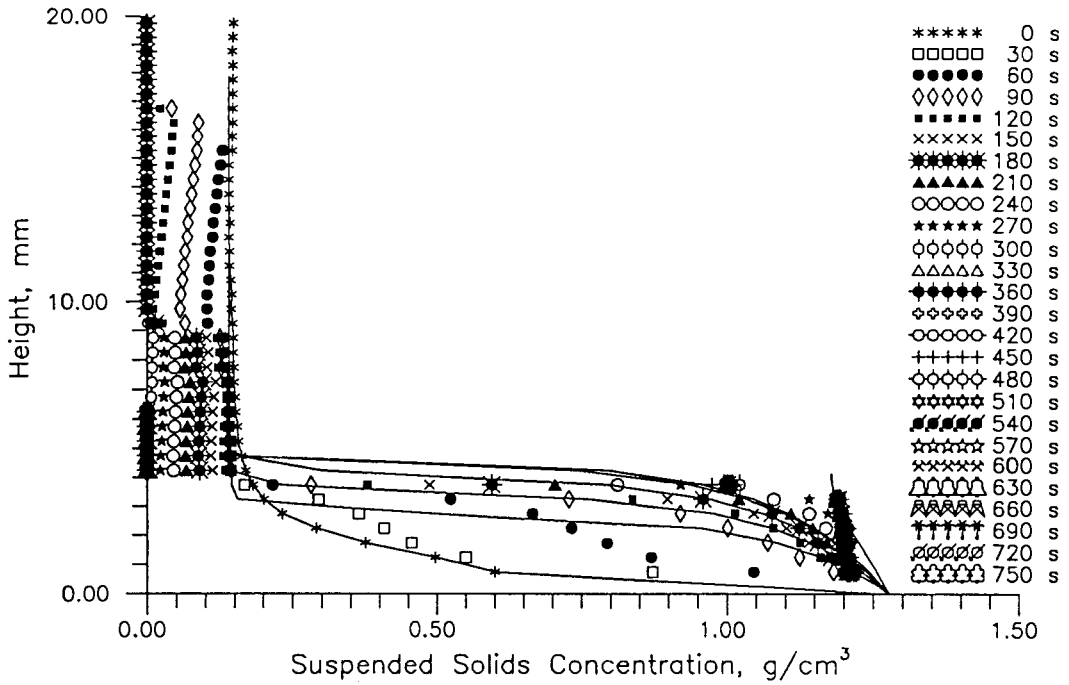


Figure 131. Data-model comparison of concentration profiles at 30 s intervals under conditions of CHES run KDM5 using constitutive relationships calculated from specific resistance tests.

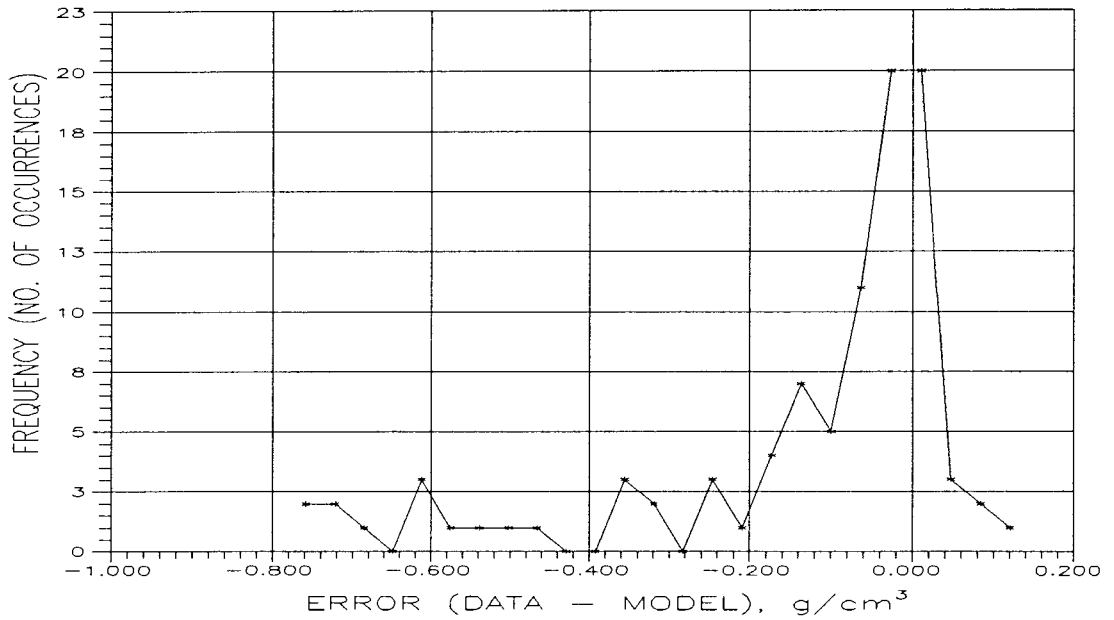


Figure 132. Error frequency histogram for calculated constitutive relationship run KDM5, paired data-model observations of porosity and time as in Figure 131.

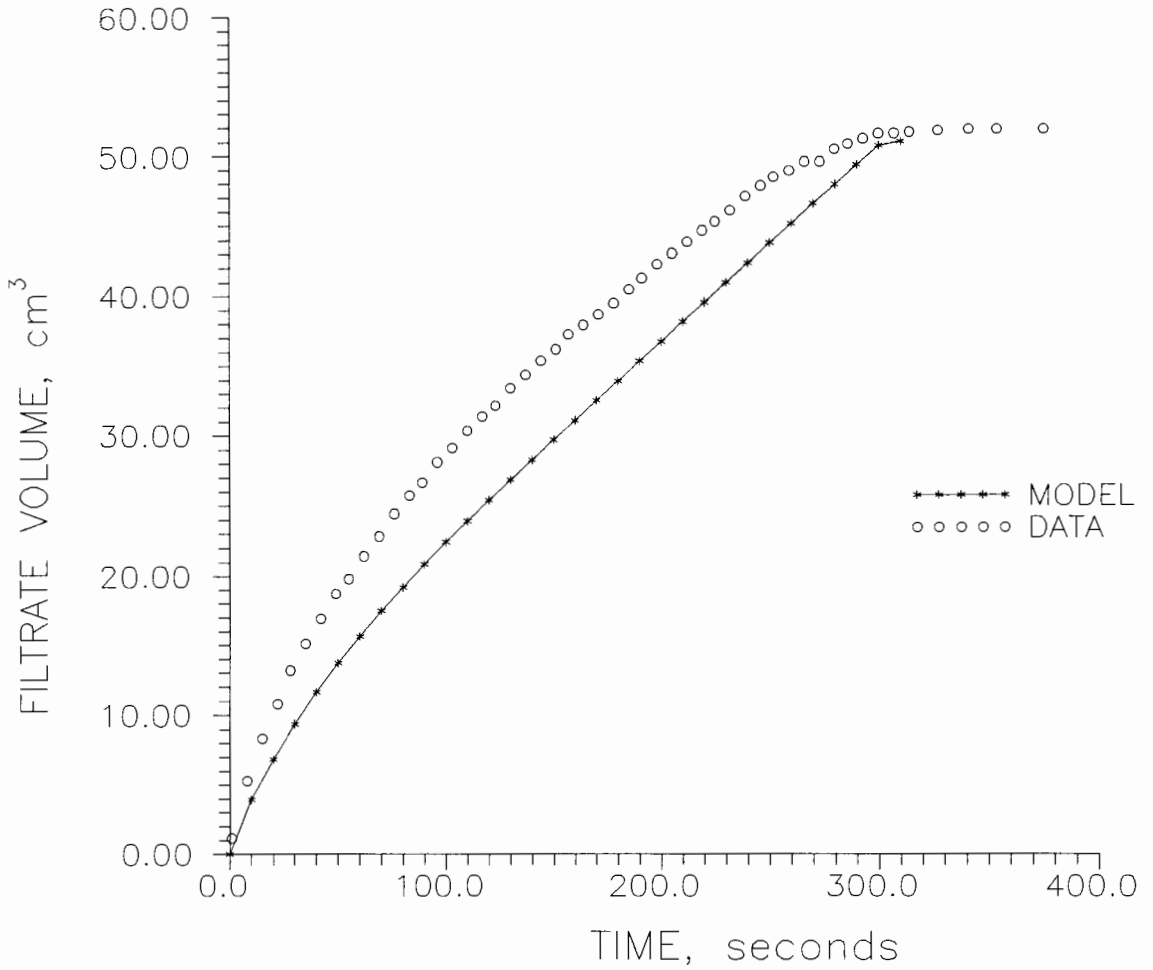


Figure 133. Data-model comparison of filtrate production with time under conditions of CHES run KDM5 using constitutive relationships calculated from specific resistance tests.

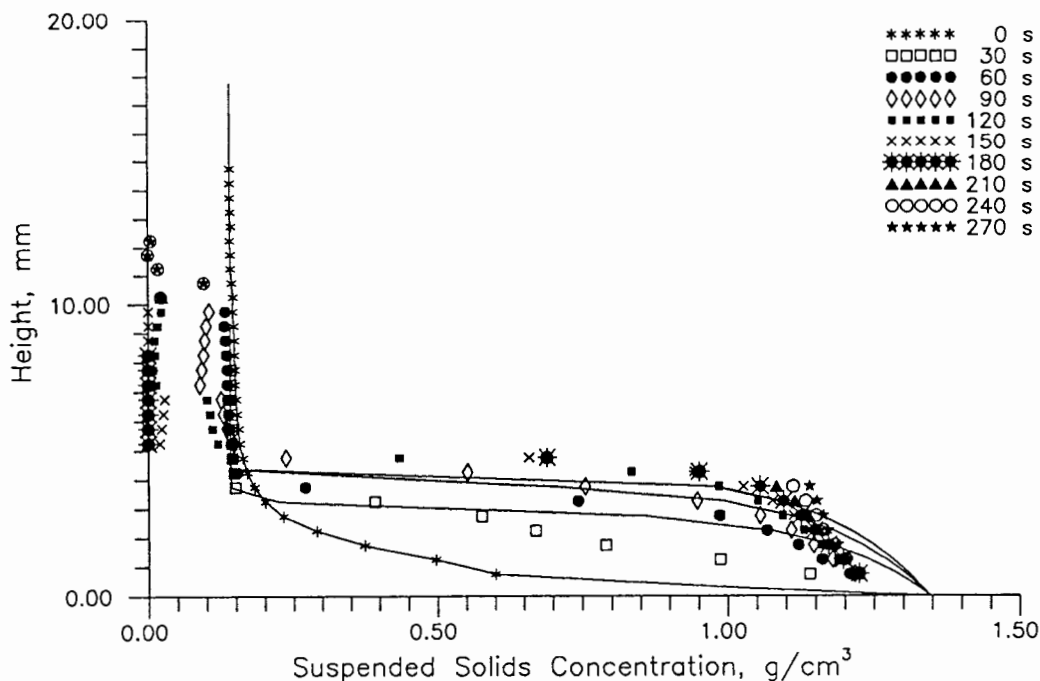


Figure 134. Data-model comparison of concentration profiles at 30 s intervals under conditions of CHES run KDM3B using constitutive relationships calculated from specific resistance tests.

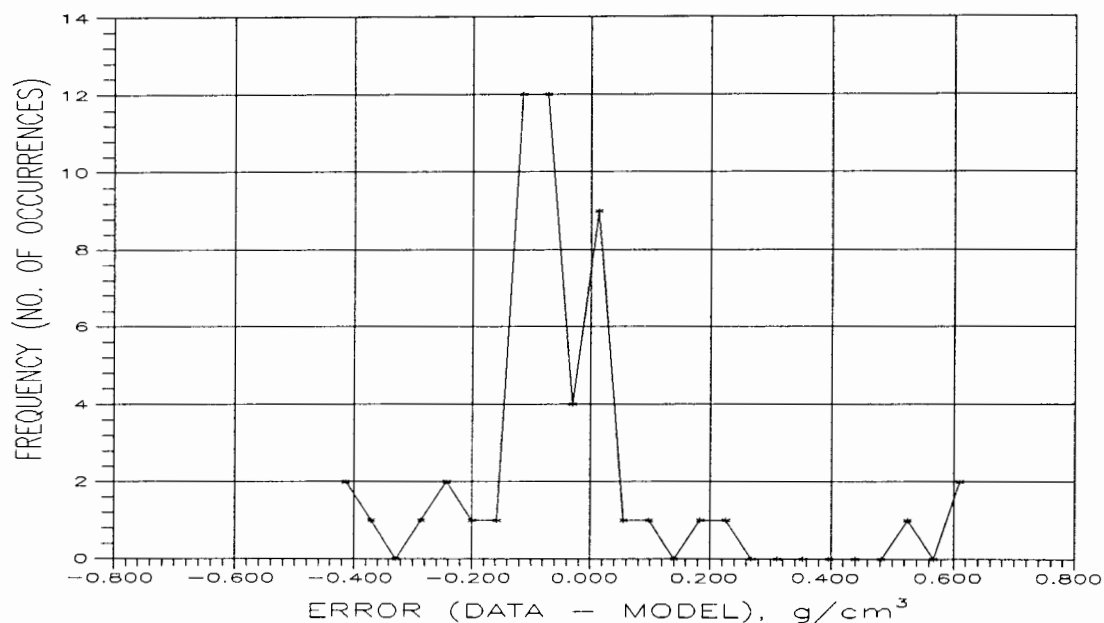


Figure 135. Error frequency histogram for calculated constitutive relationship run KDM3B, paired data-model observations of porosity and time as in Figure 134.

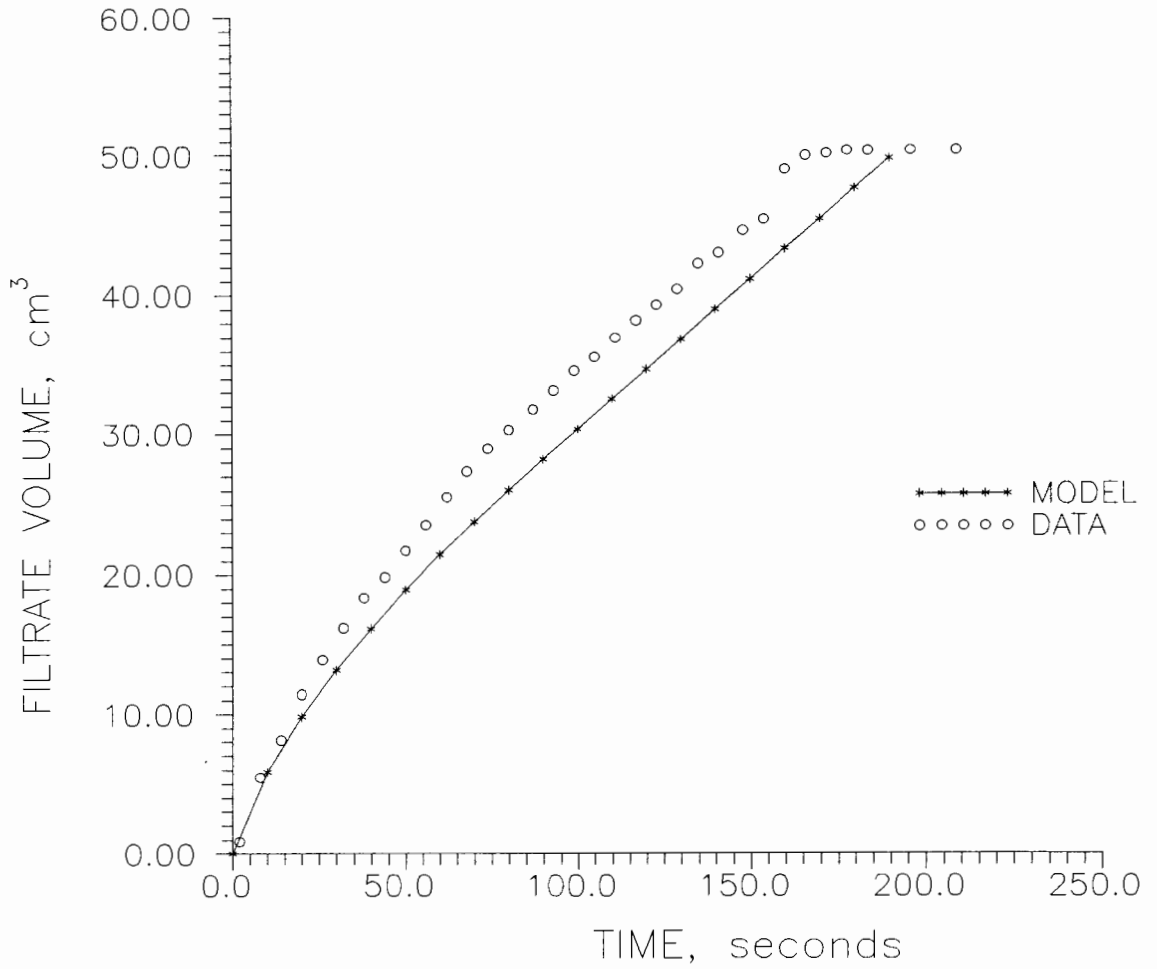


Figure 136. Data-model comparison of filtrate production with time under conditions of Chess run KDM3B using constitutive relationships calculated from specific resistance tests.

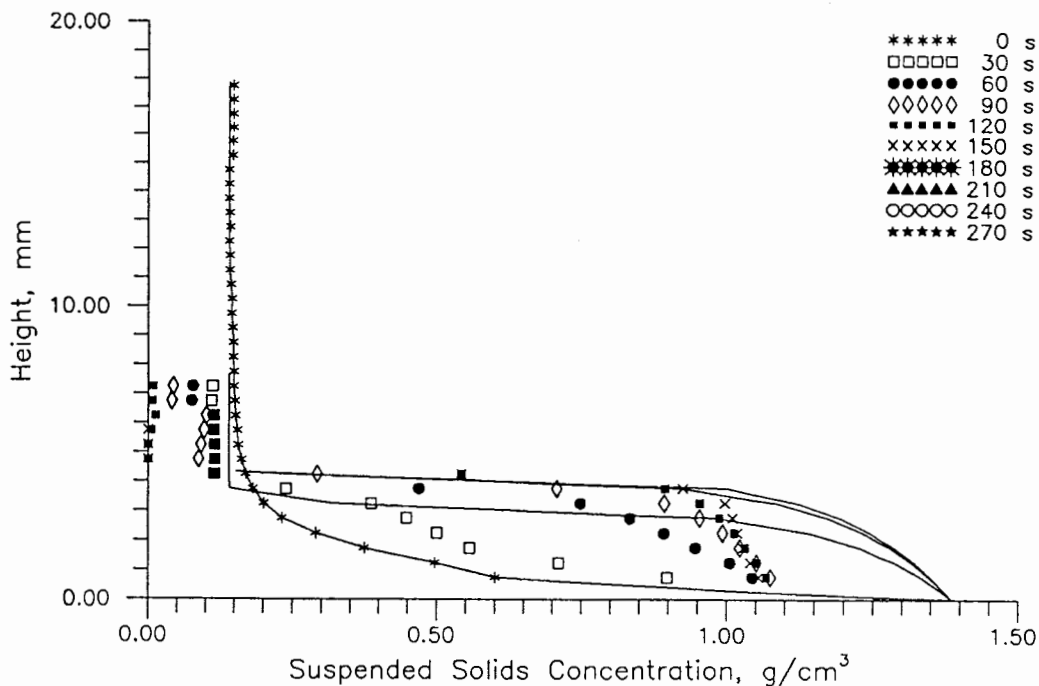


Figure 137. Data-model comparison of concentration profiles at 30 s intervals under conditions of CHES run PMK10 using constitutive relationships calculated from specific resistance tests.

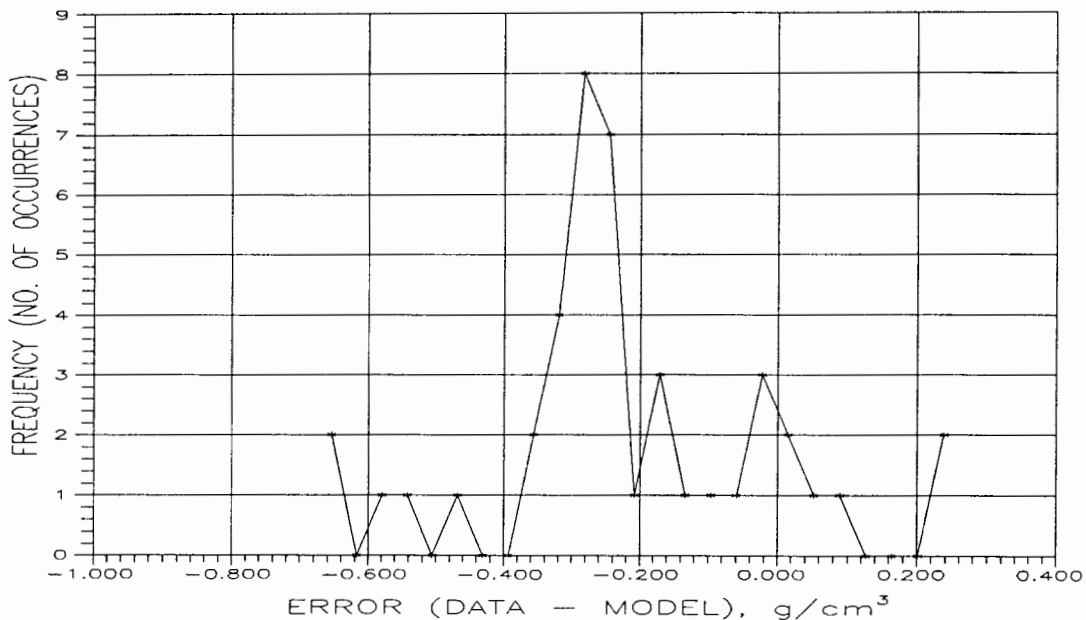


Figure 138. Error frequency histogram for calculated constitutive relationship run PMK10, paired data-model observations of porosity and time as in Figure 137.

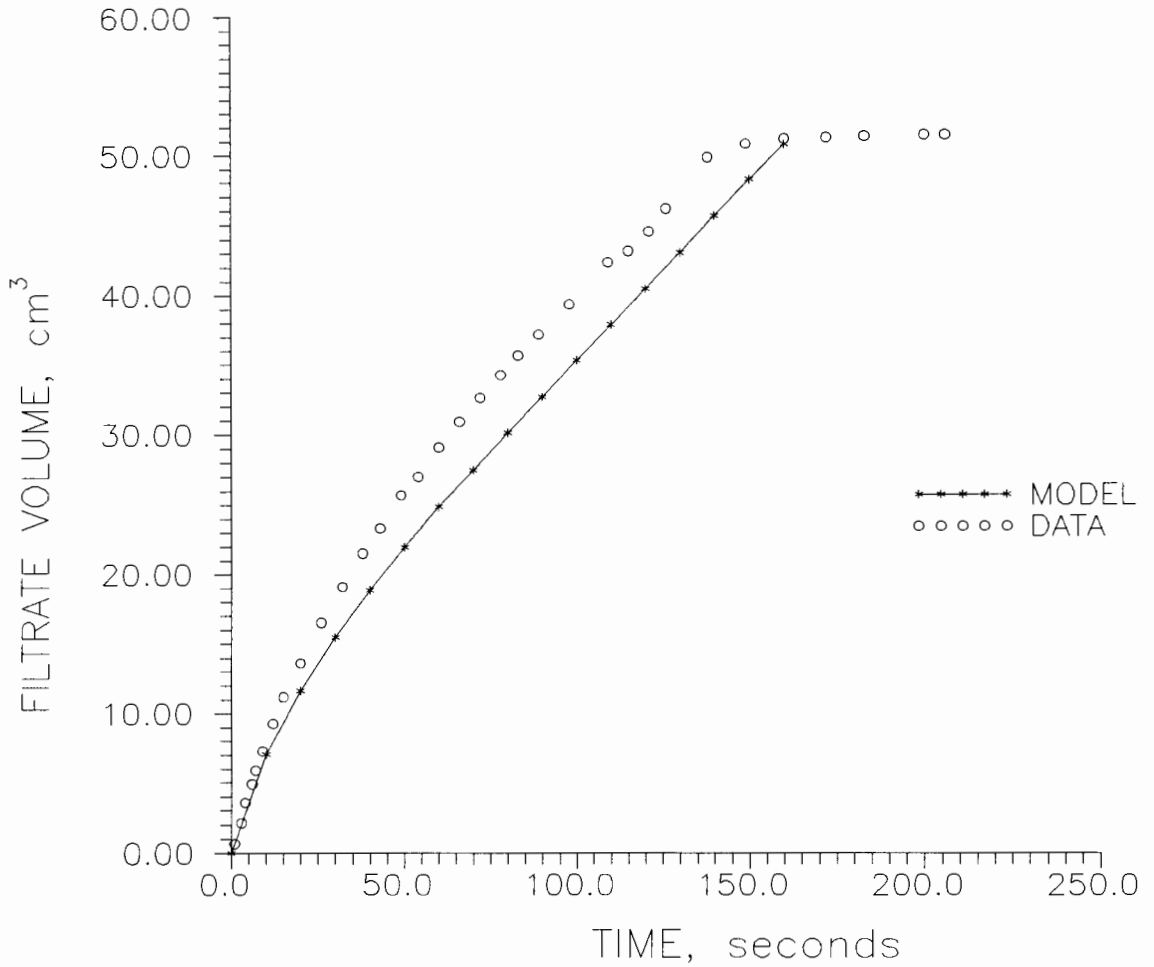


Figure 139. Data-model comparison of filtrate production with time under conditions of CHES run PMK10 using constitutive relationships calculated from specific resistance tests.

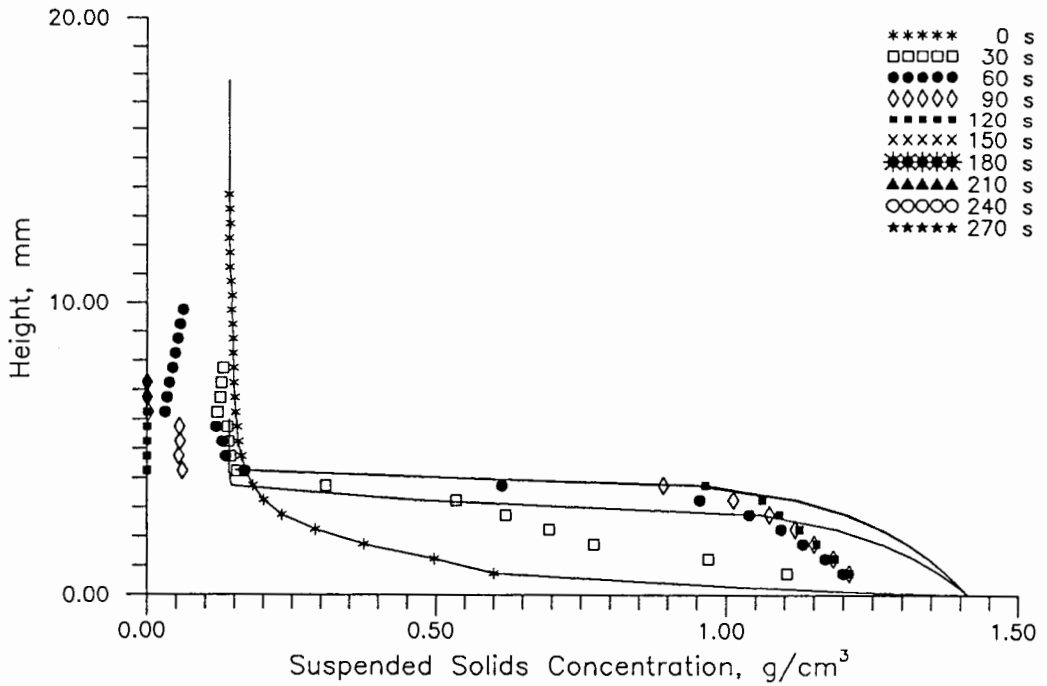


Figure 140. Data-model comparison of concentration profiles at 30 s intervals under conditions of CHES run PMK7 using constitutive relationships calculated from specific resistance tests.

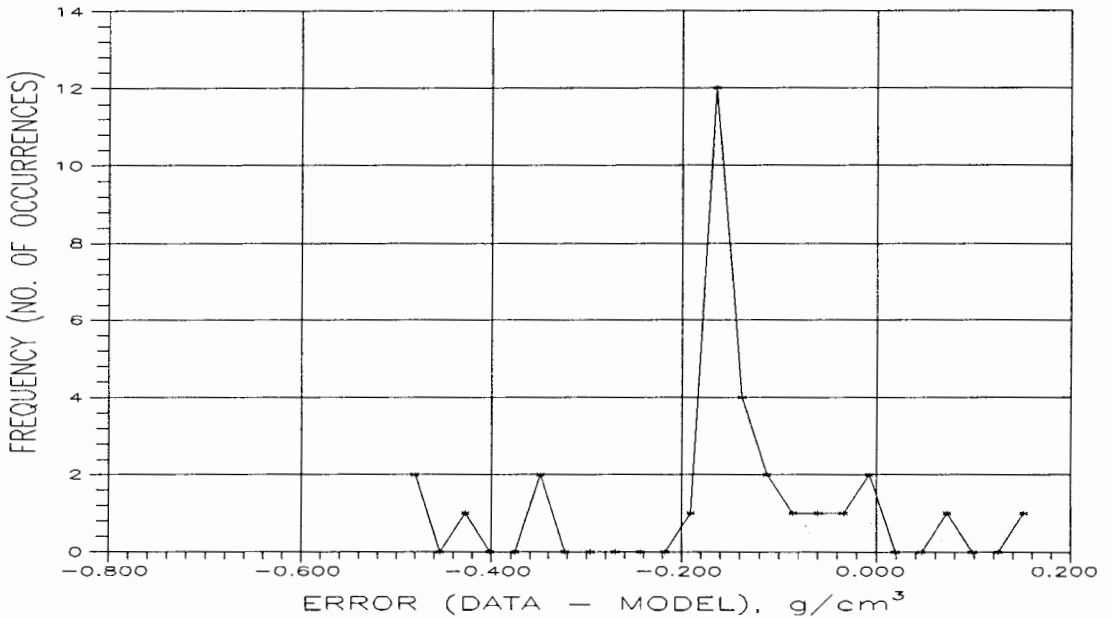


Figure 141. Error frequency histogram for calculated constitutive relationship run PMK7, paired data-model observations of porosity and time as in Figure 140.

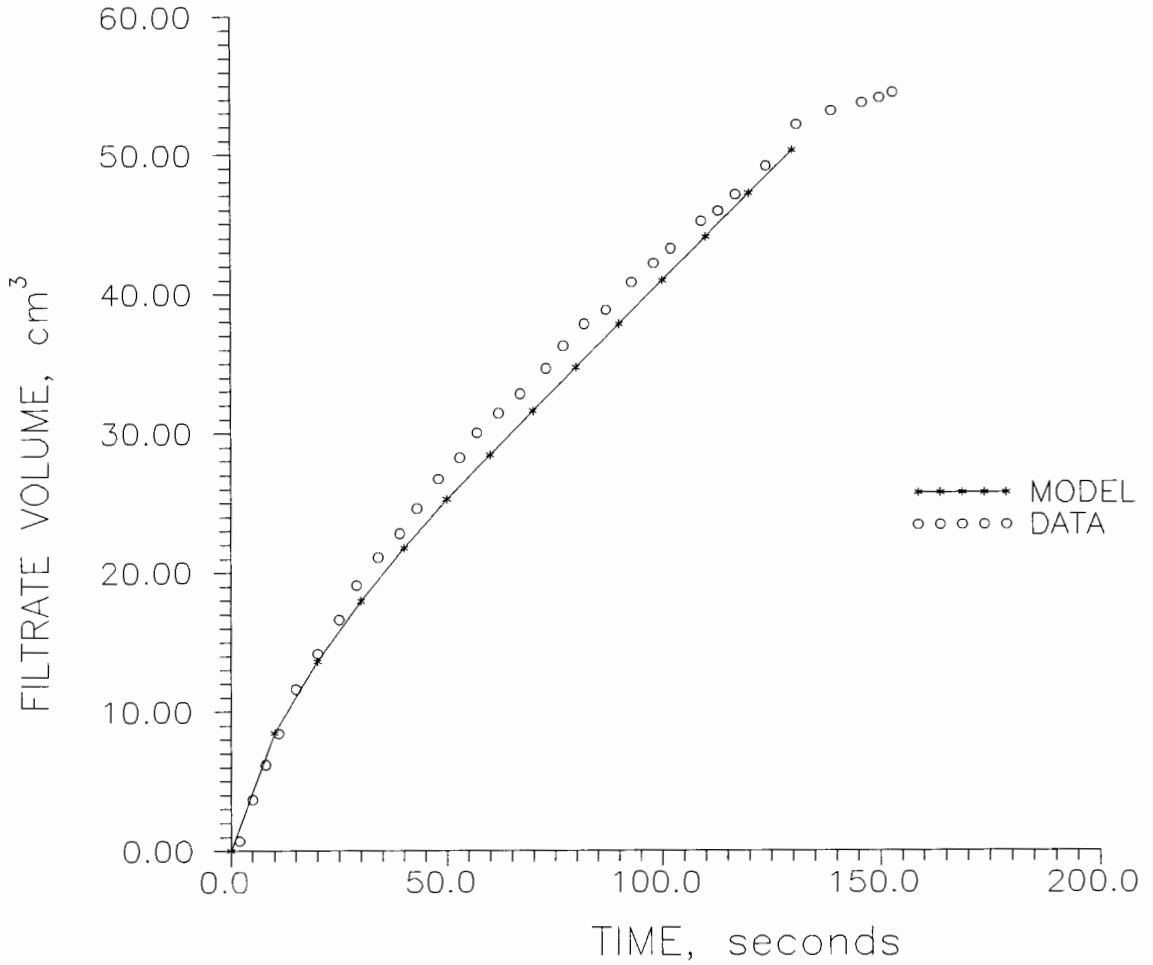


Figure 142. Data-model comparison of filtrate production with time under conditions of CHES run PMK7 using constitutive relationships calculated from specific resistance tests.

The results of simulations using constitutive equations calculated for kaolin suspensions from specific resistance tests showed the effects of changing the constants of these equations from the calibrated values. The error frequency histograms showed that the model tended to overpredict the suspended solids concentration by a relatively large amount. Table XIV gives percent changes in some of the model's predictions due to the changed constitutive relationships. In general, the cake formation time decreased, while the simulated time increased. The terminal porosity decreases. The changed parameters caused the rate of filtrate production to increase. As a result, many runs showed improved correspondence between model output and experimental data for the filtrate production versus time curves, while others were considerably worse.

Realistic results were not obtained for the conditions of CHESS run PMK6, therefore no comparisons were made using this output. Figure 143 shows the porosity gradient versus time for this run. The gradient begins to decrease, as it should, but does not continue to do so, thereby causing the model run to produce erroneous results. The conditions of this run are at one extreme (highest concentration, highest pressure) of the conditions tested. Based on this result and those of chapter 5, there does seem to be a limit to the range in which a given set of constitutive equations of the form proposed by Wells (1990a) are able to give accurate results.

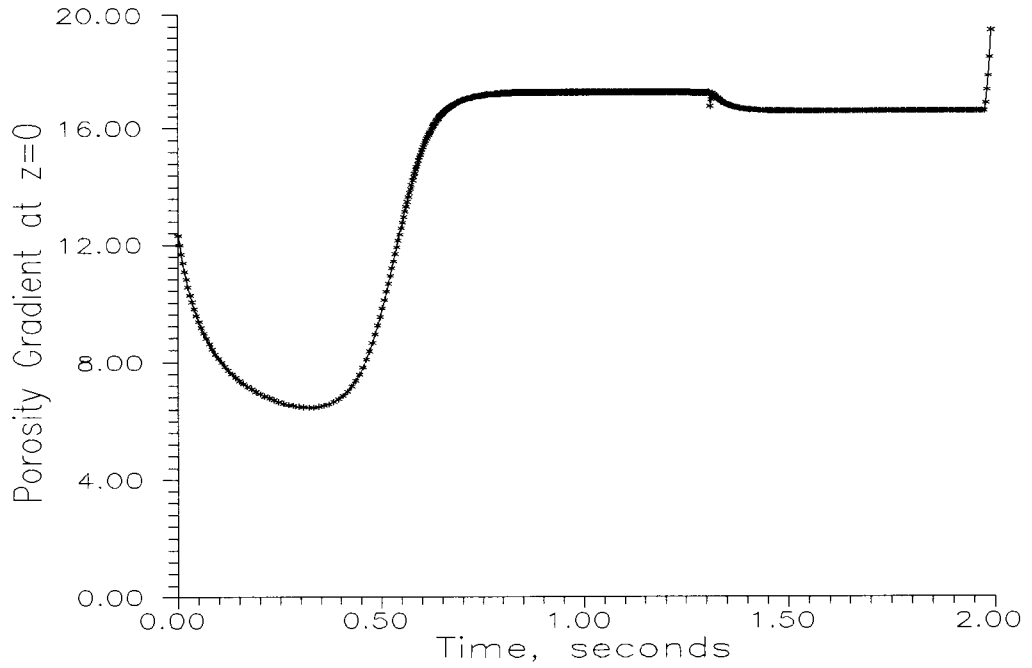


Figure 143. Plot of porosity gradient versus time for CHES run PMK6 using constitutive relationships calculated from specific resistance tests.

TABLE XIV

COMPARISON OF RESULTS FOR MODEL RUNS WITH KAOLIN SLUDGE USING CONSTITUTIVE EQUATIONS DETERMINED FROM SPECIFIC RESISTANCE TESTS. PERCENT CHANGE IN SELECTED OUTPUT FROM THAT OBTAINED FROM CALIBRATED CONSTITUTIVE RELATIONSHIPS

CHESS Run	P_{app} (kPa)	Cake Formation Time (% change)	Simulation Time (% change)	Terminal Porosity (% change)
$c_i = 0.47 \text{ g/cm}^3$				
KDMK8	103	-7.2	0.0	-7.6
KDM6	172	-11.2	+22.8	-8.2
KDM4	345	-17.4	+24.1	-8.9
PMK9	517	-23.0	+28.0	-9.4
PMK6	682	---	---	---
$c_i = 0.31 \text{ g/cm}^3$				
KDMK9	103	-19.4	0.0	-7.6
KDM2	172	-26.2	+25.7	-8.2
PMK3	345	-22.8	+22.2	-8.9
PMK4	517	-26.4	+23.9	-9.4
PMK5	682	-30.2	+25.7	-9.8
$c_i = 0.14 \text{ g/cm}^3$				
KDM7	103	-12.0	+19.1	-7.6
KDM5	172	-17.3	+19.0	-8.2
KDM3B	345	-21.4	+22.6	-8.9
PMK10	517	-24.7	+24.7	-9.4
PMK7	682	-28.7	+27.8	-9.8

TABLE XV

STATISTICS FROM DATA-MODEL COMPARISONS OF POROSITY AND DISTANCE OVER TIME FOR SIMULATIONS OF A KAOLIN SUSPENSION USING CONSTITUTIVE EQUATIONS CALCULATED FROM SPECIFIC RESISTANCE TESTS

CHESS Run	Number of Comparisons	Mean Error	Standard Deviation of Error	Skewness	Coef. of Variation
$c_i = 0.47 \text{ cm}^3$					
KDMK8	749	-0.047	0.058	0.200	-1.219
KDM6	429	-0.076	0.091	0.438	-1.190
KDM4	213	-0.103	0.116	0.613	-1.130
PMK9	184	-0.181	0.109	1.902	-0.600
PMK6	---	---	---	---	---
$c_i = 0.31 \text{ cm}^3$					
KDMK9	447	-0.064	0.062	3.000	-0.977
KDM2	266	-0.074	0.083	5.999	-1.115
PMK3	150	-0.111	0.095	-2.606	-0.858
PMK4	114	-0.070	0.087	-0.908	-1.253
PMK5	117	-0.133	0.146	-2.688	-1.099
$c_i = 0.14 \text{ cm}^3$					
KDM7	122	-0.108	0.135	0.224	-1.251
KDM5	94	-0.139	0.215	-0.165	-1.550
KDM3B	52	-0.460	0.199	1.598	-4.335
PMK10	42	-0.219	0.202	0.150	-0.922
PMK7	31	-0.162	0.143	-0.539	-0.886

Table XVI summarizes the results of model runs using the constitutive equations calculated for anaerobic sludge with and without conditioning. Figures 144-157 show these results

graphically. Since no initial sedimentation profile was available, uniform initial porosity profiles were used. Also, no tests were conducted to determine the breakthrough stress of the anaerobic sludge, therefore the value used for the kaolin suspension was also used for these runs. The numerical model became unstable during the simulation of anaerobic sludge without conditioner at a pressure of 69 kPa. No graphical results are therefore presented for this run. The important result that these experiments show is how the constitutive relationships are related to the dewaterability of the sludge, and the model's ability to predict improvement in dewaterability due to the use of conditioner on the sludge. This method for calculating the model's constitutive equations can be used to obtain a good first estimate of the model parameters as opposed to tedious trial and error calibration methods. The parameters can later be fine-tuned, and the model calibrated using vastly fewer trials and computer time.

TABLE XVI

SUMMARY OF RESULTS FROM COMPUTER SIMULATIONS USING
CONSTITUTIVE RELATIONSHIPS CALCULATED FROM SPECIFIC
RESISTANCE TESTS FOR ANAEROBIC SLUDGE WITH AND WITHOUT
CHEMICAL CONDITIONING

Anaerobic Sludge Without Conditioner $c_i=0.022$						
P_{app} (kPa)	Temp. (° C)	CPU Time (S)	Cake Form. Time (S)	Simu- lation Time (S)	Term. Poro- sity	Filt. Volume (cm ³)
69	25.5	0.03	0.0	0.01	0.9400	0.001
207	25.5	921.5	401.6	900.0	0.9315	19.3
345	25.5	1090.4	361.2	900.0	0.9275	19.2
483	25.5	1256.2	341.7	900.0	0.9249	19.2
Anaerobic Sludge With Conditioner $c_i=0.025$						
P_{app}	Temp. (° C)	CPU Time (S)	Cake Form. Time (S)	Simu- lation Time (S)	Term. Poro- sity	Filt. Volume (cm ³)
69	25.5	16.3	437.0	900.0	0.8236	88.2
207	25.5	13.2	386.9	718.4	0.8008	89.0
345	25.5	11.9	366.4	625.0	0.7902	88.9
483	25.5	11.5	354.0	583.7	0.7832	88.9

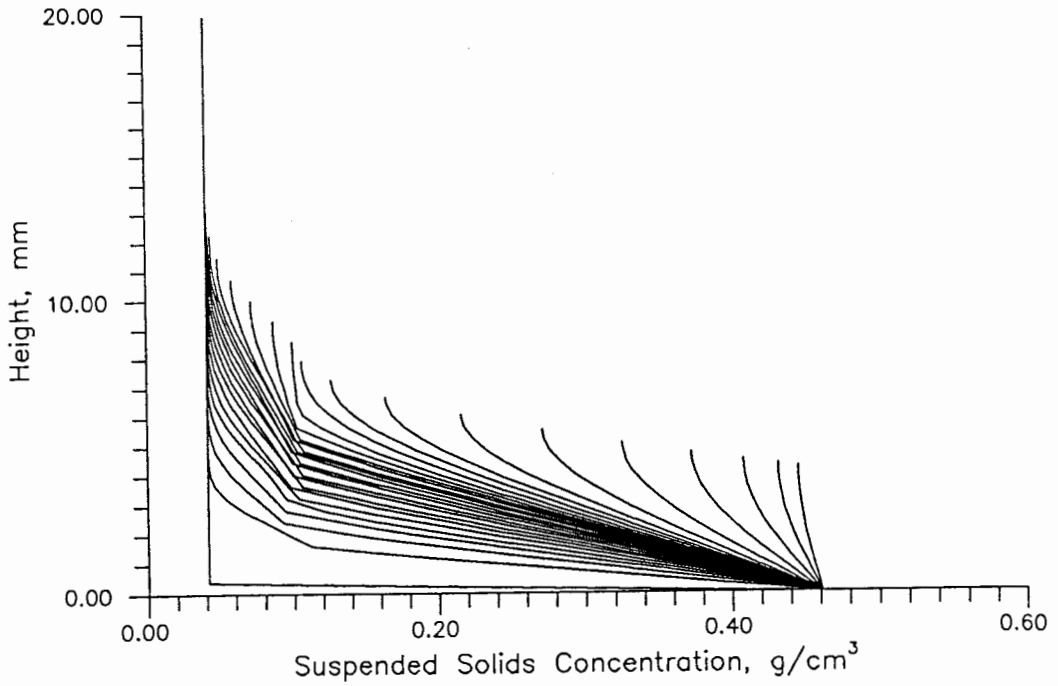


Figure 144. Plot of suspended solids concentration profiles over time for anaerobic sludge with conditioning predicted by Wells (1990a) ($c_i=0.025$ g/cm³, $P_{app}=69$ kPa) dewatering model.

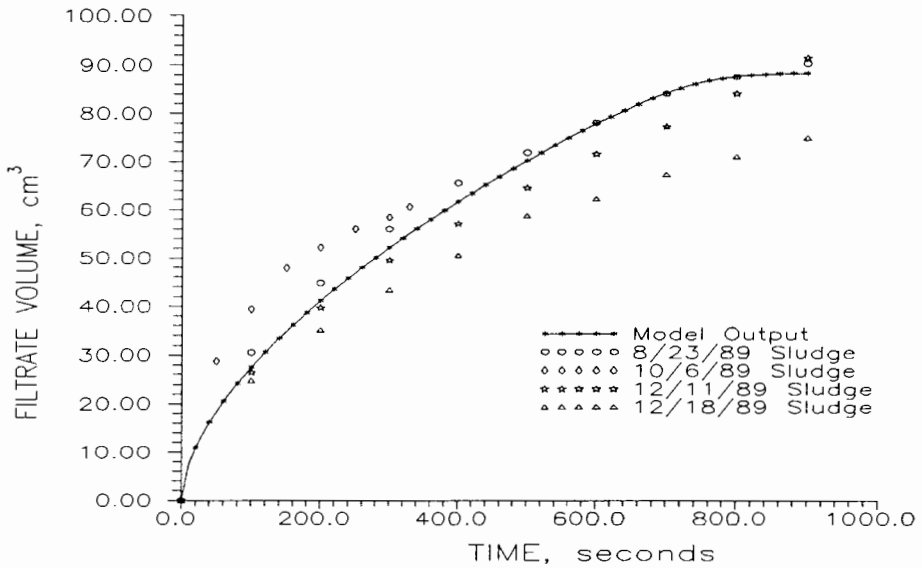


Figure 145. Filtrate production vs. time as predicted by the Wells (1990a) dewatering model compared to specific resistance test results using anaerobic sludge with conditioner ($c_i=0.025$ g/cm³, $P_{app}=69$ kPa).

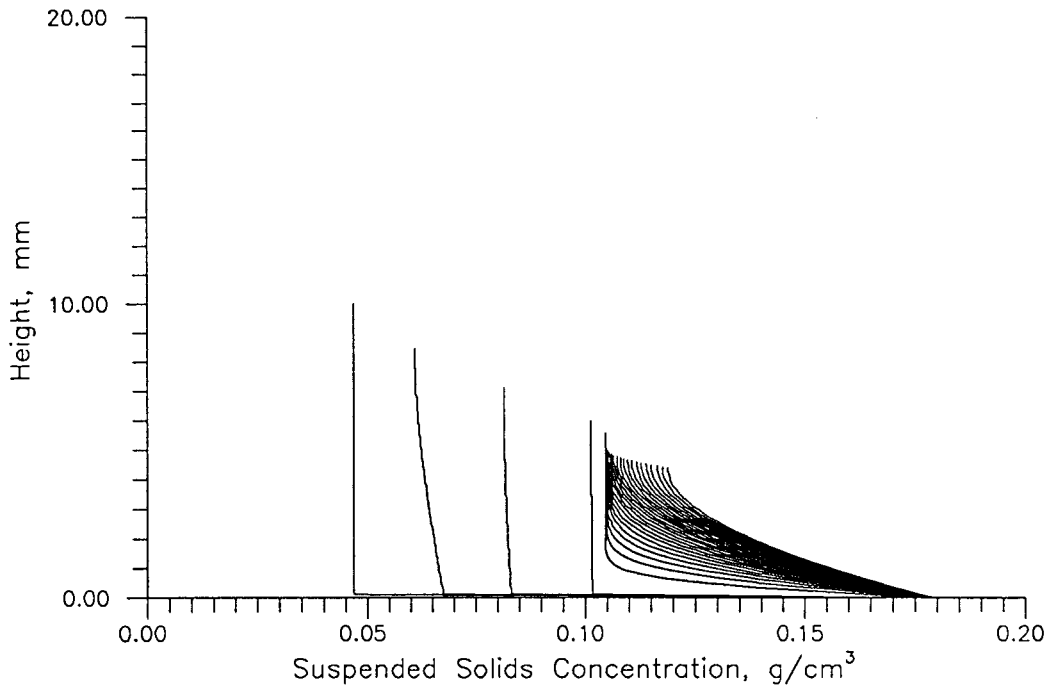


Figure 146. Plot of suspended solids concentration profiles over time for anaerobic sludge w/out conditioning predicted by Wells (1990a) ($c_i=0.022$ g/cm³, $P_{app}=207$ kPa) dewatering model.

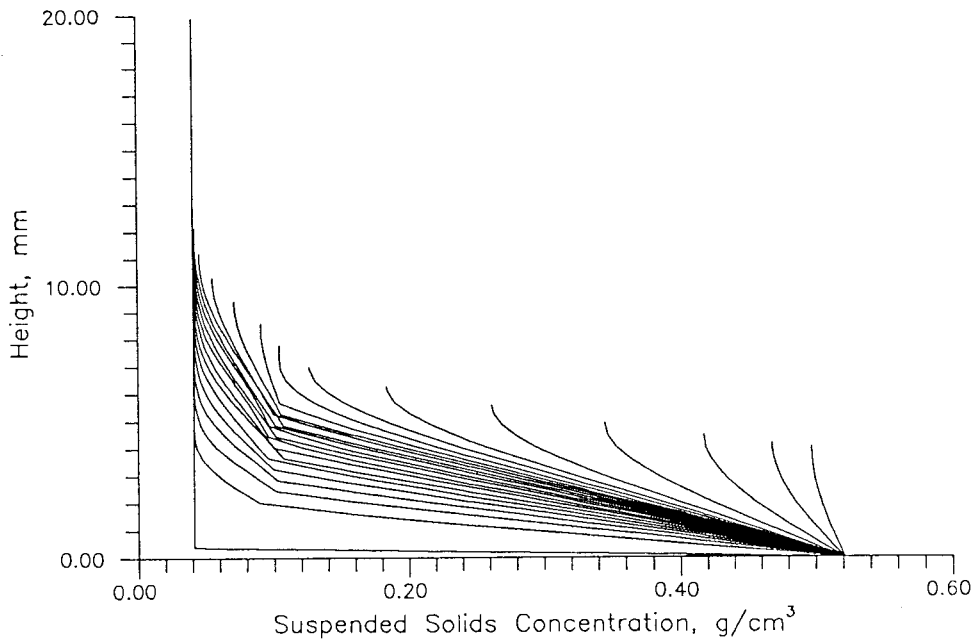


Figure 147. Plot of suspended solids concentration profiles over time for anaerobic sludge with conditioning predicted by Wells (1990a) ($c_i=0.025$ g/cm³, $P_{app}=207$ kPa) dewatering model.

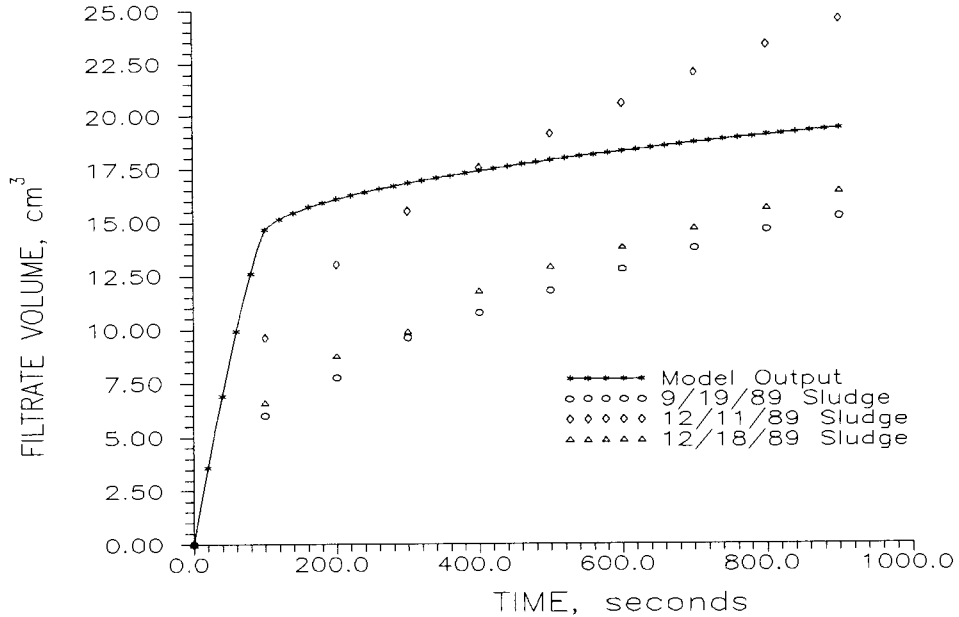


Figure 148. Filtrate production vs. time as predicted by the Wells (1990a) dewatering model compared to specific resistance test results using anaerobic sludge without conditioner ($c_i=0.022$ g/cm³, $P_{app}=207$ kPa).

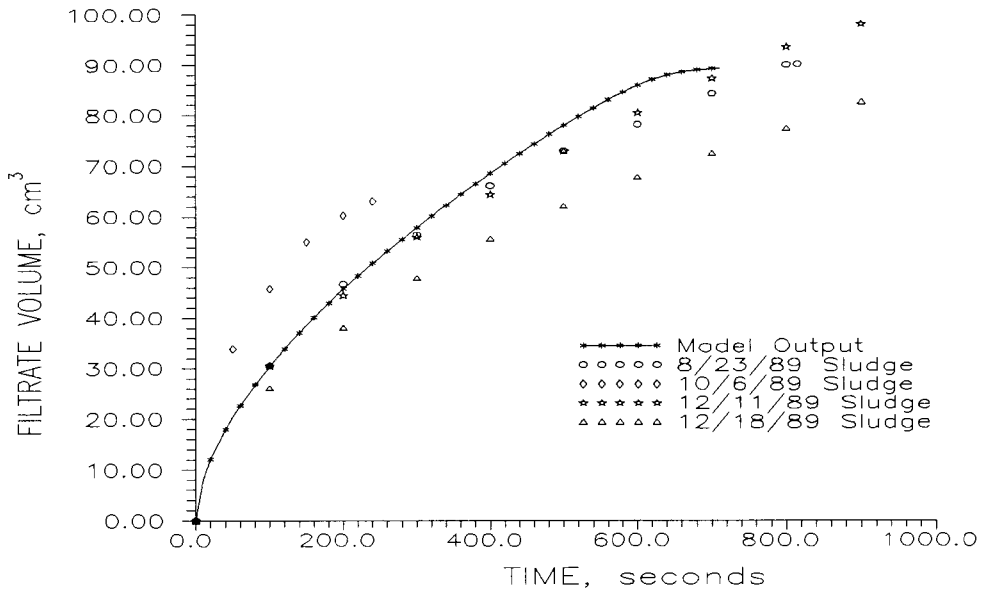


Figure 149. Filtrate production vs. time as predicted by the Wells (1990a) dewatering model compared to specific resistance test results using anaerobic sludge with conditioner ($c_i=0.025$ g/cm³, $P_{app}=207$ kPa).

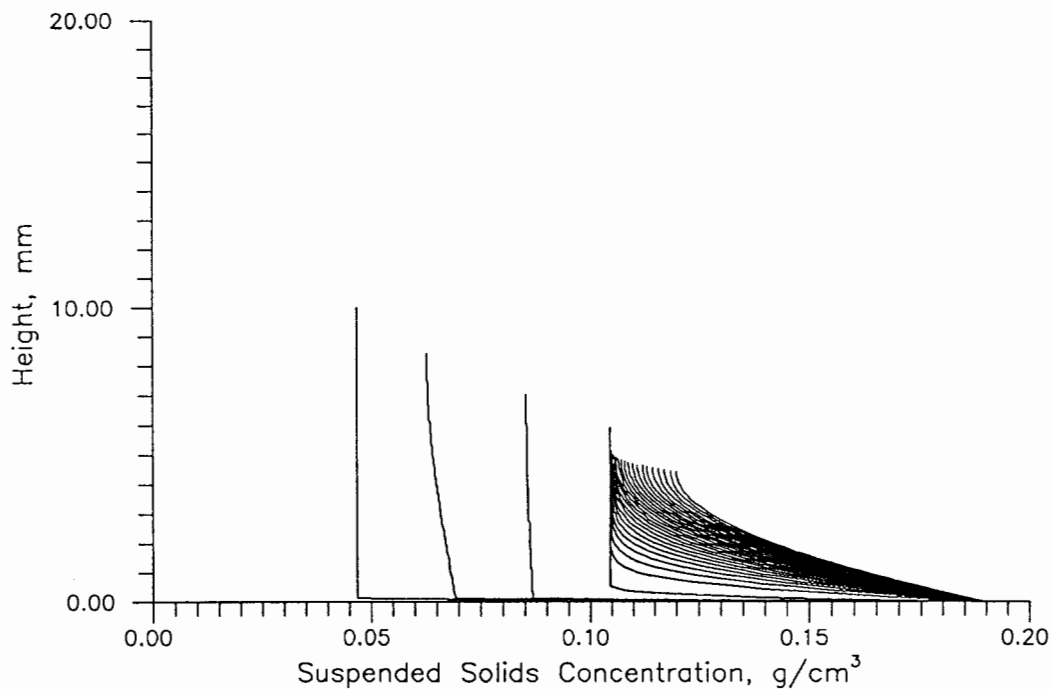


Figure 150. Plot of suspended solids concentration profiles over time for anaerobic sludge w/out conditioning predicted by Wells (1990a) ($c_i=0.022$ g/cm³, $P_{app}=345$ kPa) dewatering model.

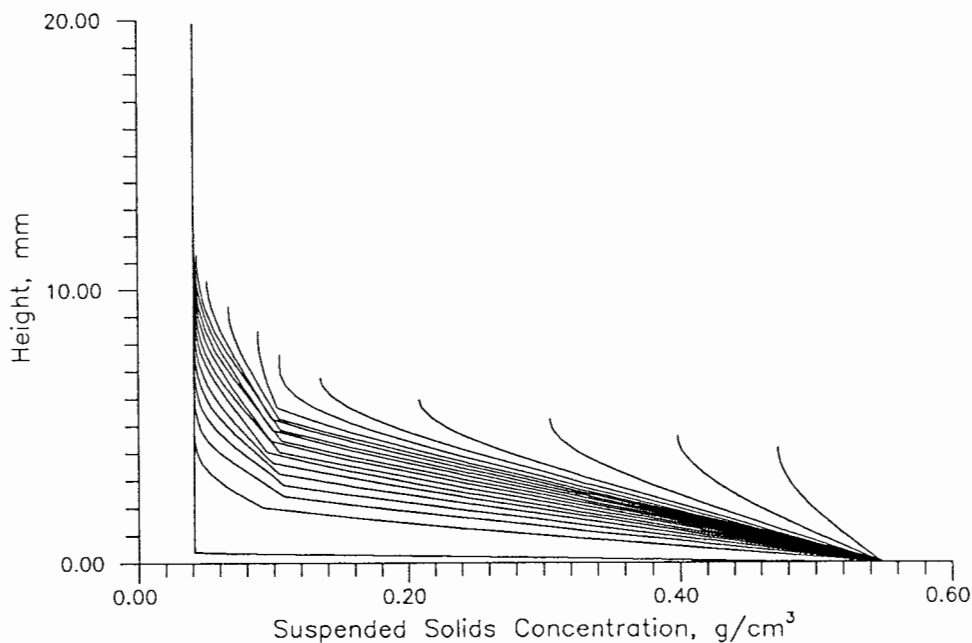


Figure 151. Plot of suspended solids concentration profiles over time for anaerobic sludge with conditioning predicted by Wells (1990a) ($c_i=0.025$ g/cm³, $P_{app}=345$ kPa) dewatering model.

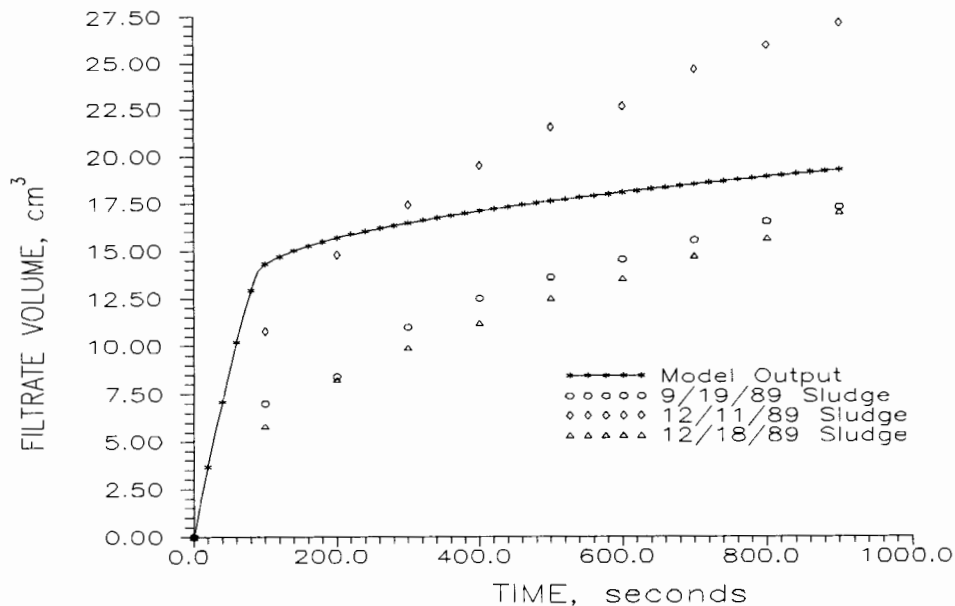


Figure 152. Filtrate production vs. time as predicted by the Wells (1990a) dewatering model compared to specific resistance test results using anaerobic sludge without conditioner ($c_i=0.022$ g/cm³, $P_{app}=345$ kPa).

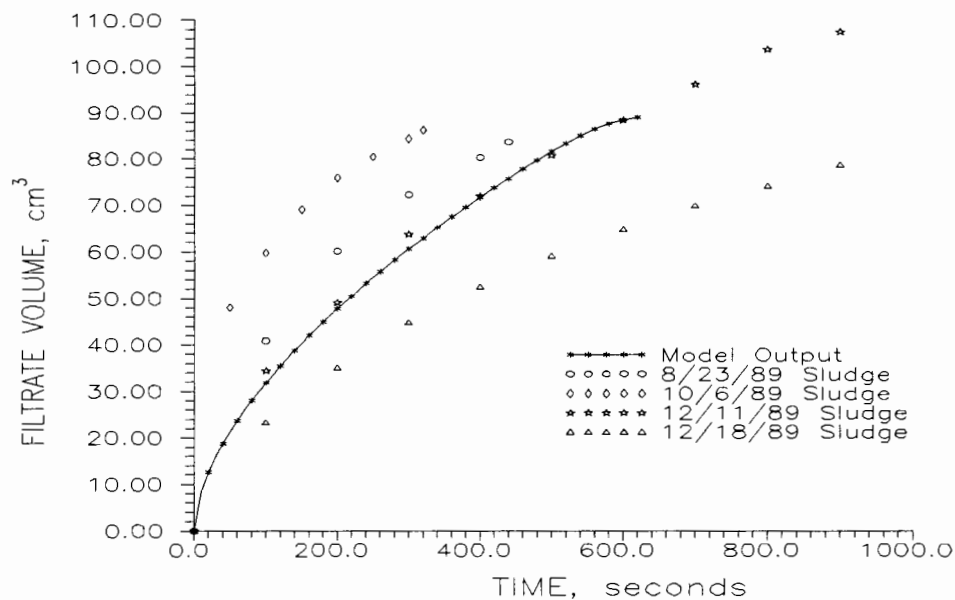


Figure 153. Filtrate production vs. time as predicted by the Wells (1990a) dewatering model compared to specific resistance test results using anaerobic sludge with conditioner ($c_i=0.025$ g/cm³, $P_{app}=345$ kPa).

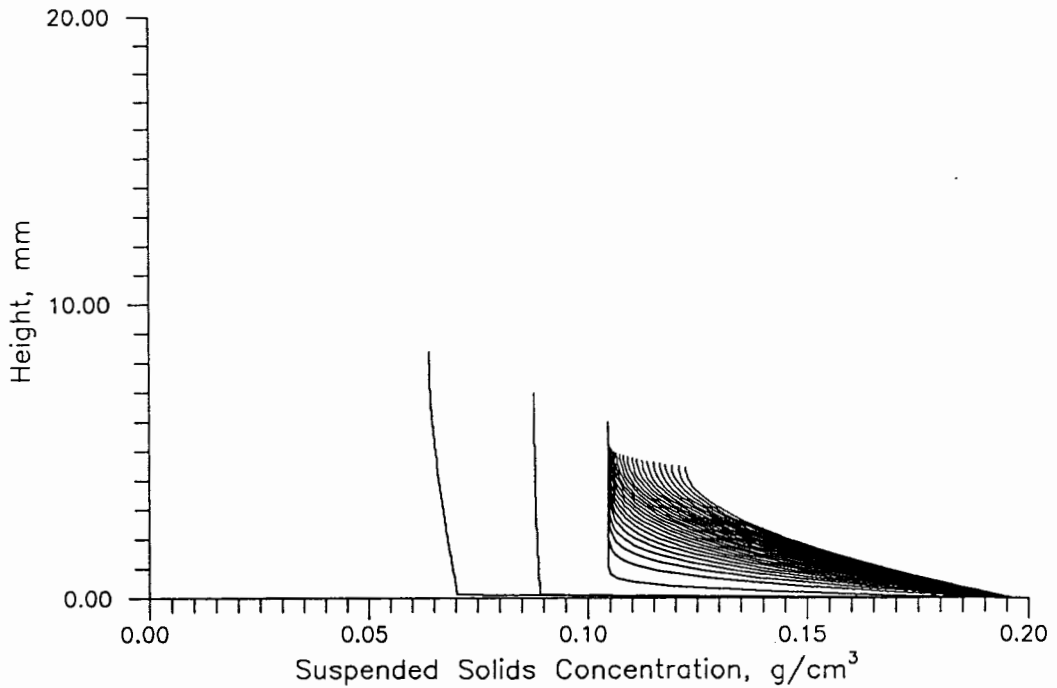


Figure 154. Plot of suspended solids concentration profiles over time for anaerobic sludge w/out conditioning predicted by Wells (1990a) ($c_i=0.022$ g/cm³, $P_{app}=483$ kPa) dewatering model.

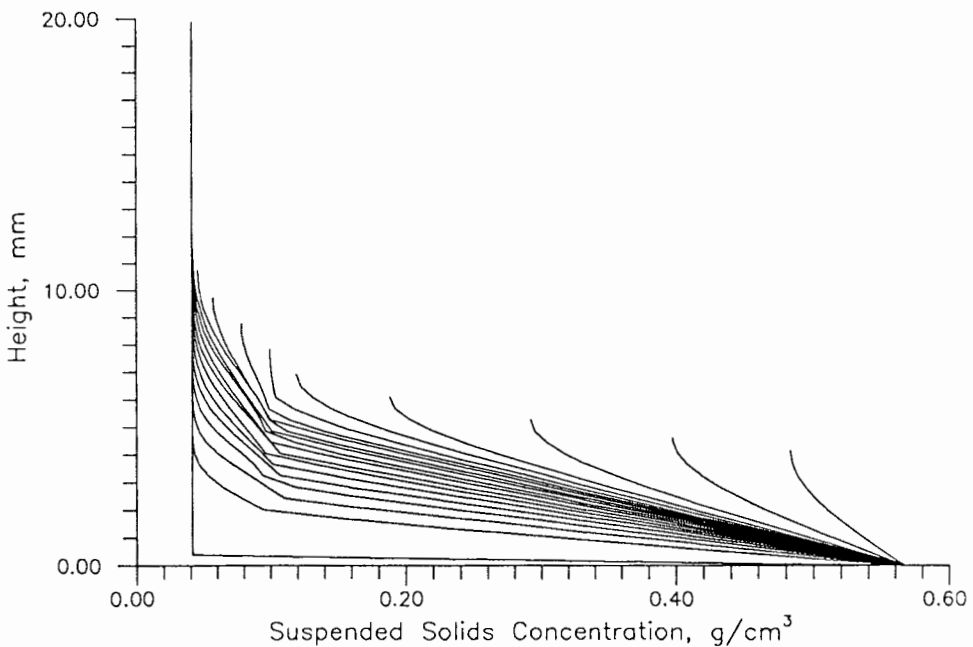


Figure 155. Plot of suspended solids concentration profiles over time for anaerobic sludge with conditioning predicted by Wells (1990a) ($c_i=0.025$ g/cm³, $P_{app}=483$ kPa) dewatering model.

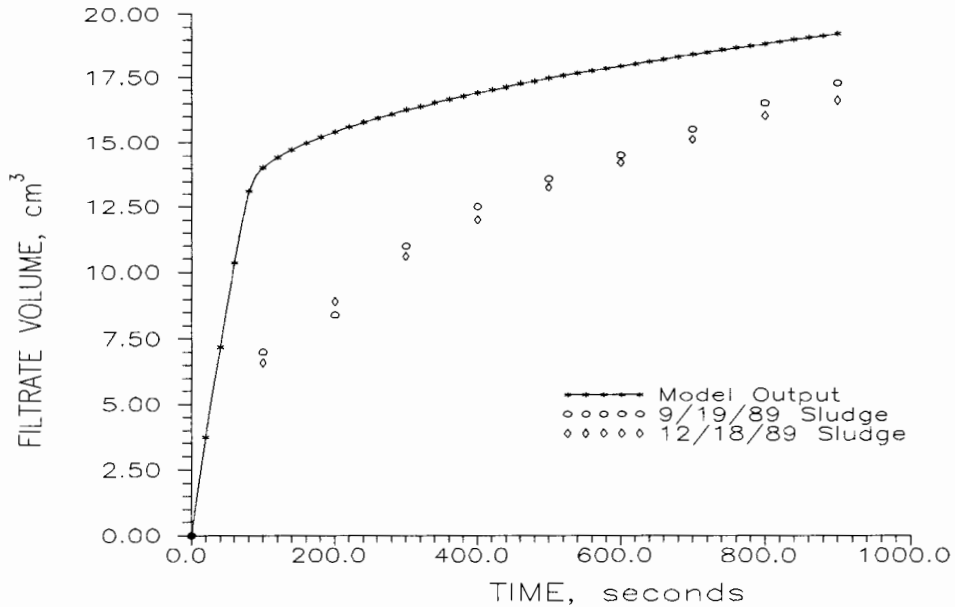


Figure 156. Filtrate production vs. time as predicted by the Wells (1990a) dewatering model compared to specific resistance test results using anaerobic sludge w/out conditioner ($c_1=0.022 \text{ g/cm}^3$, $P_{app}=483 \text{ kPa}$).

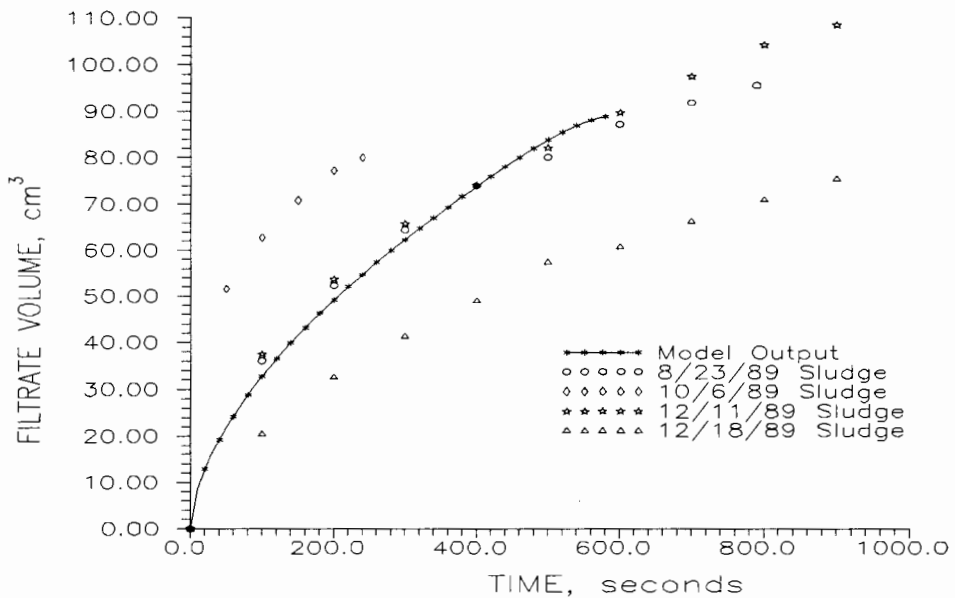


Figure 157. Filtrate production vs. time as predicted by the Wells (1990a) dewatering model compared to specific resistance test results using anaerobic sludge w/out conditioner ($c_1=0.022 \text{ g/cm}^3$, $P_{app}=483 \text{ kPa}$).

The calculated parameters for anaerobic sludge without conditioner seem to be in error. The rate of filtrate production is much greater than it should be in every case. The reasonable values for the total filtrate production were obtained only by decreasing the domain length of the problem unrealistically, thereby making less liquid available to be filtered.

The results for the simulations of conditioned anaerobic sludge, however, are quite good given the variability of sludge properties over time.

As noted previously, the model is quite sensitive to the values of the dewaterability parameters. It is very possible to be close to the correct set of parameter values yet still not obtain accurate simulation results. In any case, it is unlikely that the calculated parameters will yield the best agreement between model output and actual sludge dewatering behavior. The parameters must be fine-tuned before an optimum set of parameters can be obtained. The process of fine-tuning the model was not performed in this study, since the only method available is trial and error parameter substitution, which is both tedious and time-consuming. However, it is apparent that the parameter calculation technique outlined by Wells (1990b) can give one an excellent place to start in the process of model calibration and optimization.

CHAPTER VIII

MODELING OF CAKE FILTRATION WITH UNCERTAINTY

The Wells (1990a) compressible cake filtration model relies upon two constitutive equations related to sludge dewaterability for its solution. The equation for m_v relates effective stress and porosity. The permeability equation relates k and n . These constitutive equations were given previously in Equations 33 and 34. The calibrated parameter values for these equations were given in Equation 47.

The parameters in the constitutive equations are related to the slopes and ordinate intercepts of straight lines fit to semi-log plots of experimental data as in Figures 8 and 9. The values of these parameters have a significant effect on the modeled dewaterability of a particular sludge. The 'best' parameters are those which produce the closest agreement between model output and experimental data for a given simulation. A simulation is one run of the computer model using a particular set of constitutive equations with their associated parameter values. Parameter values chosen during calibration may not be unique, in that other parameter combinations may also produce good model-data agreement. The calibrated set of parameters represent unique dewaterability

characteristics for a particular sludge. The scatter in the data of Figures 8 and 9 indicates uncertainty in both the slope and intercept. This scatter is a result of experimental errors and changes in the physical properties of the material from experiment to experiment.

The relative importance of input parameters on the model output is essential in defining the confidence placed in the parameter calibration. The results can then be used as a guide for further study of the parameters to which the model is most sensitive. Relationships between parameters can also be explored.

The amount of uncertainty in the lines representing the constitutive equations can be quantified by calculating confidence intervals. By treating the effective stress and permeability as random variables, and assuming their logarithms are normally distributed about the lines representing the constitutive equations, the 95% confidence interval estimates for randomly selected ordinate values can be calculated from

$$y_c = \hat{y} \pm z\left(\frac{\theta}{2}\right) \cdot s_e \sqrt{1 + \frac{1}{N_d} + \frac{(x-\bar{x})^2}{\sum (x-\bar{x})^2}} \quad (76)$$

where

y_c = upper (lower) 95% confidence interval estimate
for y at x

\hat{y} = point estimate for the true value of y
(predicted value) at x

N_d = sample size (number of data points)

\bar{x} = sample mean for abscissa values

θ = probability of a Type I error = 0.05

z = standard normal deviate = 1.96 for 95%
confidence

$$s_e = \sqrt{\frac{\sum (y - \hat{y})^2}{d_f}} = \text{standard deviation of error}$$

d_f = number of degrees of freedom

The 68% and 95% confidence interval estimates for randomly selected σ' and k values are shown in Figures 158 and 159. The 95% confidence interval envelopes are seen to be rather wide due to the scatter in the data and the functional forms chosen for the constitutive relationships. Although the confidence limit envelopes should diverge as they get farther from the mean of the data sample, the envelopes were found to be rather straight when plotted on a logarithmic scale. Therefore, for convenience, an exponential curve was fit through the confidence limit envelopes calculated from Equation 76. The log-normal distribution was chosen 1) for convenience; 2) because both permeability, k , and the coefficient of volume compressibility, m_v , are bounded below by zero, and 3) because the data and past experience with the

model indicate that there is a greater probability of accurate model results using constitutive equations near the calibrated, or mean constitutive equations.

A simple means of determining the effect of parameter uncertainty on the model's performance would be to vary the values of these parameters over their ranges and examine the results of several model runs. By doing many simulations using a different set of model parameters for each run, distributions of input parameters and model results are obtained. These distributions can then be analyzed statistically. This process is termed a sensitivity analysis. A sensitivity analysis provides a means of identifying and quantifying those parameters or variables to which model performance is particularly sensitive. Sampling values of dewaterability parameters at random from a particular probability distribution can simulate the inherent uncertainty and variability in the dewaterability characteristics of sludges. Simulations can then be performed using these randomly generated parameters to determine the effect of parameter variability on the model results. Ranges of dewatering behavior can be predicted based upon the variability of sludge characteristics. This process is a stochastic, or Monte Carlo simulation.

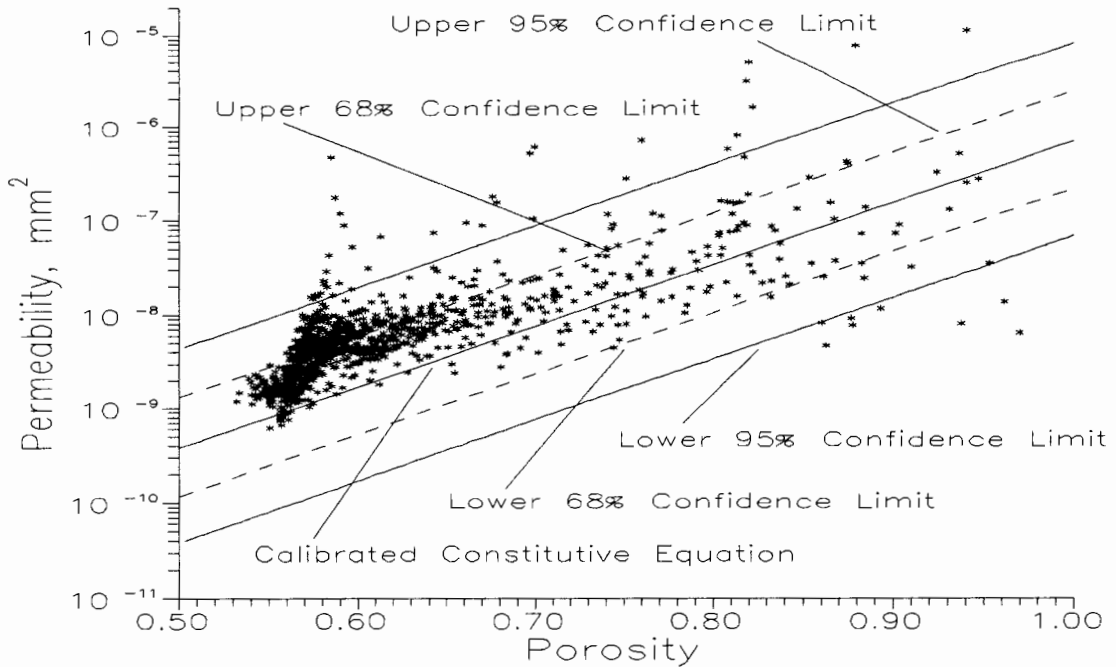


Figure 158. Confidence interval estimates for normally distributed, randomly selected values of permeability at various values of porosity.

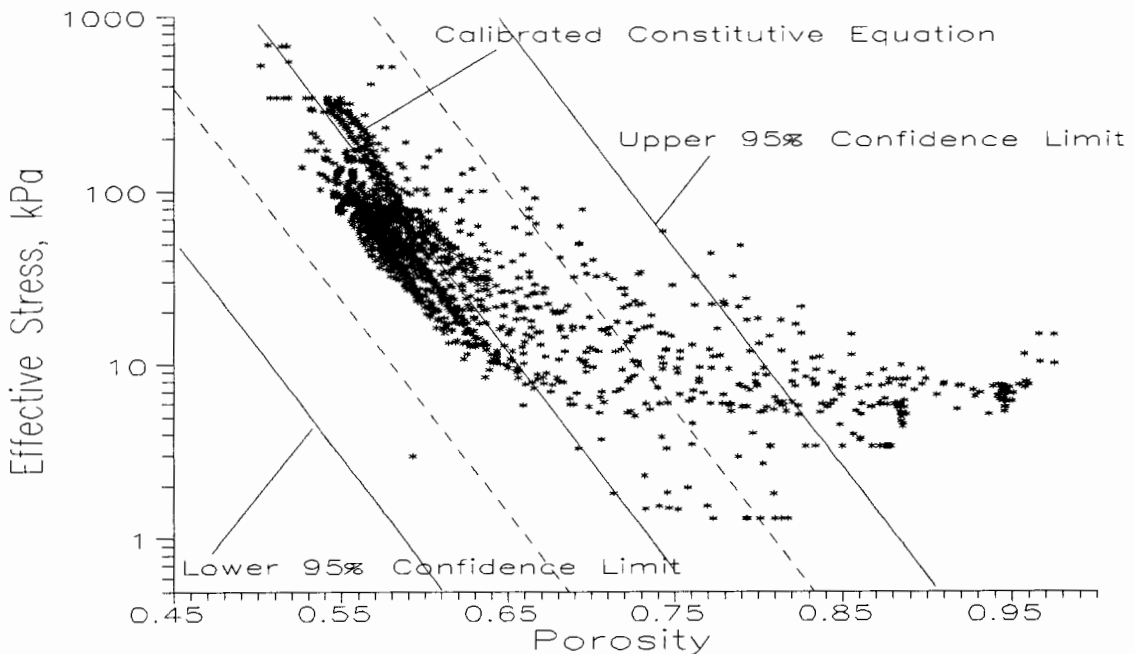


Figure 159. Confidence interval estimates for normally distributed, randomly selected values of effective stress at various values of porosity.

The straight lines in Figures 158 and 159 give the conditional mean, or predicted constitutive equations as determined by the calibrated parameters α , β , γ , and δ . For a given value of suspended solids concentration, the ordinate value is assumed to be distributed normally about the mean value with an associated standard deviation. These straight lines are uncertain, and the slopes and intercepts may vary within the confidence interval envelopes. By taking one normally distributed random value of the ordinate at each extreme of the suspended solids concentration axis, a new constitutive equation within the 95% confidence region can be calculated. The parameters from the new equation can then be used in a computer simulation. Repeating this procedure many times gives a distribution of constitutive equations about the predicted constitutive equation.

DEWATERING MODEL UNCERTAINTY ANALYSIS

The Monte Carlo simulation algorithm used in this study is shown in Figure 160. The computer code used to calculate constitutive equations within the confidence limits is given in Appendix C.

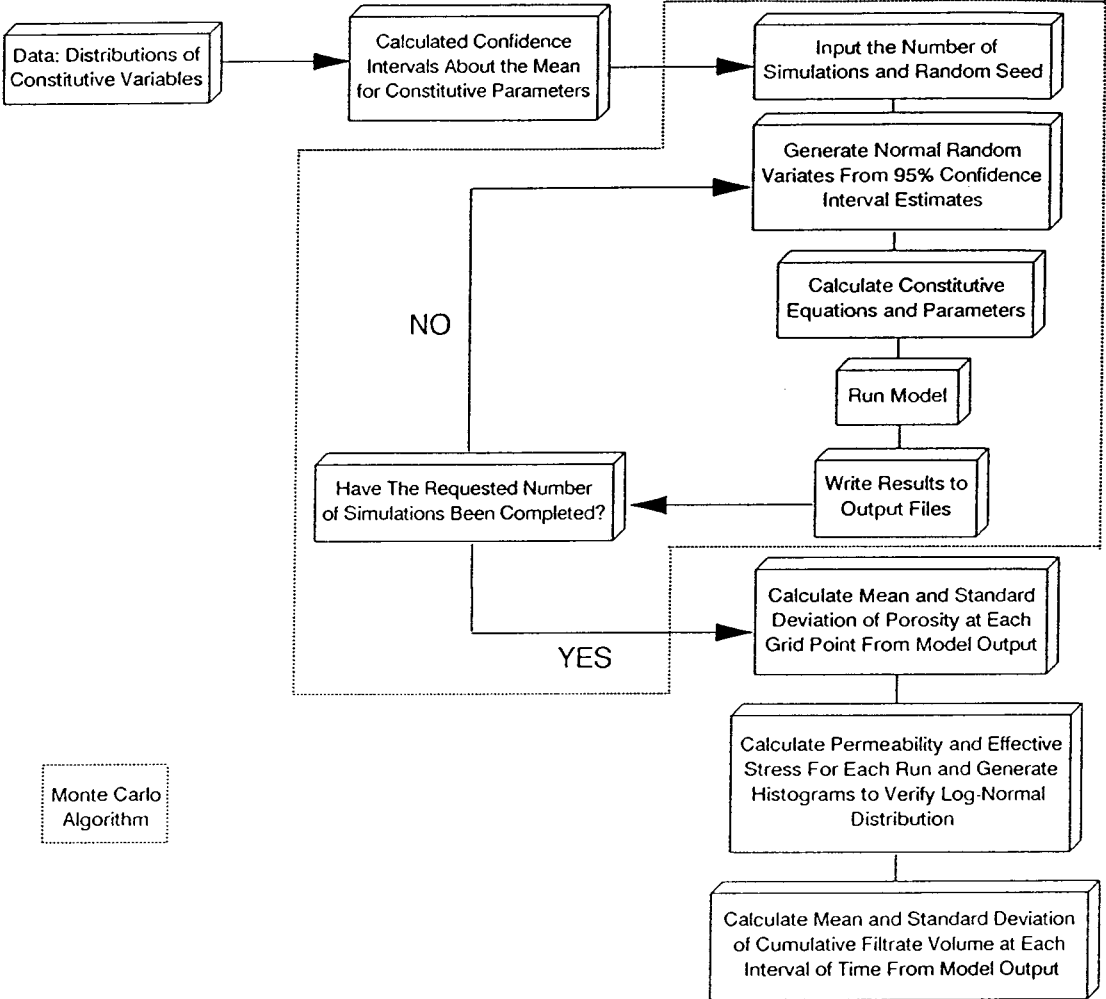


Figure 160. Monte Carlo simulation algorithm.

A total of 500 simulations were performed using the conditions of the model calibration run (CHESS run KDMK9) as input. Only the parameters associated with the constitutive equations were varied. Figures 161 and 162 give the distributions of values of k and m_v (for a single value of porosity, $n=0.8815$) which resulted from all simulations. These give an indication of the distributions of the constitutive equations. The distributions should be lognormal, and indeed, seem to be.

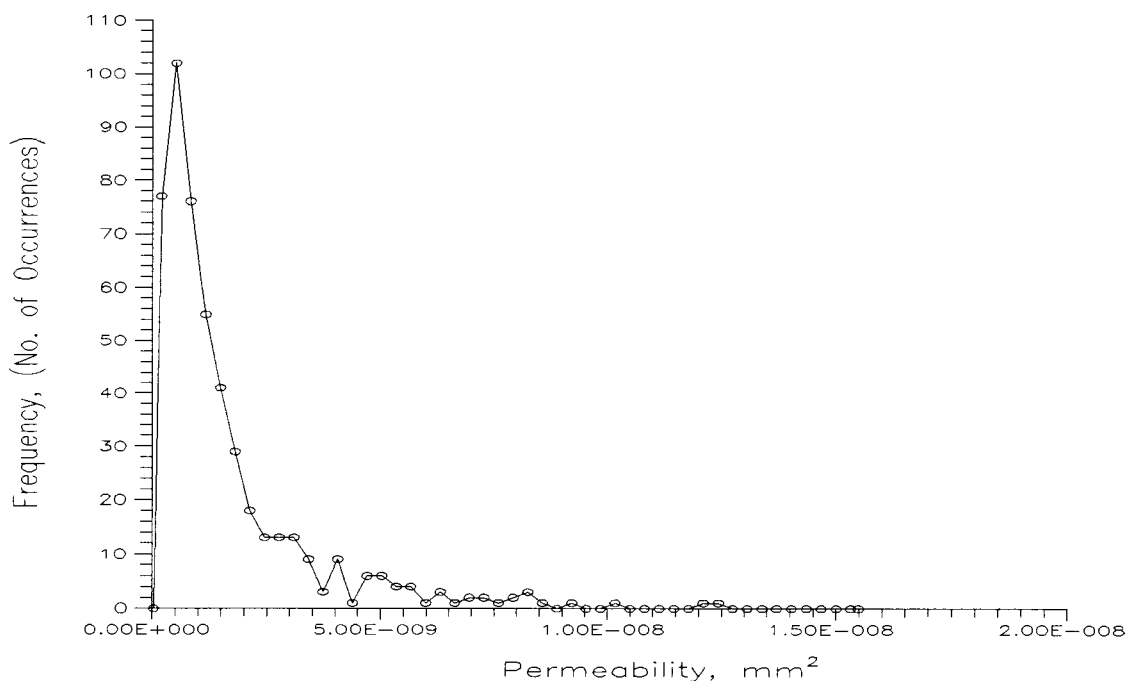


Figure 161. Frequency histogram for permeability, k , for 500 runs of parameter picking algorithm using UNIX system pseudo-random number generator at initial porosity of 0.88 g/cm^3 .

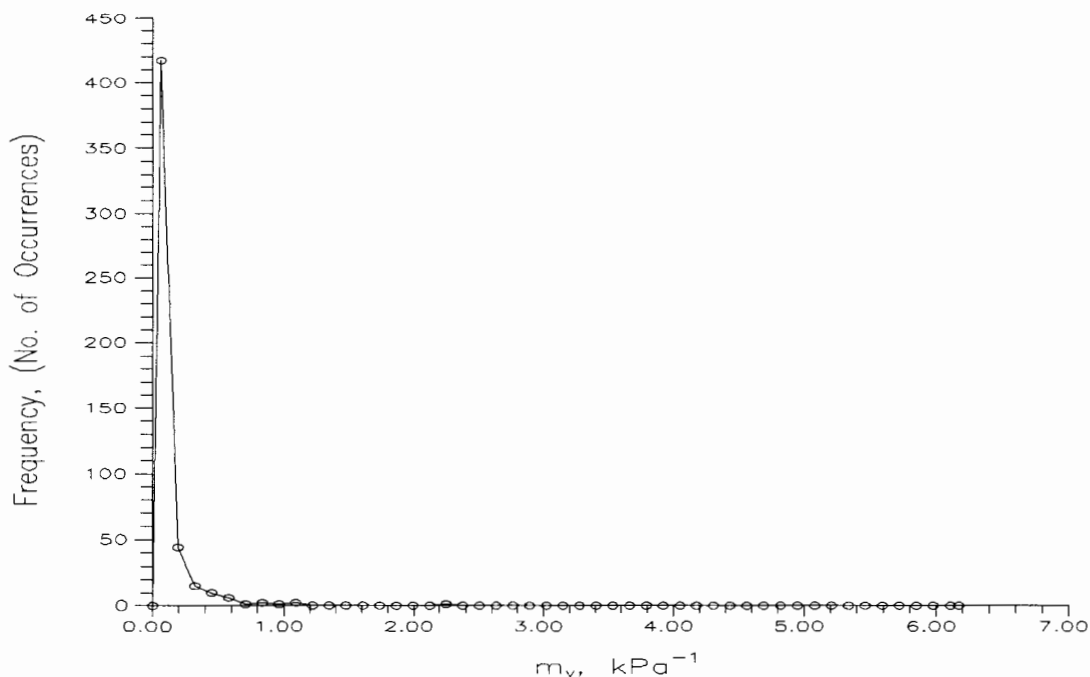


Figure 162. Frequency histogram for m_v for 500 runs of parameter picking algorithm using UNIX system pseudo-random number generator at initial porosity of 0.88 g/cm^3 .

Table XVII presents statistics for several parameter-dependent quantities calculated by the dewatering model. Figures 163-167 give mean suspended solids concentration profiles and approximate 68% confidence limits at 60, 90, 120, 180, and 300 seconds for the 500 runs of the computer model. These figures give an idea of the expected values of model predictions and the uncertainty in these predictions of suspended solids concentrations at various points in space and time considering the inherent variability in the dewaterability of the kaolin sludge used in the CHESSE experiments.

TABLE XVII

MEAN AND STANDARD DEVIATION OF PARAMETER-DEPENDENT QUANTITIES FOR 500 RUNS OF WELLS (1990a) DEWATERING MODEL

Variable	Simulations	Mean	Std. Dev.
Terminal Porosity	500	0.3977	9.32×10^{-3}
	400	0.3961	1.06×10^{-3}
	300	0.3997	6.23×10^{-3}
	200	0.4030	2.69×10^{-3}
	100	0.3979	4.64×10^{-3}
CPU Time, seconds	500	3205	143
	400	3219	161
	300	3259	188
	200	3540	259
	100	3332	389
Iterations	500	466,726	20,853
	400	462,303	23,078
	300	477,669	27,572
	200	509,421	13,422
	100	466,327	31,363

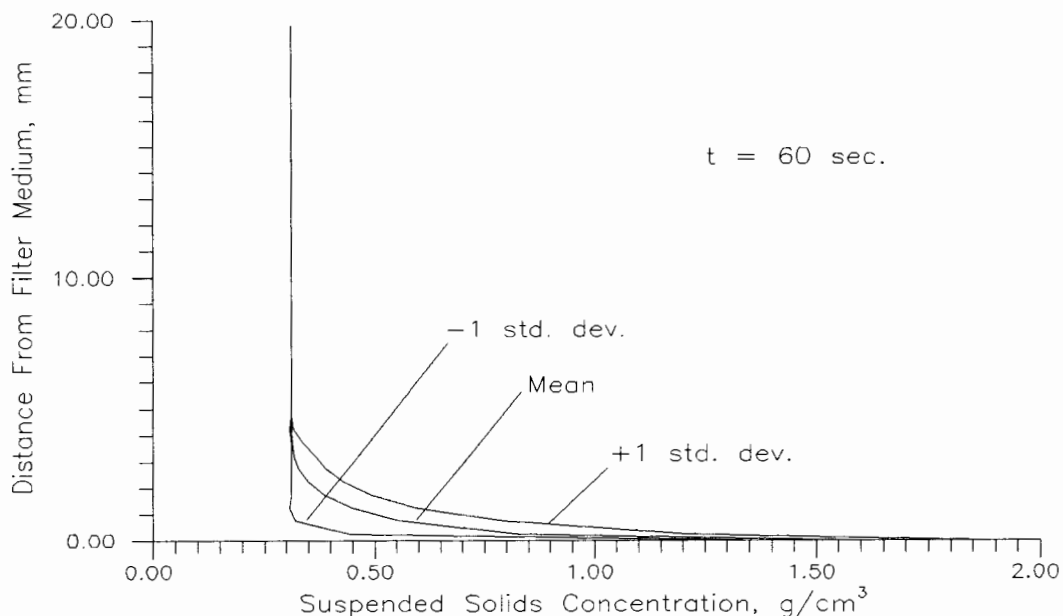


Figure 163. Mean values of suspended solids concentration versus distance from the filter medium with approximate 68% confidence limits as predicted by Wells (1990a) sludge dewatering model for 500 model simulations.

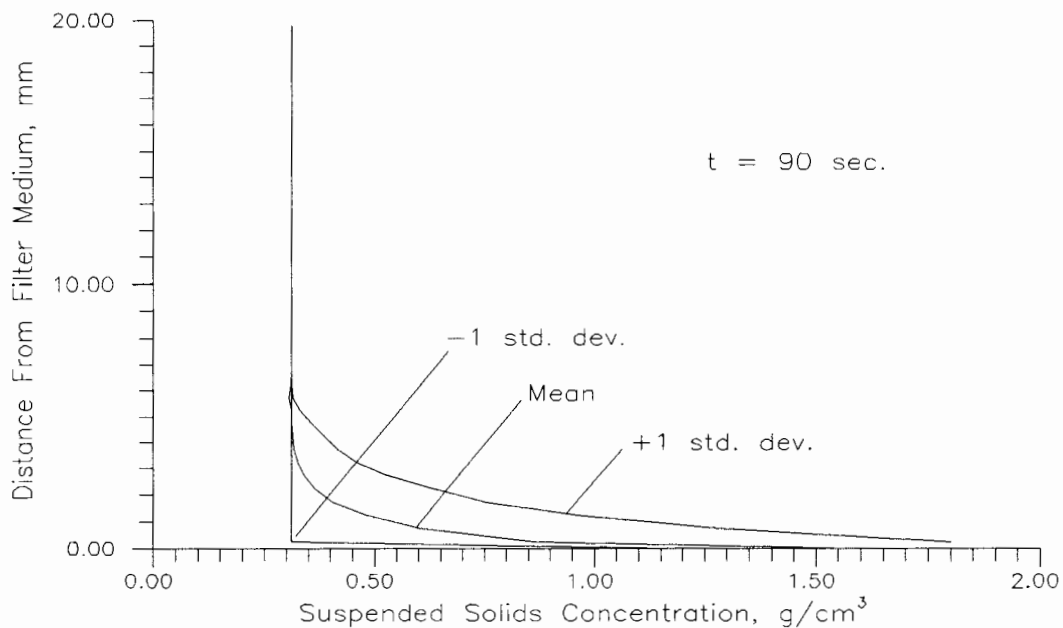


Figure 164. Mean values of suspended solids concentration versus distance from the filter medium with approximate 68% confidence limits as predicted by Wells (1990a) sludge dewatering model for 500 model simulations.

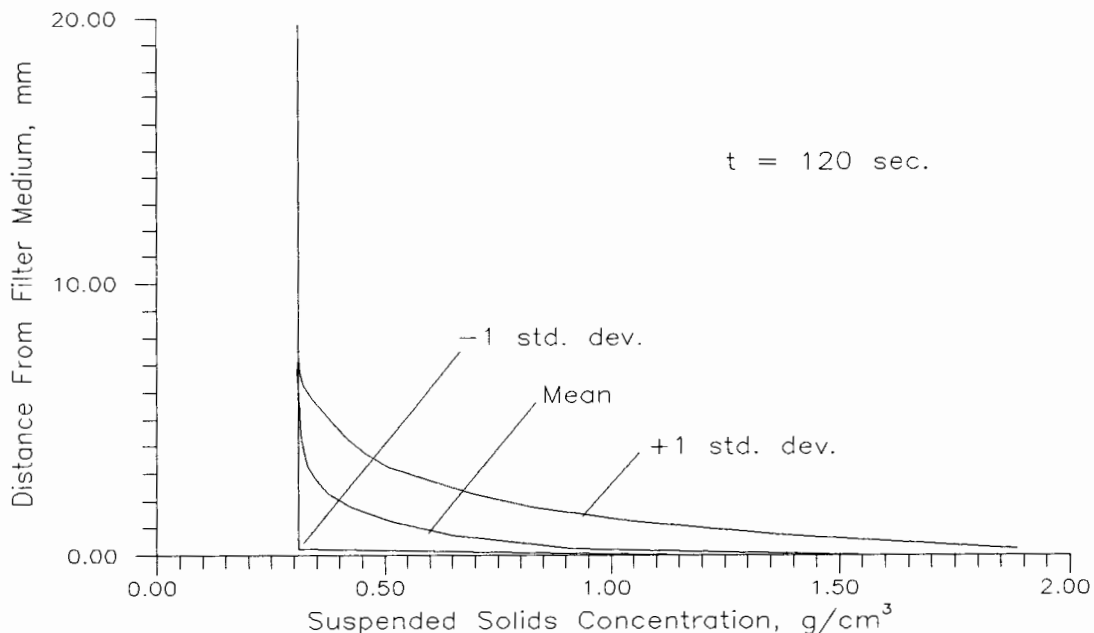


Figure 165. Mean values of suspended solids concentration versus distance from the filter medium with approximate 68% confidence limits as predicted by Wells (1990a) sludge dewatering model for 500 model simulations.

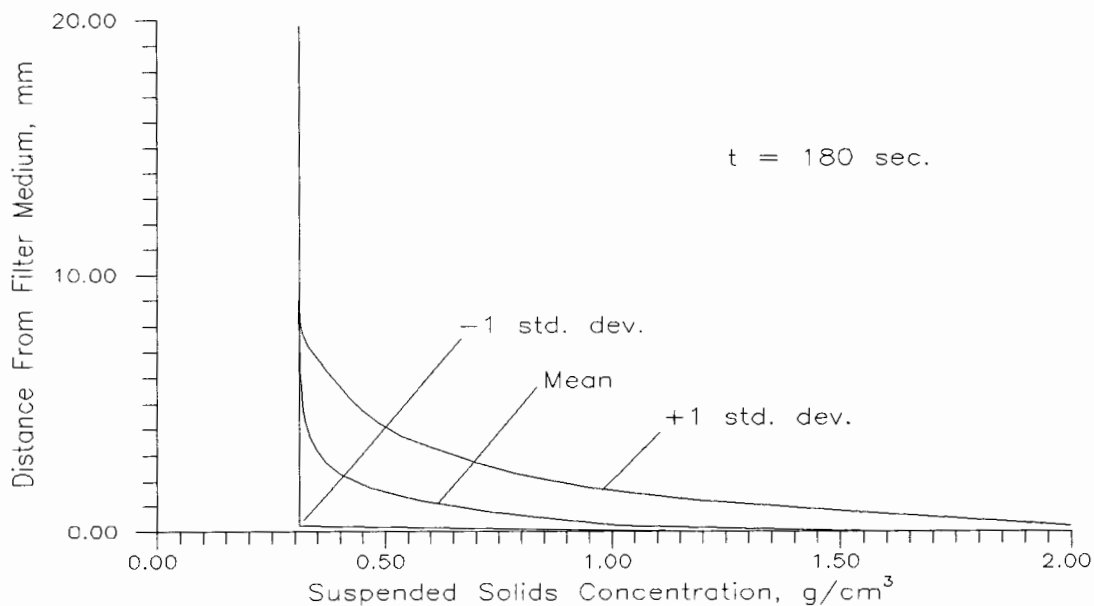


Figure 166. Mean values of suspended solids concentration versus distance from the filter medium with approximate 68% confidence limits as predicted by Wells (1990a) sludge dewatering model for 500 model simulations.

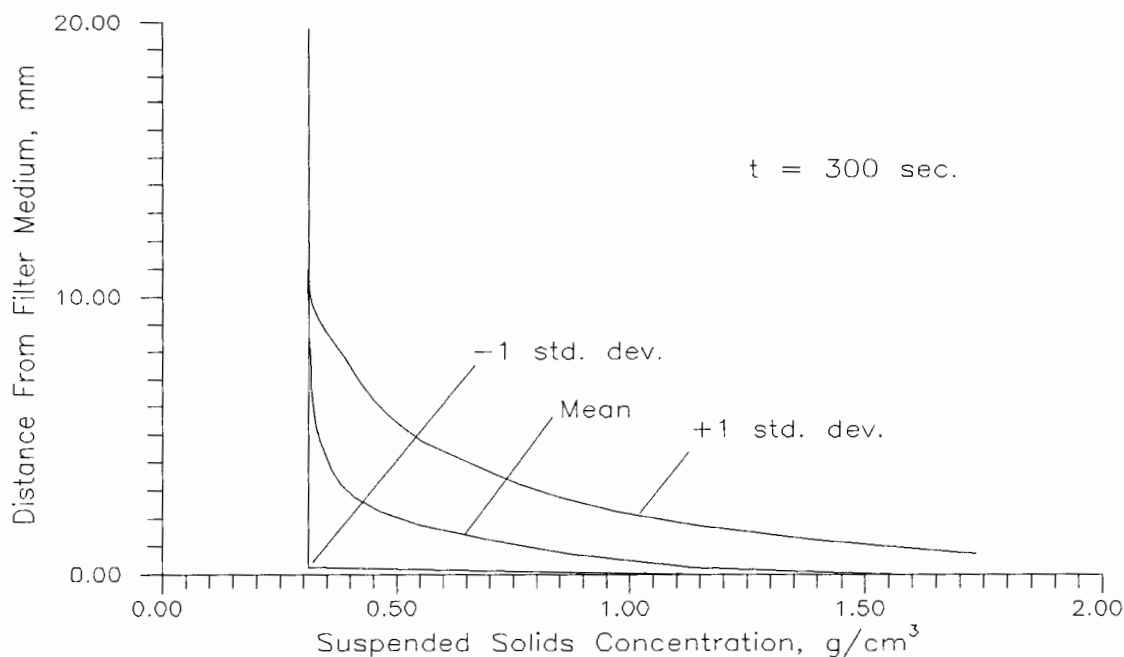


Figure 167. Mean values of suspended solids concentration versus distance from the filter medium with approximate 68% confidence limits as predicted by Wells (1990a) sludge dewatering model for 500 model simulations.

As can be seen from Figures 163-167, the large degree of uncertainty in the parameters of the constitutive equations produces a large uncertainty in the model predictions of suspended solids concentration at various distances from the filter medium. The lower confidence limit is not symmetrical about the mean with the upper confidence limit, since it is physically impossible for the suspended solids concentration to be lower than the initial concentration under these conditions.

Figure 168 shows expected values of model predictions for filtrate volume versus time and the 68% confidence limit estimates.

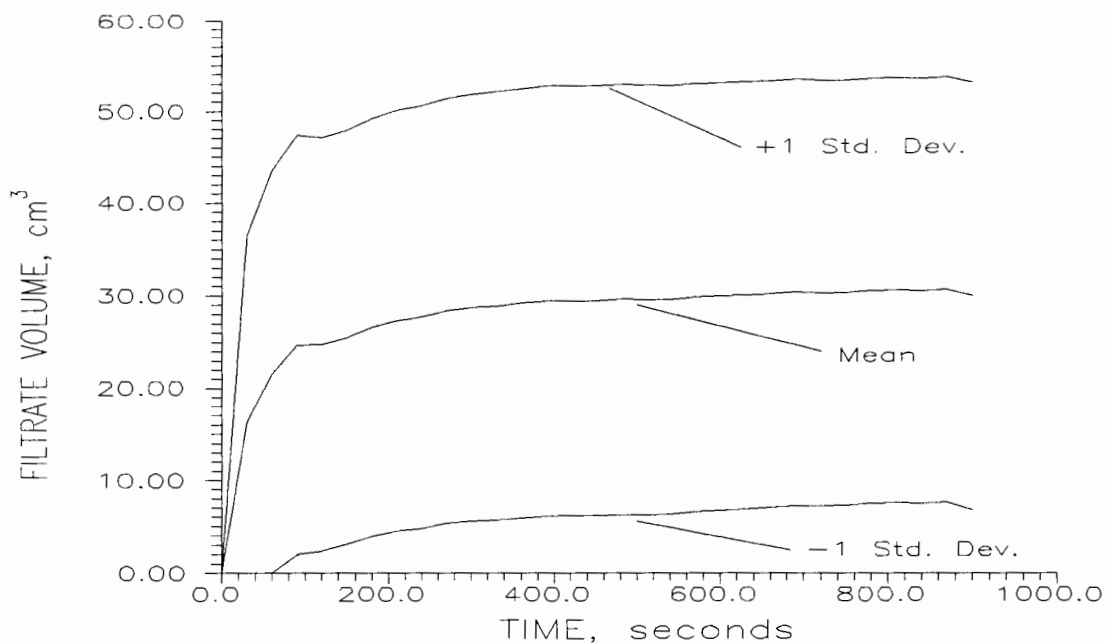


Figure 168. Mean values of filtrate volume versus time with approximate 68% confidence limits as predicted by Wells (1990a) sludge dewatering model for 500 model simulations.

These results show the sensitivity of the model results to the constitutive equation parameters and indicate that more research should be conducted on the functional forms of the constitutive equations and the relationship of the two constitutive equations to each other.

An important point to be considered in any application of stochastic, or Monte Carlo simulation is the number of simulations that were required to be performed. Statistically, the more simulations performed, the better. However, it would be a waste of time to perform 1000 simulations if similar results could be obtained by performing only 500. Figures 169-173 give the differences in mean

suspended solids concentration at different distances from the filter medium between those calculated after 500 simulations and those calculated after 400, 300, 200, and 100 simulations.

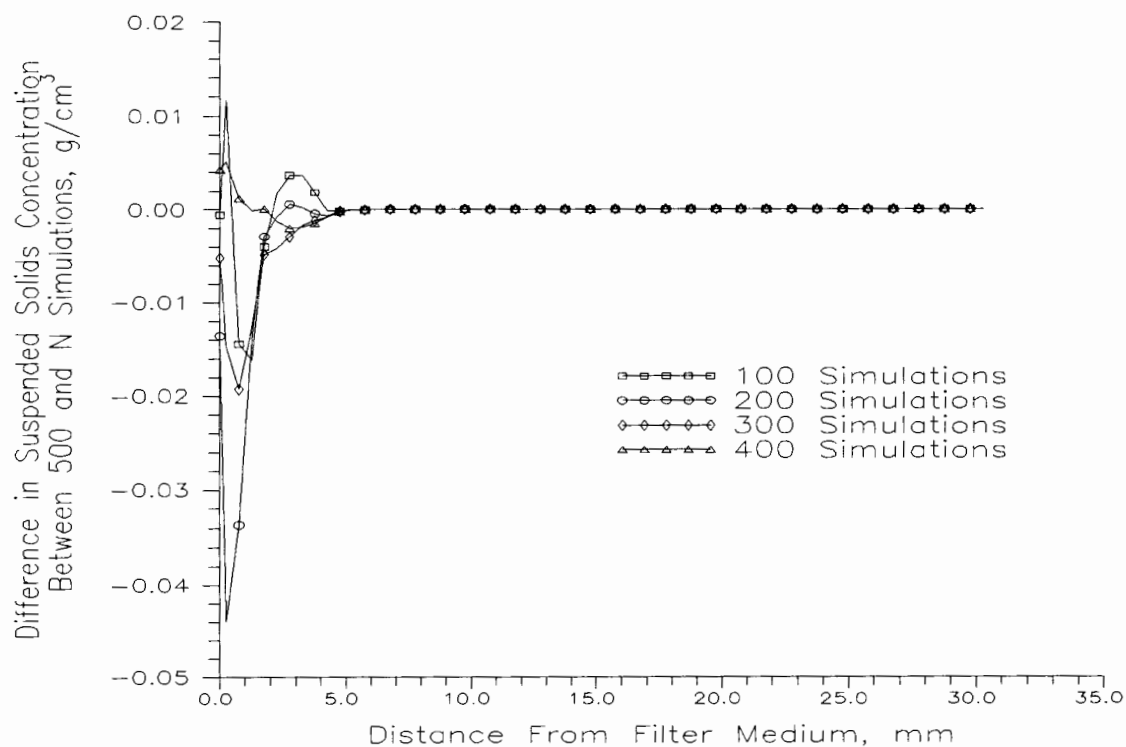


Figure 169. Plot of differences between mean suspended solids concentration obtained after 500 and N model runs at a simulated time of 60 seconds.

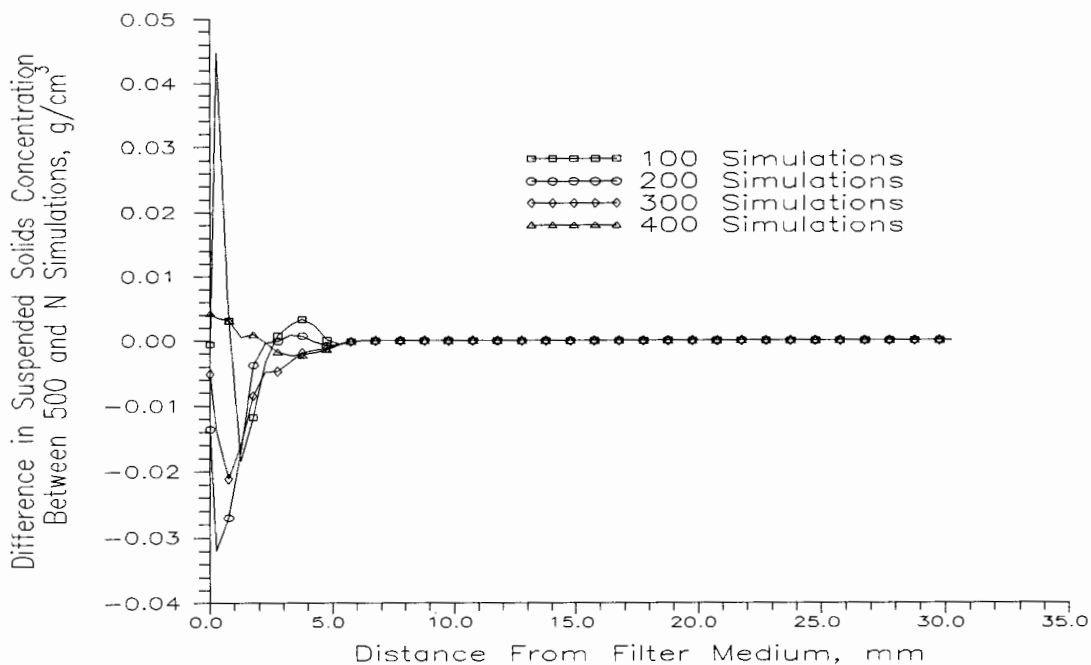


Figure 170. Plot of differences between mean suspended solids concentration obtained after 500 and N model runs at a simulated time of 90 seconds.

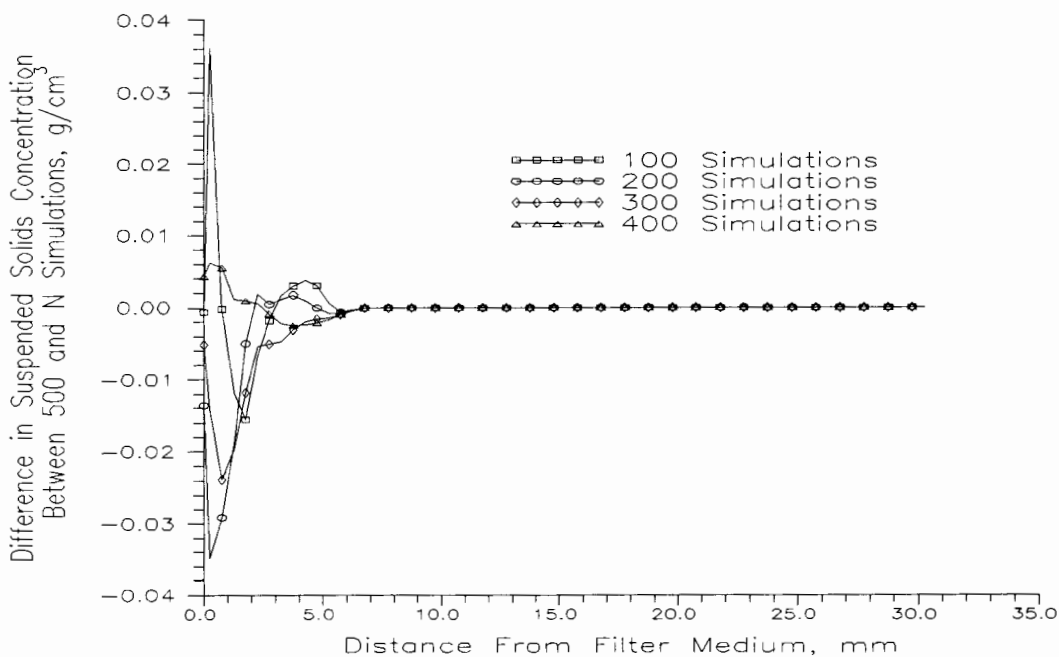


Figure 171. Plot of differences between mean suspended solids concentration obtained after 500 and N model runs at a simulated time of 120 seconds.

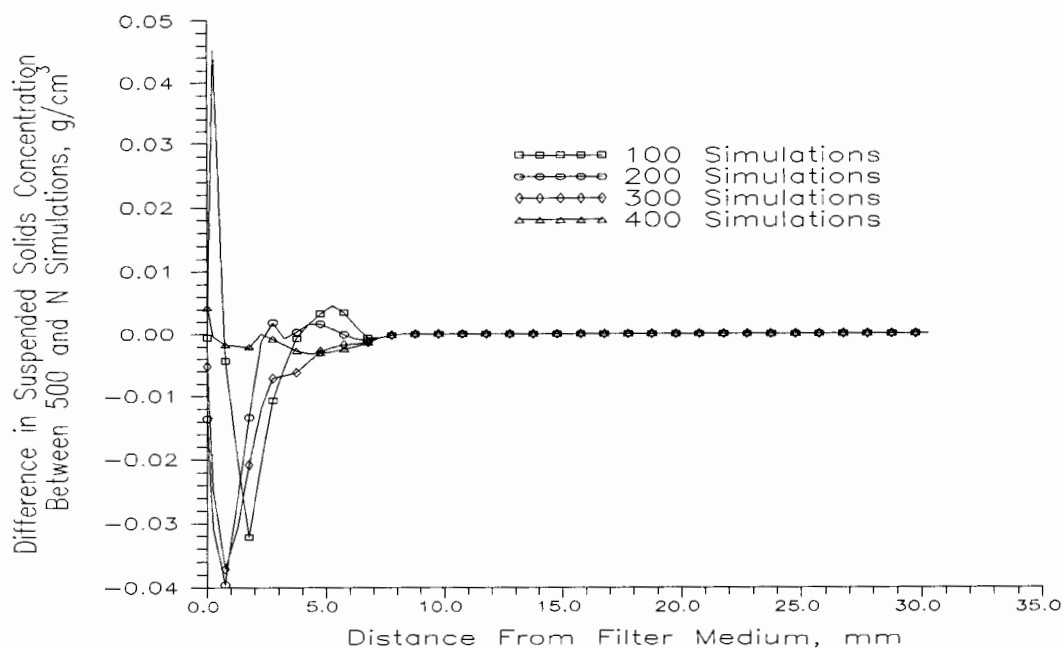


Figure 172. Plot of differences between mean suspended solids concentration obtained after 500 and N model runs at a simulated time of 180 seconds.

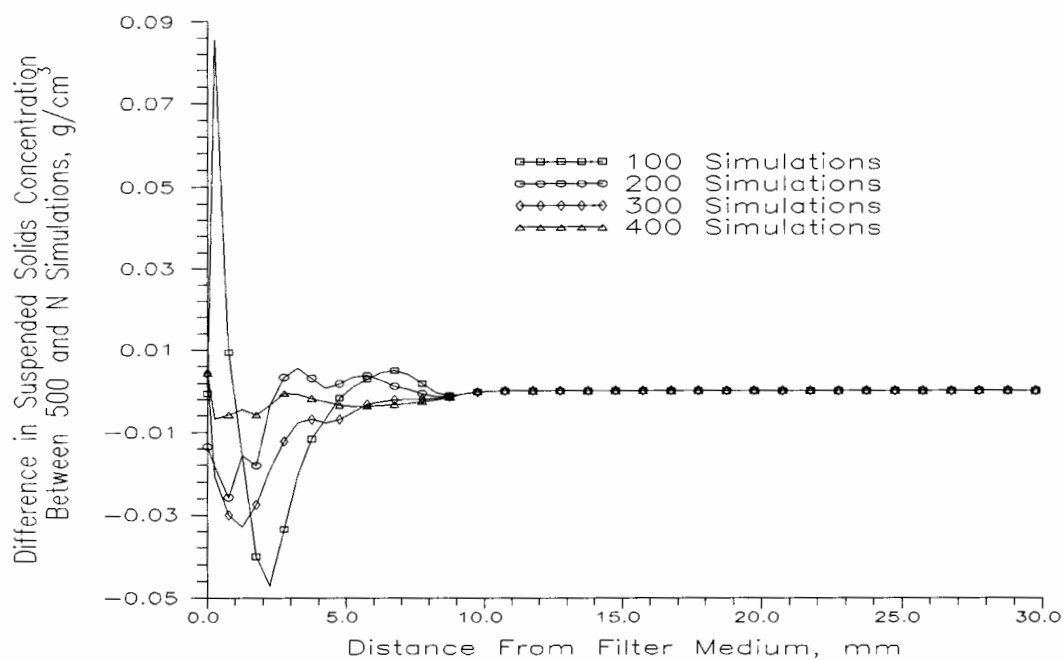


Figure 173. Plot of differences between mean suspended solids concentration obtained after 500 and N model runs at a simulated time of 300 seconds.

It would be expected that the differences in the mean suspended solids concentration values would be inversely proportional to the number of simulations performed. As can be seen from the figures, in general, the mean error decreases as the number of simulations increases. As expected, the largest error occurs near the filter medium ($z=0$). The figures show that similar results can be obtained by performing either 400 or 500 simulations.

Figure 174 is a plot of the differences between mean filtrate volume obtained after 500 and those obtained after 100, 200, 300, and 400 runs of the dewatering model.

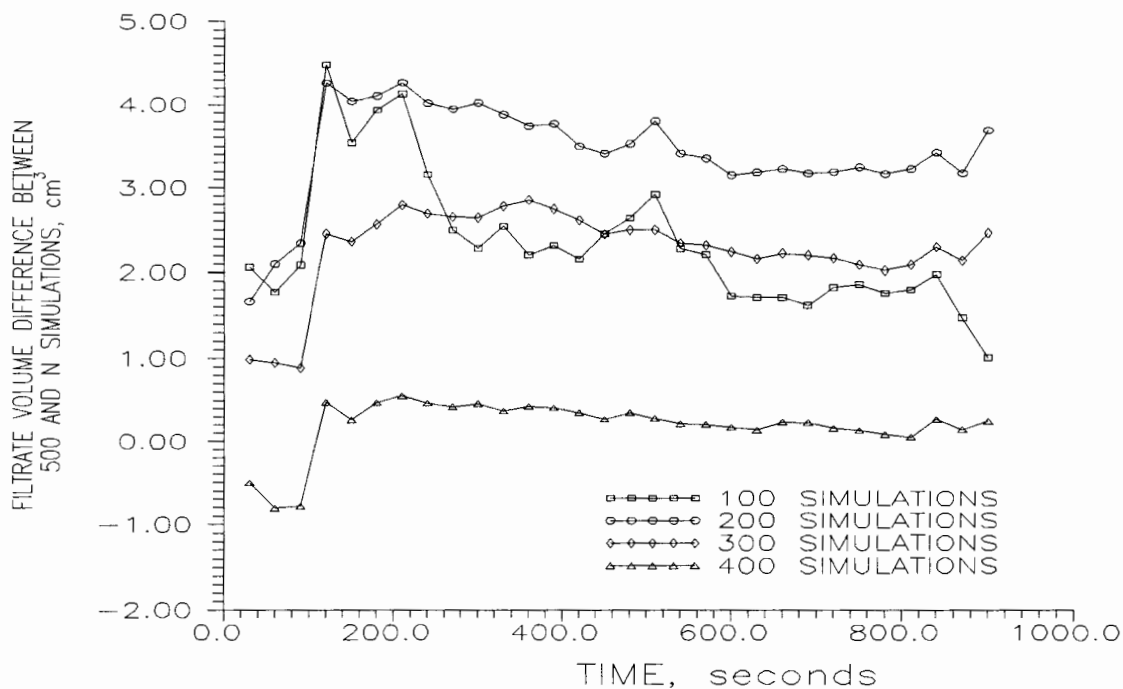


Figure 174. Plot of differences between mean filtrate volume obtained after 500 and N model runs at various times.

As with the plots of differences in suspended solids concentrations at various distances from the filter medium, the mean differences after 200 simulations were quite large, but were offset by the results of subsequent simulations.

A check was made of the parameter picking algorithm for possible bias. Another pseudo-random number generator was substituted for that used in the Monte Carlo simulation. Initially, the pseudo-random number generator was intended to be included within the computer code of the parameter-picking algorithm in order to make it completely portable. This initial pseudo-random number generator was a subroutine (RAN1) taken from the book Numerical Recipes by Press, Flannery, Teukolsky and Vetterling.

Figures 175 and 176 show the distributions of k and m_v resulting from substitution of a call to the Numerical Recipes pseudo-random number generator in place of the call to the system resident pseudo-random number generator in the computer code of the parameter picking algorithm. A total of 500 values of each parameter were picked.

Comparing these figures to Figures 161 and 162 show significant differences in the parameters obtained from each pseudo-random number generator. The Numerical Recipes pseudo-random number generator gave a narrower spread of values. It also seemed to pick values in certain intervals much more frequently than it should, for instance near the tail of the distribution. This should not happen if the pseudo-random

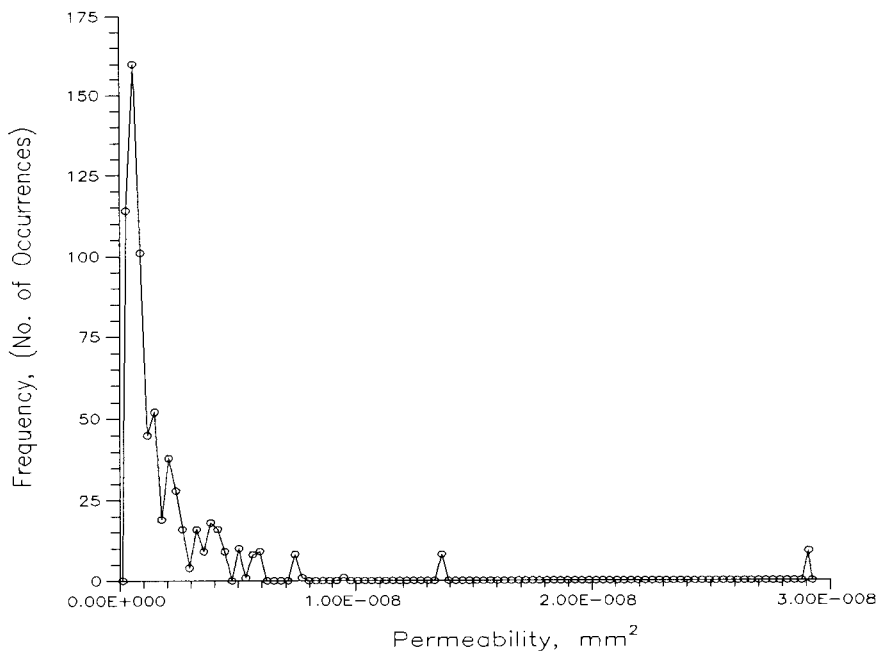


Figure 175. Frequency histogram for permeability, k , for 500 simulations of Wells (1990a) dewatering model at initial porosity of 0.88 g/cm^3 .

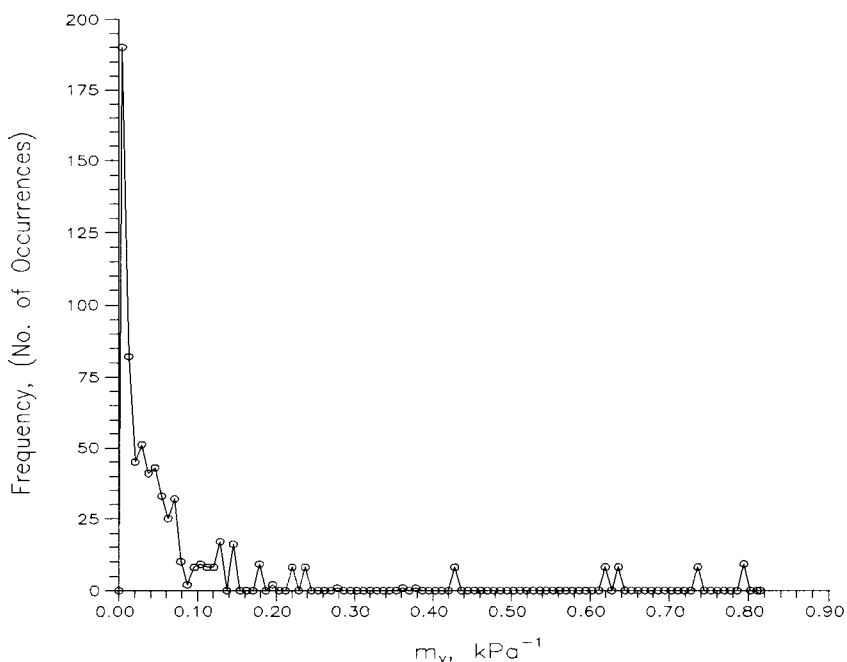


Figure 176. Frequency histogram for the coefficient of volume compressibility, m_v , for 500 simulations of Wells (1990a) dewatering model at initial porosity of 0.88 g/cm^3 .

number generator was truly unbiased. The probability of picking values near the tail of the distribution should be extremely small. If any parameter values near the tail of the distribution were chosen at all, it seems improbable that ten m_v values would be chosen in one class interval near the tail of the distribution. The parameters chosen by the UNIX system pseudo-random number generator seemed much more reasonable. For this reason, the system resident pseudo-random number generator was used in the computer code used to generate the constitutive equation parameters.

A NEW CONSTITUTIVE EQUATION FOR m_v

As can be observed in Figure 159, the constitutive equation for m_v causes the confidence interval envelope to be rather wide. Previous results have indicated that the constitutive equations used to solve the model's governing equations may not be adequate during high porosity (low concentration) conditions. Equation 77 gives an alternative functional form for the constitutive equation for m_v , which better fit the experimental data from Bierck, Wells and Dick (1988).

$$n = (v\sigma')^{\frac{\omega}{(\sigma' - \sigma'_l)}} - n_l \quad (77)$$

This constitutive equation requires the user to calibrate the three parameters ω , σ'_l , and n_l . The constant, v , is required solely for dimensional consistency. Even with the additional parameter, however, the new constitutive equation should be no more difficult to calibrate than the exponential constitutive equation previously used by Wells (1990), since the new parameters vary over a much narrower range. The parameter σ'_l corresponds to a limiting effective stress, while n_l is a limiting value of porosity. This equation has not yet been incorporated into the computer model. Figure 174 shows a comparison between experimental data and the new constitutive equation using the following parameter values:

$$v = 1.0$$

$$\omega = 0.54$$

$$\sigma'_l = 2.0$$

$$n_l = 0.46$$

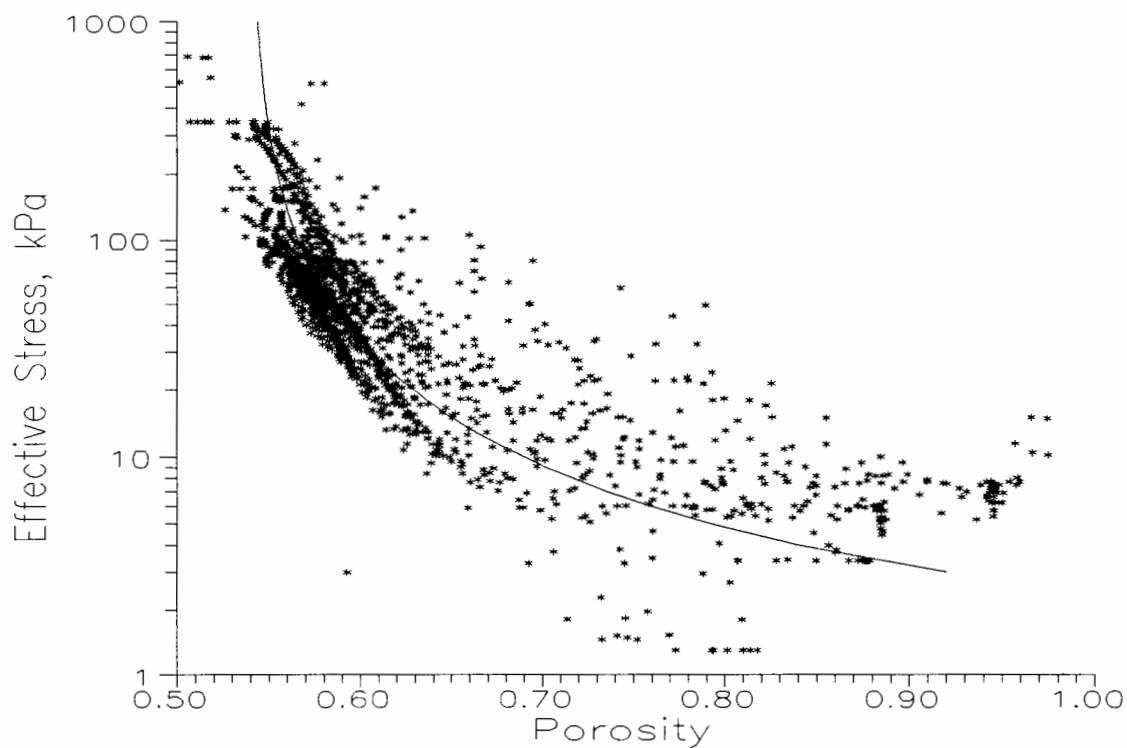


Figure 177. Plot of data obtained from Bierck, Wells and Dick (1988) versus new constitutive equation for the coefficient of volume compressibility, m_v .

CHAPTER IX

CONCLUSIONS AND RECOMMENDATIONS FOR FURTHER RESEARCH

This study has shown the ability of the Wells (1990a) sludge dewatering model to simulate the dewatering behavior of sludges under the conditions of the typical specific resistance test. This is an important first step toward the development of a more comprehensive model which would simulate real-world dewatering processes, such as vacuum filters and belt filter presses. Such a model would be a valuable aid in the rational design of dewatering equipment.

Because the Wells (1990a) sludge dewatering model did not give accurate results when the initial porosity profile used as input to the model was uniform, the method of artificial viscosity, first proposed by von Neumann and Richtmeyer (1950), was incorporated into the model to smooth out the discontinuity in the initial porosity profile. This was shown to be a significant improvement, thus extending the usefulness of the model.

A procedure for calculating dewaterability parameters used in the Wells (1990b) dewatering model from specific resistance tests was shown to yield good results in two of the three sludges studied. The procedure outlined by Wells (1990b) results in a great savings of time and effort during

the process of calibrating the model for different sludges. Even so, this procedure gives only a somewhat rough calibration. There is a need for more rapid and automatic calibration techniques (such as direct search computer methods) to be applied to the Wells (1990a) dewatering model, which are able to fine-tune, or optimize, the calibration of model parameters for any given sludge.

Because sludge properties exhibit great variability, and determination and characterization of these properties is somewhat uncertain, stochastic, or Monte Carlo simulation was used in an attempt to characterize the model's response to this parameter variability and uncertainty. The model was shown to be quite sensitive to the values of the input parameters.

This study has produced some evidence that the constitutive equations used to solve the model's governing equations may not be adequate during high porosity (low concentration) conditions. An alternative form for the constitutive equation for the coefficient of volume compressibility, m_v , was proposed which better fit the CHES data than that of Wells (1990a). Because of the importance of the constitutive equations to the dewatering model's performance, further research into this and other possible functional forms for these constitutive equations is needed. There is also a need to study the relationships between the constitutive equations.

The less accurate results for the high initial porosity runs may also be the result of neglecting the effect of gravity in the dewatering model. In the region above the propagating sludge solids cake there is no particle to particle contact, hence no effective stress. In this region the dominant physical process would be gravity sedimentation. This process cannot be completely taken into account using the constitutive equation for m_v ($=-\partial n/\partial \sigma'$) alone.

As Wells (1990a) has pointed out, comprehensive simulation of sludge dewatering by belt filter press would require models of gravity sedimentation; cake filtration in a laterally unconfined domain, taking into account the effect of shear between the belts; stress on the cake due to machine design factors (such as roller geometry) and operational parameters (such as belt speed and tension); and permeability of the belt as a function of belt tension and washing efficiency.

REFERENCES

- Atsumi, K. and T. Akiyama. 1975. "A Study of Cake Filtration - Formulation as a Stefan Problem," Journal of Chemical Engineering of Japan, 8 (6) 487-492.
- Benson, R. E. 1987. "A Consolidation Model For Sludge Dewatering," in Proceedings of the 1987 Environmental Engineering Specialty Conference, ed. by John D. Dietz, American Society of Civil Engineers, New York.
- Bierck, B. R., S. A. Wells and R. I. Dick. 1988. "Compressible Cake Filtration: Monitoring Cake Formation and Shrinkage Using Synchrotron X-rays," Journal of the Water Pollution Control Federation, 60 (5) 645-649.
- Biot, M. A. 1941. "General Theory of Three-Dimensional Consolidation," Journal of Applied Physics, 12, 155-164.
- Bowles, J. E. 1984. Physical and Geotechnical Properties of Soils, McGraw Hill, New York.
- Chang, C. S. 1985. "Uncertainty of One-Dimensional Consolidation Analysis," Journal of Geotechnical Engineering, 111, 1411-1424.
- Christensen, G. L. and R. I. Dick. 1985. "Specific Resistance Measurements: Methods and Procedures," Journal of Environmental Engineering, 111, 258-271.
- Davis, E. H. and G. P. Raymond. 1965. "A Non-Linear Theory of Consolidation," Geotechnique, 15, 161-173.
- Dick, R. I., and R. O. Ball. 1980. "Sludge Dewatering," Critical Reviews in Environmental Control, 10, 269-337.
- Doctor, P. G. 1989. "Sensitivity and Uncertainty Analyses for Performance Assessment Modeling," Engineering Geology, 26, 411-429.
- Dunn, I. S., L. R. Anderson, and F. W. Kiefer. 1980. Fundamentals of Geotechnical Analysis. John Wiley and Sons, New York.

- Evans, B., and D. Filman. 1988. "Solids Handling Costs at Large Sewage Treatment Plants," Specialty Conference Proceedings - Joint CSCE-ASCE National Conference on Environmental Engineering.
- Gibson, R. E., G. L. England and M. J. L. Hussey. 1967. "The Theory of One-Dimensional Consolidation of Saturated Clays. 1. Finite Non-Linear Consolidation of Thin Homogeneous Layers," Geotechnique, 17 (3) 261-273.
- Gibson, R. E., R. L. Schiffman and K. W. Cargill. 1981. "The Theory of One-dimensional Consolidation of Saturated Clays. II. Finite Non-linear Consolidation of Thick Homogeneous Layers," Canadian Geotechnical Journal, 8, 280-293.
- Herath, B., P. Geladi and C. Albano. 1989. "Developing and Empirical Model for Dewatering - and its Application to Peat," Filtration & Separation, 53-56.
- Johnson, R. 1984. Elementary Statistics, Duxbury Press, Boston.
- Koch, R. W. and G. M. Smillie. 1986. "Bias in Hydrologic Prediction Using Log-transformed Regression Models," Water Resources Bulletin, 22, 717-723.
- Kos, P. and D. D. Adrian. 1975. "Transport Phenomena Applied to Sludge Dewatering," Journal of the Environmental Engineering Division, ASCE, 101, 947-965.
- Lee, I. K. 1968. Soil Mechanics Selected Topics, Butterworths, London.
- Lee, K. and G. L. Sills. 1979. "A Moving Boundary Approach to Large Strain Consolidation of a Thin Soil Layer," in Numerical Methods in Geomechanics Aachen 1979, ed. by W. Wittke, A. A. Balkema, Rotterdam, 163-173.
- McNabb, A. 1960. "A Mathematical Treatment of One-Dimensional Soil Consolidation," Quarterly of Applied Mathematics, 17, (4), 337-347.
- Monte, J. L. and R. J. Krizek. 1976. "One-dimensional Mathematical Model For Large-strain Consolidation," Geotechnique, 26, (3), 495-510.
- Morse, D. 1989. "Sludge in the Nineties," Civil Engineering, 47-50.

- von Neumann, J. and R. D. Richtmyer. 1950. "A Method for the Numerical Calculation of Hydrodynamic Shocks," Journal of Applied Physics, 21, 232-237.
- Nystrom, G. A. 1984. "Reporter Summary Sedimentation-Consolidation Models: Theory," in Sedimentation Consolidation Models Predictions and Validation, ed. by R. N. Yong and F. C. Townsend, American Society of Civil Engineers, New York, 1-29.
- Philip, J. R. 1955. "Numerical Solution of Equations of the Diffusion Type with Diffusivity Concentration-Dependent," Transactions of the Faraday Society, 51, 885-892.
- Philip, J. R. 1968. "Kinetics of Sorption and Volume Change in Clay-Colloid Pastes," Australian Journal of Soil Research, 6, 249-267.
- Press, W. H., B. P. Flannery, S. A. Teukolsky and W. T. Vetterling. 1986. Numerical Recipes The Art of Scientific Computing. Cambridge University Press, New York.
- Quinney, D. 1985. An Introduction to the Numerical Solution of Differential Equations. John Wiley and Sons Inc., New York.
- Richtmyer, R. D. and K. W. Morton. 1967. Difference Methods for Initial-value Problems. Wiley Interscience Publishers, New York.
- Scheidegger, A. E. 1974. The Physic of Flow Through Porous Media. University of Toronto Press, Canada.
- Schiffman, R. L. and R. E. Gibson. 1964. "Consolidation of Nonhomogeneous Clay Layers," Proceedings of the American Society of Civil Engineers, 90, SM5, 1-30.
- Schiffman, R. L. 1980. "Finite and Infinitesimal Strain Consolidation," Proceedings of the American Society of Civil Engineers, 106, GT2, 203-207.
- Schiffman, R. L., V. Pane and R. E. Gibson. 1984. "The Theory of One-Dimensional Consolidation of Saturated Clays. IV. An overview of Non-linear Finite Strain Sedimentation and Consolidation," in Sedimentation Consolidation Models Predictions and Validation, ed. by R. N. Yong and F. C. Townsend, American Society of Civil Engineers, New York, 1-29.

- Sills, G. C. and K. Lee. 1980. "Assumptions Underlying Soil Consolidation Theories," University of Oxford Department of Engineering Science, S.M. Report No. SM008/ESD/80, Engineering Laboratory, Parks Road, Oxford.
- Smiles, D. E., and M. J. Rosenthal. 1968. "The Movement of Water in Swelling Materials," Australian Journal of Soil Research, 6, 237-248.
- Smiles, D. E., and H. G. Poulos. 1969. "The One-Dimensional Consolidation of Columns of Soil of Finite Length," Australian Journal of Soil Research, 7, 285-291.
- Smiles, D. E. 1970. "A Theory of Constant Pressure Filtration," Chemical Engineering Science, 25, 985-996.
- Smith, G. D. 1978. Numerical Solution of Partial Differential Equations: Finite Difference Methods. Oxford University Press, Oxford.
- Task Committee on Belt Filter Presses. 1988. "Belt Filter Press Dewatering of Wastewater Sludge," Journal of Environmental Engineering, 114, (5), 991-1006.
- Terzaghi, K. 1943. Theoretical Soil Mechanics. John Wiley and Sons, Inc., New York.
- Thomann, R. V. 1972. "Value and General Concepts of Modeling," in Mathematical Modeling in Environmental Engineering, ed. by T. M. Keinath and M. P. Wanielista, Association of Environmental Engineering Professors.
- Tiller, F. M., 1975. "Compressible Cake Filtration," in Scientific Basis of Filtration, ed by K. Ives, Noordhoff, London, 315-397.
- Tiller, F. M. and Liou-Liang Horng. 1983. "Hydraulic Deliquoring of Compressible Filter Cakes," AIChE Journal, 29, 297-305.
- Tosun, I. 1986. "Formulation of Cake Filtration," Chemical Engineering Science, 41, 2563-2568.
- Wakeman, R. J. 1978. "A Numerical Integration of the Differential Equations Describing the Formation of and Flow in Compressible Filter Cakes," Transactions Institute Chemical Engineering, 56, 1978.
- Walpole, R. E. and R. H. Myers. 1985. Probability and Statistics for Engineers and Scientists, Macmillan Publishing Company, New York.

- Wells, S. A. 1989. "Mathematical Modeling of Compressible Cake Filtration," in ASCE Environmental Engineering Proceedings, ed. by J. Malina, 788-795.
- Wells, S. A. 1990a. Compressible Cake Filtration Modeling and Analysis. Ph.D. Dissertation, School of Civil and Environmental Engineering, Cornell University, Ithaca, N.Y.
- Wells, S. A. 1990b. "Determination of Sludge Properties for Modeling Compressible Cake Filtration From Specific Resistance Tests," Proceedings ASCE National Conference on Environmental Engineering, ed. by C. O'Melia, 125.
- Wells, S. A. and J. H. Plaskett. 1991. "Modeling Compressible Cake Filtration With Uncertainty," presented at conference Separation Problems and the Environment co-sponsored by U.S. Environmental Protection Agency and Georgia Institute of Technology, Oct. 20-23, 1991.
- Willis, M. S. 1983. "A Multiphase Theory of Filtration," in Progress in Filtration and Separation, ed. by R. J. Wakeman, Elsevier Scientific, New York, 1-56.

APPENDIX A

MODIFIED SLUDGE DEWATERING MODEL COMPUTER CODE

```

*****C
C COMPRESSIBLE CAKE FILTRATION MODEL WITH CONSTANT GRID SPACING
C ...cake.FOR.....
C SCOTT WELLS
C JULY 1987...DECEMBER 1987
C HOLLISTER HALL SCHOOL OF CIVIL AND ENVIRONMENTAL ENGINEERING
C CORNELL UNIVERSITY
C ITHACA, NEW YORK 14853
C MODIFIED 1991: PORTLAND STATE UNIVERSITY-PORTLAND, OREGON
*****C
C POROSITY OR CONCENTRATION OF SOLIDS (IF DENSITY OF SOLIDS ARE KNOWN)
C ARE CALCULATED AS A FUNCTION OF TIME AND SPACE ABOVE THE FILTRATION
C MEDIA WHEN THE FOLLOWING INPUT DATA IS AVAILABLE:
C     TEMPERATURE OF SUSPENSION
C     AREA OF FILTRATION CELL
C     COEFFICIENT OF COMPRESSIBILITY, MV AS A
C     F(STRESS,TIME,POROSITY)
C     TERMINAL POROSITY AS A F(TIME)
C     INITIAL POROSITY OF THE SUSPENSION
C     APPLIED PRESSURE
*****C
C NUMERICAL SCHEME IS EXPLICIT UPWIND FTCS FINITE DIFFERENCE
C ALGORITHM WITH STABILITY CRITERION BASED ON SEMI-EMPIRICAL ANALYSIS
C WHICH REDUCES TO THE VON NUEMANN CONDITIONS FOR SIMPLE CASES
*****C
C COMPUTATIONAL SWITCHES: IDIAG(1-8) FLAG IS ON IF IDIAG(I)<>0
C IDIAG(1):NOT USED
C IDIAG(2):INCLUDE ARTIFICIAL VISCOSITY IN DIFFUSIVE TERM
C IDIAG(3):WRITE EACH TERM OF GOVERNING EQ. TO FILE
C IDIAG(4):NOT USED
C IDIAG(5):INCLUDE ARTIFICIAL VISCOSITY IN CALCULATION OF V0
C IDIAG(6):WRITE POROSITY PROFILES AT 30 SEC. INTERVALS
C IDIAG(7):WRITE VALUES ASSOCIATED WITH THE CALCULATION OF V0
C IDIAG(8):NOT USED
*****C
****
IMPLICIT DOUBLE PRECISION (A-H,O-Z)
external etime
COMMON/DOMN/ DIST(200),EET(200)
COMMON/PERMC/ PERMZ(200)
COMMON/PRIM/ U(200),US(200),P(200),SIGMA(200)
COMMON/PAR/ V0,ET,avisc
COMMON/POR/ DT,DZ,AREA,DVIS,K,EE(200),S0,TIM,TEMP,
1     EO,PAPP,RM,DL,NFIL,NSOL,FACT,EYLD
COMMON/VOLUME/ V(50),T1(50),NVOL
COMMON/PORTERM/ ETERM(50),T2(50),NETERM
COMMON/OUT/ TIML,NPR,NITL,INPOR
COMMON/STAT/ NSD,INTV
COMMON/DIAG/ IDIAG(8),IPLLOT,IDT,A,SYLD,A2
COMMON/PERMCAL/ PKA1,PKB1,NKC,PKA2,PKB2,EKP
COMMON/AVCAL/ AVA,AVB
COMMON/TERMS/DF1(12),CV1(12),CV2(12),M
real tarray(2)
character divider(80)
CHARACTER*4 FNAME
CHARACTER*8 INFILE
CHARACTER*11 OUT1,OUT2,OUT3,OUT4,OUT5,OUT6,OUT7,OUT8,OUT9,
1     OUT10
CHARACTER*9 WHY

```

```

OPEN(8,FILE='FAMILY')
OPEN(9,FILE='IRUNS')
READ(8,'(a4)')FNAME
READ(9,*)IRUNS
CLOSE(9)
INFILE=FNAME//' .dat'
OUT1=FNAME//'out1'
OUT2=FNAME//'out2'
OUT3=FNAME//'out3'
OUT4=FNAME//'out4'
OUT5=FNAME//'out5'
OUT6=FNAME//'out6'
OUT7=FNAME//'out7'
OUT8=FNAME//'out8'
OUT9=FNAME//'out9'
OUT10=FNAME//'out0'
OPEN(10,FILE=INFILE)
OPEN(11,FILE=OUT1,STATUS='NEW')
OPEN(12,FILE=OUT2,STATUS='NEW')
OPEN(13,FILE=OUT3,STATUS='NEW')
OPEN(14,FILE=OUT4,STATUS='NEW')
OPEN(15,FILE=OUT5,STATUS='NEW')
OPEN(16,FILE=OUT6,STATUS='NEW')
OPEN(17,FILE=OUT7,STATUS='NEW')
OPEN(18,FILE=OUT8,STATUS='NEW')
OPEN(19,FILE=OUT9,STATUS='NEW')
OPEN(20,FILE=OUT10,STATUS='NEW')
C
C READ IN INITIAL DATA
C
CALL INIT(E1)
  IF (IDIAG(3).NE.0)OPEN(5,FILE='wave.dat',STATUS='NEW')
  IF (IDIAG(7).EQ.1)OPEN(21,FILE='grad.dat',STATUS='NEW')
TIM=0.0
SUMQ=0.0
NSTOP=0
VOLCUM=0.0
DLL=DL
DL2=DL
NIT=0
  N30=1
  NP30=1
EE(1)=E1
  DIST(1)=0.0
NHOLD=0
  NFILT=1
  RNS=1
  TVAL=1.
C
C NFILT: COUNTER INDICATING END OF FILTRATION PERIOD
C NP30: COUNTER INVOLVED IN PRINTING OUT OUTPUT EVERY 30 S
C NHOLD: COUNTER INVOLVED IN HOLDING BC AT K+1 DURING WATER FILTRATION
C DL2:DOMAIN DIST(CM) CALCULATED FROM FILTRATE LOST
C VOLCUM:CUMULATIVE VOLUME OF FILTRATE(CM**3) BASED ON VO*ET*DT
C NIT:TIME STEP COUNTER
C SUMQ:FILTRATE VOLUME DURING BC HOLD CONDITION
C
  IF(INPOR.NE.1)GO TO 65
  DZ=DIST(K+1)-DIST(K)
  DIST(K+2)=DIST(K+1)+DZ
  DIST(K+3)=DIST(K+2)+DZ
C REDO DOMAIN IF NO SOLIDS IN CELLS DUE TO SEDIMENTATION

```

```

        DO 64 J=1,K+1
64      IF(EE(J).EQ.1.0)GO TO 63
C      DVOL IS THE TOTAL VOLUME OF WATER ABOVE THE CAKE AFTER CAKE FORMATION
PERIOD
63      DVOL=AREA*(K-J+2)*DZ
        K=J-2
        DL=DIST(K+1)
        DLL=DL
        DL2=DL
        GO TO 1

C
65      DZ=DL/REAL(K)
C
        DO 4381 J=1,K+3
4381    DIST(J)=REAL(J-1)*DZ
C
1      AV=AVV(EE(1))
        GRAD=(EE(2)-EE(1))/(DIST(2)-DIST(1))
        gr1=grad
        DZ1=DIST(2)-DIST(1)
        DZ2=DIST(3)-DIST(2)
        DZ3=DZ1+DZ2
        GRAD1=(-EE(1)*(DZ3/DZ1-DZ1/DZ3)+EE(2)*(DZ3/DZ1)-EE(3)*(DZ1/DZ3))
1      /DZ2
        grad2=(ee(3)-ee(2))/(dist(3)-dist(2))

C
        if(grad1.gt.0.0)grad=grad1
        avisc=0.0
        gr=grad

C
        V0=GRAD*PERM(EE(1))/(DVIS*EE(1)*AV)
        if(idiag(7).eq.1)write(21,28)tim,gr,grad1,grad2,v0,volcum
1      avisc
        if(idiag(5).eq.1)v0=v0-avisc
        RM = PAPP/(V0*EE(1)*DVIS)
        VL=V0*EE(1)

C
        BETA=(1.-E0)*PERM(E0)/(DVIS*AVV(E0))
        DT1=FACT*(DZ**2)/(2.*BETA)
        DT2=FACT*2.*BETA/(EE(1)*V0)**2
        DT=MIN(DT1,DT2)
        ddt=dt
        IF(DT.LT.0.001)NOUT=2000
        IF(DT.GE.0.001.AND.DT.LT.0.01)NOUT=700
        IF(DT.GE.0.01.AND.DT.LT.0.1)NOUT=90
        IF(DT.GE.0.1)NOUT=8

C
C      COMPUTATION OF ALPHA1
C
        ALPHA1=(1.-EE(1))*EE(1)/(DL*GRAD)

C
C      PRINT INITIAL DATA
C
        IF(IRUNS.EQ.1)THEN
            WRITE(19,541)
            WRITE(19,542)
            WRITE(19,543)TEMP,E0,PAPP/10000,SYLD,DL,AREA,K,
1      dvol,DVIS,TIML
            do 57 kj=1,80
                divider(kj)='_ '
57      continue
            WRITE(19,*)(divider(jj),jj=1,80)

```

```

        WRITE(19,*)
        WRITE(19,551)
        WRITE(19,552)
        WRITE(19,553)
        WRITE(19,554)
        WRITE(19,*)
    ENDIF
CALL SMASS(XMASS)
    IF((IRUNS.EQ.1).AND.(INPOR.EQ.1))THEN
        DO 6 I=1,K+1
6         WRITE(11,507)DIST(I),EE(I)
        ELSEIF((IRUNS.EQ.1).AND.(INPOR.EQ.0))THEN
            write(11,507)dist(1),ee(1)
            DO 8 I=2,K+1
8             WRITE(11,507)DIST(I),EO
        ENDIF
C
C  TIME STEPPING LOOP
C
100    CONTINUE
        NIT=NIT+1
        IF(ABS((EE(K+1)-EO)/EO).GT.0.005)NFILT=NFILT+1
        IF(NFILT.EQ.2)NHOLD=1
        IF(NHOLD.NE.1)GO TO 4200
        DVOL1=V0*EE(1)*AREA*DT
        IF(NFILT.EQ.2)THEN
            BBC=TIM
        ENDIF
        DVOL=DVOL-DVOL1
        IF(DVOL.LE.0.0)NHOLD=2
        IF(NHOLD.EQ.2)THEN
            EBC=TIM
        ENDIF
4200   CONTINUE
        IF(NFILT.EQ.2)THEN
            CFTIM=TIM
        ENDIF
        IF(EE(K+1).LE.EYLD)THEN
            ENDTIM=TIM
            WHY='CRACKING'
            GO TO 50
        ENDIF
C
C  COMPUTE VELOCITY AT Z=0
C
        AV=AVV(EE(1))
        GRAD=(EE(2)-EE(1))/(DIST(2)-DIST(1))
        gr1=grad
        grad2=(ee(3)-ee(2))/(dist(3)-dist(2))
        if(grad2.lt.0.0)grad2=0.0
        DZ1=DIST(2)-DIST(1)
        DZ2=DIST(3)-DIST(2)
        DZ3=DZ1+DZ2
        GRAD1=(-EE(1)*(DZ3/DZ1-DZ1/DZ3)+EE(2)*(DZ3/DZ1)-EE(3)*(DZ1/DZ3))
1         /DZ2
C
        IF((GRAD1.GT.0.0).and.(idiag(8).eq.1))GRAD=GRAD1
C
C  THIS IS NECESSARY IN CASES WHERE GRAD1 BECOMES NEGATIVE-PHYSICALLY
C  UNREALISTIC
        avisc=0.0
        v0=grad*perm(ee(1))/(dvis*ee(1)*av)

```

```

C
C COMPUTATION OF V0 USING ARTIFICIAL VISCOSITY
C
      u(1)=v0
      if(idiag(5).eq.1)then
1         vg1=(u(2)-(ee(1)*v0-ee(2)*u(2))*ee(2)/(1-ee(2)))*ee(2)
           /perm(ee(2))
1         vg2=(u(1)-(ee(1)*v0-ee(1)*u(1))*ee(1)/(1-ee(1)))*ee(1)
           /perm(ee(1))
1         vg3=(u(3)-(ee(1)*v0-ee(3)*u(3))*ee(3)/(1-ee(3)))*ee(3)
           /perm(ee(3))
      vgrad1=(vg1-vg2)/dz1
      vgrad2=(vg3-vg1)/dz2
      q1=((a2**2)*(dz1**2))*dvis*(vgrad1)
C      if(vgrad1.gt.0.0)q1=0.0
      q2=((a2**2)*(dz2**2))*dvis*(vgrad2)
C      if(vgrad2.gt.0.0)q2=0.0
      dpv=q2-q1
      avisc=(perm(ee(1))*(q2-q1))/(dz1*ee(1)*dvis)
C      avsc=avisc
C      dzq2=dist(4)-dist(3)
C      g1=(-3*u(1)+4*u(2)-u(3))/(2*dz2)
C      g2=(-3*u(2)+4*u(3)-u(4))/(2*dzq2)
C      dzq3=dist(5)-dist(4)
C      g3=(-3*u(3)+4*u(4)-u(5))/(2*dzq3)
C      q1=((a2**2)*(dz2**2))*g1*abs(g1)
C      if(g1.gt.0.0)q1=0.0
C      q2=((a2**2)*(dzq2**2))*g2*abs(g2)
C      if(g2.gt.0.0)q2=0.0
C      q3=((a2**2)*(dz2**2))*g3*abs(g3)
C      if(g3.gt.0.0)q3=0.0
C      avisc2=(perm(ee(1))*(-3*q1+4*q2-q3))/(2*dz2*ee(1)*dvis)
C      avc=avisc2
C      if((grad1.gt.0.0))then
C          avisc=avisc2
C      endif
      if(avisc.lt.0.0)avisc=0.0
      endif
      gr=grad
C
      v0=v0-avisc
      if((idiag(7).eq.1).and.(mod(nit,100).eq.0))write(21,28)
1         tim,gr,dpv,v0,volcum,avisc
      if(idiag(5).eq.1)v0=v0-avisc
C
C COMPUTE MAXIMUM ALLOWABLE TIME STEP BASED ON STABILITY RESTRICTIONS
C
      DO 4431 J=1,K+1
4431 PERMZ(J)=PERM(EE(J))
      IF(IDT.EQ.1)GO TO 21
      DT=1.0
C
      DO 22 J=1,K
      E5=(EE(J+1)+EE(J))*0.5
      PERM5=SQRT(PERMZ(J+1)*PERMZ(J))
      DZZ=DIST(J+1)-DIST(J)
      BETA=(1.-E5)*PERM5/(AVV(E5)*DVIS)
      DT1=FACT*(DZZ**2)/(2.*BETA)
          DT2=FACT*(2.*BETA)/(E0*V0)**2
          DT1=MIN(DT1,DT2)
      DT3=FACT*(DZ**2)/(EE(1)*V0*DZ + 2.*BETA)
      DT1=MIN(DT1,DT3)

```

```

22  DT=MIN(DT1,DT)
      DTT=DT
      T30=REAL(N30)*30.
      NP30=1
      IF((TIM+DT).GT.T30)DDT=T30-TIM
      IF((TIM+DT).GT.T30)N30=N30+1
      IF((TIM+DT).GT.T30)NP30=2
      DT=DTT
C
21  CONTINUE
      IF(DT.LE.0.0)THEN
        ENDTIM=TIM
        WHY='DT<=0.0'
        GOTO 50
      ENDIF
      IF((TIM+DT).GT.TIML)DT=TIML-TIM
      TIM=TIM+DT
C
      CALL INTER(TIM,1,ET)
      EE(1)=ET
C
      IF(DT.LT.0.0001)THEN
        ENDTIM=TIM
        WHY='DT<0.0001'
        GOTO 50
      ENDIF
      CALL SOLV1(NIT,NHOLD)
C
      IF(NFILT.EQ.2)DLFR=DL
      Q=VO*EE(1)*AREA
      VOLCUM=VOLCUM+Q*DT
C
      CALL SMASS(XMASS)
C
C THIS PRINTS DATA FOR PLOTTING AT SPECIFIED TIMES
C
      IF(RNS.EQ.1)THEN
        WRITE(12,*)'RUN = ',IRUNS
        WRITE(13,*)'RUN = ',IRUNS
        WRITE(14,*)'RUN = ',IRUNS
        WRITE(15,*)'RUN = ',IRUNS
        WRITE(16,*)'RUN = ',IRUNS
        WRITE(17,*)'RUN = ',IRUNS
        WRITE(18,*)'RUN = ',IRUNS
        RNS=0
      ENDIF
      IF(IPLOT.EQ.1)GO TO 300
      GO TO 301
300  IF(NP30.EQ.1)GO TO 301
      IF((TIM.GT.60.).AND.(TIM.LT.65.))THEN
        DO 302 J=1,K+1
1     IF(J.EQ.1)WRITE(12,507)DIST(J),EE(J),PERMZ(J),TIM,VOLCUM,DL
302  1     ,DL2
      IF(J.NE.1)WRITE(12,507)DIST(J),EE(J),PERMZ(J)
      ENDIF
      IF((TIM.GT.90.).AND.(TIM.LT.95.))THEN
        DO 312 J=1,K+1
1     IF(J.EQ.1)WRITE(13,507)DIST(J),EE(J),PERMZ(J),TIM,VOLCUM,DL
312  1     ,DL2
      IF(J.NE.1)WRITE(13,507)DIST(J),EE(J),PERMZ(J)
      ENDIF

```

```

IF ((TIM.GT.120.).AND.(TIM.LT.125.))THEN
DO 322 J=1,K+1
IF(J.EQ.1)WRITE(14,507)DIST(J),EE(J),PERMZ(J),TIM,VOLCUM,DL
1      ,DL2
322  IF(J.NE.1)WRITE(14,507)DIST(J),EE(J),PERMZ(J)
ENDIF
IF ((TIM.GT.180.).AND.(TIM.LT.185.))THEN
DO 332 J=1,K+1
IF(J.EQ.1)WRITE(15,507)DIST(J),EE(J),PERMZ(J),TIM,VOLCUM,DL
1      ,DL2
332  IF(J.NE.1)WRITE(15,507)DIST(J),EE(J),PERMZ(J)
ENDIF
IF ((TIM.GT.300.).AND.(TIM.LT.305.))THEN
DO 342 J=1,K+1
IF(J.EQ.1)WRITE(16,507)DIST(J),EE(J),PERMZ(J),TIM,VOLCUM,DL
1      ,DL2
342  IF(J.NE.1)WRITE(16,507)DIST(J),EE(J),PERMZ(J)
ENDIF
IF ((TIM.GT.500.).AND.(TIM.LT.505.))THEN
DO 352 J=1,K+1
IF(J.EQ.1)WRITE(17,507)DIST(J),EE(J),PERMZ(J),TIM,VOLCUM,DL
1      ,DL2
352  IF(J.NE.1)WRITE(17,507)DIST(J),EE(J),PERMZ(J)
ENDIF
if(idiag(6).ne.1)goto 301
ir=int(TIM)
if(mod(ir,1).eq.0)then
do 392 j=1,k+1
if(j.eq.1)write(11,507)dist(j),ee(j),u(j),tim,volcum,dl
1      ,dl2
392  if(j.ne.1)write(11,507)dist(j),ee(j),u(j)
endif
301  CONTINUE
C
      IF(NP30.EQ.2)WRITE(18,508)TIM,VOLCUM
IF((NIT.GE.NITL.OR.TIM.GE.TIML).AND.(TIM.GE.90.))THEN
      ENDTIM=TIM
      WHY='NITL/TIML'
      GO TO 200
ENDIF
IF((VOLCUM.EQ.VCPREV).AND.(TIM.GT.90))THEN
      ENDTIM=TIM
      WHY='VC=CONST'
      GOTO 200
ENDIF
VCPREV=VOLCUM
IF((NIT/NPR)*NPR.NE.NIT)GO TO 150
C
150  CONTINUE
GO TO 100
200  CONTINUE
C
C  PRINT FINAL SOLUTION
C
      GO TO 51
50  CONTINUE
51  CONTINUE
xp=0.6
RAT=PERM(xp)/AVV(xp)
if(iruns.eq.1)then
write(20,570)
write(20,572)

```

```

        write(20,*)
    endif
    call etime(tarray)
    eta=tarray(1)
    WRITE(19,555)IRUNS,AVA,AVB,PKA1,PKB1,RAT,eta,CFTIM,EBC,ENDTIM,
1    WHY
    call etime(tarray)
    write(20,571)iruns,nit,tarray(1),tarray(2),volcum,ddt,et,rm
    IRUNS=IRUNS+1
    OPEN(9,FILE='IRUNS')
    WRITE(9,*)IRUNS
STOP
C
C  FORMAT STATEMENTS
C
28    format(1x,7e11.3)
507  FORMAT(1X,F10.5,4X,F7.4,4X,E10.4,4(1X,F10.4))
508  FORMAT(1X,F10.3,5X,E12.4)
509  FORMAT(1X,'END OF CAKE FORMATION PERIOD AT NIT:',I7,
1    2X,'AND AT TIME(S):',F10.4)
510  FORMAT(1X,'END OF RUN DUE TO NITL/TIML EXCEEDED AT',1X,
1    F8.2,'S')
511  FORMAT(1X,'END OF RUN DUE TO CRACKING, EE(K+1).LE.EYLD',
1    1X,'AT',1X,F8.2,'S')
512  FORMAT(1X,'DVOL=',F12.5,'ml')
513  FORMAT(1X,'END OF HOLDING BC AT TIM=',F10.3,'S')
514  FORMAT(1X,'AT BEGINNING OF BC HOLD: '/
1    1X,'TIM:',F10.3,2X,'PKZB:',E14.4,2X,'DVOL1:',E12.4,2X,
1    'DVOL:',E12.4,2X,'DT:',F10.5)
541  FORMAT(1X,'TEMP',4X,'E0',5X,'PAPP',4X,'SYLD',3X,'DOMAIN',
1    3X,'AREA',3X,'VERT.',3X,'DVOL',3X,'MED.RES',4X,'TIML')
542  FORMAT(2X,'(C)',10X,'(kPa)',4X,'(Pa)',4X,'(CM)',3X,
1    '(CM^2)',2X,'STEPS',3X,'(ml)',3X,'(CM^-1)',4X,'(S)')
543  FORMAT(1X,F4.1,2X,F5.4,2X,F6.2,2X,E7.2,2X,F6.3,3X,F5.2,
1    1X,I4,3X,F6.3,2X,E9.3,3X,F4.0)
551  FORMAT(1X,'RUN',4X,'AVA',4X,'AVB',3X,'PKA1',3X,'PKB1',3X,
1    'k/mv',4X,'CPU',4X,'CAKE',4X,'END',4X,'END',5X,'DUE TO')
552  FORMAT(34X,'(E=.6)',3X,'TIME',3X,'FORM.',4X,'BC',5X,'OF')
553  FORMAT(50X,'TIME',3X,'HOLD',4X,'RUN')
554  FORMAT(43X,'(S)',5X,'(S)',4X,'(S)',4X,'(S)')
555  FORMAT(1X,I3,1X,E8.2,1X,F4.1,1X,E8.2,1X,F4.1,1X,E7.2,2X,
1    F6.2,1X,F6.2,1X,F6.2,1X,F6.2,2X,A9)
570  format(1x,'RUN',5x,'NIT',4x,'CPU TIME',3x,'SYS TIME',
1    4x,'VOLCUM',7x,'DT',8x,'ETERM',5x,'MED.RES.')
571  format(1x,i3,1x,i8,1x,f10.2,1x,f9.2,2x,f9.3,4x,e10.4,
1    1x,f8.4,3x,e9.3)
572  format(18x,'(SEC)',6x,'(SEC)',5x,'(CM^3)',6x,'(SEC)',16x,
1    '(CM^-1)')
900  FORMAT(1X,'DT:',E13.5,2X,'NOUT:',I5)
END
C*****
SUBROUTINE SOLV1(NIT,NHOLD)
C*****
C
C  SOLV1 SOLVES THE EXPLICIT FINITE DIFFERENCE EQUATIONS FOR POROSITY
C  AS A FUNCTION OF TIME AND SPACE USING THE UPWIND FTCS
C  EQUATIONS WHICH ARE THIRD ORDER ACCURATE IN DZ AND FIRST ORDER IN DT
C  WHEN GRID SPACING IS CONSTANT
    IMPLICIT DOUBLE PRECISION (A-H,O-Z)
    DIMENSION UT(200)
    COMMON/OUT/ TIML,NPR,NITL,INPOR
    COMMON/PAR/ V0,ET,avisc

```

```

COMMON/PRIM/U(200),US(200),P(200),SIGMA(200)
COMMON/POR/ DT,DZ,AREA,DVIS,K,EE(200),SO,TIM,TEMP,
1      EO,PAPP,RM,DL,NFIL,NSOL,FACT,EYLD
COMMON/DIAG/ IDIAG(8),IPLOT,IDT,A,crap,a2
COMMON/DOMN/ DIST(200),EET(200)
COMMON/PERMC/ PERMZ(200)
COMMON/AVCAL/AVA,AVB
COMMON/PERMCAL/PKA1,PKB1,NKC,PKA2,PKB2,EKP
COMMON/TERMS/ DF1(12),CV1(12),CV2(12),M,CV3(12),DF2(12)

C
VPREV=0.0
NNN=K
IF(NHOLD.EQ.1)NNN=K-1

EE(K+2)=EE(K)
u(k+2)=u(k)
ut(1)=v0

C
EE(NNN+3)=EE(NNN+1)
u(nnn+3)=u(nnn+1)
DO 10 I=2,NNN+1
DZP=DIST(I+1)-DIST(I)
DZM=DIST(I)-DIST(I-1)
DZB=0.5*(DZM+DZP)
EE1=(EE(I+1)+EE(I))/2.
EE2=(EE(I-1)+EE(I))/2.
EEU1=EE(I+1)-EE(I)
EEU2=EE(I+2)-EE(I+1)
AV1=AVA*EXP(AVB*EE1)
AV2=AVA*EXP(AVB*EE2)
IF(NKC.EQ.1)GO TO 11
IF(EE1.LE.EKP)PERM1=PKA1*EXP(PKB1*EE1)
IF(EE1.GT.EKP)PERM1=PKA2*EXP(PKB2*EE1)
GO TO 12
11 PERM1=EE1**3/(((1.-EE1)**2)*5.*S0**2)
12 CONTINUE
IF(NKC.EQ.1)GO TO 13
IF(EE2.LE.EKP)PERM2=PKA1*EXP(PKB1*EE2)
IF(EE2.GT.EKP)PERM2=PKA2*EXP(PKB2*EE2)
GO TO 14
13 PERM2=EE2**3/(((1.-EE2)**2)*5.*S0**2)
14 CONTINUE
BETA1=(1.-EE1)*PERM1/(AV1*DVIS)
BETA2=(1.-EE2)*PERM2/(AV2*DVIS)

C
C COMPUTATION OF DIFFUSIVE TERM USING ARTIFICIAL VISCOSITY
C
if(idiag(2).eq.1)then
dz2p=dist(i+2)-dist(i+1)
um=(u(i)+u(i-1))/2
up=(u(i)+u(i+1))/2
u32p=(u(i+2)+u(i+1))/2
dzi=((dist(i+1)+dist(i))/2)-((dist(i)+dist(i-1))/2)
u12p=(up-((ee(1)*v0-ee1*up)*ee1/(1-ee1)))*ee1/perm1
u12m=(um-((ee(1)*v0-ee2*um)*ee2/(1-ee2)))*ee2/perm2
dui=(u12p-u12m)/dzi
coef1=((a2**2)*(dzi**2))*dvis
dz3hp=((dist(i+2)+dist(i+1))/2)-((dist(i+1)+dist(i))/2)
ee3=(ee(i+2)+ee(i+1))/2
perm3=pkcal*exp(pkb1*ee3)
u32u=(u32p-((ee(1)*v0-ee3*u32p)*ee3/(1-ee3)))*ee3/perm3
if(i.gt.2)then

```

```

        ee4=(ee(i-2)+ee(i-1))/2
        u32m=(u(i-2)+u(i-1))/2
        dz2m=dist(i-2)
    endif
    if(i.eq.2)then
        ee4=ee(1)-(ee(2)-ee(1))
        u32m=(u(1)-(u(2)-u(1))+u(1))/2
        dz2m=dist(1)
    endif
    perm4=pk1*exp(pk2*ee4)
    u32d=(u32m-((ee(1)*v0-ee4*u32m)*ee4/(1-ee4)))*ee4
1    /perm4
    dulp=(u32u-u12p)/dz3hp
    dz3hm=((dist(i)+dist(i-1))/2)-((dist(i-1)+dz2m)/2)
    dulm=(u32d-u12m)/dz3hm
    coefp=((a2**2)*(dz3hp**2))*dvis
    coefm=((a2**2)*(dz3hm**2))*dvis
    qip1=coefp*dulp
    qi=coef1*dui
    qim1=coefm*dulm
    part1=beta1*av1*(qip1-qi)/dzp
    part2=beta2*av2*(qi-qim1)/dzm
    diff2=dt*(part1-part2)/dzi
    endif
C
    DIFF=(DT/(DZB))*((BETA1*(EE(I+1)-EE(I))/DZP)
1    -(BETA2*(EE(I)-EE(I-1))/DZM))
C
    CONV=(VO*DT*ET/DZP)*EEU1
    conv2=(avisc*dt*et*eeu1)/dzp
C
    IF ((IDIAG(3).NE.0).AND.(MOD(NIT,100).eq.0))THEN
        NODE=IDIAG(3)
        if(i.eq.node)then
            WRITE(5,89)TIM,(DIFF),(DIFF2),(CONV),
1            (CONV2)
        endif
    ENDIF
    if((idiag(2).eq.1))diff=diff-diff2
C
    EET(I)=EE(I) + DIFF + CONV
C
C COMPUTATION OF VELOCITY PROFILE
C
    if(idiag(2).eq.1)then
        eet(1)=ee(1)
        ee1=(eet(i-1)+eet(i))/2
        ee2=(ee(i)+ee(i-1))/2
        ee11=0.5*(ee(i-1)+eet(i-1))
        ee22=0.5*(ee(i)+eet(i))
        dzi=(dist(i+1)+dist(i))/2-(dist(i)+dist(i-1))/2
        ut(i)=((ee1-ee2)/dt)*dzi+ut(i-1)*ee11/ee22
    endif
10    CONTINUE
    IF(NHOLD.EQ.1)EET(K+1)=EE(K+1)
C
    EET(1)=EE(1)
C
    if(idiag(2).eq.1)u(k+2)=u(k)
    EET(K+2)=EET(K)
C COMPUTE NEW DOMAIN

```

```

do 970 i=2,nnn+1
970   u(i)=ut(i)
C
CALL SOLV2(NIT,NHOLD)
C
89   FORMAT(1X,F10.5,5(2X,E12.5))
RETURN

END
C*****
SUBROUTINE SOLV2(NIT,NHOLD)
C*****
C COMPUTES NEW DOMAIN AND
C SOLV2 SOLVES FOR LIQUID VELOCITY(CM/SEC)-U,
C SOLID VELOCITY(CM/SEC)-US,PORE WATER PRESSURE(GM/CM/SEC/SEC)-P,
C AND SOLID STRESS(GM/CM/SEC/SEC)-SIGMA,AND PERMEABILITY(CM*CM)
C
IMPLICIT DOUBLE PRECISION (A-H,O-Z)
DIMENSION E(200),D(200)
COMMON/PERMC/ PERMZ(200)
COMMON/DIAG/ IDIAG(8),IPLOT,IDT
COMMON/PRIM/ U(200),US(200),P(200),SIGMA(200)
COMMON/POR/ DT,DZ,AREA,DVIS,K,EE(200),SO,TIM,TEMP
1     ,EO,PAPP,RM,DL,NFIL,NSOL,FACT,EYLD
COMMON/PAR/ VO,ET
COMMON/DOMN/ DIST(200),EET(200)
C
C RECOMPUTE DOMAIN AND NEW DZ
C
C DIST:DIST FROM POROUS PLATE CORRESPONDING TO EE
C
C DURING NHOLD=1 NO DOMAIN HEIGHT CHANGE
C
IF(NHOLD.EQ.1)GO TO 678
DH=VO*DT*EE(1)
DL=DL-DH
KK=0
SK1=(DL/DZ)+0.5
SK2=SK1-INT(SK1)
IF (SK2 .NE. 0.0)KK=1
K=INT(SK1)+KK
DIST(K+1)=DL
DIST(K+2)=DL+(DIST(K+1)-DIST(K))
DIST(K+3)=DIST(K+2)+(DIST(K+1)-DIST(K))
C
C CREATE LARGER CELL AT UPPER BOUNDARY IF DZ GETS TOO SMALL
C
DZ1=DIST(K+1)-DIST(K)
DZ2=DZ/4.
IF(DZ1.LT.DZ2)GO TO 897
GO TO 898
897 CONTINUE
K=K-1
DIST(K+1)=DL
DIST(K+2)=DL+(DIST(K+1)-DIST(K))
DIST(K+3)=DIST(K+2)+(DIST(K+1)-DIST(K))
898 CONTINUE
CALL INTER(DIST(K+1),4,E1)
EET(K+1)=E1
CALL INTER(DIST(K+2),4,E1)
EET(K+2)=E1
C

```

```

C CONVERT TEMPORARY VARIABLES TO PERMANENT ONES
C
678 DO 3 J=1,K+2
3 EE(J)=EET(J)
C
IF(NSOL.EQ.0)GO TO 50
C
50 RETURN
END
C*****
SUBROUTINE INIT(ET)
C*****
C
C INIT READS IN INPUT DATA AND INITIALIZES POROSITY ARRAY
C
IMPLICIT DOUBLE PRECISION (A-H,O-Z)
COMMON/DOMN/ DIST(200),EET(200)
COMMON/PORTERM/ ETERM(50),T2(50),NETERM
COMMON/POR/ DT,DZ,AREA,DVIS,K,EE(200),SO,TIM,TEMP,
1 EO,PAPP,RM,DL,NFIL,NSOL,FACT,EYLD
COMMON/OUT/ TIML,NPR,NITL,INPOR
COMMON/VOLUME/ V(50),T1(50),NVOL
COMMON/DIAG/ IDIAG(8),IPLOT,IDT,A,SYLD,A2
COMMON/AVCAL/ AVA,AVB
COMMON/PERMCAL/ PKA1,PKB1,NKC,PKA2,PKB2,EKP
C
C DEFINITION OF VARIABLES:
C AREA:AREA OF FILTRATION CELL IN CM**2
C AVA,AVB:PARAMETERS USED IN AV CALCULATION IN AVV SUBROUTINE
C (NOTE:AVA IN UNITS OF GM/CM/S/S)
C EE:POROSITY AT EACH SPATIAL STEP FROM THE MEDIA
C EKP:POROSITY AT WHICH PKA1,PKB1 IS VALID IN PERM SUBROUTINE
C EO:INITIAL POROSITY OF THE SUSPENSION
C DL:LENGTH OF DOMAIN(CM)
C DT:TIME STEP IN SECONDS
C DVIS:DYNAMIC VISCOSITY IN GM/CM/SEC
C DZ:VERTICAL SPATIAL STEP IN CM
C FACT:SAFETY FACTOR FOR TIME STEP STABILITY ANALYSIS 1.0>FACT>0.0
C IDIAG:DIAGNOSTIC FLAGS THAT PRINT INTERMEDIATE CALCULATIONS
C IDT:IF IDT=1, TIME STEP IS SET TO DT IN INPUT DATA FILE
C IPLOT:IF EQUAL TO '1' AN OUTPUT FILE SUITABLE FOR PLOTTING IS MADE
C K:NUMBER OF SPATIAL STEPS IN VERTICAL DOMAIN
C NETERM:NUMBER OF TERMINAL POROSITY WITH TIME DATA
C NITL:TIME LIMIT IN TIME STEPS FOR RUN TO CEASE
C NKC:FLAG THAT USES CARMEN-KOZENY PERM IF NKC=1
C NPR:FULL OUTPUT PRINTED EVERY NPR TIME CYCLES
C NSOL:PARAMETER TO TURN ON(=1)OR OFF(=0)THE CALCULATION OF
VS,VL,P,SIGMA
C NVOL:NUMBER OF FILTRATE VOLUME WITH TIME DATA
C PAPP:APPLIED PRESSURE DIFFERENTIAL IN PASCALS(N/M**2)
C PKA,PKB:PARAMETERS USD IN PERM VS POROSITY CALCULATION IN PERM
C (NOTE:PKA IN UNITS OF CM*CM)
C SO:SPECIFIC SURFACE(1/CM)(USED IN PERM IF NKC=1)
C SYLD:EFFECTIVE STRESS AT WHICH SOLID PHASE YIELDS(PASCALS)
C TEMP:TEMPERATURE OF THE SUSPENSION IN DEGREES CELSIUS
C TIM:TIME SINCE BEHINNING OF THE RUN UPDATED IN MAIN SEC
C TIML:TIME LIMIT IN SEC TO STOP CALCULATIONS
C
READ(10,200)
READ(10,100)DL,AREA,TEMP,EO,PAPP,EKP,TIML,SYLD
READ(10,200)
READ(10,110)AVA,AVB,PKA1,PKB1,DT,FACT,PKA2,PKB2

```

```

C CALCULATE DVIS BASED ON TEMP
  CALL INTER(TEMP,3,DVIS)
C CONVERT TO CGS SYSTEM, PASCALS(KG/M/SEC/SEC) TO (GM/CM/SEC/SEC)
  PAPP=10.*PAPP
  SYLD=10.*SYLD
C COMPUTE POROSITY AT WHICH CRACKING BEGINS...FILTRATION CEASES
  EYLD=(-1./AVB)*LOG((EXP(-AVB*EO))+AVA*AVB*SYLD)
C IF INPOR=1,INITIAL POROSITY DISTRIBUTION IS GIVEN TO ALLOW FOR
SEDIMENTATION
  READ(10,200)
  READ(10,101)INPOR,NVOL,NETERM,K,NPR,NITL,NFIL,NKC
  READ(10,200)
  READ(10,104)IPLOT,NSOL,IDT,IETERM,A,DENS,A2
  READ(10,200)
  READ(10,101)IDIAG
C INITIALIZE POROSITY ARRAY
  DO 10 I=1,K+1
10   EE(I)=EO
  READ(10,200)
  IF(INPOR.NE.1)GO TO 11
  DO 13 J=2,K+1
13   READ(10,103)DIST(J),EE(J)
11   READ(10,200)
C
C TERMINAL POROSITY AS A FUNCTION OF TIME
  IF(IETERM.EQ.1)GO TO 14
  DO 12 J=1,NETERM
12   READ(10,103)ETERM(J),T2(J)
  ET=ETERM(1)
  GO TO 15
C COMPUTE ETERM FROM MV RELATIONSHIP
14   ET=(-1./AVB)*LOG((PAPP*AVA*AVB)+EXP(-AVB*EO))
  ETERM(1)=ET
15   CONTINUE
  RETURN
C
C FORMAT STATEMENTS
C
100  FORMAT(8F10.5)
101  FORMAT(8I10)
102  FORMAT(F10.5)
103  FORMAT(2F10.5)
104  FORMAT(4I10,4F10.5)
110  FORMAT(8E10.5)
200  FORMAT(1X)
201  FORMAT(1X,'SYLD:',E12.4,2X,'EYLD:',F7.3,1X,'ET:',F7.4)
  END
C*****
  SUBROUTINE INTER(T,N,Z)
C*****
C
C INTER INTERPOLATES INPUT DATA TO OBTAIN DYNAMIC VISCOSITY, LIQUID
C VELOCITY AT Z=0, TERMINAL POROSITY
C
C T..TIME IN SEC OR TEMP IN DEG C OR POROSITY
C N..SPECIFIC VARIABLE TO INTERPOLATE:1=TERM POR
C                                     2=LIQ VEL
C                                     3=DVIS
C                                     4=NEW POROSITY
C
C Z..RETURNED VARIABLE
  IMPLICIT DOUBLE PRECISION (A-H,O-Z)
  DIMENSION VIS(15),VTEMP(15),X(200),Y(200)

```

```

COMMON/DIAG/ IDIAG(8), IPLOT, IDT
COMMON/PORTERM/ ETERM(50), T2(50), NETERM
COMMON/POR/ DT, DZ, AREA, DVIS, K, EE(200), SO, TIM, TEMP,
1      EO, PAPP, RM, DL, NFIL, NSOL, FACT, EYLD
COMMON/VOLUME/ V(50), T1(50), NVOL
COMMON/DOMN/ DIST(200), EET(200)

C
C   THE FOLLOWING VISCOSITY(GM/CM/SEC)-TEMP(C) DATA IS FROM G. K.,
BACHELOR
C   AN INTRODUCTION TO FLUID DYNAMICS P.595,1967
C
      DATA VIS/1.781,1.514,1.304,1.137,1.002,0.891,0.798,
1      0.720,0.654,0.548,0.467,0.405,0.355,0.316,
1      0.283/
      DATA VTEMP/0.,5.,10.,15.,20.,25.,30.,35.,40.,50.,60.,
1      70.,80.,90.,100./
10     IF(N-2)10,20,30
      NY=NETERM
      DO 1 J=1,NY
      X(J)=T2(J)
1      Y(J)=ETERM(J)
      GO TO 5
20     NY=NVOL
      DO 2 J=1,NY
      X(J)=T1(J)
2      Y(J)=V(J)
      GO TO 5
30     IF(N.EQ.4)GO TO 40
      NY=15
      DO 3 J=1,NY
      X(J)=VTEMP(J)
3      Y(J)=VIS(J)*0.01
      GO TO 5
40     NY=K+1
      DO 4 J=1,NY
      Y(J)=EET(J)
4      X(J)=DIST(J)
5      CONTINUE
C
C   LINEAR INTERPOLATION
C
      IF(N.EQ.1.AND.NETERM.EQ.1)GO TO 204
      IF(T.LE.X(1))GO TO 206
      IF(T.GE.X(NY))GO TO 207
C
      DO 6 J=1,NY
      IF(T.EQ.X(J))GO TO 201
6      IF(T.LT.X(J))GO TO 50
C
50     CONTINUE
      DX=X(J-1)-X(J)
      DY=Y(J-1)-Y(J)
      SLOPE=DY/DX
      Z=Y(J-1) + SLOPE*(T-X(J-1))
      IF(N.EQ.2)Z=SLOPE/AREA
      GO TO 202
C
201    Z=Y(J)
C   AVERAGE SLOPE ON EITHER SIDE OF THE POINT
      IF(N.EQ.2)Z=((Y(J+1)-Y(J))/(X(J+1)-X(J))*0.5 +
1      (Y(J)-Y(J-1))/(X(J)-X(J-1))*0.5)/AREA
      GO TO 202

```

```

206  Z=Y(1)
      IF(N.EQ.2)Z=(Y(1)-Y(2))/(X(1)-X(2))/AREA
      GO TO 202
207  Z=Y(NY)
      IF(N.EQ.2)Z=(Y(NY-1)-Y(NY))/(X(NY-1)-X(NY))/AREA
      GO TO 202
204  Z=ETERM(1)
202  CONTINUE
      RETURN
C
C  FORMAT STATEMENTS
C
101  FORMAT(1X,'N=',I2,1X,'NY=',I2,1X,'T=',E10.3,1X,'Z=',E10.3,
1     1X,'SLOPE=',E10.3)
      END
C*****
      FUNCTION AVV(E)
C*****
      IMPLICIT DOUBLE PRECISION (A-H,O-Z)
      COMMON/AVCAL/ AVA,AVB
      AVV=AVA*EXP(AVB*E)
      RETURN
      END
C*****
      FUNCTION PERM(E)
C*****
      IMPLICIT DOUBLE PRECISION (A-H,O-Z)
      COMMON/PERMCAL/PKA1,PKB1,NKC,PKA2,PKB2,EKP
      COMMON/POR/ DT,DZ,AREA,DVIS,K,EE(200),SO,TIM,TEMP,
1     EO,PAPP,RM,DL,NFIL,NSOL,FACT,EYLD
      IF(NKC.EQ.1)GO TO 10
      IF(E.LE.EKP)PERM=PKA1*EXP(PKB1*E)
      IF(E.GT.EKP)PERM=PKA2*EXP(PKB2*E)
      GO TO 11
10   PERM=E**3/(((1.-E)**2)*5.*SO**2)
11   CONTINUE
      RETURN
      END
C*****
      SUBROUTINE SMASS(X)
C*****
C  COMPUTES THE MASS IN THE DOMAIN
C  [THE CALCULATION IS REALLY THE VOLUME OCCUPIED BY SOLIDS, TO OBTAIN
C  THE MASS MULTIPLY BY THE MASS DENSITY OF SOLIDS]
C
      IMPLICIT DOUBLE PRECISION (A-H,O-Z)
      COMMON/DOMN/ DIST(200),EET(200)
      COMMON/POR/ DT,DZ,AREA,DVIS,K,EE(200),SO,TIM,TEMP
1     ,EO,PAPP,RM,DL,NFIL,NSOL,FACT,EYLD
C
      X=0.0
      DO 10 J=1,K
      DZZ=DIST(J+1)-DIST(J)
      E5=(EE(J+1)+EE(J))*0.5
10   X=X+DZZ*(1.-E5)*AREA
      RETURN
      END
C*****

```

APPENDIX B

RESULTS OF DEWATERING MODEL SIMULATIONS

SUMMARY OF MODEL RESULTS FOR CHESS RUNS WITH 3 MINUTES OF GRAVITY SEDIMENTATION

RUN	TEMP. (C)	POR (z=0)	Papp (kPa)	Syd (kPa)	DOMAIN LENGTH (cm)	AREA VERT. (cm ²)	SLDG. VOL. (cm ³)	MEDIA RESIST. (SEC.)	TML	GAMMA	DELTA	ALPHA	BETA	k/mv	CAKE FORM TIME (SEC.)	BC HOLD (SEC.)	END OF RUN (SEC.)	DUE TO ITERA- TIONS	CPU TIME (SEC.)	SYS. TIME (SEC.)	CUM. FILT. (cm ³)	dt AT t=dt (z=0)	POR (z=0)		
KDM6	26.0	0.820	103	1700000	3.225	15.28	85	4.587	0.00872	900	2.0E-15	28.9	2.1E-15	15.0	0.00025	404.1	572.2	900.0	TML	46060	325.5	1.3	31.01	1.2E-02	0.5750
KDM8	26.0	0.820	172	1700000	3.125	15.28	83	7.845	0.00872	900	2.0E-15	28.9	2.1E-15	15.0	0.00025	301.2	513.5	771.0	CRACK	55760	344.7	0.9	33.98	9.1E-03	0.5572
KDM4	26.0	0.820	345	1700000	3.175	15.28	84	10.703	0.00872	900	2.0E-15	28.9	2.1E-15	15.0	0.00025	224.6	431.9	498.8	CRACK	52597	328.7	2.9	37.97	3.1E-03	0.5331
PMK9	24.0	0.820	517	1700000	2.925	15.28	59	14.525	0.00913	900	2.0E-15	28.9	2.1E-15	15.0	0.00025	185.1	384.7	421.5	CRACK	53110	298.9	3.1	36.87	5.3E-03	0.5182
PMK8	24.0	0.820	882	1700000	2.125	15.28	43	19.877	0.00913	900	2.0E-15	28.9	2.1E-15	15.0	0.00025	78.8	289.6	284.6	CRACK	41745	182.3	0.4	38.11	1.2E-03	0.5098
KDMK9	25.5	0.882	103	1700000	3.025	15.28	61	9.838	0.00882	900	2.0E-15	28.9	2.1E-15	15.0	0.00025	385.6	626.9	900.0	TML	47893	241.4	1.1	40.87	1.1E-02	0.5750
KDM2	26.0	0.882	172	1700000	3.325	15.28	67	9.174	0.00872	900	2.0E-15	28.9	2.1E-15	15.0	0.00025	334.8	527.7	676.8	CRACK	48638	308.4	3.3	43.69	1.0E-02	0.5572
PMK3	24.0	0.882	345	1700000	3.325	15.28	67	4.587	0.00913	900	2.0E-15	28.9	2.1E-15	15.0	0.00025	281.2	329.4	374.8	CRACK	37412	228.3	2.8	39.35	3.3E-03	0.5332
PMK4	24.0	0.882	517	1700000	3.325	15.28	67	4.587	0.00913	900	2.0E-15	28.9	2.1E-15	15.0	0.00025	212.8	287.4	296.1	CRACK	38942	226.1	2.5	39.52	6.6E-03	0.5182
PMK5	24.0	0.882	682	1700000	3.325	15.28	67	8.174	0.00913	900	2.0E-15	28.9	2.1E-15	15.0	0.00025	183.9	302.7	326.5	CRACK	44028	232.6	3.1	44.21	6.4E-03	0.5098
KDM7	26.0	0.847	103	1700000	1.775	15.28	36	22.171	0.00872	900	2.0E-15	28.9	2.1E-15	15.0	0.00025	131.4	382.3	517.0	d(FV)=0	27457	63.5	1.6	42.74	1.6E-02	0.5750
KDM5	26.0	0.847	172	1700000	1.775	15.28	36	29.816	0.00872	900	2.0E-15	28.9	2.1E-15	15.0	0.00025	101.4	358.4	382.5	CRACK	26778	63.0	1.8	50.56	1.1E-02	0.5572
KDM3B	26.0	0.847	345	1700000	1.775	15.28	36	29.816	0.00872	900	2.0E-15	28.9	2.1E-15	15.0	0.00025	71.5	247.6	255.2	CRACK	28455	60.7	1.4	50.84	2.2E-03	0.5332
PMK10	24.0	0.847	517	1700000	1.775	15.28	36	29.816	0.00913	900	2.0E-15	28.9	2.1E-15	15.0	0.00025	80.0	208.3	214.7	CRACK	27000	63.8	1.3	50.57	7.3E-03	0.5182
PMK7	24.0	0.847	682	1700000	1.775	15.28	36	29.818	0.00913	900	2.0E-15	28.9	2.1E-15	15.0	0.00025	51.6	179.9	184.2	CRACK	27482	67.1	1.2	50.57	9.4E-04	0.5098

SUMMARY OF MODEL RESULTS FOR CHESS RUNS WITHOUT GRAVITY SEDIMENTATION USING ARTIFICIAL VISCOSITY

RUN	TEMP.	FOR	Papp	Syld	DOMAIN	AREA	VERT.	MEDIA	TIML	GAMMA	DELTA	ALPHA	BETA	K/mv	CAKE	END	END	ITERA-	CPU	SYS.	CUM.	dt AT	POR	
(C)	(=0)	(kPa)	(kPa)	(kPa)	LENGTH	(cm ²)	STEP	RESIST.	(SEC.)	(cm ⁻¹)	(cm ⁻²)	(cm ⁻¹)	(cm ⁻¹)	(cm ⁻¹)	FORM	BC	OF	TO	TIME	TIME	FILT.	t=dt	(z=0)	
					(cm)			(cm ⁻¹)							TIME	HOLD	RUN		(SEC.)	(SEC.)	(cm ³)	(SEC.)	(SEC.)	
KDM6	26.0	0.620	103	1700000	3.675	15.26	71	0.00672	900	2.0E-15	26.9	2.1E-15	15.0	0.00025	520.7	520.7	900.0	TIML	12189	140.3	0.8	33.75	7.3E-03	0.5750
KDM6	26.0	0.620	172	1700000	3.675	15.26	73	0.00672	900	2.0E-15	26.9	2.1E-15	15.0	0.00025	267.5	267.5	563.8	CRACK	27611	314.5	1.4	34.25	3.7E-04	0.5572
KDM4	26.0	0.620	345	1700000	3.675	15.26	78	0.00672	900	2.0E-15	26.9	2.1E-15	15.0	0.00025	278.9	278.9	365.0	CRACK	11761	187.1	0.7	35.61	2.1E-02	0.5331
PMK9	24.0	0.620	517	1700000	3.675	15.26	78	0.00613	900	2.0E-15	26.9	2.1E-15	15.0	0.00025	232.0	232.0	307.6	CRACK	10667	173.6	0.7	36.59	4.8E-03	0.5192
PMK6	24.0	0.620	682	1700000	3.675	15.26	89	0.00613	900	2.0E-15	26.9	2.1E-15	15.0	0.00025	186.0	186.0	239.4	CRACK	8270	118.3	0.8	37.70	3.3E-04	0.5096
KDMK9	25.5	0.662	103	1700000	3.725	15.26	74	0.00662	900	2.0E-15	26.9	2.1E-15	15.0	0.00025	396.7	396.7	900.0	TIML	25634	253.8	1.0	41.16	1.4E-02	0.5750
KDM2	26.0	0.662	172	1700000	3.625	15.26	79	0.00672	900	2.0E-15	26.9	2.1E-15	15.0	0.00025	327.7	327.7	463.8	CRACK	13027	185.4	0.8	44.19	3.6E-02	0.5572
PMK3	24.0	0.662	345	1700000	3.625	15.26	73	0.00613	900	2.0E-15	26.9	2.1E-15	15.0	0.00025	239.8	239.8	265.8	CRACK	10370	160.0	0.7	39.63	7.6E-03	0.5332
PMK4	24.0	0.662	517	1700000	3.625	15.26	73	0.00613	900	2.0E-15	26.9	2.1E-15	15.0	0.00025	201.0	201.0	239.8	CRACK	10767	172.0	0.6	39.45	1.8E-02	0.5192
PMK5	24.0	0.662	682	1700000	3.625	15.26	78	0.00613	900	2.0E-15	26.9	2.1E-15	15.0	0.00025	187.1	187.1	218.4	CRACK	13052	235.5	0.8	43.67	1.6E-02	0.5096
KDM7	26.0	0.647	103	1700000	3.675	15.26	65	0.00672	900	2.0E-15	26.9	2.1E-15	15.0	0.00025	350.1	350.1	726.3	d(FV)=0	20089	262.5	0.9	48.48	8.4E-02	0.5750
KDM5	26.0	0.647	172	1700000	3.675	15.26	75	0.00672	900	2.0E-15	26.9	2.1E-15	15.0	0.00025	280.3	280.3	358.4	CRACK	19448	356.6	1.2	48.58	1.4E-02	0.5572
KDM3B	26.0	0.647	345	1700000	3.675	15.26	75	0.00672	900	2.0E-15	26.9	2.1E-15	15.0	0.00025	218.7	218.7	248.8	CRACK	21765	445.0	1.2	47.84	3.4E-02	0.5332
PMK10	24.0	0.647	517	1700000	3.675	15.26	75	0.00613	900	2.0E-15	26.9	2.1E-15	15.0	0.00025	168.5	168.5	195.6	CRACK	27163	562.5	1.1	49.21	9.0E-03	0.5192
PMK7	24.0	0.647	682	1700000	3.675	15.26	75	0.00613	900	2.0E-15	26.9	2.1E-15	15.0	0.00025	139.5	139.5	155.1	CRACK	35465	754.8	1.4	48.59	9.7E-03	0.5096

**SUMMARY OF MODEL RESULTS FOR CHESS RUNS WITH 3 MINUTES OF GRAVITY SEDIMENTATION
USING PARAMETERS CALCULATED FROM SPECIFIC RESISTANCE TESTS**

RUN	TEMP. (C)	POR ($\phi=0$)	Papp (MPa)	Syld (MPa)	DOMAIN LENGTH (cm)	AREA (cm ²)	VERT. STEP	SLOG. VOL (cm ³)	MEDIA RESIST. (SEC.) (cm ⁻¹)	TIML GAMMA	DELTA	ALPHA	BETA	K/mv	CAKE FORM TIME (SEC.)	END BC HOLD (SEC.)	END OF RUN (SEC.)	DUE TO TIML	ITERA- TIONS	CPU TIME (SEC.)	SYS. TIME (SEC.)	CUM. FILT. VOL (cm ³)	dtAT t=dt (SEC.)	POR (z=0)	
KDMK8	26.0	0.820	103	1700000	3.225	15.26	65	4.567	0.00872	900	2.8E-14	26.5	2.1E-14	12.3	0.00015	375.2	512.6	900.0	TIML	60989	369.0	1.3	33.26	3.8E-03	0.5311
KDM6	26.0	0.820	172	1700000	3.125	15.26	63	7.645	0.00872	900	2.8E-14	26.5	2.1E-14	12.3	0.00015	297.4	434.1	585.2	CRACK	55311	325.3	1.0	36.18	1.7E-03	0.5117
KDM4	26.0	0.820	345	1700000	3.175	15.26	64	10.703	0.00872	900	2.8E-14	26.5	2.1E-14	12.3	0.00015	165.6	340.0	378.6	CRACK	53890	310.9	0.8	40.35	4.6E-04	0.4855
PMK9	24.0	0.820	517	1700000	2.925	15.26	59	14.325	0.00913	900	2.8E-14	26.5	2.1E-14	12.3	0.00015	127.2	263.5	303.5	CRACK	53287	271.3	0.6	42.35	4.4E-03	0.4702
PMK6	24.0	0.820	862	1700000	2.125	15.26	43	19.877	0.00913	900	2.8E-14	26.5	2.1E-14	12.3	0.00015	1.3	2.0	2.0	CRACK	66645	181.9	1.0	52.12	1.2E-04	0.4597
KDMK9	25.5	0.862	103	1700000	3.025	15.26	61	9.958	0.00882	900	2.8E-14	26.5	2.1E-14	12.3	0.00015	308.1	512.3	900.0	TIML	63641	275.4	0.9	42.85	8.0E-03	0.5311
KDM2	26.0	0.862	172	1700000	3.325	15.26	67	8.174	0.00872	900	2.8E-14	26.5	2.1E-14	12.3	0.00015	265.2	413.5	502.6	CRACK	49170	298.7	0.9	45.84	5.8E-03	0.5117
PMK3	24.0	0.862	345	1700000	3.325	15.26	67	4.567	0.00913	900	2.8E-14	26.5	2.1E-14	12.3	0.00015	212.7	265.0	291.7	CRACK	38859	227.0	0.5	40.78	8.3E-04	0.4855
PMK4	24.0	0.862	517	1700000	3.325	15.26	67	4.567	0.00913	900	2.8E-14	26.5	2.1E-14	12.3	0.00015	166.3	206.0	225.3	CRACK	38548	225.9	0.3	41.02	4.5E-04	0.4702
PMK5	24.0	0.862	862	1700000	3.325	15.26	67	8.174	0.00913	900	2.8E-14	26.5	2.1E-14	12.3	0.00015	142.8	213.3	224.7	CRACK	45746	250.4	0.5	45.81	3.1E-03	0.4588
KDM7	26.0	0.847	103	1700000	1.775	15.26	36	22.171	0.00872	900	2.8E-14	26.5	2.1E-14	12.3	0.00015	114.6	324.3	416.1	d(FV)=0	27839	63.1	0.3	43.18	3.2E-03	0.5311
KDM9	26.0	0.847	172	1700000	1.775	15.26	36	26.816	0.00872	900	2.8E-14	26.5	2.1E-14	12.3	0.00015	63.9	282.5	310.4	CRACK	29266	68.2	0.3	50.81	2.3E-03	0.5117
KDM3B	26.0	0.847	345	1700000	1.775	15.26	36	26.816	0.00872	900	2.8E-14	26.5	2.1E-14	12.3	0.00015	58.2	163.0	187.6	CRACK	32296	68.3	0.2	51.18	1.1E-03	0.4855
PMK10	24.0	0.847	517	1700000	1.775	15.26	36	26.816	0.00913	900	2.8E-14	26.5	2.1E-14	12.3	0.00015	45.2	156.3	161.6	CRACK	36188	118.5	0.2	51.12	4.3E-03	0.4702
PMK7	24.0	0.847	862	1700000	1.775	15.26	36	26.816	0.00913	900	2.8E-14	26.5	2.1E-14	12.3	0.00015	36.9	130.5	133.0	CRACK	46750	166.6	0.4	51.17	1.3E-03	0.4598

SUMMARY OF MODEL RESULTS USING PARAMETER CALCULATED FROM SPECIFIC RESISTANCE TESTS FOR ANAEROBIC SLUDGE WITHOUT CONDITIONING AND NO PRIOR SEDIMENTATION

TEMP. (C)	POR (t=0)	P _{app} (kPa)	Sy/d	DOMAIN LENGTH (cm)	AREA (cm ²)	VERT. STEP (cm ⁻¹)	MEDIA RESIST. (SEC.)	TIML (SEC.)	GAMMA	DELTA	ALPHA	BETA	K/mv	CAKE FORM TIME (SEC.)	END BC HOLD (SEC.)	END OF RUN (SEC.)	DUE TO (NITL)	ITERATIONS	CPU TIME (SEC.)	SYS. TIME (SEC.)	CUM. FILT. VOL (cm ³)	dt/dt (t=dt)	POR (z=0)
25.5	0.982	89	2700000	1.00	34.21	74	0.00882	900	5.7E-61	128.1	7.8E-71	140.0	1.8E-07	0.0	0.0	563.8	dt<0.0	2	0.0	0.18	0.001	7.7E-03	0.9400
25.5	0.982	207	2700000	1.00	34.21	74	0.00882	900	5.7E-61	128.1	7.8E-71	140.0	1.8E-07	28.1	28.1	395.0	NITL	1060683	8163.0	9.62	19.33	3.8E-01	0.8315
25.5	0.982	345	2700000	1.00	34.21	74	0.00882	900	5.7E-61	128.1	7.8E-71	140.0	1.8E-07	26.0	26.0	307.6	NITL	1127709	9483.0	13.08	19.25	1.4E-01	0.9275
25.5	0.982	483	2700000	1.00	34.21	74	0.00882	900	5.7E-61	128.1	7.8E-71	140.0	1.8E-07	24.9	24.8	238.4	NITL	1011847	8712.9	9.03	19.20	2.1E-02	0.9249

SUMMARY OF MODEL RESULTS USING PARAMETER CALCULATED FROM SPECIFIC RESISTANCE TESTS FOR ANAEROBIC SLUDGE WITH CONDITIONING AND NO PRIOR SEDIMENTATION

25.5	0.984	89	1700000	3.00	34.21	74	0.00882	900	1.7E-25	48.2	3.2E-29	47.2	0.0001	437.0	437.0	900.0	TIML	3541	16.3	0.78	86.238	5.6E-02	0.8238
25.5	0.984	207	1700000	3.00	34.21	74	0.00882	900	1.7E-25	48.2	3.2E-29	47.2	0.0001	388.9	388.9	718.4	CRACK	2628	13.2	0.36	89.014	3.1E-02	0.8008
25.5	0.984	345	1700000	3.00	34.21	74	0.00882	900	1.7E-25	48.2	3.2E-29	47.2	0.0001	366.4	366.4	625.0	CRACK	2285	11.8	0.50	88.929	2.8E-01	0.7802
25.5	0.984	483	1700000	3.00	34.21	74	0.00882	900	1.7E-25	48.2	3.2E-29	47.2	0.0001	354.0	354.0	583.7	CRACK	2139	11.5	0.35	88.867	2.0E-01	0.7832

APPENDIX C

COMPUTER CODE FOR GENERATING MODEL PARAMETER VALUES

```

program parms
implicit double precision (a-h,o-z)
dimension cnum(1000),esl(1000),pl(1000),sigma(1000),ee(200)
dimension dist(200),id(10),por(1000)
real*8 k1,k2,ka,ksig,ksig2,kslope,kint,k2sig,k2sig2
character*4 fname
character*8 infile
character*80 c1,c2,c3,c4,c5,c6
open(7,file='parms')
open(8,file='IRUNS')
read(8,*)IRUNS
close(8)
open(9,file='line.dat',status='new')
C*****
C
C READ INPUT DATA FILE
C
open(8,file='FAMILY')
read(8,'(a4)')fname
infile=fname//'.dat'
open(11,file=infile)
read(11,400)c1
read(11,300)d1,area,temp,e0,papp,ekp,timl,syld
read(11,400)c2
read(11,300)av1,av2,pka,pkb,dt, fact ,pka2,pkb2
read(11,400)c3
read(11,320)inpor,nvol,neterm,ks,npr,nitl,nfil,nkc
read(11,400)c4
read(11,310)iplot,nsol,idt,ieterm,ap,dens,a2
read(11,400)c5
read(11,320)id(1),id(2),id(3),id(4),id(5),id(6),id(7),
1 id(8)
read(11,400)c6
do 10 i=1,ks+1
read(11,*,end=11)dist(i),ee(i)
10 continue
11 continue
C*****
C
C GENERATE RANDOM PAIR FOR DETERMINING EFFECTIVE STRESS
C INTERCEPT.
C
open(10,file='seed')
read(10,*)irnd
close(10)
call tworands(irnd,x1,x2)
open(20,file='mflag.rnd')
read(20,*)mflag
open(21,file='sig.rnd')
n=21
call dev(n,mflag,x1,x2,sig)
close(21)
open(10,file='seed')
write(10,*)irnd
close(10)
C*****
C
C GENERATE RANDOM PAIR FOR DETERMINING EFFECTIVE STRESS
C FAR BOUND.
C
call tworands(irnd,x1,x2)

```

```

open(24,file='sig2.rnd')
n=24
call dev(n,mflag,x1,x2,e2sig)
close(24)
C*****
C
C   CALCULATION OF SLOPE AND INTERCEPT FOR SCOTT'S BEST FIT
C   OF THE EFFECTIVE STRESS VS. POROSITY RELATIONSHIP.
C
    yeu=-3.37982
    yel=-11.9381
    yem=-7.65896
    y2eu=12.08
    y2el=3.536
    y2em=7.808
    e1=(yeu-yem)*sig/2.00+yem
    e2=(y2eu-y2em)*e2sig/2.00+y2em
    conc1=0.0
    conc2=1.4
    por1=1.0
    por2=1-conc2/dens
    b=(e2-e1)/(conc2-conc1)
    a=e1
    eslope=b
    eint=a
C*****
C
C   CALCULATION OF EFFECTIVE STRESS PARAMETERS
C
    c=exp(a)
    d=b*dens
    avb=d
    f=exp(d)
    g=f*c/100
    h=g*d
    ava=1e-4/h
C*****
C
C   GENERATE RANDOM PAIR FOR DETERMINING PERMEABILITY
C   INTERCEPT.
C
    call tworands(irnd,x1,x2)
    open(23,file='ksig.rnd')
    n=23
    call dev(n,mflag,x1,x2,ksig)
    close(23)
C*****
C
C   GENERATE RANDOM PAIR FOR DETERMINING PERMEABILITY
C   FAR BOUND.
C
    call tworands(irnd,x1,x2)
    open(25,file='ksig2.rnd')
    n=25
    call dev(n,mflag,x1,x2,k2sig)
    close(25)
C*****
C
C   CALCULATION OF SLOPE AND INTERCEPT FOR SCOTT'S PERMEABILITY
C   VS. POROSITY RELATIONSHIP.
C
    yku=-11.7332

```

```

ykl=-16.501
ykm=-14.192
yk2u=-19.775
yk2l=-24.514
yk2m=-22.219
k1=(yku-ykm)*ksig/2.00+ykm
k2=(yk2u-yk2m)*k2sig/2.00+yk2m
concl=0.0
conc2=1.3
por1=1.0
por2=1-conc2/dens
b=(k2-k1)/(conc2-concl)
a=k1
kslope=b
kint=a
C*****
C
C   CALCULATION OF PERMEABILITY PARAMETERS
C
      c=exp(a)
      d=b*dens
      pkb1=-d
      pka1=exp(d)*c/100
C*****
C
C   WRITE A RECORD OF PARAMETERS, SLOPES AND INTERCEPTS USED.
C
      if(IRUNS.eq.1)write(9,500)
      write(9,510) sig,ksig,eslope,eint,kslope,kint
500   format(5x,'ESDEV',7x,'KSDEV',7x,'ESLOPE',6x,'EINT',7x,
1     'KSLOPE',7x,'KINT')
510   format(6e12.3)
      close(20)
      open(20,file='mflag.rnd')
      if (mflag.eq.200)write(20,*)100
      if (mflag.eq.100)write(20,*)200
      close(20)
      write(7,550)ava,avb,pka1,pkb1
550   format(4e10.3)
C*****
C
C   WRITE INPUT DATA FILE WITH NEW PARAMETERS
C
      rewind 11
      read(11,400)
      read(11,400)
      read(11,400)
      write(11,300)ava,avb,pka1,pkb1,dt, fact, pka2, pkb2
      write(11,400)c3
      write(11,320)inpor,nvol,neterm,ks,npr,nit1,nfil,nkc
      write(11,400)c4
      write(11,310)iplot,nsol,idt,ieterm,ap,dens,a2
      write(11,400)c5
      write(11,320)id(1),id(2),id(3),id(4),id(5),id(6),id(7),
1     id(8)
      write(11,*)' INITPOR'
      do 12 i=1,ks+1
          write(11,305)dist(i),ee(i)
12     continue
300   format(8e10.5)
305   format(2f10.5)
310   format(4i10,4e10.5)

```

```

320  format(8i10)
400  format(a80)
end
C*****
SUBROUTINE TWORANDS(IRND,X1,X2)
implicit double precision (a-h,o-z)
m=2147483647
x1=(real(irand(irnd)))/m
20  irnd=int(x1*100000)
if(irnd.eq.0)goto 20
x2=(real(irand(irnd)))/m
30  irnd=int(x2*10000000)
if(irnd.eq.0)goto 30
return
end
C*****
SUBROUTINE DEV(N,MFLAG,X1,X2,sig)
implicit double precision (a-h,o-z)
rewind n
atest=log(x1)
if(mflag.eq.200)then
  read(n,*)sig
endif
if(mflag.eq.100)then
  sig=(((-2*atest)**.5)*cos(6.2831853*x2))
  sig2=(((-2*atest)**.5)*sin(6.2831853*x2))
  write(n,*)sig2
endif
return
end
C*****

```

APPENDIX D

UNIX SHELL PROCEDURE TO CONTROL MONTE CARLO SIMULATION

```
name=$1
echo $name>FAMILY
sims=$2
echo $sims>RUNS
seed=$3
echo $seed>seed
echo 1 > IRUNS
rm linop
rm parmop
echo > kdk9op1
echo > kdk9op2
echo > kdk9op3
echo > kdk9op4
echo > kdk9op5
echo > kdk9op6
echo > kdk9op7
echo > kdk9op8
echo > kdk9op9
echo > kdk9op10
echo > linop
echo > parmop
rm MVHST.DAT
rm MV.DAT
rm PRMHST.DAT
rm PRM.DAT
rm ESTHST.DAT
rm volstats.dat
rm vol13.dat
rm kdk9out*
while test $sims -gt 0
do echo $sims
  sims=`expr $sims - 1`
  rm parms
  rm line.dat
  slope3
  cat line.dat >> linop
  cat parms >> parmop
  ckadtm
  cat kdk9out1 >> kdk9op1
  cat kdk9out2 >> kdk9op2
  cat kdk9out3 >> kdk9op3
  cat kdk9out4 >> kdk9op4
  cat kdk9out5 >> kdk9op5
  cat kdk9out6 >> kdk9op6
  cat kdk9out7 >> kdk9op7
  cat kdk9out8 >> kdk9op8
  cat kdk9out9 >> kdk9op9
  cat kdk9out10 >> kdk9op10
  rm kdk9out*
done
```

APPENDIX E

MONTE CARLO SIMULATION RESULTS

SUMMARY OF MONTE CARLO SIMULATION RESULTS (500 MODEL RUNS) FOR
CONDITIONS OF CHESS RUN KDMK9 WITH PRIOR GRAVITY SEDIMENTATION

RUN	GAMMA	DELTA	ALPHA	BETA	k/mv	CAKE FORM TIME (sec.)	END BC HOLD (sec.)	END OF RUN (sec.)	END DUE TO	ITERA- TIONS	CPU TIME (sec.)	SYS. TIME (sec.)	CUM. FILT. VOL (cm ^ 3)	dt AT t=dt (sec.)	POR (Z=0)
1	2.7E-15	33.5	2.5E-17	20.6	4.5E-06	72.4	87.8	90.1	d(FV)=0	139347	647.9	7.3	56.0	6.8E-03	0.4825
2	2.7E-10	20.0	2.6E-16	16.5	3.9E-07	0.0	0.0	900.0	TIML	955	9.3	0.6	3.8	7.1E-01	0.2593
3	4.7E-11	21.3	3.2E-17	17.1	5.4E-08	0.0	0.0	900.0	TIML	1026	10.8	0.2	1.9	9.3E-01	0.3218
4	9.1E-13	25.1	6.6E-19	23.3	2.5E-07	0.0	0.0	900.0	TIML	900	9.4	0.5	1.9	0.0E+00	0.4248
5	3.9E-11	27.3	3.0E-15	15.0	4.8E-06	0.0	0.0	18.8	T>2HR	721859	7200.0	47.8	3.2	3.9E-04	0.2494
6	2.5E-08	17.3	1.9E-15	15.0	2.0E-06	0.0	0.0	900.0	TIML	25774	263.1	1.8	2.0	1.4E-01	0.0479
7	1.6E-14	30.8	5.6E-16	18.1	1.7E-05	15.5	18.9	90.0	d(FV)=0	183073	832.7	9.9	56.0	7.8E-03	0.4714
8	3.6E-14	30.7	8.1E-16	16.2	2.7E-06	47.3	57.3	90.5	d(FV)=0	725179	3327.5	37.9	56.0	5.5E-01	0.4447
9	2.4E-13	25.8	4.0E-15	13.9	1.3E-05	20.3	24.6	90.0	d(FV)=0	145534	665.6	7.6	56.0	1.8E-02	0.4630
10	2.4E-13	28.9	9.3E-15	13.5	3.9E-06	0.0	0.0	8.0	TIME>2H	827909	7200.0	54.1	22.9	7.9E-05	0.4106
11	1.0E-14	32.5	9.0E-16	15.7	3.6E-06	31.3	37.7	90.3	d(FV)=0	1466887	6621.2	77.8	56.0	7.0E-01	0.4577
12	2.5E-15	33.2	9.1E-14	10.8	5.4E-05	0.0	0.0	0.4	TIME>2H	761536	7200.0	47.9	7.8	3.6E-06	0.4910
13	1.2E-13	29.7	1.4E-15	15.0	1.7E-06	48.4	58.5	90.6	d(FV)=0	1299591	5913.5	68.9	56.0	4.4E-01	0.4205
14	5.7E-17	37.6	4.6E-14	9.8	4.4E-05	0.0	0.0	0.6	TIME>2H	726907	7200.0	47.8	3.9	3.6E-06	0.5295
15	6.2E-14	30.7	7.1E-17	18.8	8.9E-07	172.9	210.4	215.8	d(FV)=0	299928	1398.5	17.0	56.0	9.4E-04	0.4278
16	2.1E-16	39.2	5.0E-16	15.7	1.7E-06	0.0	0.0	3.4	TIME>2H	719932	7200.0	45.8	3.2	2.4E-05	0.4737
17	8.5E-12	24.6	1.2E-16	19.4	6.2E-07	0.0	0.0	900.0	TIML	1573	15.9	0.3	5.9	6.0E-02	0.3425
18	3.5E-13	29.7	4.7E-16	15.1	2.1E-07	0.0	0.0	88.1	TIME>2H	862669	7200.0	52.7	17.9	7.0E-05	0.3663
19	3.2E-12	23.7	1.5E-16	18.5	2.2E-06	0.0	0.0	900.0	TIML	1325	12.3	0.4	9.1	2.9E-01	0.4001
20	4.0E-13	30.7	4.9E-16	17.0	3.3E-07	0.0	0.0	57.1	TIME>2H	888594	7200.0	53.0	19.8	7.1E-06	0.3676
21	2.3E-12	25.0	4.6E-16	15.7	7.5E-07	216.9	264.7	271.7	d(FV)=0	161815	769.0	8.6	56.0	7.4E-01	0.3892
22	3.3E-13	27.5	9.3E-17	18.6	1.3E-06	213.8	259.4	266.0	d(FV)=0	73140	346.0	3.9	56.0	1.5E-03	0.4205
23	4.0E-13	29.6	1.1E-13	10.1	2.2E-06	0.0	0.0	0.3	TIME>2H	707377	7200.0	46.5	1.4	2.3E-06	0.3819
24	5.4E-12	25.0	8.3E-17	17.9	2.1E-07	0.0	0.0	900.0	TIML	59766	353.9	3.4	38.9	6.1E-03	0.3552
25	4.3E-17	38.8	1.2E-14	13.6	7.5E-05	0.0	0.0	0.5	TIME>2H	756989	7200.0	49.0	6.9	3.7E-06	0.5206
26	6.9E-12	26.1	1.3E-14	12.7	6.0E-07	0.0	0.0	8.6	TIME>2H	769311	7200.0	51.0	8.8	1.2E-04	0.3285
27	1.6E-15	33.1	3.0E-17	18.9	3.8E-06	104.3	126.2	129.8	d(FV)=0	157011	724.3	8.0	56.0	6.4E-04	0.5052
28	1.4E-15	34.5	2.9E-17	20.4	4.3E-06	65.9	79.9	90.6	d(FV)=0	231873	1071.2	12.6	56.0	4.4E-01	0.4865
29	3.9E-11	24.4	3.4E-14	11.1	3.1E-07	0.0	0.0	4.3	TIME>2H	724392	7200.0	45.9	3.8	7.1E-05	0.2845
30	3.8E-11	22.0	4.4E-17	21.1	6.8E-07	0.0	0.0	900.0	TIML	907	9.4	0.2	4.2	6.5E-01	0.3216
31	3.1E-16	37.1	1.4E-15	15.4	1.0E-05	0.0	0.0	3.3	TIME>2H	789133	7200.0	50.1	10.7	2.9E-05	0.4923
32	1.7E-11	21.0	4.7E-15	13.2	2.5E-06	88.4	107.8	110.6	d(FV)=0	81094	389.8	4.1	56.0	2.3E-03	0.3768
33	5.6E-14	30.1	2.3E-14	13.1	1.5E-05	0.0	0.0	2.4	TIEM>2H	894034	7200.0	54.6	20.4	2.3E-05	0.4401
34	8.6E-15	33.8	1.9E-15	14.5	2.2E-06	0.0	0.0	5.6	TIME>2H	766575	7200.0	48.1	8.1	5.2E-05	0.4452
35	5.4E-16	33.8	6.2E-15	12.7	3.8E-05	8.5	10.1	90.2	d(FV)=0	1324625	5896.6	70.0	56.0	7.6E-01	0.5266

36	3.7E-14	31.5	1.9E-15	15.1	2.8E-06	0.0	0.0	14.1	TIME>2H	928926	7200.0	56.6	23.2	1.3E-04	0.4327
37	5.4E-15	34.4	1.9E-15	15.5	4.0E-06	0.0	0.0	4.2	TIME>2H	788450	7200.0	48.6	10.2	4.0E-05	0.4493
38	3.5E-14	30.6	1.2E-16	17.7	1.5E-06	117.4	142.6	146.6	d(FV)=0	309191	1430.1	16.8	56.0	3.3E-04	0.4490
39	3.5E-14	30.0	8.1E-16	15.1	2.2E-06	67.1	81.2	90.7	d(FV)=0	634000	2898.1	33.3	56.0	3.0E-01	0.4578
40	3.5E-12	28.5	7.0E-15	14.1	1.2E-06	0.0	0.0	26.5	TIME>2H	1067676	7200.0	64.0	32.3	2.8E-04	0.3485
41	2.6E-13	30.6	1.1E-16	18.3	4.9E-07	188.7	229.7	235.8	d(FV)=0	530632	2463.6	28.3	56.0	3.0E-04	0.3823
42	3.9E-15	32.2	3.1E-17	19.3	3.4E-06	110.3	133.5	137.3	d(FV)=0	122506	564.6	6.7	56.0	6.4E-04	0.4931
43	3.7E-12	23.6	1.0E-17	22.9	1.7E-06	0.0	0.0	900.0	TIML	903	9.0	0.4	6.2	9.0E-01	0.3909
44	3.6E-11	23.9	3.0E-15	15.2	4.5E-07	145.0	177.1	181.8	d(FV)=0	585113	2770.8	31.8	56.0	8.6E-02	0.2950
45	2.0E-10	17.9	1.7E-16	18.0	9.0E-07	0.0	0.0	900.0	TIML	802	9.3	0.3	4.6	5.2E-02	0.3116
46	1.6E-14	30.5	1.2E-17	20.6	2.0E-06	0.0	0.0	900.0	TIML	1857	18.5	0.4	7.3	1.8E-01	0.4753
47	2.0E-12	25.6	7.7E-16	16.4	1.4E-06	105.5	128.8	132.2	d(FV)=0	194347	918.7	10.6	56.0	7.7E-04	0.3815
48	1.7E-10	21.7	7.7E-17	20.5	2.3E-07	0.0	0.0	900.0	TIML	918	9.6	0.2	2.6	8.9E-01	0.2583
49	1.6E-13	28.5	1.5E-16	14.9	2.8E-07	429.8	521.4	532.5	d(FV)=0	615554	2838.5	32.7	56.0	7.0E-04	0.4319
50	6.7E-12	21.9	2.8E-13	8.5	1.3E-05	5.8	7.1	90.2	NITL	1094483	5029.1	59.7	56.0	6.2E-01	0.4012
51	3.0E-12	31.0	9.5E-14	10.6	1.6E-07	0.0	0.0	0.0	TIME>2H	697198	7200.0	44.6	0.1	4.1E-07	0.2991
52	9.9E-18	41.4	3.1E-15	13.4	1.6E-05	0.0	0.0	0.9	TIME>2H	720911	7200.0	48.8	3.0	5.6E-06	0.5220
53	5.4E-17	37.8	6.2E-19	23.5	2.1E-06	0.0	0.0	900.0	TIML	2604	26.7	0.4	5.9	5.5E-01	0.5282
54	1.7E-14	33.4	6.1E-15	13.7	2.7E-06	0.0	0.0	1.8	TIME>2H	726796	7200.0	49.7	4.6	1.6E-05	0.4299
55	2.8E-06	17.0	1.6E-15	15.7	2.7E-06	0.0	0.0	900.0	TIML	10068	103.0	0.8	1.5	5.5E-02	0.0428
56	5.0E-15	32.9	4.3E-16	18.6	1.7E-05	13.1	15.9	90.3	d(FV)=0	321569	1474.6	17.1	56.0	7.5E-01	0.4743
57	4.5E-14	29.6	5.7E-14	10.1	1.0E-05	0.0	0.0	1.7	TIME>2H	784132	7200.0	50.6	9.7	1.6E-05	0.4569
58	3.6E-13	24.9	4.6E-16	17.7	1.8E-05	0.0	0.0	900.0	TIML	7944	57.0	0.6	23.5	8.7E-02	0.4656
59	1.4E-16	38.6	1.1E-16	20.5	1.3E-05	13.5	16.2	90.5	NITL	1210964	5455.3	64.7	56.1	4.6E-01	0.4901
60	3.3E-13	26.4	3.4E-17	20.0	2.2E-06	0.0	0.0	900.0	TIML	1243	12.2	0.1	7.9	5.2E-02	0.4400
61	3.8E-12	21.9	2.8E-17	19.9	2.3E-06	0.0	0.0	900.0	TIML	808	8.5	0.5	7.1	3.7E-01	0.4288
62	2.9E-11	22.6	5.1E-14	10.8	1.5E-06	0.0	0.0	11.9	TIME>2H	921551	7200.0	55.3	22.4	1.6E-04	0.3225
63	4.0E-11	22.9	1.3E-14	12.7	7.0E-07	64.1	78.1	90.8	NITL	1240986	5776.6	63.9	56.0	2.4E-01	0.3042
64	1.5E-16	37.5	1.2E-14	12.6	2.5E-05	0.0	0.0	0.7	TIME>2H	739904	7200.0	47.7	4.9	5.1E-06	0.5050
65	1.8E-15	34.5	1.3E-15	15.0	7.0E-06	0.0	0.0	10.9	TIME>2H	944814	7200.0	57.2	23.8	9.2E-05	0.4851
66	1.6E-15	34.6	2.9E-16	16.2	2.6E-06	0.0	0.0	44.1	TIME>2H	1154243	7200.0	64.7	36.6	6.8E-06	0.4792
67	7.3E-14	30.7	7.8E-17	18.5	7.2E-07	188.8	229.3	235.0	d(FV)=0	378903	1757.4	21.3	56.0	4.0E-04	0.4222
68	8.8E-13	28.9	2.1E-14	13.0	1.7E-06	0.0	0.0	1.9	TIME>2H	738951	7200.0	48.2	5.5	2.2E-05	0.3656
69	7.3E-12	25.0	3.3E-16	16.7	3.1E-07	409.8	500.9	514.8	d(FV)=0	197103	937.9	11.1	56.0	4.7E-01	0.3426
70	6.1E-16	34.1	1.6E-14	15.6	3.9E-04	0.8	1.0	90.0	d(FV)=0	637302	2868.6	33.9	56.1	9.8E-01	0.5181
71	6.8E-13	27.9	8.0E-18	22.5	4.4E-07	0.0	0.0	900.0	TIML	1168	11.9	0.4	4.0	8.8E-02	0.3877
72	8.5E-16	29.8	4.9E-16	16.3	1.7E-04	606.2	0.0	900.0	TIML	27375	159.7	1.8	34.0	1.4E-02	0.5857
73	3.2E-10	18.6	1.3E-16	19.6	7.2E-07	0.0	0.0	900.0	TIML	900	9.3	0.4	3.7	0.0E+00	0.2729
74	3.5E-13	28.7	9.9E-16	16.2	1.6E-06	57.4	69.7	90.2	d(FV)=0	693265	3187.8	37.1	56.0	8.4E-01	0.3999
75	2.9E-12	23.3	1.4E-16	18.0	1.9E-06	0.0	0.0	900.0	TIML	1105	10.7	0.5	7.9	8.8E-02	0.4106
76	1.0E-13	28.8	2.7E-16	16.5	1.6E-06	109.0	132.6	136.5	d(FV)=0	275976	1281.8	14.8	56.0	5.2E-04	0.4414
77	2.9E-12	26.0	1.3E-16	18.3	4.2E-07	459.9	561.9	578.1	d(FV)=0	97295	467.9	5.3	55.9	3.3E-01	0.3637
78	9.7E-13	28.4	1.4E-14	11.5	5.5E-07	0.0	0.0	3.5	TIME>2H	727099	7200.0	45.7	3.6	3.7E-05	0.3686
79	3.2E-12	25.5	2.7E-16	16.8	4.7E-07	321.2	392.4	402.9	d(FV)=0	159704	758.3	8.3	56.0	2.4E-03	0.3681
80	1.5E-15	36.4	7.1E-18	21.5	6.0E-07	251.2	304.1	311.0	d(FV)=0	647137	2961.5	34.1	56.0	5.6E-04	0.4581

81	9.2E-13	27.8	1.6E-14	11.8	1.1E-06	0.0	0.0	4.5	TIME>2H	753741	7200.0	48.2	6.9	5.1E-05	0.3790
82	4.2E-10	20.3	1.7E-17	20.6	4.8E-08	0.0	0.0	900.0	TIML	900	9.2	0.3	0.8	0.0E+00	0.2339
83	1.1E-15	36.0	1.4E-14	13.4	1.6E-05	0.0	0.0	0.5	TIME>2H	731255	7200.0	45.5	4.3	4.0E-06	0.4715
84	9.5E-11	21.8	2.8E-16	17.9	3.0E-07	0.0	0.0	900.0	TIML	1438	14.6	0.5	4.2	8.1E-01	0.2825
85	1.3E-15	33.3	7.5E-17	19.8	1.7E-05	27.2	32.7	90.0	d(FV)=0	115349	516.7	6.2	56.0	6.8E-04	0.5086
86	8.2E-13	26.0	1.9E-17	19.6	4.9E-07	0.0	0.0	900.0	TIML	1233	12.6	0.4	4.0	3.9E-02	0.4125
87	7.3E-12	23.1	2.0E-18	21.8	1.3E-07	0.0	0.0	900.0	TIML	900	9.5	0.4	1.4	0.0E+00	0.3752
88	8.3E-11	23.3	2.7E-16	17.3	8.6E-08	0.0	0.0	900.0	TIML	79765	597.8	4.7	25.2	2.7E-04	0.2665
89	3.9E-09	19.7	1.9E-14	13.2	9.7E-08	0.0	0.0	99.5	TIME>2H	806942	7200.0	49.4	12.7	5.2E-05	0.1281
90	8.9E-13	27.1	3.5E-18	15.4	3.5E-07	269.9	328.4	336.1	d(FV)=0	565098	2621.3	31.3	56.0	7.3E-04	0.3908
91	7.0E-16	33.8	3.9E-15	13.6	3.1E-05	9.2	11.0	90.2	NITL	1153831	5170.0	60.5	56.0	8.4E-01	0.5194
92	6.6E-13	30.1	3.3E-18	23.3	8.2E-08	0.0	0.0	900.0	TIML	3343	33.3	0.3	4.8	7.8E-01	0.3584
93	1.1E-14	33.0	4.0E-17	19.1	8.5E-07	175.5	212.9	218.2	d(FV)=0	499227	2287.3	27.7	56.0	4.6E-04	0.4474
94	1.5E-09	17.4	3.7E-18	23.5	9.6E-08	0.0	0.0	900.0	TIML	900	9.7	0.1	0.2	0.0E+00	0.2095
95	2.3E-11	24.1	1.4E-15	15.9	4.4E-07	209.6	256.3	262.2	CRACKIN	323473	1535.8	17.4	56.0	7.2E-04	0.3096
96	1.2E-09	17.1	1.1E-15	15.5	3.4E-07	0.0	0.0	900.0	TIML	1038	10.3	0.3	3.9	9.8E-01	0.2248
97	5.9E-14	29.3	1.3E-14	11.8	8.1E-06	0.0	0.0	7.8	TIME>2H	929980	7200.0	56.0	22.8	6.9E-05	0.4521
98	8.9E-14	30.0	4.9E-15	13.0	2.0E-06	0.0	0.0	9.4	TIME>2H	819994	7200.0	51.1	13.7	9.5E-05	0.4263
99	1.6E-15	36.0	7.2E-16	13.3	5.8E-07	0.0	0.0	9.2	TIME>2H	725044	7200.0	46.5	3.3	6.6E-05	0.4627
100	8.0E-15	34.0	1.5E-15	15.1	2.2E-06	0.0	0.0	6.3	TIME>2H	778383	7200.0	49.3	9.1	6.0E-05	0.4441
101	2.2E-13	33.5	2.2E-16	18.2	9.9E-08	0.0	0.0	29.9	TIME>2H	739708	7200.0	47.4	5.4	3.6E-04	0.3517
102	5.6E-14	30.8	1.0E-13	7.1	1.3E-06	0.0	0.0	0.5	TIME>2H	706163	7200.0	43.1	1.0	3.4E-06	0.4329
103	1.3E-12	25.7	1.6E-17	19.1	2.5E-07	0.0	0.0	900.0	TIML	1346	13.9	0.3	3.1	5.0E-01	0.4016
104	8.8E-17	43.6	3.2E-15	15.1	1.7E-06	0.0	0.0	0.1	TIME>2H	698731	7200.0	41.5	0.2	3.5E-07	0.4495
105	1.1E-10	24.1	5.2E-17	20.5	5.4E-08	0.0	0.0	900.0	TIML	1517	15.6	0.5	2.3	4.1E-02	0.2447
106	1.4E-14	30.7	3.8E-16	15.8	3.6E-06	59.5	72.1	90.6	d(FV)=0	406830	1859.3	22.2	56.0	4.2E-01	0.4766
107	1.3E-11	21.9	4.3E-15	14.6	4.1E-06	62.8	76.1	90.1	d(FV)=0	63878	301.0	3.1	55.9	4.5E-03	0.3703
108	5.6E-13	29.5	1.3E-15	15.6	5.8E-07	0.0	0.0	33.7	TIME>2H	886658	7200.0	54.5	19.8	2.5E-05	0.3727
109	8.6E-15	31.4	8.7E-17	19.2	6.5E-06	51.6	62.5	63.8	CRACKIN	119289	553.3	6.4	56.0	5.1E-04	0.4799
110	6.2E-14	29.8	1.0E-16	17.7	1.1E-06	161.5	196.4	201.2	d(FV)=0	247618	1152.2	13.3	56.0	1.9E-04	0.4418
111	5.9E-12	23.9	1.2E-14	14.2	5.9E-06	19.1	23.3	90.0	d(FV)=0	301844	1402.6	16.5	56.0	8.1E-03	0.3666
112	4.9E-12	26.4	1.1E-15	14.8	2.2E-07	0.0	0.0	170.0	NITL	1001100	6342.4	57.2	36.2	6.3E-05	0.3380
113	1.4E-15	32.1	1.5E-13	10.4	2.4E-04	0.0	0.0	1.0	TIME>2H	1132065	7200.0	65.7	35.3	6.9E-06	0.5249
114	9.1E-14	31.1	1.0E-17	20.7	2.3E-07	730.9	890.8	900.0	TIML	186378	874.4	10.1	55.6	9.1E-04	0.4104
115	2.3E-17	38.2	4.5E-16	16.5	4.4E-05	10.9	13.0	90.1	d(FV)=0	967127	4316.8	50.5	56.0	8.6E-01	0.5448
116	2.3E-10	21.5	1.5E-18	24.6	4.4E-08	0.0	0.0	900.0	TIML	900	9.7	0.3	0.4	0.0E+00	0.2471
117	3.9E-13	28.3	3.5E-17	19.1	3.6E-07	563.6	687.3	706.0	d(FV)=0	116233	550.3	6.3	55.9	6.8E-03	0.4027
118	5.5E-09	15.3	5.4E-15	12.0	1.4E-07	0.0	0.0	900.0	TIML	4327	43.7	0.3	4.2	3.1E-01	0.1606
119	3.0E-11	24.2	1.2E-14	12.9	4.9E-07	0.0	0.0	24.4	TIME>2H	858772	7200.0	52.9	17.5	4.0E-04	0.2987
120	7.3E-15	35.5	5.1E-16	15.8	5.0E-07	0.0	0.0	8.0	TIME>2H	728454	7200.0	46.0	4.0	6.8E-05	0.4258
121	1.5E-15	34.2	2.6E-17	19.0	1.8E-06	140.9	170.6	175.1	d(FV)=0	352822	1618.8	18.9	56.0	5.3E-04	0.4888
122	3.4E-13	29.5	3.0E-15	12.3	3.0E-07	0.0	0.0	12.6	TIME>2H	738428	7200.0	47.7	5.2	1.3E-04	0.3898
123	5.1E-11	24.2	2.3E-14	13.3	6.3E-07	0.0	0.0	11.6	TIME>2H	813182	7200.0	48.3	12.9	2.2E-04	0.2749
124	1.9E-14	35.1	2.1E-17	20.4	1.6E-07	0.0	0.0	237.9	TIME>2H	995958	7200.0	58.9	27.6	7.5E-05	0.4034
125	5.3E-16	33.5	2.2E-13	9.9	3.0E-04	0.0	0.0	0.4	TIME>2H	870655	7200.0	54.9	17.7	3.6E-06	0.5317

126	8.6E-11	22.0	1.8E-16	19.7	5.9E-07	0.0	0.0	900.0	TIML	1002	10.2	0.4	4.9	5.7E-01	0.2950
127	1.3E-17	39.0	1.4E-16	15.8	9.5E-06	50.1	59.3	90.2	NITL	1499629	6631.5	77.7	56.1	8.1E-01	0.5479
128	1.9E-12	23.2	5.5E-15	13.9	1.1E-05	27.2	33.0	90.7	d(FV)=0	75700	356.0	3.6	56.0	2.8E-01	0.4297
129	3.4E-12	29.4	2.7E-15	13.5	5.7E-06	0.0	0.0	7.4	TIME>2H	709927	7200.0	47.2	1.6	9.3E-05	0.3119
130	6.0E-15	32.6	7.0E-17	18.6	2.8E-06	87.1	105.7	106.9	d(FV)=0	297341	1365.0	18.8	56.1	7.2E-05	0.4735
131	2.2E-14	33.2	3.0E-17	19.3	3.5E-07	299.5	363.1	371.0	d(FV)=0	786459	3594.9	41.1	56.0	6.5E-05	0.4256
132	9.1E-12	25.0	5.4E-17	19.7	2.5E-07	0.0	0.0	900.0	TIML	1654	17.0	0.4	3.9	1.2E-01	0.3348
133	3.7E-11	23.7	4.9E-15	13.2	2.3E-07	0.0	0.0	95.4	TIME>2H	994002	7200.0	57.8	27.9	8.3E-05	0.2949
134	1.3E-11	23.2	7.7E-17	19.5	6.4E-07	0.0	0.0	900.0	TIML	1042	10.5	0.5	4.9	1.2E-01	0.3489
135	7.8E-15	33.7	1.9E-16	17.4	1.3E-06	75.0	0.0	90.0	NITL	1484452	6747.5	80.0	55.0	4.3E-05	0.4483
136	7.2E-12	23.6	1.7E-14	10.8	1.1E-06	46.0	55.8	90.8	NITL	1523363	6987.9	82.3	56.0	1.6E-01	0.3675
137	1.7E-12	26.9	4.1E-16	16.0	3.5E-07	244.1	297.3	304.7	d(FV)=0	528896	2465.9	28.7	56.0	3.1E-04	0.3708
138	1.1E-15	37.5	2.5E-15	18.8	8.9E-06	0.0	0.0	0.9	TIME>2H	743155	7200.0	49.8	5.3	7.5E-06	0.4529
139	4.8E-13	29.1	1.6E-15	15.3	8.4E-07	0.0	0.0	38.1	TIME>2H	990683	7200.0	57.1	27.8	1.5E-05	0.3825
140	2.0E-14	27.9	6.4E-17	18.7	1.3E-05	0.0	0.0	900.0	TIML	4381	37.3	0.5	14.7	1.6E-01	0.5150
141	4.7E-14	30.2	3.7E-15	18.0	1.5E-05	8.7	10.6	90.8	d(FV)=0	629774	2692.5	31.1	56.0	2.4E-01	0.4444
142	1.0E-11	24.8	5.8E-16	16.6	4.2E-07	279.7	342.0	351.2	d(FV)=0	215722	1026.7	12.0	56.0	3.6E-04	0.3326
143	1.0E-14	29.2	1.4E-16	17.9	1.5E-05	0.0	0.0	900.0	TIML	6496	53.4	0.7	16.9	3.0E-02	0.5135
144	2.5E-13	28.1	8.9E-15	13.5	5.5E-06	15.0	18.1	90.5	NITL	1274311	5613.5	67.0	56.0	5.3E-01	0.4205
145	2.9E-12	26.1	2.3E-15	15.0	1.0E-06	71.7	87.2	90.1	d(FV)=0	728143	3374.3	37.4	56.0	9.1E-01	0.3621
146	2.6E-15	33.2	5.0E-15	12.7	8.4E-06	0.0	0.0	5.8	TIME>2H	842527	7200.0	51.8	15.4	5.1E-05	0.4683
147	2.5E-14	30.8	1.2E-15	16.4	8.1E-06	19.5	23.7	90.1	d(FV)=0	535166	2455.2	29.1	56.0	8.6E-01	0.4563
148	8.0E-15	34.5	4.1E-15	15.8	7.0E-06	0.0	0.0	1.6	TIME>2H	765580	7200.0	47.4	8.2	1.5E-05	0.4368
149	7.6E-14	28.6	2.1E-15	14.4	5.7E-06	28.5	34.5	90.2	d(FV)=0	482548	2209.9	25.1	56.0	8.5E-01	0.4553
150	6.5E-15	29.5	1.8E-16	16.4	7.5E-06	0.0	0.0	900.0	TIML	4786	43.5	0.7	12.5	8.5E-02	0.5150
151	3.1E-14	31.7	9.5E-16	16.1	2.8E-06	34.8	41.7	90.4	NITL	1488815	8727.1	74.1	56.0	6.0E-01	0.4355
152	2.4E-12	28.5	1.5E-15	15.2	2.0E-07	0.0	0.0	35.0	TIME>2H	794098	7200.0	50.1	10.9	3.1E-05	0.3354
153	1.1E-13	29.1	8.2E-15	12.7	4.1E-06	0.0	0.0	10.9	TIME>2H	964525	7200.0	57.9	25.7	9.8E-05	0.4343
154	5.6E-14	30.5	1.0E-16	18.9	1.7E-06	104.8	127.6	131.4	d(FV)=0	228376	1060.8	12.9	56.0	7.1E-04	0.4346
155	3.3E-15	34.5	2.1E-14	15.0	5.5E-05	0.0	0.0	0.5	TIME>2H	806228	7200.0	50.2	11.9	4.2E-06	0.4633
156	4.4E-12	24.5	2.5E-16	17.4	7.6E-07	0.0	0.0	900.0	TIML	3651	35.6	0.5	8.9	5.9E-01	0.3715
157	5.2E-16	30.8	1.1E-18	23.1	2.1E-05	0.0	0.0	900.0	TIML	3224	28.5	0.4	12.6	2.4E-01	0.5817
158	1.1E-12	26.9	3.1E-16	18.9	2.4E-06	98.1	119.4	122.2	CRACKIN	76564	363.6	4.5	56.0	1.7E-03	0.3868
159	9.7E-09	17.6	1.2E-15	15.0	2.4E-08	0.0	0.0	900.0	TIML	7769	79.3	1.0	2.3	2.0E-01	0.0984
160	8.3E-13	24.4	7.2E-14	11.4	4.7E-05	4.0	4.9	91.0	d(FV)=0	297184	1369.5	16.2	56.0	4.3E-02	0.4530
161	8.3E-14	30.8	4.2E-17	18.7	3.6E-07	351.9	428.0	437.9	d(FV)=0	400032	1856.8	21.5	56.0	7.7E-04	0.4170
162	8.1E-17	36.6	3.9E-14	12.0	1.8E-04	0.0	0.0	0.6	TIME>2H	823969	7200.0	51.7	13.4	4.8E-06	0.5357
163	2.2E-11	24.7	2.0E-15	14.5	2.0E-07	0.0	0.0	194.2	NITL	1001100	5865.6	54.6	40.4	1.5E-04	0.3039
164	2.2E-16	35.7	5.9E-17	18.4	8.2E-06	47.3	57.1	90.2	d(FV)=0	376590	1704.3	19.9	56.0	8.2E-01	0.5211
165	3.3E-14	31.6	1.4E-17	20.8	6.1E-07	345.3	420.3	431.2	d(FV)=0	154334	724.7	8.3	56.0	1.3E-03	0.4347
166	1.2E-11	25.2	1.1E-15	15.4	2.4E-07	247.7	302.2	309.8	d(FV)=0	756087	3524.6	39.5	56.0	1.4E-04	0.3194
167	1.4E-10	21.4	2.5E-15	14.9	3.7E-07	315.5	386.8	398.0	d(FV)=0	204630	995.3	11.5	55.9	2.0E-03	0.2706
168	9.3E-14	30.1	5.7E-17	18.6	6.0E-07	262.0	318.9	326.6	d(FV)=0	269416	1252.5	14.7	56.0	1.1E-03	0.4236
169	2.2E-14	30.9	2.3E-15	13.6	3.3E-06	0.0	0.0	24.4	TIME>2H	1094416	7200.0	62.6	33.5	1.9E-04	0.4586
170	1.3E-11	25.0	2.2E-16	17.2	1.6E-07	741.8	0.0	900.0	TIML	207696	1002.3	11.8	54.5	1.1E-03	0.3206

171	2.7E-14	33.1	2.8E-17	18.4	1.5E-07	0.0	0.0	462.9	NITL	1001100	5905.9	55.5	40.1	1.9E-04	0.4197
172	1.4E-12	27.2	1.1E-15	14.9	5.2E-07	125.5	0.0	151.7	NITL	1001100	4670.0	52.3	54.6	1.8E-04	0.3745
173	4.4E-11	25.3	1.7E-15	14.8	7.2E-08	0.0	0.0	123.8	TIME>2H	834958	7200.0	52.4	15.0	5.7E-05	0.2679
174	9.3E-14	30.9	8.0E-15	13.3	2.3E-06	0.0	0.0	3.3	TIME>2H	758418	7200.0	47.1	7.4	3.3E-05	0.4123
175	4.3E-14	31.1	2.7E-17	20.2	8.8E-07	235.0	286.1	293.4	d(FV)=0	162453	759.7	6.1	56.0	2.3E-03	0.4336
178	3.3E-15	33.5	5.2E-16	15.1	2.6E-06	0.0	0.0	41.8	TIME>2H	1130888	7200.0	64.0	35.7	2.7E-05	0.4778
177	4.4E-11	22.4	1.7E-15	14.1	2.6E-07	312.4	382.0	392.4	d(FV)=0	359943	1706.2	18.6	56.0	7.6E-01	0.3060
178	3.4E-13	30.6	4.8E-16	16.4	2.9E-07	0.0	0.0	55.4	TIME>2H	856926	7200.0	51.7	16.9	4.2E-05	0.3742
179	4.4E-14	32.2	7.7E-17	20.8	1.9E-06	79.3	96.6	99.0	d(FV)=0	284102	1321.8	14.6	56.0	4.8E-04	0.4171
180	3.4E-13	28.5	1.1E-16	16.7	2.6E-07	422.3	513.9	526.6	d(FV)=0	448756	2084.8	24.1	56.0	1.2E-03	0.4037
181	6.6E-12	21.4	2.8E-15	13.5	3.8E-06	0.0	0.0	900.0	TIML	4212	37.3	0.6	14.5	2.6E-02	0.4127
182	4.9E-12	26.0	3.8E-15	13.9	1.7E-07	0.0	0.0	12.9	TIME>2H	739596	7200.0	48.8	5.0	1.8E-04	0.3171
183	2.0E-14	33.1	3.1E-16	18.9	2.9E-06	34.4	41.6	90.4	d(FV)=0	900338	4125.1	45.1	56.0	8.1E-01	0.4285
184	1.2E-14	32.5	1.2E-17	21.6	1.6E-06	184.8	224.5	230.0	d(FV)=0	103570	484.8	5.6	56.0	1.3E-03	0.4543
185	6.6E-13	24.5	2.8E-15	16.4	3.2E-05	623.1	0.0	900.0	TIML	19582	106.2	1.1	37.3	1.6E-02	0.4485
186	1.6E-10	20.0	3.4E-16	17.7	5.3E-07	0.0	0.0	900.0	TIML	1008	10.0	0.2	4.7	2.7E-01	0.2848
187	1.6E-14	28.6	2.2E-16	17.9	2.3E-05	0.0	0.0	900.0	TIML	9523	71.2	0.9	21.8	9.0E-02	0.5093
188	6.0E-13	26.3	4.0E-14	11.8	1.1E-05	7.3	8.8	91.0	NITL	1246417	5698.9	63.9	56.0	1.9E-02	0.4187
189	1.3E-12	26.0	1.3E-16	18.4	1.0E-06	0.0	0.0	900.0	TIML	2857	28.3	0.3	8.6	5.6E-01	0.3951
190	2.2E-16	35.9	1.0E-14	13.1	5.6E-05	0.0	0.0	1.5	TIME>2H	846060	7200.0	53.8	15.9	1.3E-05	0.5192
191	3.0E-12	25.3	6.8E-15	14.6	3.5E-06	26.4	32.2	90.9	d(FV)=0	459319	2145.1	25.0	56.0	1.2E-01	0.3730
192	2.1E-15	33.8	2.4E-15	14.8	1.1E-05	0.0	0.0	8.1	TIME>2H	994287	7200.0	57.2	27.3	6.5E-05	0.4861
193	4.1E-15	31.4	5.7E-16	17.1	2.6E-05	14.6	17.7	90.0	d(FV)=0	167674	771.8	6.2	56.0	9.7E-01	0.5043
194	2.4E-14	31.5	5.7E-15	12.4	2.6E-06	0.0	0.0	5.6	TIME>2H	774244	7200.0	49.9	9.0	5.3E-05	0.4472
195	2.5E-13	27.3	7.3E-18	15.8	2.5E-06	70.3	85.6	90.1	d(FV)=0	242113	1125.0	13.0	56.0	4.3E-03	0.4339
196	6.5E-15	35.0	1.1E-15	17.5	4.8E-06	0.0	0.0	4.9	TIME>2H	826289	7200.0	50.7	14.3	4.8E-05	0.4369
197	1.8E-13	29.8	6.2E-15	13.1	1.4E-06	0.0	0.0	6.2	TIME>2H	772300	7200.0	47.9	8.9	6.6E-05	0.4051
198	7.9E-14	26.8	8.8E-14	6.9	7.1E-06	0.0	0.0	8.5	TIME>2H	879175	7200.0	55.3	18.9	7.4E-05	0.4864
199	5.2E-15	33.9	5.2E-13	8.7	2.7E-05	0.0	0.0	0.0	TIME>2H	704098	7200.0	47.1	1.0	2.5E-07	0.4574
200	8.7E-17	43.9	1.9E-16	17.7	3.3E-07	0.0	0.0	0.7	TIME>2H	698760	7200.0	44.3	0.4	4.2E-06	0.4406
201	3.2E-18	41.0	5.0E-17	19.0	2.8E-05	21.1	25.1	90.5	VC=COST	829437	3683.7	44.5	56.1	4.6E-01	0.5541
202	1.6E-12	26.3	1.5E-14	11.7	1.5E-06	0.0	0.0	10.9	TIME>2H	848946	7200.0	52.1	16.2	1.2E-04	0.3817
203	1.6E-11	24.3	5.5E-18	20.9	4.6E-08	0.0	0.0	900.0	TIML	905	9.6	0.3	1.5	6.9E-01	0.3223
204	1.3E-15	36.0	6.8E-16	14.8	1.6E-06	0.0	0.0	8.1	TIME>2H	751362	7200.0	46.1	6.6	6.8E-05	0.4681
205	6.6E-10	21.2	4.0E-16	17.4	6.3E-08	0.0	0.0	900.0	TIML	3425	34.4	0.4	3.2	1.6E-01	0.2001
206	2.2E-13	31.0	2.2E-15	14.7	5.8E-07	0.0	0.0	8.6	TIME>2H	751404	7200.0	47.6	6.7	9.5E-05	0.3830
207	4.6E-13	26.9	1.1E-16	16.7	5.2E-07	380.2	463.3	475.5	d(FV)=0	148902	700.8	8.8	56.0	4.6E-03	0.4190
208	2.7E-14	31.2	3.1E-17	18.1	4.2E-07	392.5	476.7	487.7	d(FV)=0	372199	1720.9	20.2	56.0	1.2E-03	0.4462
209	4.7E-12	28.0	2.8E-15	14.1	1.4E-07	0.0	0.0	17.6	ATIME>2	742787	7200.0	47.4	5.4	2.5E-04	0.3176
210	3.8E-11	25.8	4.2E-14	11.8	2.6E-07	0.0	0.0	1.5	TIME>2H	712128	7200.0	46.3	1.8	2.5E-05	0.2670
211	2.0E-14	32.2	7.4E-18	22.4	1.0E-06	291.5	353.2	362.4	d(FV)=0	77555	361.9	3.9	56.0	9.1E-01	0.4422
212	2.0E-16	35.9	1.7E-16	17.6	1.4E-05	24.9	30.0	90.5	d(FV)=0	537131	2422.4	28.0	56.0	4.6E-01	0.5220
213	3.7E-10	18.8	1.4E-15	14.8	3.3E-07	0.0	0.0	900.0	TIML	1914	18.7	0.6	5.1	8.6E-01	0.2627
214	2.1E-12	26.6	5.1E-17	18.8	2.3E-07	869.9	0.0	900.0	TIML	87350	453.8	4.5	46.6	1.4E-02	0.3679
215	6.4E-14	31.1	1.7E-16	17.5	7.3E-07	137.3	166.6	170.9	d(FV)=0	777382	3555.8	40.4	56.0	1.3E-04	0.4211

216	1.5E-11	24.7	5.1E-16	15.2	1.1E-07	585.2	714.2	733.0	d(FV)=0	620550	2903.9	31.7	56.0	3.1E-04	0.3182
217	2.1E-12	26.6	6.9E-17	21.2	1.5E-06	0.0	0.0	900.0	TIML	1628	15.9	0.4	6.6	6.1E-01	0.3642
218	3.6E-13	30.4	4.6E-15	14.6	9.9E-07	0.0	0.0	5.3	TIME>2H	759830	7200.0	50.4	7.2	6.0E-05	0.3753
219	5.0E-12	20.8	2.2E-16	16.7	3.6E-06	0.0	0.0	900.0	TIML	1263	11.8	0.5	9.8	3.2E-01	0.4389
220	7.6E-15	31.4	1.6E-15	17.0	3.5E-05	7.3	8.8	91.0	d(FV)=0	285082	1313.9	13.4	56.0	1.3E-02	0.4834
221	1.4E-12	28.1	1.4E-15	13.4	1.5E-07	0.0	0.0	43.6	TIME>2H	777634	7200.0	48.3	9.2	2.4E-05	0.3612
222	4.3E-14	27.5	1.1E-15	15.8	2.4E-05	0.0	0.0	900.0	TIML	14211	98.2	1.0	26.6	1.0E-02	0.4951
223	7.1E-14	33.4	3.5E-17	20.1	1.7E-07	0.0	0.0	330.9	NITL	1001100	5806.1	56.0	40.6	1.8E-04	0.3872
224	8.2E-14	29.5	3.0E-15	13.6	2.7E-06	33.5	40.3	90.1	NITL	1535341	6960.4	81.8	56.0	9.5E-01	0.4381
225	2.8E-11	22.5	9.0E-16	20.3	8.9E-06	0.0	0.0	900.0	TIML	900	9.5	0.5	1.8	0.0E+00	0.3271
226	1.8E-14	33.1	4.6E-15	13.2	1.7E-06	0.0	0.0	3.0	TIME>2H	733566	7200.0	47.4	4.6	2.6E-05	0.4332
227	2.9E-10	22.2	6.5E-16	16.0	5.5E-06	0.0	0.0	900.0	TIML	162028	1233.8	9.7	24.1	4.5E-03	0.2261
228	8.7E-15	33.7	7.6E-14	11.5	1.4E-05	0.0	0.0	0.2	TIME>2H	718509	7200.0	48.4	2.5	1.4E-06	0.4459
229	2.2E-13	29.2	9.5E-16	17.5	4.0E-06	31.3	38.1	90.0	d(FV)=0	375713	1742.3	20.1	56.0	1.9E-02	0.4094
230	7.4E-17	36.5	1.6E-17	21.8	3.2E-05	0.0	0.0	900.0	TIML	12447	93.9	0.9	21.8	2.4E-02	0.5395
231	1.0E-13	26.7	2.3E-15	13.6	8.8E-06	32.4	39.3	90.0	d(FV)=0	184312	844.6	9.2	56.0	2.5E-02	0.4788
232	9.9E-11	19.7	1.4E-16	18.0	5.3E-07	0.0	0.0	900.0	TIML	925	9.5	0.2	4.0	8.4E-01	0.3150
233	2.6E-14	33.0	6.0E-18	15.7	6.7E-07	0.0	0.0	18.2	TIME>2H	784725	7200.0	48.5	10.2	1.9E-04	0.4200
234	2.6E-12	25.9	1.6E-16	19.3	1.3E-06	0.0	0.0	900.0	TIML	2384	23.0	0.5	9.2	7.4E-01	0.3699
235	2.6E-13	29.6	6.6E-16	16.3	9.2E-07	81.3	0.0	94.0	NITL	1001100	4804.5	51.6	52.5	5.4E-06	0.3978
236	1.7E-12	23.8	5.3E-17	19.7	2.6E-06	0.0	0.0	900.0	TIML	1008	9.8	0.3	8.5	3.3E-01	0.4242
237	2.1E-13	28.6	5.0E-16	15.5	9.4E-07	115.8	140.6	144.6	d(FV)=0	613908	2818.8	33.3	56.0	1.9E-04	0.4200
238	1.4E-11	23.2	4.9E-17	21.1	1.0E-06	0.0	0.0	900.0	TIML	935	8.9	0.5	5.6	3.8E-01	0.3454
239	3.8E-13	29.9	2.4E-17	22.0	5.8E-07	389.4	474.7	487.7	d(FV)=0	79786	380.7	4.0	55.9	5.2E-03	0.3817
240	1.4E-11	20.9	9.4E-17	18.6	1.6E-06	0.0	0.0	900.0	TIML	923	8.6	0.4	6.7	6.1E-01	0.3865
241	4.8E-11	19.4	3.9E-16	17.1	2.0E-06	0.0	0.0	900.0	TIML	945	9.1	0.4	8.4	7.8E-01	0.3571
242	5.4E-12	25.0	1.8E-17	20.4	2.2E-07	0.0	0.0	900.0	TIML	1092	11.3	0.2	2.9	2.9E-01	0.3559
243	4.9E-13	27.3	4.3E-17	20.8	1.8E-06	0.0	0.0	900.0	TIML	1515	14.8	0.5	8.3	3.2E-01	0.4099
244	8.9E-11	21.9	2.6E-15	13.8	2.2E-07	315.4	385.6	395.9	d(FV)=0	518083	2459.1	28.9	56.0	2.1E-02	0.2831
245	1.8E-11	21.4	1.8E-14	12.6	5.0E-06	28.2	34.5	90.0	d(FV)=0	181853	858.0	10.3	56.0	2.4E-02	0.3648
246	2.3E-14	32.7	8.3E-16	15.3	1.1E-06	0.0	0.0	16.5	TIME>2H	805794	7200.0	51.0	12.3	1.6E-04	0.4304
247	8.5E-16	34.6	1.5E-17	20.7	4.3E-06	87.6	106.1	109.3	d(FV)=0	160627	740.3	8.1	56.0	2.4E-04	0.5002
248	1.5E-13	30.3	1.4E-15	16.3	2.1E-06	33.9	41.0	90.8	NITL	1296042	5924.5	69.5	56.0	2.3E-01	0.4057
249	1.1E-10	21.5	1.6E-16	18.9	2.9E-07	0.0	0.0	900.0	TIML	1048	10.7	0.5	3.6	1.0E-01	0.2781
250	5.6E-14	28.7	1.2E-15	15.6	8.1E-06	27.8	33.8	90.5	d(FV)=0	240450	1113.6	12.3	56.0	5.2E-01	0.4647
251	2.1E-12	24.4	3.7E-17	19.1	7.2E-07	0.0	0.0	900.0	TIML	1083	11.0	0.2	4.7	4.5E-01	0.4036
252	8.1E-14	29.8	5.5E-17	18.0	5.6E-07	304.2	370.1	379.0	d(FV)=0	258570	1200.2	14.6	56.0	1.9E-03	0.4327
253	2.7E-11	24.2	2.3E-16	18.8	3.4E-07	0.0	0.0	900.0	TIML	2955	29.3	0.4	5.9	2.9E-01	0.3029
254	1.4E-11	25.9	3.8E-16	17.3	1.5E-07	488.4	596.8	612.6	d(FV)=0	485666	2291.2	25.4	56.0	4.0E-04	0.3036
255	1.1E-12	24.7	8.2E-18	21.1	9.1E-07	0.0	0.0	900.0	TIML	922	9.4	0.4	4.4	3.0E-01	0.4263
256	4.9E-13	27.1	7.7E-16	18.1	6.9E-06	35.2	42.9	43.8	CRACKIN	68239	416.5	5.0	56.0	2.4E-04	0.4130
257	3.3E-10	20.9	8.8E-16	15.7	1.2E-07	0.0	0.0	900.0	TIML	69989	496.0	4.4	28.3	2.2E-03	0.2373
258	1.4E-13	25.8	4.0E-15	13.7	2.0E-05	18.5	22.4	90.9	d(FV)=0	101666	467.6	5.8	56.0	1.3E-01	0.4845
259	1.3E-13	29.6	1.8E-16	16.6	5.7E-07	196.5	238.7	244.6	d(FV)=0	582417	2677.4	31.2	56.0	1.1E-04	0.4201
260	1.1E-14	32.8	1.4E-15	15.6	4.4E-06	0.0	0.0	12.9	TIME>2H	982968	7200.0	56.6	26.7	1.1E-04	0.4517

261	2.0E-12	28.1	5.5E-16	15.8	1.7E-07	0.0	0.0	166.1	NITL	1001100	7047.6	58.1	29.7	1.2E-04	0.3471
262	5.4E-14	29.8	7.6E-17	17.5	6.7E-07	221.1	268.8	275.4	d(FV)=0	243131	1126.2	13.0	56.0	5.2E-04	0.4466
263	2.9E-13	29.4	5.3E-17	19.3	4.3E-07	340.7	415.4	426.3	d(FV)=0	212486	998.0	10.8	56.0	4.3E-04	0.3959
264	8.4E-12	26.7	5.2E-15	13.6	2.4E-07	0.0	0.0	16.5	TIME>2H	763664	7200.0	48.9	7.7	2.5E-04	0.3135
265	1.4E-11	23.8	2.2E-15	15.4	1.1E-06	106.5	130.1	133.1	CRACKIN	223737	1083.4	12.2	56.0	3.4E-04	0.3366
266	6.7E-15	33.0	2.4E-15	15.7	1.1E-05	10.5	0.0	12.0	TIME>2H	1515619	7200.0	80.2	52.2	6.7E-05	0.4631
267	2.6E-14	30.1	1.0E-16	19.1	5.2E-06	65.7	79.5	81.2	CRACKIN	88027	409.3	5.2	56.0	2.6E-04	0.4667
268	2.2E-14	29.8	1.3E-15	17.2	3.3E-05	9.7	11.8	90.0	d(FV)=0	130247	603.6	7.3	56.0	9.6E-01	0.4795
269	4.6E-12	24.2	2.4E-15	14.5	1.5E-06	81.4	99.3	101.9	d(FV)=0	261444	1229.1	13.5	56.0	3.5E-06	0.3745
270	6.1E-14	27.2	9.5E-17	18.7	9.3E-06	0.0	0.0	900.0	TIML	4069	34.7	0.6	14.7	1.5E-01	0.4882
271	2.5E-14	31.6	8.0E-16	17.6	7.3E-06	18.8	22.8	90.2	d(FV)=0	568601	2604.7	30.4	56.0	7.6E-01	0.4438
272	5.2E-12	24.8	9.7E-18	22.1	3.6E-07	0.0	0.0	900.0	TIML	923	9.5	0.4	3.1	5.3E-01	0.3596
273	1.3E-13	26.5	4.2E-16	15.7	4.8E-06	0.0	0.0	900.0	TIML	5159	46.6	0.4	14.1	2.3E-01	0.4718
274	2.3E-10	19.3	2.8E-16	17.1	3.1E-07	0.0	0.0	900.0	TIML	991	10.2	0.3	3.5	7.2E-01	0.2786
275	4.8E-13	29.5	2.1E-16	17.9	4.0E-07	192.7	234.4	240.4	d(FV)=0	717728	3312.1	39.0	56.0	5.8E-01	0.3767
276	8.8E-13	27.4	2.2E-16	18.2	9.9E-07	164.2	200.4	205.8	d(FV)=0	157022	747.0	8.1	56.0	2.4E-05	0.3864
277	1.3E-12	26.1	3.1E-15	12.5	6.6E-07	0.0	0.0	90.0	NITL	1130644	6364.5	62.8	42.4	6.1E-05	0.3921
278	1.2E-12	25.5	1.6E-16	16.7	6.5E-07	347.7	423.7	435.2	d(FV)=0	92599	437.7	5.4	55.9	7.5E-03	0.4046
279	1.9E-14	34.8	1.4E-14	12.5	1.2E-06	0.0	0.0	0.3	TIME>2H	704783	7200.0	45.6	0.8	2.4E-06	0.4084
280	2.3E-12	28.0	4.1E-17	19.8	1.3E-07	0.0	0.0	900.0	TIML	145813	846.9	8.3	40.5	1.3E-03	0.3434
281	1.3E-15	34.8	1.1E-16	18.2	3.8E-06	51.9	62.8	90.8	d(FV)=0	718495	3266.8	37.3	56.0	2.3E-01	0.4843
282	2.1E-11	22.9	1.6E-18	18.0	3.8E-07	0.0	0.0	900.0	TIML	1526	15.6	0.4	4.8	7.2E-01	0.3320
283	4.4E-12	25.6	2.2E-18	22.5	7.9E-08	0.0	0.0	900.0	TIML	900	9.5	0.4	1.8	0.0E+00	0.3543
284	2.2E-12	26.0	1.2E-15	13.6	3.1E-07	206.7	0.0	227.3	NITL	1001100	4984.5	52.5	49.7	1.3E-04	0.3745
285	3.1E-09	18.6	3.8E-17	20.5	3.9E-06	0.0	0.0	900.0	TIML	900	9.7	0.2	0.5	0.0E+00	0.1522
286	9.5E-14	33.0	2.7E-14	12.1	9.8E-07	0.0	0.0	0.2	TIME>2H	701184	7200.0	45.3	0.7	2.0E-06	0.3825
287	2.3E-11	21.8	1.8E-15	13.8	6.4E-07	225.4	275.6	283.2	d(FV)=0	155154	740.7	8.6	56.0	1.2E-03	0.3467
288	4.3E-18	35.5	4.6E-15	13.3	1.8E-05	0.0	0.0	3.2	TIME>2H	818582	7200.0	50.9	13.4	2.8E-05	0.5064
289	4.3E-14	32.8	6.6E-14	11.5	4.8E-06	0.0	0.0	0.2	TIME>2H	710391	7200.0	44.7	1.6	1.5E-06	0.4118
290	8.8E-15	33.5	5.1E-14	10.8	6.9E-06	0.0	0.0	0.4	TIME>2H	714918	7200.0	47.8	2.1	2.4E-06	0.4480
291	9.5E-17	36.4	4.4E-15	15.0	1.2E-04	3.1	3.7	90.7	NITL	1183475	5277.5	63.7	56.0	2.8E-01	0.5348
292	1.6E-16	37.6	4.8E-16	17.4	1.6E-05	0.0	0.0	7.9	TIME>2H	1013713	7200.0	57.0	28.8	6.2E-05	0.5023
293	8.2E-15	30.8	3.7E-15	12.8	9.3E-06	21.0	25.3	90.7	NITL	1028147	4639.4	57.8	56.0	3.5E-01	0.4923
294	3.4E-13	26.9	1.5E-17	18.5	2.8E-07	0.0	0.0	900.0	TIML	1991	20.3	0.3	3.7	2.0E-02	0.4299
295	1.3E-14	34.3	2.4E-17	20.1	3.6E-07	267.2	323.6	330.8	d(FV)=0	962243	4404.6	50.2	56.0	1.8E-01	0.4251
296	1.4E-10	25.1	3.4E-15	14.0	3.3E-08	0.0	0.0	38.9	TIME>2H	731179	7200.0	48.7	4.1	1.0E-05	0.2254
297	5.3E-11	22.6	7.4E-16	15.8	2.4E-07	557.1	682.6	704.8	d(FV)=0	162440	785.2	9.5	55.9	3.1E-03	0.2968
298	1.4E-14	32.4	1.5E-17	21.2	1.4E-06	186.0	226.1	231.8	d(FV)=0	134916	631.5	7.4	56.0	5.0E-04	0.4510
299	1.7E-13	29.5	2.4E-15	15.3	2.7E-06	28.2	34.1	90.8	NITL	1313875	5972.7	71.3	56.1	2.3E-01	0.4115
300	1.1E-10	20.8	1.4E-17	21.0	1.5E-07	0.0	0.0	900.0	TIML	900	9.0	0.4	1.5	0.0E+00	0.2920
301	2.3E-14	30.4	1.4E-15	16.0	1.1E-05	17.4	21.1	90.6	d(FV)=0	408011	1867.4	22.4	56.1	4.5E-01	0.4665
302	1.4E-10	21.0	2.9E-16	16.3	1.3E-07	0.0	0.0	900.0	TIML	2328	23.7	0.4	3.6	4.9E-01	0.2772
303	5.8E-14	29.2	8.3E-16	14.2	1.8E-06	77.2	93.5	96.4	d(FV)=0	683922	3130.7	34.7	56.1	1.3E-04	0.4546
304	8.5E-13	28.7	2.6E-15	15.5	1.1E-06	0.0	0.0	30.2	TIME>2H	1041274	7200.0	61.3	30.8	1.8E-05	0.3696
305	1.6E-13	32.0	8.6E-17	18.1	1.3E-07	0.0	0.0	201.7	TIME>2H	936382	7200.0	55.5	23.4	6.7E-05	0.3795

306	2.0E-14	30.0	7.9E-18	22.9	5.5E-08	0.0	0.0	900.0	TIML	2249	20.6	0.2	11.2	6.8E-02	0.4766
307	6.4E-12	25.8	4.4E-16	16.0	1.9E-07	388.2	473.6	485.7	d(FV)=0	547143	2565.0	30.5	56.0	1.1E-01	0.3366
308	3.2E-10	18.0	4.4E-16	18.3	1.6E-08	0.0	0.0	900.0	TIML	907	6.7	0.3	6.6	6.4E-01	0.2836
309	4.2E-13	29.2	3.8E-14	9.6	7.2E-07	0.0	0.0	1.0	TIME>2H	710923	7200.0	46.1	1.6	8.7E-06	0.3862
310	3.6E-13	25.5	5.8E-16	18.2	1.9E-05	0.0	0.0	900.0	TIML	10126	68.7	0.6	26.8	1.7E-02	0.4532
311	3.0E-18	39.4	6.3E-18	21.6	5.3E-07	0.0	0.0	135.6	NITL	1001100	7053.5	57.6	29.2	1.2E-04	0.4626
312	2.3E-13	25.7	3.7E-17	18.6	2.6E-08	0.0	0.0	900.0	TIML	1169	11.4	0.3	7.5	7.8E-01	0.4687
313	5.1E-10	19.6	1.7E-15	15.4	2.4E-07	0.0	0.0	900.0	TIML	4087	40.6	0.6	5.6	2.0E-02	0.2305
314	2.7E-11	24.7	3.6E-17	19.6	6.6E-08	0.0	0.0	900.0	TIML	2094	21.5	0.5	2.9	6.6E-01	0.2951
315	4.4E-14	30.0	6.5E-14	10.6	1.3E-05	0.0	0.0	1.1	TIME>2H	770902	7200.0	51.4	8.3	9.6E-08	0.4496
316	2.7E-11	23.2	1.6E-15	14.1	2.7E-07	262.2	320.1	327.3	CRACKIN	528057	2477.6	29.1	56.0	1.0E-04	0.3164
317	1.1E-18	37.9	2.6E-15	15.9	4.5E-05	0.0	0.0	1.6	TIME>2H	853588	7200.0	52.9	18.3	1.4E-05	0.5097
318	4.4E-14	32.2	1.8E-17	19.2	1.7E-07	641.2	778.6	797.4	d(FV)=0	615409	2830.0	33.1	56.0	1.1E-03	0.4176
319	2.0E-14	29.3	2.7E-15	15.0	2.5E-05	11.6	14.0	90.3	d(FV)=0	246695	1131.3	13.2	56.0	6.9E-01	0.4891
320	9.8E-11	23.9	6.9E-17	16.6	1.3E-08	0.0	0.0	900.0	TIML	43804	424.7	3.1	5.9	3.6E-03	0.2526
321	2.0E-14	30.8	7.8E-16	16.9	9.3E-06	20.6	25.2	90.7	d(FV)=0	361830	1666.6	20.0	56.0	3.3E-01	0.4636
322	6.7E-12	27.9	4.6E-15	14.3	2.0E-07	0.0	0.0	11.1	TIME>2H	741507	7200.0	46.3	5.3	1.7E-04	0.3074
323	1.5E-13	27.7	8.8E-16	13.9	1.5E-06	98.2	119.2	122.6	d(FV)=0	492354	2258.4	25.6	56.0	8.7E-05	0.4470
324	8.0E-15	31.9	1.0E-15	16.2	9.8E-06	18.5	22.4	90.9	d(FV)=0	618798	2811.2	33.9	56.0	1.4E-01	0.4749
325	1.5E-13	32.5	1.0E-15	15.6	2.6E-07	0.0	0.0	9.5	TIME>2H	731941	7200.0	49.2	4.1	9.8E-05	0.3751
326	1.0E-13	28.9	3.1E-16	22.9	8.3E-07	0.0	0.0	900.0	TIML	1029	10.5	0.4	4.4	3.9E-01	0.4402
327	1.0E-13	29.9	4.2E-15	15.9	9.2E-06	10.7	12.9	90.2	d(FV)=0	885143	4056.1	46.3	56.0	8.5E-01	0.4241
328	1.7E-09	18.0	1.3E-17	20.3	3.2E-06	0.0	0.0	900.0	TIML	900	9.7	0.2	0.3	0.0E+00	0.1928
329	8.2E-15	29.4	6.5E-16	16.1	2.7E-05	0.0	0.0	900.0	TIML	13896	100.0	1.4	24.7	6.5E-02	0.5172
330	1.5E-10	22.1	6.5E-14	9.4	2.1E-07	0.0	0.0	3.9	TIME>2H	716605	7200.0	46.3	3.0	7.4E-05	0.2569
331	2.1E-13	29.0	1.4E-15	15.7	2.4E-06	39.7	48.2	90.1	d(FV)=0	779172	3571.6	40.3	56.0	8.8E-01	0.4128
332	1.2E-16	39.8	2.3E-15	14.0	3.8E-06	0.0	0.0	0.9	TIME>2H	709849	7200.0	47.2	1.8	5.3E-06	0.4813
333	5.4E-14	29.6	2.6E-16	17.3	3.1E-06	64.4	78.3	90.0	d(FV)=0	233351	1084.7	12.7	56.0	9.9E-01	0.4496
334	2.7E-14	32.3	1.1E-15	15.6	1.8E-08	0.0	0.0	15.2	TIME>2H	863080	7200.0	53.2	17.7	1.5E-04	0.4302
335	8.8E-13	27.1	2.5E-16	17.7	1.1E-06	180.2	195.4	200.4	d(FV)=0	154013	726.9	8.2	56.0	7.3E-04	0.3920
336	6.6E-14	29.8	1.1E-16	16.7	5.1E-07	257.7	313.1	320.6	d(FV)=0	481348	2224.1	24.4	56.0	4.4E-04	0.4313
337	9.9E-13	26.4	1.0E-14	14.0	6.1E-06	15.0	18.2	90.6	d(FV)=0	665950	3079.8	34.9	56.0	3.9E-01	0.3992
338	4.6E-12	28.0	7.2E-17	20.4	1.7E-07	749.7	0.0	900.0	TIML	186278	909.6	9.8	53.9	7.5E-03	0.3197
339	2.0E-15	32.4	3.8E-17	19.6	8.2E-06	0.0	0.0	900.0	TIML	5691	50.7	0.5	14.1	5.6E-04	0.5090
340	7.7E-12	22.1	4.2E-17	17.6	3.8E-07	0.0	0.0	900.0	TIML	987	10.3	0.1	3.3	4.3E-02	0.3916
341	2.5E-11	23.4	2.2E-17	21.2	2.4E-07	0.0	0.0	900.0	TIML	920	9.5	0.5	2.7	6.5E-01	0.3171
342	2.3E-11	26.5	1.3E-15	15.1	5.8E-08	0.0	0.0	86.2	TIME>2H	783362	7200.0	48.7	9.9	4.4E-05	0.2777
343	6.0E-11	20.7	8.6E-16	12.8	1.3E-07	898.7	0.0	900.0	TIML	183557	981.3	10.7	45.0	4.4E-03	0.3229
344	6.9E-14	30.7	1.1E-16	18.0	7.8E-07	161.2	195.9	201.0	d(FV)=0	466707	2149.2	25.2	56.0	4.7E-04	0.4248
345	1.7E-13	34.2	2.0E-15	16.1	2.2E-07	0.0	0.0	1.8	TIME>2H	707964	7200.0	46.7	1.3	1.8E-05	0.3511
346	4.1E-12	26.0	1.0E-16	19.3	4.5E-07	0.0	0.0	900.0	TIML	3789	37.6	0.4	7.5	9.9E-01	0.3513
347	2.9E-14	29.0	5.9E-17	18.1	2.8E-06	0.0	0.0	900.0	TIML	3122	29.6	0.6	9.5	2.9E-01	0.4805
348	4.5E-12	23.8	1.4E-16	17.5	7.1E-07	0.0	0.0	900.0	TIML	1562	15.8	0.4	5.8	2.6E-01	0.3826
349	1.2E-11	25.8	8.1E-15	12.1	1.8E-07	0.0	0.0	12.9	TIME>2H	741276	7200.0	49.5	5.3	1.9E-04	0.3110
350	2.8E-12	26.6	4.2E-14	12.6	3.2E-06	0.0	0.0	2.6	TIME>2H	799006	7200.0	50.7	11.4	3.4E-05	0.3539

351	3.5E-15	35.5	7.4E-15	13.5	4.0E-06	0.0	0.0	0.9	TIME>2H	717766	7200.0	45.7	2.8	6.2E-06	0.4473
352	1.9E-16	34.6	7.8E-18	20.1	6.8E-06	0.0	0.0	900.0	TIML	2991	28.4	0.4	8.6	8.5E-02	0.5430
353	3.7E-15	33.2	2.1E-16	16.9	3.1E-06	56.7	70.9	90.3	d(FV)=0	734960	3344.8	38.6	56.1	6.6E-01	0.4785
354	3.9E-10	22.4	1.7E-15	13.6	2.2E-08	0.0	0.0	361.3	TIME>2H	793811	7200.0	177.9	13.5	3.0E-04	0.2108
355	1.5E-12	27.8	8.1E-14	10.7	2.0E-06	0.0	0.0	0.6	TIME>2H	629315	7200.0	425.8	2.6	7.3E-06	0.3618
358	5.0E-14	33.0	2.0E-16	17.7	4.2E-07	0.0	0.0	44.2	TIME>2H	728040	7200.0	431.7	15.2	9.1E-06	0.4020
357	7.0E-17	37.7	9.2E-18	23.1	2.0E-05	27.5	32.9	90.6	d(FV)=0	123235	660.8	46.1	56.0	4.2E-01	0.5237
358	1.5E-12	26.3	6.1E-15	13.1	1.5E-06	0.0	0.0	34.2	TIME>2H	972131	7200.0	438.5	37.9	2.0E-05	0.3849
359	2.5E-10	17.7	2.7E-14	11.2	2.3E-06	71.7	87.9	90.4	d(FV)=0	114416	710.6	42.5	55.9	6.6E-02	0.3047
360	5.3E-15	33.8	5.7E-16	17.2	5.1E-06	23.2	27.9	90.4	NITL	1320643	6292.4	227.9	56.1	5.8E-01	0.4583
361	4.5E-18	36.8	1.1E-17	21.0	1.8E-08	121.7	147.1	151.0	d(FV)=0	508998	2326.8	25.2	56.0	2.0E-02	0.4853
362	2.5E-13	27.2	2.8E-17	19.2	9.6E-07	0.0	0.0	900.0	TIML	1515	15.2	0.3	5.5	1.1E-01	0.4371
363	2.0E-10	21.1	4.2E-15	12.0	9.1E-08	0.0	0.0	325.9	NITL	1001100	6461.0	58.1	35.2	3.8E-05	0.2591
364	4.2E-11	23.9	1.1E-16	16.0	2.1E-06	0.0	0.0	900.0	TIML	80551	738.5	4.9	10.4	1.6E-03	0.2669
365	1.1E-14	35.7	3.4E-13	7.8	1.8E-06	0.0	0.0	0.0	TIME>2H	698470	7200.0	43.4	0.1	5.3E-08	0.4124
366	5.0E-12	29.2	1.2E-15	17.2	1.8E-07	0.0	0.0	39.1	TIME>2H	800042	7200.0	50.6	11.9	3.4E-05	0.3018
367	7.5E-18	42.5	1.8E-16	17.9	9.4E-06	0.0	0.0	3.4	TIME>2H	756181	7200.0	48.8	7.0	2.7E-05	0.5139
368	7.1E-14	27.2	1.0E-16	20.4	2.5E-05	0.0	0.0	900.0	TIML	9045	61.5	0.9	25.5	6.1E-02	0.4834
369	1.8E-12	26.0	5.3E-16	14.9	3.7E-07	254.6	310.1	317.7	d(FV)=0	485432	2263.7	24.6	56.0	8.2E-05	0.3811
370	4.0E-12	22.1	4.1E-17	19.5	2.2E-06	0.0	0.0	900.0	TIML	917	9.1	0.3	7.3	8.1E-02	0.4212
371	3.3E-13	30.9	5.0E-16	15.3	1.3E-07	0.0	0.0	39.1	TIME>2H	760354	7200.0	47.4	7.3	3.7E-05	0.3711
372	2.1E-11	23.4	2.2E-15	17.1	2.3E-06	92.3	112.8	116.0	d(FV)=0	76147	368.0	4.5	55.9	4.3E-04	0.3230
373	3.6E-13	30.3	2.2E-18	23.0	7.5E-06	0.0	0.0	900.0	TIML	3112	31.2	0.4	4.7	6.0E-01	0.3765
374	2.3E-14	27.4	2.3E-16	18.5	4.5E-05	849.8	0.0	900.0	TIML	14292	90.3	1.1	29.2	2.5E-02	0.5193
375	3.2E-09	17.8	1.4E-16	17.1	2.9E-06	0.0	0.0	900.0	TIML	900	9.4	0.3	1.0	0.0E+00	0.1598
376	1.2E-12	25.2	1.0E-15	15.5	2.7E-06	76.5	93.3	96.4	d(FV)=0	123715	583.1	6.7	56.0	7.4E-04	0.4137
377	2.9E-12	27.3	3.9E-15	13.4	3.1E-07	0.0	0.0	19.3	TIME>2H	776272	7200.0	48.5	9.4	2.6E-04	0.3443
378	9.8E-14	30.0	9.0E-17	19.9	2.2E-06	99.5	121.2	124.9	d(FV)=0	126852	596.3	7.0	56.0	1.5E-03	0.4240
379	1.1E-14	33.4	1.4E-15	17.1	7.2E-06	0.0	0.0	11.5	TIME>2H	1237096	7200.0	67.8	40.8	8.2E-05	0.4425
380	5.3E-12	22.9	5.8E-17	20.0	2.0E-06	0.0	0.0	900.0	TIML	936	9.1	0.4	7.6	8.4E-01	0.3936
381	5.2E-14	27.4	6.0E-16	15.5	9.6E-06	0.0	0.0	900.0	TIML	7510	63.1	0.6	17.8	1.0E-01	0.4907
382	1.2E-11	22.7	7.7E-16	16.7	1.9E-06	0.0	0.0	900.0	TIML	2315	22.1	0.4	10.8	2.4E-01	0.3630
383	2.6E-13	29.9	4.0E-16	15.0	2.1E-07	0.0	0.0	101.2	TIME>2H	880267	7200.0	51.9	18.9	1.6E-05	0.3933
384	1.5E-13	28.0	2.2E-17	19.6	9.3E-07	0.0	0.0	900.0	TIML	1658	16.7	0.3	5.6	5.9E-01	0.4416
385	5.5E-13	30.7	2.1E-15	14.5	2.4E-07	0.0	0.0	8.7	TIME>2H	731224	7200.0	46.9	4.1	9.8E-05	0.3571
386	6.6E-11	23.4	1.1E-16	16.6	2.7E-08	0.0	0.0	900.0	TIML	37581	349.9	2.3	9.1	1.0E-03	0.2759
387	3.1E-14	31.5	7.8E-18	20.8	4.1E-07	567.1	690.1	708.6	d(FV)=0	134283	627.5	7.7	56.0	4.7E-03	0.4388
388	4.9E-12	28.2	9.6E-16	15.0	7.2E-08	0.0	0.0	52.4	TIME>2H	757401	7200.0	48.3	7.4	3.2E-05	0.3137
389	3.6E-10	21.4	6.5E-17	20.1	8.3E-08	0.0	0.0	900.0	TIML	910	9.7	0.2	1.7	9.8E-01	0.2252
390	1.2E-13	30.7	2.5E-16	15.5	2.4E-07	0.0	0.0	127.0	TIME>2H	929566	7200.0	56.5	22.9	8.5E-05	0.4073
391	9.3E-12	22.4	5.7E-17	19.0	7.9E-07	0.0	0.0	900.0	TIML	962	9.8	0.4	4.9	5.6E-01	0.3761
392	1.2E-12	29.9	1.8E-16	16.3	4.3E-08	0.0	0.0	169.0	TIME>2H	789486	7200.0	49.7	10.8	1.7E-04	0.3421
393	1.2E-11	24.2	2.0E-16	18.8	6.0E-07	0.0	0.0	900.0	TIML	1932	19.4	0.3	6.3	6.0E-01	0.3333
394	2.0E-12	28.7	1.8E-15	14.2	1.5E-07	0.0	0.0	22.2	TIME>2H	747097	7200.0	47.0	6.2	2.9E-04	0.3388
395	1.4E-12	24.7	1.8E-15	13.7	1.7E-06	90.7	110.5	113.3	d(FV)=0	246069	1151.1	14.0	56.0	1.2E-04	0.4145

396	2.0E-11	20.6	6.3E-16	14.8	7.6E-07	0.0	0.0	900.0	TIML	1714	16.6	0.3	6.3	5.9E-01	0.3728
397	2.1E-10	16.0	1.1E-17	20.9	2.9E-07	0.0	0.0	900.0	TIML	900	9.5	0.2	1.4	0.0E+00	0.3076
398	2.6E-13	31.4	1.6E-16	18.0	2.0E-07	0.0	0.0	156.3	NITL	1001100	7183.9	60.3	28.3	2.8E-05	0.3727
399	2.1E-10	21.2	7.9E-15	12.5	2.2E-07	0.0	0.0	199.0	NITL	1001100	5390.6	56.2	45.0	6.3E-05	0.2555
400	2.3E-12	25.9	2.9E-17	20.3	4.4E-07	0.0	0.0	900.0	TIML	1313	13.3	0.3	4.3	2.2E-01	0.3749
401	4.0E-12	22.7	1.0E-15	14.4	1.7E-06	163.9	196.2	203.4	d(FV)=0	64790	302.5	4.2	55.9	3.6E-03	0.4077
402	1.5E-16	36.1	1.6E-17	21.5	1.6E-05	0.0	0.0	900.0	TIML	9729	81.1	0.9	18.7	1.1E-01	0.5259
403	1.1E-13	31.8	4.8E-16	16.9	6.2E-07	0.0	0.0	38.5	TIME>2H	897055	7200.0	56.3	20.3	1.2E-05	0.3959
404	1.0E-10	20.3	1.9E-15	14.9	7.1E-07	0.0	0.0	900.0	TIML	3030	30.0	0.5	8.4	6.6E-01	0.3023
405	3.4E-13	27.7	1.2E-14	12.6	4.1E-06	0.0	0.0	14.1	TIME>2H	1157345	7200.0	66.5	36.6	1.1E-04	0.4172
406	3.6E-14	31.0	6.4E-16	15.1	1.7E-06	56.6	68.3	90.5	NITL	1409654	6389.6	70.9	56.0	5.2E-01	0.4419
407	1.7E-15	34.6	6.7E-17	16.9	9.3E-07	0.0	0.0	154.7	NITL	1001100	5587.6	57.2	42.5	3.9E-05	0.4782
408	1.5E-13	30.6	7.2E-16	23.3	5.9E-07	0.0	0.0	900.0	TIML	1983	19.9	0.4	5.5	2.9E-01	0.4007
409	1.1E-11	27.6	3.1E-14	12.0	2.4E-07	0.0	0.0	1.0	TIME>2H	705649	7200.0	45.5	1.2	1.4E-05	0.2923
410	3.8E-10	17.4	1.6E-16	18.4	7.5E-07	0.0	0.0	900.0	TIML	900	9.2	0.4	3.7	0.0E+00	0.2872
411	3.4E-16	35.7	6.1E-17	20.3	1.7E-05	21.9	26.4	91.0	d(FV)=0	238405	1086.2	12.6	56.0	5.5E-02	0.5098
412	2.2E-12	25.3	5.3E-16	16.4	1.2E-06	150.5	183.7	188.6	d(FV)=0	128276	609.5	6.7	56.0	1.5E-03	0.3858
413	1.0E-11	22.3	9.7E-16	16.8	3.6E-06	0.0	0.0	900.0	TIML	2775	24.5	0.4	13.9	2.1E-01	0.3753
414	2.9E-13	28.4	4.6E-16	16.7	1.4E-06	89.9	109.4	112.1	d(FV)=0	376720	1750.7	20.0	56.0	2.8E-04	0.4101
415	1.0E-13	27.8	7.5E-17	18.2	2.3E-06	0.0	0.0	900.0	TIML	2660	25.8	0.2	9.2	2.9E-02	0.4587
416	3.8E-13	28.0	3.0E-14	12.1	6.0E-06	0.0	0.0	3.3	TIME>2H	850785	7200.0	50.0	16.2	3.4E-05	0.4086
417	8.1E-12	25.8	6.7E-17	17.4	6.3E-08	0.0	0.0	900.0	TIML	88864	706.4	5.8	21.0	3.0E-03	0.3304
418	3.5E-16	35.4	1.1E-15	15.9	2.6E-05	10.0	12.0	90.2	NITL	1072824	4794.6	55.2	56.0	7.9E-01	0.5132
419	1.0E-11	26.8	5.7E-14	12.1	7.8E-07	0.0	0.0	1.0	TIME>2H	716831	7200.0	45.9	2.6	1.4E-05	0.3041
420	8.5E-14	29.3	3.0E-17	21.4	3.1E-06	0.0	0.0	900.0	TIML	2418	22.2	0.4	10.5	2.4E-01	0.4397
421	1.2E-16	35.5	4.5E-14	9.8	7.5E-05	0.0	0.0	1.3	TIME>2H	798247	7200.0	48.7	11.1	1.1E-05	0.5421
422	3.4E-11	20.4	3.7E-14	11.3	4.6E-06	24.8	30.1	30.7	CRACKIN	264603	1245.7	14.0	56.0	1.0E-04	0.3545
423	2.1E-16	39.2	1.3E-14	12.6	6.9E-06	0.0	0.0	0.2	TIME>2H	707471	7200.0	42.8	1.0	1.1E-06	0.4737
424	2.6E-16	36.7	4.3E-16	16.1	6.9E-06	0.0	0.0	13.7	TIME>2H	930972	7200.0	54.3	22.9	1.1E-04	0.5016
425	1.5E-15	34.7	3.1E-15	13.6	6.4E-06	0.0	0.0	4.0	TIME>2H	784408	7200.0	50.6	9.9	3.6E-05	0.4819
426	4.3E-13	29.0	3.4E-17	20.0	3.5E-07	505.1	616.4	633.0	d(FV)=0	136955	647.0	7.8	56.0	9.7E-02	0.3881
427	1.7E-14	33.0	1.4E-17	22.0	1.1E-06	191.5	233.1	239.0	d(FV)=0	164564	768.6	8.1	56.0	1.7E-04	0.4352
428	2.9E-11	22.7	3.0E-17	20.0	2.0E-07	0.0	0.0	900.0	TIML	944	9.9	0.3	2.6	9.1E-01	0.3207
429	1.3E-10	19.4	9.1E-18	20.6	1.4E-07	0.0	0.0	900.0	TIML	900	9.2	0.3	1.2	0.0E+00	0.3061
430	3.5E-11	22.7	2.4E-15	13.3	2.3E-07	266.8	325.6	333.8	d(FV)=0	685297	3214.0	34.7	56.0	6.3E-04	0.3119
431	2.8E-10	21.6	9.9E-16	16.7	1.9E-07	0.0	0.0	900.0	TIML	11586	110.3	1.0	10.1	7.9E-01	0.2346
432	2.8E-14	33.5	6.4E-15	13.5	1.9E-06	0.0	0.0	1.1	TIME>2H	718277	7200.0	45.8	2.7	8.8E-06	0.4140
433	9.8E-14	28.0	2.5E-15	14.2	6.4E-06	27.8	33.8	90.5	d(FV)=0	391398	1802.2	19.5	56.0	5.4E-01	0.4570
434	2.9E-15	33.2	4.9E-17	21.1	1.2E-05	33.1	40.0	90.8	d(FV)=0	97543	447.4	4.9	56.0	1.7E-01	0.4863
435	2.4E-14	32.1	2.3E-16	17.3	1.3E-06	81.3	98.3	101.2	d(FV)=0	961746	4385.2	50.6	56.0	6.5E-05	0.4370
436	1.5E-11	21.0	3.1E-17	21.1	2.3E-06	0.0	0.0	900.0	TIML	901	8.8	0.4	7.2	9.4E-01	0.3844
437	1.2E-12	27.0	7.6E-16	16.2	9.0E-07	109.9	133.9	137.6	d(FV)=0	433401	2020.3	22.9	56.0	3.2E-05	0.3804
438	3.2E-11	20.9	1.6E-15	13.8	6.8E-07	292.6	357.6	367.7	d(FV)=0	67468	421.3	5.1	55.9	2.4E-03	0.3480
439	1.6E-13	28.9	7.0E-17	19.6	1.6E-06	159.5	193.9	199.0	d(FV)=0	83596	393.8	4.9	56.0	2.2E-04	0.4233
440	5.4E-14	32.7	1.7E-15	15.3	9.0E-07	0.0	0.0	6.4	TIME>2H	750790	7200.0	48.5	6.4	6.5E-05	0.4036

441	6.3E-12	23.3	1.2E-15	18.0	1.8E-06	134.4	163.6	168.1	d(FV)=0	69129	327.9	4.0	55.9	1.5E-03	0.3660
442	4.3E-14	30.3	3.2E-15	14.0	4.3E-06	23.1	27.8	90.3	NITL	1488688	6708.1	75.6	56.1	7.3E-01	0.4470
443	7.8E-14	29.1	4.4E-17	19.0	1.3E-06	224.8	272.9	279.9	d(FV)=0	86220	402.5	5.0	56.0	4.6E-03	0.4446
444	1.5E-14	32.4	5.3E-16	16.2	2.1E-06	49.1	59.1	90.2	NITL	1445121	6510.8	75.0	56.0	8.3E-01	0.4471
445	2.0E-11	24.2	2.9E-15	14.6	4.7E-07	132.1	161.1	165.6	d(FV)=0	708609	3315.7	38.1	56.0	3.1E-04	0.3145
446	3.0E-13	28.9	2.2E-15	15.0	1.8E-06	39.8	48.2	90.1	NITL	1318568	6020.5	69.2	56.0	8.6E-01	0.4024
447	1.8E-14	31.4	1.1E-16	19.0	3.9E-06	59.0	71.7	90.3	d(FV)=0	196242	912.0	9.8	56.0	7.0E-01	0.4585
448	2.7E-14	30.8	6.4E-18	17.4	7.5E-06	23.5	28.5	90.1	d(FV)=0	358359	1645.0	20.1	56.0	8.7E-01	0.4534
449	3.7E-12	24.3	1.6E-17	19.8	2.6E-07	0.0	0.0	900.0	TIML	1020	10.5	0.5	2.9	9.6E-01	0.3825
450	2.0E-13	26.9	6.1E-16	14.9	2.2E-06	94.8	115.2	118.6	d(FV)=0	203406	946.3	10.7	56.0	2.8E-04	0.4496
451	1.1E-10	23.3	2.5E-15	15.4	2.0E-07	289.0	353.4	363.0	d(FV)=0	730467	3481.8	38.8	56.0	2.8E-01	0.2538
452	2.7E-13	30.9	4.0E-15	13.5	4.3E-07	0.0	0.0	4.6	TIME>2H	724688	7200.0	46.1	3.5	4.6E-05	0.3778
453	2.1E-14	30.1	3.5E-15	13.9	1.0E-05	18.7	20.2	90.5	d(FV)=0	761183	3445.3	40.7	56.0	5.0E-01	0.4732
454	1.1E-14	33.2	2.5E-18	22.6	4.0E-07	659.1	801.3	822.9	d(FV)=0	109932	515.7	5.8	56.0	3.6E-03	0.4458
455	1.3E-14	32.5	1.8E-15	14.4	2.6E-06	0.0	0.0	10.5	TIME>2H	832805	7200.0	49.7	14.8	1.0E-04	0.4492
456	2.4E-09	18.5	1.9E-15	14.5	7.3E-08	0.0	0.0	900.0	TIML	9963	99.2	0.8	4.9	7.3E-01	0.1672
457	4.0E-14	31.7	3.9E-14	10.7	3.3E-06	0.0	0.0	0.8	TIME>2H	716478	7200.0	48.8	2.4	4.8E-06	0.4268
458	3.7E-14	31.8	6.8E-17	19.2	1.0E-06	142.4	173.2	177.6	d(FV)=0	357645	1649.2	20.1	56.0	3.7E-04	0.4312
459	2.5E-16	37.7	1.6E-15	17.0	2.5E-05	0.0	0.0	1.8	TIME>2H	829654	7200.0	51.8	14.5	1.6E-05	0.4891
460	9.5E-12	24.0	6.8E-17	19.0	3.6E-07	0.0	0.0	900.0	TIML	1329	13.0	0.6	4.1	9.5E-01	0.3485
461	4.1E-14	27.8	6.3E-16	19.0	8.8E-05	342.0	579.8	900.0	TIML	53838	225.9	2.7	42.6	6.3E-03	0.4952
462	9.2E-12	24.3	3.3E-15	13.8	5.7E-07	111.8	136.2	140.0	d(FV)=0	799063	3712.5	41.8	56.0	1.7E-04	0.3444
463	1.8E-13	24.3	2.1E-17	21.9	2.7E-05	893.6	0.0	900.0	TIML	5359	38.2	0.6	23.7	4.5E-02	0.5052
464	1.5E-14	33.0	9.0E-14	10.9	1.0E-05	0.0	0.0	0.2	TIME>2H	715273	7200.0	47.0	2.1	1.4E-06	0.4377
465	6.1E-11	19.6	3.2E-16	15.4	4.4E-07	0.0	0.0	900.0	TIML	1119	11.1	0.5	4.3	8.0E-01	0.3425
466	5.7E-17	37.4	5.7E-19	25.0	6.0E-06	0.0	0.0	900.0	TIML	2364	22.6	0.3	8.4	3.4E-01	0.5328
467	7.9E-13	30.0	7.9E-13	8.3	2.1E-06	0.0	0.0	0.0	TIME>2H	700026	7200.0	45.8	0.2	1.2E-07	0.3535
468	3.0E-08	14.5	3.3E-15	13.0	4.4E-08	0.0	0.0	900.0	TIML	8277	84.6	0.8	1.9	6.9E-03	0.0545
469	1.6E-18	41.7	1.7E-17	19.8	2.0E-05	35.4	42.3	90.9	d(FV)=0	652323	2907.4	35.1	56.0	8.1E-02	0.5608
470	1.6E-14	34.0	1.0E-16	18.0	4.2E-07	0.0	0.0	80.4	TIME>2H	923781	7200.0	54.4	22.3	3.7E-05	0.4234
471	1.0E-10	23.0	2.3E-15	14.5	1.4E-07	364.5	445.3	456.9	d(FV)=0	922148	4323.2	51.0	56.0	2.0E-04	0.2621
472	4.9E-12	26.0	9.4E-16	14.3	1.8E-07	0.0	0.0	248.6	NITL	1001100	5884.6	56.4	40.3	1.2E-05	0.3445
473	2.7E-14	31.6	1.9E-16	16.1	6.2E-07	0.0	0.0	158.6	NITL	1001100	5453.7	55.6	44.1	4.3E-05	0.4409
474	1.3E-13	31.8	9.8E-16	15.4	4.0E-07	0.0	0.0	14.7	TIME>2H	761801	7200.0	48.2	7.3	1.6E-04	0.3888
475	1.9E-12	29.0	1.2E-15	13.1	4.6E-08	0.0	0.0	25.5	TIME>2H	720126	7200.0	45.9	3.0	3.0E-04	0.3369
476	1.1E-13	30.1	1.4E-15	16.5	3.8E-06	25.6	31.1	90.7	d(FV)=0	790471	3610.7	41.9	56.0	3.5E-01	0.4184
477	9.5E-14	33.8	5.9E-18	21.8	4.9E-08	0.0	0.0	900.0	TIML	450727	3241.9	27.7	27.8	1.6E-03	0.3739
478	5.3E-14	28.3	2.6E-15	15.7	2.6E-05	11.0	13.4	90.7	d(FV)=0	159025	735.1	8.2	56.0	3.5E-01	0.4732
479	5.6E-10	19.7	1.8E-15	13.3	6.8E-08	0.0	0.0	900.0	TIML	261968	1728.4	15.5	33.3	2.7E-03	0.2273
480	2.0E-14	29.6	2.7E-15	12.5	4.7E-06	38.2	46.0	90.8	d(FV)=0	879203	3963.1	47.7	56.0	2.4E-01	0.4833
481	4.7E-14	33.5	3.9E-17	19.4	1.8E-07	0.0	0.0	271.0	NITL	1001100	6532.1	58.1	34.3	2.2E-04	0.3985
482	2.4E-14	34.7	2.8E-15	14.4	5.8E-07	0.0	0.0	1.7	TIME>2H	713287	7200.0	45.8	1.7	1.3E-05	0.4020
483	2.4E-11	23.6	3.2E-15	15.3	8.7E-07	104.3	127.6	131.0	d(FV)=0	337754	1604.1	18.3	56.0	1.5E-04	0.3150
484	1.9E-14	31.7	4.3E-16	17.9	5.5E-06	28.5	34.6	90.3	d(FV)=0	463620	2120.3	25.6	56.0	7.4E-01	0.4503
485	1.4E-14	30.4	7.3E-16	18.3	3.7E-05	9.7	11.7	90.0	d(FV)=0	114230	491.4	6.4	56.0	4.4E-03	0.4818

486	3.9E-13	26.2	1.4E-14	13.0	1.3E-05	11.3	13.7	91.0	d(FV)=0	443527	2045.7	21.9	56.0	1.5E-02	0.4385
487	1.5E-13	25.4	7.0E-17	20.0	1.8E-05	0.0	0.0	900.0	TIML	5359	40.5	0.6	20.4	1.5E-01	0.4895
488	1.3E-15	34.1	1.2E-14	13.5	4.0E-05	0.0	0.0	1.7	TIME>2H	883670	7200.0	53.4	19.1	1.5E-05	0.4953
489	8.2E-12	22.6	6.6E-16	17.2	3.1E-06	0.0	0.0	900.0	TIML	2334	20.9	0.5	12.4	1.4E-01	0.3784
490	1.6E-15	33.1	3.0E-14	10.1	1.9E-05	0.0	0.0	1.9	TIME>2H	780083	7200.0	49.0	9.1	1.6E-05	0.5047
491	1.9E-13	27.2	3.7E-15	13.1	4.0E-06	34.3	41.6	90.5	d(FV)=0	583003	2662.4	31.1	56.1	5.2E-01	0.4454
492	4.2E-16	36.7	2.0E-16	16.2	2.2E-06	0.0	0.0	6.3	TIME>2H	760971	7200.0	48.7	7.5	5.5E-05	0.4625
493	1.3E-14	33.8	1.2E-16	19.0	1.3E-06	73.1	88.4	90.1	NITL	1086017	4947.7	57.2	56.1	2.5E-01	0.4321
494	1.4E-12	25.5	2.0E-15	15.1	2.7E-06	52.4	63.9	65.3	CRACKGN	243664	1142.4	13.8	56.0	1.2E-04	0.3989
495	3.2E-12	24.3	6.7E-15	13.0	2.4E-06	41.8	50.9	91.0	d(FV)=0	462461	2151.4	24.2	56.0	9.1E-04	0.3886
496	3.2E-14	30.6	2.9E-15	14.6	6.0E-06	18.6	22.5	90.8	NITL	1208357	5478.7	62.9	56.0	1.7E-01	0.4516
497	4.6E-15	34.0	1.4E-16	18.7	3.2E-06	46.8	56.7	90.8	d(FV)=0	708857	3235.3	35.1	56.0	2.1E-01	0.4600
498	1.8E-14	31.5	6.3E-18	19.9	3.4E-07	750.2	0.0	900.0	TIML	140392	665.2	6.9	54.2	8.4E-03	0.4567
499	2.7E-12	24.7	4.1E-17	21.2	1.8E-06	0.0	0.0	900.0	TIML	974	9.6	0.4	7.6	2.4E-01	0.3880
500	5.6E-10	22.8	1.0E-17	22.9	1.8E-08	0.0	0.0	900.0	TIML	900	9.6	0.4	0.5	0.0E+00	0.1896